



# Grasping the Complexity of Anti-Tumor Immunity

Vivien Veninga

# Grasping the Complexity of Anti-Tumor Immunity

Looking at T cells and beyond

Vivien Veninga

Printed by: Gildeprint  
Layout: Vivien Veninga  
Cover design: Enis Nart  
DOI: <https://doi.org/10.33540/2220>  
ISBN: 978-94-6496-091-4

Copyright © Vivien Veninga, 2024. All rights reserved.

**Grasping the Complexity of Anti-Tumor Immunity**  
Looking at T cells and beyond

Het beginnen te begrijpen van de complexiteit van  
anti tumor immuniteit

(met een samenvatting in het Nederlands)

**Proefschrift**

ter verkrijging van de graad van doctor aan de  
Universiteit Utrecht  
op gezag van de  
rector magnificus, prof. dr. H.R.B.M. Kummeling,  
ingevolge het besluit van het college voor promoties  
in het openbaar te verdedigen op

dinsdag 7 mei 2024 des middags te 2.15 uur

door

**Vivien Veninga**

geboren op 13 mei 1992  
te Nienburg (Weser), Duitsland

**Promotor:**

Prof. dr. E. E. Voest

**Copromotor:**

Dr. N. F. de Miranda

**Beoordelingscommissie:**

Prof. dr. R. Bernardis

Prof. dr. J.H.E. Kuball (voorzitter)

Prof. dr. S.M.A. Lens

Prof. dr. R.H. Medema

Prof. dr. W. Zwart

# Contents

<b>Chapter 1</b>	General Introduction and Outline	7
<b>Chapter 2</b>	Tumor organoids: Opportunities and challenges to guide precision medicine	17
<b>Chapter 3</b>	Whole genome CRISPR screen of patient-derived tumor organoids to identify mediators of autologous T cell killing	49
<b>Chapter 4</b>	CD8 <sup>+</sup> T cell dynamics in patient-derived tumor organoid co-cultures	81
<b>Chapter 5</b>	$\gamma\delta$ T cells are effectors of immunotherapy in cancers with HLA class I defects	109
<b>Chapter 6</b>	Making mismatch repair proficient colorectal cancer visible to $\gamma\delta$ T cells	159
<b>Chapter 7</b>	Unveiling determinants driving CD34 <sup>+</sup> progenitor-derived NK cell reactivity against patient-derived tumor organoids	177
<b>Chapter 8</b>	General Discussion and Summary	215
<b>Addendum</b>	Addendum	225
	Nederlandse samenvatting	227
	Curriculum vitae	230
	List of publications	231
	Acknowledgements	233

Only a few know, how much one must know, to know  
how little one knows

Werner Heisenberg

# General Introduction and Outline

1





The concept of leveraging the body's immune system to combat cancer has roots dating back 133 years. In 1891, William Coley, a distinguished American cancer researcher and orthopedic surgeon, made a groundbreaking observation. He witnessed the regression of sarcomas by administering a mix of heat-inactivated bacteria. Coley's pioneering work earned him the title of the father of immunotherapy<sup>1,2</sup>.

Since then, the field of cancer immunotherapy has made significant advancements, especially gaining momentum in the latter half of the 20th century<sup>3</sup>. The discovery of T cells and B cells in 1967, along with the successful regression of advanced cancers through the administration of autologous lymphocytes in combination with interleukin 2 (IL-2) by Rosenberg and his team in 1985, paved the way for the success of cancer immunotherapy<sup>4,5</sup>.

Around a decade ago, immune checkpoint inhibitor drugs targeting CTLA-4 and PD-1 received FDA approval in 2011 and 2014, respectively<sup>6,7,8</sup>. Meanwhile, Carl June treated the first child with CAR-T cells against leukemia in 2012<sup>9</sup>. These success stories of immune checkpoint inhibitors (ICI) and adoptive cell therapies have significantly influenced the trajectory of the field, fundamentally changing the clinical treatment of cancer patients and fueling a large proportion of cancer immunotherapy research. The significance and growth of the field are also reflected in a global market size of 84 billion USD in 2021, with an estimated increase to reach 306 billion USD by 2030<sup>10</sup>.

In the coming years, we anticipate significant progress that will deepen our understanding and open new avenues for groundbreaking treatments for cancer patients. Nevertheless, crucial questions remain: Can we effectively develop cancer immunotherapies tailored for currently unresponsive tumor types? How much untapped potential remains in the continued exploration of immune checkpoint inhibitor (ICI) treatments? When might the next major breakthrough emerge to revolutionize our perspective on anti-tumor immunity?

ICI treatment has produced remarkable clinical outcomes, particularly in melanoma and microsatellite instability-high (MSI-H) tumors<sup>6,11</sup>. In 2019, response rates for these specific tumors were reported at an impressive 45-60%. However, the response rates in the majority of other solid tumors ranged from 15-30%<sup>12</sup>. Shortly thereafter, Chalabi

et al. reported an astonishing success rate of 100% in early-stage mismatch repair deficient (MMR-d) colon cancers by administering ICI as neoadjuvant treatment<sup>13</sup>.

To further improve clinical response rates, a primary area of research emphasis, both past and present, revolves around predicting ICI treatment response, discerning biomarkers, and comprehending the underlying mechanism. To date, tumor mutational burden (TMB), mismatch repair (MMR) deficiency, and PD-L1 expression have been shown to robustly correlate with anti-PD-(L)1 treatment response<sup>14</sup>. MMR deficiency, as well as TMB, enhances the probability of neoantigens presented by cancer cells, which can be recognized by T cells<sup>15</sup>. Blocking the inhibitory receptor ligand pair PD-1/PD-L1 allows for T cell activation<sup>16</sup>. Thus, providing an explanation for the mentioned correlation of TMB and MMR deficiency with patient response.

In line with this, Ribas and colleagues described that mutations of the antigen presenting machinery (APM) and IFN $\gamma$  pathway lead to acquired resistance to anti-PD1 immunotherapy in patients with melanoma<sup>17</sup>. Additionally, they showed that for melanoma, ICI response requires pre-existing intratumoral CD8<sup>+</sup> T cells and that T cell-induced IFN $\gamma$  is a main driver of clinical response<sup>18,19</sup>. Contrary, Yost et al. reported that in their basal and squamous cell carcinoma cohort newly infiltrating T cell clones proved to be relevant for T cell response to immune checkpoint blockade<sup>20</sup>.

While the question of which T cells, T cell states, and perhaps T cell behavior are relevant for the response to ICI treatment remains not fully answered, another crucial consideration arises—how translatable are findings from one tumor (type) to another? The beauty, but simultaneously the challenge, of cancer immunotherapy is that it targets the interplay of cancer cells and immune cells. Therefore, to understand and predict its outcome, one likely needs to analyze two unique and vastly complex parameters: the tumor itself and the patient's immune system.

The intricate composition of the tumor microenvironment (TME) is influenced by multiple factors, such as the genetic make-up of the tumor, its location, as well as the tumor stage, which ultimately determine the exposure to a selected subset of immune cells under specific conditions<sup>21</sup>. Underlining the importance to investigate whether certain resistance mechanisms or the influence of IFN $\gamma$  on ICI treatment response is broadly applicable or only relevant for specific tumor types. Moreover, questioning

which immune cells are key to a successful anti-tumor immune response. An in vivo CRISPR screen demonstrated that, controversially to previous findings, loss of IFN $\gamma$  signaling resulted in enhanced immune response, partly mediated by natural killer (NK) cells and the inhibiting effect of major histocompatibility complex (MHC) class I expression<sup>22</sup>. Likewise, we have discovered that colorectal cancers with defects in the antigen presenting machinery are able to respond to immune checkpoint blockade, again contrary to our knowledge based on melanoma studies<sup>23</sup>. Emphasizing that ICI response may be mediated by different cellular mechanisms depending on, for example, mutational profile or tumor type.

In summary, T cells play a major role in tumor immune responses, and the detailed understanding of underlying mechanisms governs great translational potential for future therapies. Simultaneously, the complexity of anti-tumor immunity requires us to look beyond conventional T cells to unveil the full picture. This may be especially relevant for understanding and overcoming current resistance mechanisms to ICI treatment and hence opening up opportunities to increase the response rate for those patients.

This thesis aims to understand the anti-tumor potential of different immune cell types while carefully considering the complexity of tumor-immune cell interactions. To investigate anti-tumor immunity in a personalized manner, which may support clinical translation, choosing the right model system is of high importance. Patient-derived tumor organoids (PDTOs) resemble the phenotypic and genetic characteristics of the original tumor and allow for the readout of autologous immune responses. As PDTOs are fundamental to the research of this thesis, **Chapter 2** will highlight the opportunities and challenges associated with the model system concerning precision medicine. The review will provide an extensive overview of the current state of organoids in cancer research, critically evaluating their predictive value for cancer treatments and summarizing advances in their integration into the field of immunotherapy.

Following the description of the potential of PDOs for whole-genome screens and cancer immunotherapy, **Chapter 3** reports on our attempt to perform whole-genome CRISPR Cas9 knockout screens on PDOs to identify modulators of autologous CD8<sup>+</sup> T cell killing. Based on two independent fully autologous screens of MSI CRC PDOs and expanded tumor-reactive CD8<sup>+</sup> T cells, sensitizers and resisters to T cell killing were identified and validated. This ambitious undertaking came with numerous optimizations, which will be described in this methods-oriented chapter.

In line with the goal to better understand T cell killing and reactivity, **Chapter 4** will dissect T cell dynamics during co-culture with PDOs, albeit at a much smaller scale. Here, we aimed to understand differences in T cell reactivity based on expression and chromatin accessibility profiles. Furthermore, we discuss recent advancements in identifying relevant T cell states for tumor response and provide context for the potential of our model system.

**Chapter 5** will shed light on how tumors, invisible to CD8<sup>+</sup> T cells, can respond to ICI treatment. Following a comprehensive multi-omics analysis of MMR-d B2M mutant CRC tumors and patient cohorts, we identified  $\gamma\delta$  T cells as effectors of ICI response. Differential gene expression analysis of two independent patient cohorts treated with ICI, surface marker phenotyping, and single-cell RNA analysis of tumor-infiltrating  $\gamma\delta$  T cells, along with in vitro experiments using CRC cell lines as well as isogenic B2M mutant/knockout PDOs, confirmed a cytotoxic phenotype and enhanced reactivity of V $\delta$ 1/3 T cells towards B2M mutant MMR-d CRC tumors. Thus, with these exciting findings, the thesis shifts its focus to immune cells beyond conventional T cells.

To take the discoveries of Chapter 5 one step further, we asked whether our findings of enhanced  $\gamma\delta$  T cell tumor reactivity in the context of MMR-d CRC can be translated to MMR-p CRC. These tumors generally do not respond well to ICI treatment<sup>12</sup>, and any advancement in initiating a better immune response would be a promising step forward. **Chapter 6** summarizes our most recent findings on introducing a B2M mutation in MMR-p CRC as an effort to increase  $\gamma\delta$  T cell reactivity.

Lastly, **Chapter 7** explores hematopoietic stem and progenitor cell-derived NK cell (HSPC-NK cells) reactivity towards PDOs to characterize activating and inhibiting ligands, as well as the investigating the role of IFN $\gamma$  on tumor recognition. Moreover, using pairs of CRC PDOs derived before and after ICI treatment revealed reduced HSPC-NK cell reactivity towards post ICI treatment-derived PDOs. In line with Chapter 4, this could point towards the involvement of immune cells, other than conventional T cells, to ICI response.

Taken together, the following chapters embody a journey through the complexity of anti-tumor immunity, which, I believe, we are just beginning to grasp. Starting with the challenge of pushing our boundaries in understanding T cell responses to more unexplored avenues such as the relevance of  $\gamma\delta$  T cells in ICI response or regulators of HSPC-NK cell reactivity.

## REFERENCES

1. Starnes, C. O. (1992). "Coley's toxins." *Nature* 360(6399): 23.
2. Starnes, C. O. (1992). "Coley's toxins in perspective." *Nature* 357(6373): 11-12.
3. <https://www.whatisbiotechnology.org/index.php/timeline/science/immunotherapy>
4. Miller, J. F. and G. F. Mitchell (1967). "The thymus and the precursors of antigen reactive cells." *Nature* 216(5116): 659-663.
5. Rosenberg, S. A., M. T. Lotze, L. M. Muul, S. Leitman, A. E. Chang, S. E. Ettinghausen, Y. L. Matory, J. M. Skibber, E. Shiloni, J. T. Vetto and et al. (1985). "Observations on the systemic administration of autologous lymphokine-activated killer cells and recombinant interleukin-2 to patients with metastatic cancer." *N Engl J Med* 313(23): 1485-1492.
6. Hodi, F. S., S. J. O'Day, D. F. McDermott, R. W. Weber, J. A. Sosman, J. B. Haanen, R. Gonzalez, C. Robert, D. Schadendorf, J. C. Hassel, W. Akerley, A. J. van den Eertwegh, J. Lutzky, P. Lorigan, J. M. Vaubel, G. P. Linette, D. Hogg, C. H. Ottensmeier, C. Lebbe, C. Peschel, I. Quirt, J. I. Clark, J. D. Wolchok, J. S. Weber, J. Tian, M. J. Yellin, G. M. Nichol, A. Hoos and W. J. Urba (2010). "Improved survival with ipilimumab in patients with metastatic melanoma." *N Engl J Med* 363(8): 711-723.
7. Ledford, H. (2011). "Melanoma drug wins US approval." *Nature* 471(7340): 561.
8. Brahmer, J. R., S. S. Tykodi, L. Q. Chow, W. J. Hwu, S. L. Topalian, P. Hwu, C. G. Drake, L. H. Camacho, J. Kauh, K. Odunsi, H. C. Pitot, O. Hamid, S. Bhatia, R. Martins, K. Eaton, S. Chen, T. M. Salay, S. Alparthy, J. F. Grosso, A. J. Korman, S. M. Parker, S. Agrawal, S. M. Goldberg, D. M. Pardoll, A. Gupta and J. M. Wigginton (2012). "Safety and activity of anti-PD-L1 antibody in patients with advanced cancer." *N Engl J Med* 366(26): 2455-2465.
9. Grupp, S. A., M. Kalos, D. Barrett, R. Aplenc, D. L. Porter, S. R. Rheingold, D. T. Teachey, A. Chew, B. Hauck, J. F. Wright, M. C. Milone, B. L. Levine and C. H. June (2013). "Chimeric antigen receptor-modified T cells for acute lymphoid leukemia." *N Engl J Med* 368(16): 1509-1518.
10. Bloomberg Business <https://www.bloomberg.com/press-releases/2023-08-10/cancer-immunotherapy-market-size-worth-usd-306-241-12-million-globally-by-2030-at-13-7-cagr-verified-market-research>
11. Le, D. T., J. N. Durham, K. N. Smith, H. Wang, B. R. Bartlett, L. K. Aulakh, S. Lu, H. Kemberling, C. Wilt, B. S. Luber, F. Wong, N. S. Azad, A. A. Rucki, D. Laheru, R. Donehower, A. Zaheer, G. A. Fisher, T. S. Crocenzi, J. J. Lee, T. F. Greten, A. G. Duffy, K. K. Ciombor, A. D. Eyring, B. H. Lam, A. Joe, S. P. Kang, M. Holdhoff, L. Danilova, L. Cope, C. Meyer, S. Zhou, R. M. Goldberg, D. K. Armstrong, K. M. Bever, A. N. Fader, J. Taube, F. Housseau, D. Spetzler, N. Xiao, D. M. Pardoll, N. Papadopoulos, K. W. Kinzler, J. R. Eshleman, B. Vogelstein, R. A. Anders and L. A. Diaz, Jr. (2017). "Mismatch repair deficiency predicts response of solid tumors to PD-1 blockade." *Science* 357(6349): 409-413.
12. Das, S. and D. B. Johnson (2019). "Immune-related adverse events and anti-tumor efficacy of immune checkpoint inhibitors." *J Immunother Cancer* 7(1): 306.
13. Chalabi, M., L. F. Fanchi, K. K. Dijkstra, J. G. Van den Berg, A. G. Aalbers, K. Sikorska, M. Lopez-Yurda, C. Grootsholten, G. L. Beets, P. Snaebjornsson, M. Maas, M. Mertz, V. Veninga, G. Bounova, A. Broeks, R. G. Beets-Tan, T. R. de Wijkerslooth, A. U. van Lent, H. A. Marsman, E. Nuijten, N. F. Kok, M. Kuiper, W. H. Verbeek, M. Kok, M. E. Van Leerdam, T. N. Schumacher, E. E. Voest and J. B. Haanen (2020). "Neoadjuvant immunotherapy leads to pathological responses in MMR-proficient and MMR-deficient early-stage colon cancers." *Nat Med* 26(4): 566-576.
14. Bai, R., Z. Lv, D. Xu and J. Cui (2020). "Predictive biomarkers for cancer immunotherapy with immune checkpoint inhibitors." *Biomark Res* 8: 34.

15. Schumacher, T. N. and R. D. Schreiber (2015). "Neoantigens in cancer immunotherapy." *Science* 348(6230): 69-74.
16. Freeman, G. J., A. J. Long, Y. Iwai, K. Bourque, T. Chernova, H. Nishimura, L. J. Fitz, N. Malenkovich, T. Okazaki, M. C. Byrne, H. F. Horton, L. Fouser, L. Carter, V. Ling, M. R. Bowman, B. M. Carreno, M. Collins, C. R. Wood and T. Honjo (2000). "Engagement of the PD-1 immunoinhibitory receptor by a novel B7 family member leads to negative regulation of lymphocyte activation." *J Exp Med* 192(7): 1027-1034.
17. Zaretsky, J. M., A. Garcia-Diaz, D. S. Shin, H. Escuin-Ordinas, W. Hugo, S. Hu-Lieskovan, D. Y. Torrejon, G. Abril-Rodriguez, S. Sandoval, L. Barthly, J. Saco, B. Homet Moreno, R. Mezzadra, B. Chmielowski, K. Ruchalski, I. P. Shintaku, P. J. Sanchez, C. Puig-Saus, G. Cherry, E. Seja, X. Kong, J. Pang, B. Berent-Maoz, B. Comin-Anduix, T. G. Graeber, P. C. Tumeh, T. N. Schumacher, R. S. Lo and A. Ribas (2016). "Mutations Associated with Acquired Resistance to PD-1 Blockade in Melanoma." *N Engl J Med* 375(9): 819-829.
18. Tumeh, P. C., C. L. Harview, J. H. Yearley, I. P. Shintaku, E. J. Taylor, L. Robert, B. Chmielowski, M. Spasic, G. Henry, V. Ciobanu, A. N. West, M. Carmona, C. Kivork, E. Seja, G. Cherry, A. J. Gutierrez, T. R. Grogan, C. Mateus, G. Tomasic, J. A. Glaspy, R. O. Emerson, H. Robins, R. H. Pierce, D. A. Elashoff, C. Robert and A. Ribas (2014). "PD-1 blockade induces responses by inhibiting adaptive immune resistance." *Nature* 515(7528): 568-571.
19. Grasso, C. S., J. Tsoi, M. Onyshchenko, G. Abril-Rodriguez, P. Ross-Macdonald, M. Wind-Rotolo, A. Champhekar, E. Medina, D. Y. Torrejon, D. S. Shin, P. Tran, Y. J. Kim, C. Puig-Saus, K. Campbell, A. Vega-Crespo, M. Quist, C. Martignier, J. J. Luke, J. D. Wolchok, D. B. Johnson, B. Chmielowski, F. S. Hodi, S. Bhatia, W. Sharfman, W. J. Urba, C. L. Slingluff, Jr., A. Diab, J. Haanen, S. M. Algarra, D. M. Pardoll, V. Anagnostou, S. L. Topalian, V. E. Velculescu, D. E. Speiser, A. Kalbasi and A. Ribas (2021). "Conserved Interferon-gamma Signaling Drives Clinical Response to Immune Checkpoint Blockade Therapy in Melanoma." *Cancer Cell* 39(1): 122.
20. Yost, K. E., A. T. Satpathy, D. K. Wells, Y. Qi, C. Wang, R. Kageyama, K. L. McNamara, J. M. Granja, K. Y. Sarin, R. A. Brown, R. K. Gupta, C. Curtis, S. L. Bucktrout, M. M. Davis, A. L. S. Chang and H. Y. Chang (2019). "Clonal replacement of tumor-specific T cells following PD-1 blockade." *Nat Med* 25(8): 1251-1259.
21. de Visser, K. E. and J. A. Joyce (2023). "The evolving tumor microenvironment: From cancer initiation to metastatic outgrowth." *Cancer Cell* 41(3): 374-403.
22. Dubrot, J., P. P. Du, S. K. Lane-Reticker, E. A. Kessler, A. J. Muscato, A. Mehta, S. S. Freeman, P. M. Allen, K. E. Olander, K. M. Ockerman, C. H. Wolfe, F. Wiesmann, N. H. Knudsen, H. W. Tsao, A. Iracheta-Vellve, E. M. Schneider, A. N. Rivera-Rosario, I. C. Kohnle, H. W. Pope, A. Ayer, G. Mishra, M. D. Zimmer, S. Y. Kim, A. Mahapatra, H. Ebrahimi-Nik, D. T. Frederick, G. M. Boland, W. N. Haining, D. E. Root, J. G. Doench, N. Hacohen, K. B. Yates and R. T. Manguso (2022). "In vivo CRISPR screens reveal the landscape of immune evasion pathways across cancer." *Nat Immunol* 23(10): 1495-1506.
23. de Vries, N. L., J. van de Haar, V. Veninga, M. Chalabi, M. E. Ijsselsteijn, M. van der Ploeg, J. van den Bulk, D. Ruano, J. G. van den Berg, J. B. Haanen, L. J. Zeverijn, B. S. Geurts, G. F. de Wit, T. W. Battaglia, H. Gelderblom, H. M. W. Verheul, T. N. Schumacher, L. F. A. Wessels, F. Koning, N. de Miranda and E. E. Voest (2023). "gammadelta T cells are effectors of immunotherapy in cancers with HLA class I defects." *Nature* 613(7945): 743-750.



How it all began...

Chemie: Das Basiswissen der Chemie  
Charles E. Mortimer, Ulrich Müller 9. Auflage

# Tumor organoids: Opportunities and challenges to guide precision medicine

2

Vivien Veninga <sup>1,2</sup> and Emile E. Voest<sup>1,2</sup>

<sup>1</sup>Department of Molecular Oncology and Immunology, Netherlands Cancer Institute, Amsterdam 1066CX, The Netherlands

<sup>2</sup>Oncode Institute, Utrecht, The Netherlands



## ABSTRACT

Tumor organoids have been proposed as a model system for precision medicine. The ability of tumor organoids to retain characteristics of the original tumor makes them unique for cancer research on an individual patient level. Hence, the idea to use tumor organoids for clinical decision making and optimize patient outcome is tempting. In vitro responses of tumor organoids to a wide array of drugs have been positively correlated to patient responses. However, substantial challenges remain and prospective studies with large cohorts are highly needed before implementation in clinical cancer care can be considered. Because of their personalized characteristics and the immediate link with patient data, tumor organoids also have great potential in preclinical research. Here, we provide a critical overview of both clinical and preclinical advances using tumor organoids.

## INTRODUCTION

2

In the past decade, treatment of cancer patients has evolved from treatment based on tumor type to treatment based on molecular characteristics of a tumor or its microenvironment. This approach, coined precision medicine or individualized treatment, has changed the outlook of many patients with advanced cancers and is now also incorporated in (neo-)adjuvant studies. Large-scale tumor sequencing efforts with subsequent identification of numerous targets for treatment have been the driving force behind precision medicine. Although many successes have been reported based on DNA sequencing, it is also clear that there is still a high unmet need for effective treatments in the majority of cancer patients (Cobain et al., 2021). The focus on genetic aberrations in a fraction of coding regions has significant limitations and does not appreciate or depict the complexity of the disease. So far, DNA sequencing provides information on the drivers of cancer that are fairly well preserved during disease progression but it does not include other modulators such as epigenetic changes or effects of non-coding regions. These modulators are far more dynamic and their relevance is more difficult to understand. While cancer is a genetic disease, all levels of cellular information are relevant to fully grasp the underlying malignant mechanisms to create better treatments. Clearly, the need for a dynamic, versatile model system that allows in-depth analysis of multiple dimensions of tumor biology and reflect the behavior of the original tumor in patients is high. The ability to create living, ex vivo tumors derived from individual patients has generated significant enthusiasm to improve precision medicine. With the development of new technologies, it is now possible to grow tumors in three-dimensional (3D) structures on an individualized basis. These so-called organoids are multicellular in vitro structures derived from adult or embryonic stem cells that resemble features of their original tissue and have the ability to self-organize and self-renewal (Eiraku and Sasai, 2012; Lancaster and Knoblich, 2014; Clevers, 2016). This technology provides a promising model system to facilitate translational research and may have a role in clinical decision making. In this review, we discuss the advantages and limitations of tumor organoids and their potential relevance to improve treatment outcome of patients with cancer. In the first part, we critically appraise the role of tumor organoids

in the translational research setting and report on their current applications with respect to targeted therapy, chemotherapy, and immunotherapy. In the second part we focus on further applications in basic research, highlighting genetic screens, proteomics, and other novel avenues.

## IMPLEMENTATION OF TUMOR ORGANIDS IN CLINICAL DECISION MAKING

### Recent achievements and remaining challenges

Tumor organoids preserve features of the original tumor and offer the possibility to study individual cancers as a dynamic system compared with static sequencing data. The need for such a dynamic system is emphasized by the fact that the failure rate of drugs tested in clinical trials remains extremely high, with low success rates for cancer treatments of 3.4% in phase I–III clinical trials (Wong et al. 2019). It can be hypothesized that tumor organoids could help to improve the translation from bench to bedside by offering a more versatile and personalized view on cancer biology and treatment response. Since the establishment of the first organoid cultures derived from stem cells (Sato et al., 2011), many researchers around the world have used tumor organoids to address their scientific questions and created a wealth of data. By now it is possible to generate long-term tumor organoid cultures from a wide range of human epithelial tissues, such as colon (Sato et al., 2011), liver (Broutier et al., 2017), lung (Sachs et al., 2019), pancreas (Boj et al., 2015; Huang et al., 2015), prostate (Karthaus et al., 2014; Gao et al., 2014), ovaries (Kopper et al., 2019; Hill et al., 2018), bladder (Mullenders et al., 2019), breast (Sachs et al., 2018), endometrium (Turco et al., 2017), esophagus (Sato et al., 2011), neuroendocrine cancer (Kawasaki et al., 2020; Dijkstra et al., 2021), and more (Kretzschmar, 2021). Large living biobanks of tumor organoids have been created in recent years and this work has been summarized and extensively discussed by others (Kretzschmar, 2021; Drost and Clevers, 2018). In addition to those achievements, follow-up analysis on long-term organoid cultures suggests that characteristics of the original tumor sample, like phenotype, genetic diversity, and mutational signatures, are preserved in organoids (Weeber et al., 2015; Sachs and Clevers, 2014; Blokzijl et al., 2016). Moreover, tumor organoids have superior characteristics compared with other model systems.

Their biology places them between cell lines and patient-derived xenograft (PDX) models. Compared with organoids, converting human tumors into cell lines is a much greater challenge. A success rate of around 26% across different cancer types has been reported for the generation of a cancer cell monoculture from patient tissue (Kodack et al., 2017). PDX models, on the other hand, remain the only system to capture individualized tumor growth in vivo, surrounded by and in crosstalk with the tumor microenvironment (TME) and parts of the immune system, but tumor organoids can be easier to establish, cheaper to maintain, and do not require the use of experimental animals, in line with ethical goals on animal welfare. All of the above-mentioned advantages are of profound importance for clinical implementation and they allow researchers to analyze tumor biology on a personalized level.

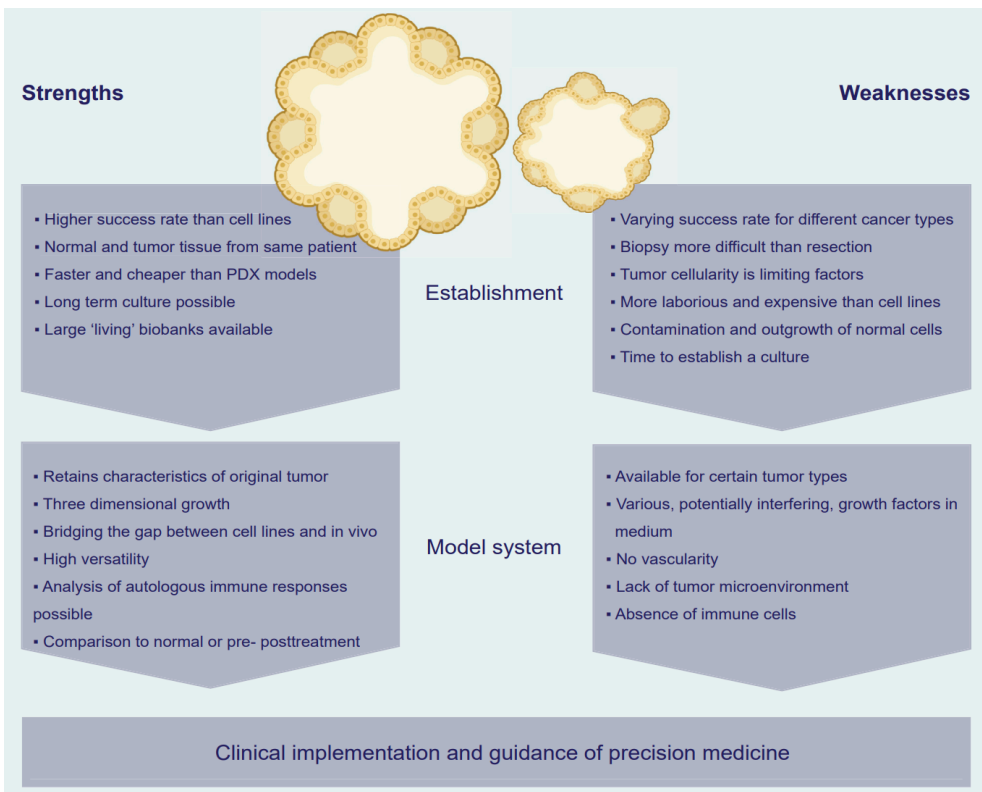


**Figure 1. Strengths and weaknesses of tumor organoids for clinical implementation.**

Summary of factors that either support or hinder the use of tumor organoids in precision medicine compared with conventional cell lines or PDX models. Two main categories of strengths and weaknesses of tumor

organoids have to be considered: the establishment of organoid cultures as a first step and the suitability of organoids as a model system. While tumor organoids, on an individual basis, are easier to establish compared with cell lines and cheaper to maintain than PDX models, their initial success rate currently hampers integration into clinical decision making. As a model system, tumor organoids represent the original tumor more closely than cell lines and at the same time are more versatile than PDX models. However, other key cellular components are lacking in organoid cultures.

Now, the concept to take a tumor specimen from a patient, create and propagate organoids, expose the patient-derived tumor organoids to a wide array of drugs, and subsequently treat the patient with the best possible drug or combination of drugs seems within reach. This would truly serve as the ultimate bench-to-bedside model for cancer therapy. Several groups, including ours, have taken this approach, and correlations were found between pre- and post-treatment organoid cultures and sensitivity to a particular drug (Mlachogiannis et al., 2018; de Witte et al., 2020; Kopper et al., 2019; Ooft et al., 2019). However, humbling experiences have also made it clear that there are challenges that need to be resolved to fully utilize the potential value of tumor organoids for clinical decision making (Figures 1 and 2). Even though the culture success rate is superior to two dimensional (2D) cultures, the success rate of culturing organoids varies across tumor types, allowing clinical translation to a fraction of cancer patients (Huang et al., 2015; van de Wetering et al., 2015; Schutte et al., 2017; Pauli et al., 2017; Table 1). We and others experienced that the available starting material, resection versus biopsy, and tumor cellularity are important factors in determining culture success (Yan et al., 2018; Ooft et al., 2019). Those factors vary greatly between tumor types and are clearly a rate-limiting step for the clinical implementation of organoids. Once established, the growth rate of a culture varies between intra- and inter-patient samples as well as tumor types and slow-growing samples could delay timely decision making. It is yet to be determined if this truly represents characteristics of the original tumor and/or if it could create unwanted biases in vitro drug assays that depend on cellular growth. In addition, culturing organoids is tedious and the need for a specific culture medium with a range of growth factors is costly and, depending on the experimental readout, has to be considered carefully. Common supplements to organoid culture medium are, for example, the ALK inhibitor A83-01 and the p38 inhibitor SB202190, which could



interfere with drugs that target the same signaling pathway. Finally, contamination of normal epithelial cells can be detrimental for the purity of organoid cultures and is a problem in prostate and non-small-cell lung cancer (Karthaus et al., 2014; Dijkstra et al., 2020). In addition to methodological challenges, tumor organoids do not capture the TME, including, for example, fibroblasts or immune cells. This has been partly resolved by the establishment of co-cultures, described below, but remains an obstacle, especially in respect to immunotherapy. In order to enable clinical implementation of tumor organoids it will be crucial to overcome current challenges.

## Evaluation of targeted therapies on an individualized level

In the past years many drug screens have been performed on a diverse set of patient-derived organoids in an attempt to analyze drug sensitivity and potentially optimize personalized therapy. Phan et al. reported a high-throughput approach to identify drug sensitivity of four different tumor organoids toward 240 kinase inhibitors and identified organoid specific responses. Their mini-ring method allowed for a rapid readout and showed potential in the discovery of effective drugs for rare cancer types (Phan et al., 2019). Although this automated screening approach has huge potential for drug development and identification, it has to be viewed critically because of a small sample size of different organoid cancer types. A drug screen in a large cohort of 28 breast cancer organoid lines and 6 EGFR/AKT/mTORC inhibitors targeting the HER signaling pathway was performed by Sachs et al. and reported to capture the heterogeneity of breast cancer subtypes. In addition, *in vitro* response of two breast cancer organoid lines to afatinib was in line with *in vivo* xeno-transplant model of the respective organoid lines (Sachs et al., 2018). More drug screens performed on tumor organoids have been reviewed by Kondo and Inoue, where it was concluded that the link between *ex vivo* sensitivity and patient response is essential for correct interpretations and needs further evaluation (Kondo and Inoue, 2019).

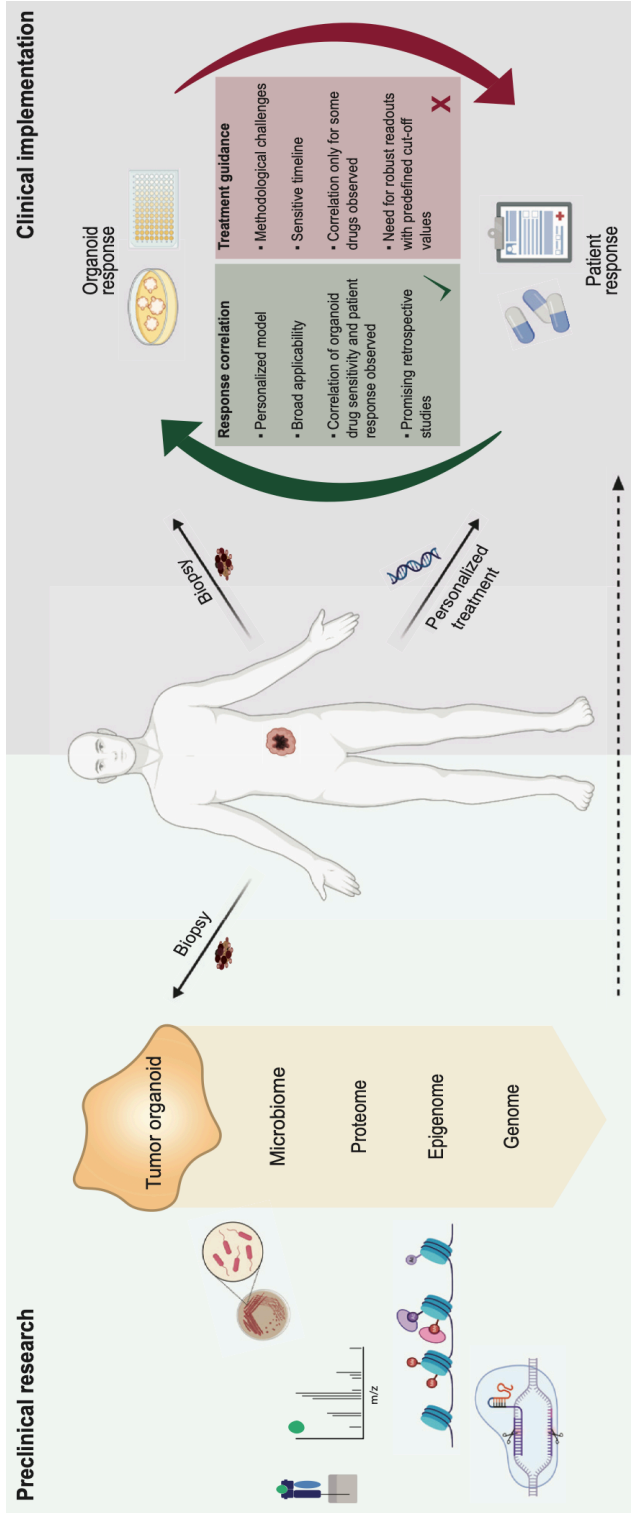


**Figure 2. Tumor organoids in preclinical research and clinical implementation.**

As a versatile model system, organoids can be used to address fundamental research questions in various omic disciplines and deepen our knowledge of cancer biology. Due to their resemblance to the original tumor, organoids offer great opportunities in preclinical research that may shape the future of precision medicine. In the clinical setting, organoids can be used to analyze sensitivity to treatments on an individual level. While retrospective correlations to patient response data are encouraging, the predictive value of tumor organoids in prospective studies is so far accompanied by methodological challenges such as initial culture success. Another major challenge for potential treatment guidance is the development of robust readouts with predefined cutoff values for drug sensitivity to allow the translation of heterogeneous intra- and inter-patient drug responses.

2

Taken together, high-throughput drug screens are feasible on a diverse range of tumor organoid types and are valuable for target identification. Equally important to drug sensitivity screens is a mechanistic understanding that allows for a rational choice of combinatorial treatments. For example, Ponsioen et al. have used KRAS or BRAF mutated colorectal cancer organoids to gain insight into MAPK signaling and showed benefit of combinatorial EGFR inhibition using a quantitative drug response assessment on the single-cell level (Ponsioen et al., 2021). Tumor organoids may provide an opportunity to identify a molecular profile that predicts outcome that would subsequently simplify clinical implementation of such a biomarker. For example, Broutier et al. compared the transcriptome of primary liver cancer organoids with healthy organoids and reported on the discovery of 11 novel genes with potential prognostic value (Broutier et al., 2017). Nonetheless, in order to facilitate clinical implementation and decision making, specific prospective intervention studies with cancer patients are needed. Positive correlation between ex vivo tumor organoid response and patient response have been observed by Vlachogiannis et al. who reported 88% positive predictive value and 100% negative predictive value (Vlachogiannis et al., 2018). This seems promising, but a critical review shows that, for example, response correlation to the EGFR inhibitor cetuximab was conducted on a cohort of only four samples. Besides a fairly small sample size, the organoids derived from a patient with stable disease showed marginal sensitivity to cetuximab compared with the non-responder samples. Although organoid sensitivity correlated to patient response, such small differences might be difficult to translate.

The group of de Witte et al. used patient-derived ovarian cancer organoids in their drug screen and discovered inter-patient heterogeneity in targeted drug responses that correlated partially with the mutational profile. Moreover, intra-patient response heterogeneity in organoids that were established from different cancer lesions or taken at different time points was observed (de Witte et al., 2020). While heterogeneous drug responses may recapitulate the unique biology of each tumor specimen, clinical translation needs robust readouts with predefined thresholds for drug sensitivity. Despite interesting correlative findings, a key limitation of these studies is the absence of such a validated organoid-based decision model on the basis of which a patient will or will not be treated. Revisiting published studies, the

correlation between clinical outcome and in vitro testing seems promising at first glance, but the sample size of most studies is too small for a reliable readout that can be used to implement in clinical practice (Table 1). In our institution, a prospective trial to evaluate feasibility of predefined organoid drug response-based treatment decisions was conducted and faced many hurdles. In the study, eight experimental drugs were included and the required level of in vitro sensitivity was defined at the start of the study and served as an inclusion criterion for patients with colorectal cancer. Expansion of organoids and drug screen readout were on average available within 10 weeks. Besides a lengthy timeline, several other obstacles were identified that could help future studies. The limited success rate of 57% of establishing organoids, the low hit rate for candidate drugs, and the clinical deterioration of patients who exhausted all other treatment opportunities need to be improved (Ooft et al., 2021). Taken together, tumor organoids and their capability to closely capture treatment response are a great asset for drug discovery and mechanistic insights but are still far away from being a predictive tool for clinical decision making (Figure 2). More correlation data, greater sample size, and improved, standardized culture and assay conditions are needed to achieve this goal. A less described application of organoids lies in a better understanding and prediction of treatment-related side effects, which is often observed with targeted therapy. Compared with cell lines, organoids offer the possibility to generate both tumor and normal organoid lines from one patient. This makes it possible to investigate the effect of drugs on normal organoids and potentially help to design targeted agents with higher selectivity. This concept has been extensively tested in cystic fibrosis, where normal colon organoids of patients with cystic fibrosis were used to test drugs that could interfere with chlorine transport channels (Berkers et al., 2019). Potentially, the best treatment could be selected for a patient with cystic fibrosis based on normal epithelial colon organoids. Despite very appealing published results, the organoid assay has not made it to the guidelines highlighting the complexities of implementation and validation of these assays.

**Table 1. Overview of publications with correlation studies of patient and tumor organoid treatment response per cancer type**

Cancer type	Study	Establishing efficiency	Treatment	Sample size	Correlation	Challenges/remarks
Breast cancer (primary)	Sachs et al., 2018	~80%	tamoxifen	2	yes	adapted protocol to achieve long-term culturing
Colorectal cancer (metastasis)	Ooft et al., 2019	~63%	irinotecan	10	yes <sup>b</sup>	
			FOLFIRI	12	yes <sup>c</sup>	
			FOLFOX	10	no	no distinct differences in organoid sensitivity to treatment
	Ooft et al., 2021	~57% <sup>a</sup>	vistusertib, capivasertib	6	no	prospective study; organoid-informed treatment decision did not lead to durable response <sup>d</sup>
Colorectal peritoneal (metastasis)	Narasimhan et al., 2020	~68% <sup>a</sup>	FOLFOX	9	no	low tumor cell content in biopsy key limitation
Esophageal adenocarcinoma	Li et al., 2018	~31%	5-FU, epirubicin and cisplatin	5	(yes)	no distinct differences in organoid sensitivity to treatment
Gastrointestinal (metastasis)	Vlachogiannis et al., 2018	~70%	paclitaxel <sup>e</sup>	3	yes	only non-responder evaluated; inter-patient heterogeneity in organoid drug sensitivity; establishing efficiency
			TAS-102 <sup>f</sup>	4	yes	
			5-FU and cisplatin <sup>g</sup>	2	yes	
			cetuximab <sup>h</sup>	4	yes	
Gastric cancer	Yan et al., 2018	>50%	cisplatin and 5-FU	2	(yes)	low tumor cell content and practical challenges in handling of biopsy; outgrowth of normal cells; only responder evaluated
	Steele et al., 2019		epirubicin, oxaliplatin, and 5-FU	2	one out of two correlated	
Glioblastoma	Jacob et al., 2020	~80% <sup>a</sup>	radiation and temozolomide	5 <sup>k</sup>		based on percentage of Ki67-expressing cells
Mesothelioma	Mazzocchi et al., 2018		displatin and pemetrexed	2	yes	
Neuroendocrine prostate CRPC-NE (metastatic)	Puca et al., 2018	~16%	alsisertib	2	yes	establishing efficiency and overgrowth by normal epithelial cells
Ovarian	Kopper et al., 2019	~65%	platinum/taxane	1	yes	two organoid lines from one patient. Primary tumor (chemotherapy sensitive); ascites (chemotherapy resistant) high growth rate variability of organoids

**Table 1. Continued**

Cancer type	Study	Establishing efficiency	Treatment	Sample size	Correlation	Challenges/remarks
	de Witte et al., 2020	<sup>1,a</sup>	carboplatin and paclitaxel	5	yes <sup>1</sup>	intra- and inter-patient response heterogeneity
Pancreatic cancer	Phan et al., 2019		carboplatin	2	(yes)	only non-responder evaluated
	Tiriac et al., 2018	~75%	5-FU, gemcitabine, nab-paclitaxel, SN-38, or oxaliplatin	9	mostly yes five sensitive out of six longer PFS; two insensitive out of three rapid progressions; one inconsistent; one intermediate	positive correlation determined if organoid was sensitive/insensitive to at least one of the treatments. Large variability in organoid sensitivity depending on treatment and inter-patient heterogeneity
Rectal cancer	Driehuis et al., 2019	~62%	gemcitabine	4	yes	outgrowth efficiency from biopsy ~31%
	Ganesh et al., 2019	~77%	5-FU or FOLFOX	7	yes	
	Yao et al., 2020	~85%	5-FU	80	mostly yes five exceptions to sensitive and 15 exceptions to insensitive	correlation of organoid single treatment to patient response of neoadjuvant chemoradiation; amount of viable tumor cells in starting material key limitation of successful culture
			irinotecan	66	mostly yes seven exceptions to sensitive; seven exceptions to insensitive	

(Yes) = positive correlation reported but only responder/non-responder included in study. PFS, progression-free survival.

<sup>a</sup>Timeline of organoid expansion and drug screen: organoid expansion and drug screen within 10 weeks (Ooft et al., 2021); organoid establishment within 1–2 weeks (Jacob et al., 2020); organoid expansion, genomic and drug profiling within 8 weeks (Narasimhan et al., 2020); organoid expansion and treatment response within 20 days. Tested for one patient sample as a pilot experiment (de Witte et al., 2020).

<sup>b</sup>Correct classification of 80% by leave-one-out cross-validation (LOOCV).

<sup>c</sup>Correct classification of 83% by LOOCV.

<sup>d</sup>Due to advanced stage of disease, clinical deterioration reduced cohort of patients from 19 to 6.

<sup>e</sup>Paclitaxel tested on mGOC.

<sup>f</sup>TAS-102 tested on mCRC.

<sup>g</sup>5-FU and cisplatin tested on mGOC.

<sup>h</sup>Cetuximab tested on mCRC.

<sup>i</sup>Similar to Kopper et al. (2019) due to shared organoid material.

<sup>j</sup>Two out of five patient-derived organoid drug responses statistically significant correlation ( $p < 0.01$ ) to histopathological, biochemical, and radiological patient response. No correlation with 6-month progressive-free survival.

<sup>k</sup>Patient data from five out of seven presented.

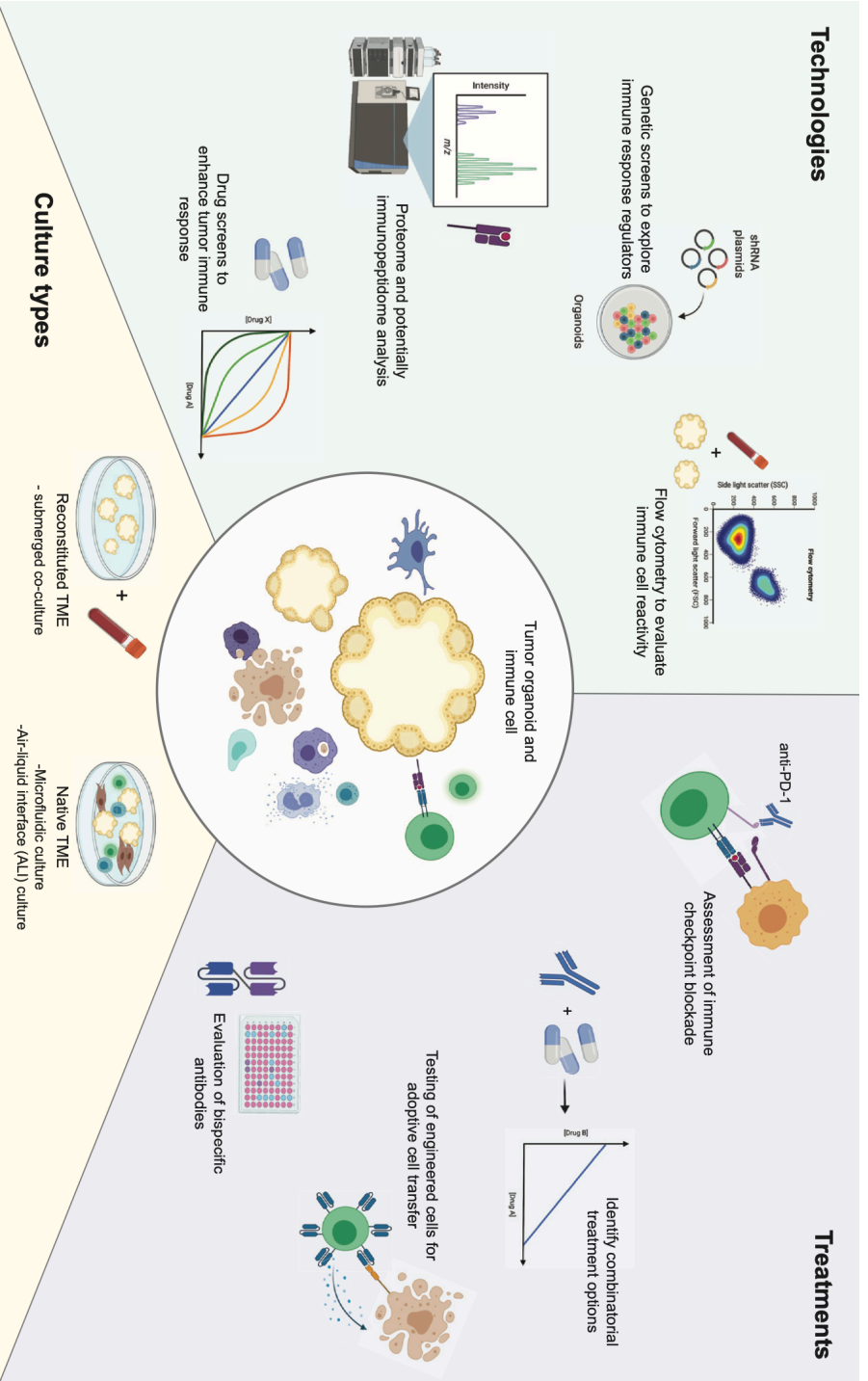
Targeted therapies also have an impact on stromal cells in the TME, which are

2

currently lacking in conventional organoid cultures. This may contribute to large variations in drug screens. Attempts have been made to maintain the TME with the generation of air-liquid interface organoid cultures or the addition of CAFs to organoids to mimic the TME (Li et al., 2016; Neal et al., 2018; Seino et al., 2018; Tsai et al., 2018). By adding another layer of complexity, it might become more difficult to use those systems in large drug screens. Studies to demonstrate the value of this approach are eagerly awaited. New insights on chemotherapy Although chemotherapy has not been considered precision medicine in the conventional sense, there are clear differences in how patients respond to this treatment. So are germline BRCA1/2 mutated metastatic breast cancer more responsive to platinum-based chemotherapy compared with BRCA1/2 wild-type (Isakoff et al., 2015). Clearly a predictive biomarker assay for chemotherapies would be beneficial. Tumor organoids could potentially identify the direct impact of chemotherapy on cancer cells. In order to discriminate responding from non-responding patients and help guide treatment decisions, patient-derived tumor organoids were proposed to capture a personalized tumor response to chemotherapy. In a retrospective study, Tiriak et al. compared chemotherapy response of nine pancreatic tumor organoids with patient response and reported correlation in most cases. Moreover, they identified gene signatures of their tumor organoid cohort that might allow *in vivo* prediction of chemosensitivity (Tiriak et al., 2018). Vlachogiannis et al. observed correlation to paclitaxel treatment in four tumor organoid lines derived from three metastatic gastroesophageal cancer (mGOC) patients. They report highest sensitivity in the sample derived from a responding lesion, whereas the three organoids derived from resistant lesions are less responsive and cluster together (Vlachogiannis et al., 2018). In order to evaluate the predictive value of colorectal cancer (CRC) organoids to the standard-of-care chemotherapy regime, we treated 35 tumor organoid lines with a combination of fluorouracil (5-FU) and oxaliplatin (FO) or irinotecan (FI), or irinotecan alone. The organoid lines were derived from metastatic colorectal cancer (mCRC) patients who had received the respective treatment. We observed a correlation of *ex vivo* treatment response and patient response for irinotecan monotherapy but not for oxaliplatin-based treatment (Ooft et al., 2019). Recently, Narasimhan et al. also reported the absence of a correlation between

sensitivity to FO for CRC organoids derived from peritoneal metastasis and patient response (Narasimhan et al., 2020). A potential link to the immune system was suggested as explanation for discrepancy of ex vivo end patient response, which has been implicated before (Zitvogel et al., 2008). Similar to others, we also observed intra- and inter-patient heterogeneity, which is not surprising due to the uniqueness of a tumor sample but is challenging for the interpretation on an individualized level. The same heterogeneity was stated by de Witte et al. in respect to drug response of ovarian cancer organoids. Besides targeted agents, they also correlated patient response to drug sensitivity of seven ovarian cancer organoids to carboplatin and paclitaxel and showed predictive value for histopathological, biochemical, and radiological responses but not progression-free survival (de Witte et al., 2020). Correlation to patient response was also observed in rectal cancer organoids treated with chemoradiation (Ganesh et al., 2019; Yao et al., 2020). Beside a highly matching response of around 80% accuracy, Yao et al. also observed inter-patient variability in response to chemoradiation treatments and stated low numbers of viable cells in the starting material as one of the major hurdles in their study (Yao et al., 2020). This is a limitation we have experienced ourselves and creates another challenge for the implementation of tumor organoids in the clinical setting. Taken together, most studies that compare tumor organoid with patient response were performed in small patient numbers, and correlations to drug responses were observed in certain tumor types and chemotherapies, but further studies are crucial to understand why this is not the case for others (Table 1). Ultimately, prospective studies are needed with predetermined thresholds for treatment or no treatment of cancer patients. Because stable diseases may already be beneficial to patients, this provides a significant challenge in organoid assay development.





Figure

**3. Overview of possibilities for tumor organoids in immunotherapy research.** In order to analyze tumor organoid and immune cell interaction, different culture types have been established. Co-culture systems (Dijkstra et al., 2018) reconstitute the TME, whereas microfluidic (Jenkins et al., 2018; Aref et al., 2018) or air-liquid interface cultures (Li et al., 2016; Neal et al., 2018) contain the native TME of the original tumor (Yuki et al., 2020). Various technologies can be used in combination with such organoid cultures and allow for optimal experimental readout. Examples are shown that address relevant research questions in the field of immunotherapy and have the potential to lead to insights in immune response mechanisms. Robust cultures and advances in technology are the foundation that enables detailed analysis of relevant immunotherapy treatments. Tumor organoids may help to understand treatment response on an individual level and can be used to evaluate novel immunotherapy approaches.

## Tumor organoids and immunotherapy

In recent years it has become clear that we are just at the start of discovering the full potential of cancer immunotherapy, with immune checkpoint therapy showing exciting successes. A variety of cancer patients, but not all, are benefiting from immunotherapy and in some instances durable responses are observed. There is significant interest to develop rational approaches to improve immunotherapy rather than initiating a multitude of clinical studies. To understand underlying mechanisms of this complex interplay between tumor and immune cells, tumor organoids and autologous immune cells could be a valuable platform. In order to capture tumor immune cell interaction, three main strategies haven been developed: (1) submerged Matrigel culture, (2) microfluidic 3D culture, and (3) air-liquid interface culture (Dijkstra et al., 2018; Jenkins et al. 2018; Aref et al., 2018; Li et al., 2016; Neal et al., 2018). Each strategy captures the TME on a different level and a detailed evaluation of those, including applications for cancer immunotherapies, has been nicely summarized by Yuki et al. (2020). Ideally, those ex vivo culture systems recapitulate responses to immune checkpoint blockade (ICB). Jenkins et al. were able to demonstrate ICB response in murine- and patient-derived organotypic tumor spheroids (Jenkins et al., 2018) and our group has been able to generate tumor reactive CD4<sup>+</sup> and CD8<sup>+</sup> T cells in a co-culture of CRC organoids, peripheral blood mononuclear cells (PBMCs), and anti-PD1 treatment (Dijkstra et al., 2018; Cattaneo et al., 2020). Clonality of the generated reactive T cells has yet to be determined and also if the tumor reactive T cells are derived from a pre-existing reactive clone or if novel reactivity is induced by the co-culture. The latter could be supported by the recent discovery that responses

2

to anti- PD1 treatment can also be attributed to T cells recruited from peripheral blood (Yost et al., 2019). In a clinical study with early stage colon cancer patients treated with neoadjuvant immunotherapy, Chalabi et al. used the same autologous organoid and PBMC co-culture system to potentially correlate ex vivo induced T cell reactivity to patient response (Chalabi et al., 2020). T cell reactivity could only be partly linked to clinical response, which might be explained by the absence of anti-CTLA4 in the co-culture system compared with combinatorial neoadjuvant treatment of anti-PD1 and anti-CTLA4 in the clinical setting or lack of key TME constituents. That said, organoid-immune assays could also provide a rationale for combination treatments of multiple ICBs or for combination with targeted drugs such as MEK or BRAF inhibitors (Ribas et al., 2019). In addition, co-culture systems may be expanded to a multitude of immune cells to analyze tumor response from the adaptive as well as innate immune side.

Due to their versatility tumor organoids have also been used for numerous other immunotherapeutic approaches (Figure 3). For example, Gonzalez-Exposito et al. gained insights into treatment response to cibisatamab, a carcinoembryonic antigen (CEA)-targeting bispecific antibody, by using patient-derived colorectal cancer organoids. They were able to group tumor or- ganoids based on their CEA surface expression and showed that treatment sensitivity/resistance correlated to high/low expression (Gonzalez-Exposito et al., 2019). We see great value in such a concept to use tumor organoids for extensive phenotyping, potential comparison with the original tumor, and evaluation of immune response. This could lead to the identification of immune escape mechanisms and offers a dynamic system to test manipulation thereof. Moreover, tumor organoids may sup- port studies in the field of adoptive cellular therapy (ACT), including the use of tumor infiltrating lymphocytes (TIL), natural killer (NK), and chimeric antigen receptor (CAR)-T cell treatments. An interesting approach is used by Schnalzger et al., who utilized the availability of matching normal and tumor organoids to explore toxicity of CAR-NK cells (Schnalzger et al., 2019). To conclude, tumor organoids are currently used as research tools to determine the effectiveness of various immunotherapeutic approaches, potentially helping to identify immune evasion mechanisms and decipher complex tumor immune cell crosstalk.

## TUMOR ORGANIDS AS A RESEARCH TOOL FOR THE IDENTIFICATION OF NOVEL APPROACHES TO IMPROVE CANCER TREATMENTS

While numerous opportunities in the use of tumor organoids have become apparent, it also highlights the complexity of cancer biology and its translation to the patient setting. Based on the current experiences and challenges, it may be difficult to incorporate tumor organoids in clinical decision making without significant improvements. However, they can greatly contribute to a better understanding of target vulnerability and thereby pave the way to improved treatment. Here, we will review recent applications of tumor organoids in different omic disciplines that can help to advance precision medicine.

### Genetic engineering and genomic screens

Han et al. used a genome-wide CRISPR screen to compare 2D and 3D lung cancer cultures and concluded that screens in 3D spheroids captured features of oncogenes and tumor suppressor genes more accurately than 2D cultures. Moreover, 3D spheroids were able to recapitulate tumor xenografts more closely. As an example, they highlighted CREBBP knockouts, which have a positive growth effect in 3D and xenografts models but a negative growth effect in lung cancer cell lines (Han et al., 2020). Because organoids maintain the genomic profile of the original tumor, it is a relevant model system for genetic analysis (van de Wetering et al., 2015). Many different techniques to genetically engineer organoids have been tested and successfully used for genetic analysis (reviewed in Teriyapirom et al., 2021). The model has shown value in the analysis of oncogenes in tumor evolution by, for example, small hairpin RNA-guided downregulation of tumor suppressor genes or CRISPR-Cas9-mediated gene knockout (Nadauld et al., 2014; Takeda et al., 2019). The availability of normal-tissue-derived organoids has been used to mimic the multi-hit oncogenesis model in colonic organoids or to model brain tumorigenesis using cerebral organoids (Drost et al., 2015; Matano et al., 2015; Bian et al., 2018). Although possibilities for low- to medium-scale CRISPR-Cas screens seem endless, limitations were encountered when performing large-scale or genome-wide screens on tumor organoids. Manual handling of organoids at sufficient numbers, single-guide RNA

2 coverage, and heterogeneous growth rates have been described as challenging (Teriyapirom et al., 2021; Ringel et al., 2020). In 2019, a targeted screen of 192 genes was performed by Planas-Paz et al. and 1 year later Ringel et al. reported the first genome-scale CRISPR screen (Planas- Paz et al., 2019; Ringel et al., 2020). They optimized their readout by single organoid instead of bulk DNA analysis and were able to identify drivers of transforming growth factor (TGF)-beta resistance (Ringel et al., 2020). Those examples illustrate the improvements in genetic engineering in organoids over the past years and will serve as a strong foundation for even more extensive screens. Large-scale screens to address resistance to immunotherapy in co-culture models are underway and results are eagerly awaited.

### Proteomics and the immunopeptidome

Proteomics has a great potential to offer valuable insights for cancer treatment but low resolution, need for large amounts of starting material, the robustness of the system, and low throughput capacity are limiting factors. Advances in sample processing and coverage have been reported and thus make personalized proteomic profiling possible (Hayes et al., 2018; Kelly, 2020). Unlimited starting material and availability of matching healthy/tumor pairs make organoids a great source for characterization of the proteome on an individualized level. In 2017, Cristobal et al. reported proteomic data of human colon organoids and identified common characteristics shared by tumor samples, such as relevant proteins for genomic instability, as well as individual features that, they speculated, could aid precision treatment (Cristobal et al., 2017). Shortly thereafter, Gonneaud et al. reviewed the analysis of organoids by proteomics, summarizing efforts in quantitative proteomics and concluding that organoids could be used for therapeutic evaluation (Gonneaud et al., 2017). The most significant contributions have been made in the field of immunotherapy. For many years the prediction of cancer neoantigens has been in the spotlight of T cell-based immunotherapy and various approaches to identify neoantigens have been pursued. In 2018, Bulik-Sullivan et al. optimized neoantigen identification by using large datasets of HLA peptide mass spectrometry and deep learning to create a model named EDGE. Their model greatly increased the positive

predictive value and could potentially improve neoantigen-targeted immunotherapies (Bulik-Sullivan et al., 2018). It is likely that the generation of new models for neoantigen prediction will further improve with more and bigger datasets. Here tumor organoids could play an important role in the identification of neoepitopes. In order to better understand HLA peptide presentation by tumors, Demmers et al. used tumor organoids to analyze their proteome and HLA ligandome. The single-cell-derived tumor organoids showed large diversity in peptide presentation. Following their analysis, it was suggested to immunize patients with multiple peptides that are conserved in their presentation in tumors with low mutational burden (Demmers et al., 2020). Another proteomic study performed on melanoma correlated immunotherapy response to mitochondrial lipid metabolism, which was subsequently linked to higher antigen presentation and IFN signaling (Harel et al., 2019). Taken together, tumor organoids-based applications of proteomics are becoming more relevant and may advance personalized treatment.

### **The versatility of tumor organoids in emerging technologies**

In the past decade, microbiome research has gained in popularity especially in the field of tumor biology. It has been shown that the microbiome affects tumors on multiple levels and the most significant immune-related discoveries are well summarized by Jain et al. (2021). Tumor organoids have been used as a model system to study inflammatory responses and bacterial interaction. *Helicobacter pylori* was microinjected into gastric organoids and was found to induce the release of interleukin (IL)-8 and other inflammatory cytokines (Bartfeld and Clevers, 2015). In addition, spheroid co-cultures with dendritic cells (DCs) showed increased DC recruitment upon *H. pylori* microinjection (Sebrell et al., 2019). Recently, Pleguezuelos-Manzano et al. observed a distinct mutational signature when CRC organoids were exposed to genotoxic bacteria that carried the pathogenic island pks. This signature was subsequently detected in human colorectal cancer genomes. The findings imply direct involvement of these bacteria in the mutagenic process (Pleguezuelos-Manzano et al., 2020). These are exciting examples of how organoids may contribute to a better understanding of the biological impact of the microbiome.

2

While it is now accepted that the mutational profile of the original tumor is well represented by tumor organoids, recent studies also suggested this for the epigenetic landscape. In 2020, Joshi et al. reported the DNA methylation landscape of 25 cancer organoids and showed that the analyzed organoids retained the epigenome of their cancer type (Joshi et al., 2020). Soon thereafter, Chen et al. identified the menin-MLL inhibitor MI-136 as a potential drug for endometrial cancer using tumor organoids in a small molecule drug screen that specifically targeted epigenetic factors (Chen et al., 2021). This opens up great opportunities to understand not only basic epigenetic mechanisms in tumor biology but also personalized treatment response to epigenetic drugs.

## CONCLUDING REMARKS AND FUTURE PERSPECTIVE

There is a high unmet need for a personalized model system that allows better translation of experimental results to clinical applications. Here, we reviewed the current use of tumor organoids as a tool for translational and basic research. Taken together, it is very tempting to implement organoid technology in clinical practice, but significant issues still have to be resolved. One major bottleneck that needs to be overcome is the low culture success rate. Although it has been shown that this could be partially improved for breast cancer organoids by optimization of the culture medium composition (Sachs et al., 2018), it is unclear to what extent this can be improved for other cancer types and if the success rate can meet the criteria for clinical use. Besides the initial culture success rate, the generation of pure tumor cultures and integration of the TME will also be relevant for clinical implementation. Although we have seen great promise in high-throughput drug screens in organoids, which may help to improve drug development, the use of tumor organoids for treatment decisions on an individual basis remains challenging. Inter- and intra-patient heterogeneity in drug sensitivity hinder direct clinical translation. Consequently, the development of standardized and robust organoid assays with predefined cutoff values for drug response will be essential for clinical use of organoids. To circumvent current limitations of organoid cultures, we highly anticipate the development of novel technologies that are also based on patient-derived samples. Recently, Wang et al.

used their micro-organosphere technology to create a microfluidic platform that overcomes certain organoid limitations and could be used as a high-throughput tool for diagnostic and drug development purposes (Wang et al., 2021). An additional restriction of current available correlation studies is the small sample size. Even though we would like to emphasize the importance of future studies with larger patient cohorts, it is important to realize that the process of taking biopsies from patients is not void of side effects. If only a fraction of the biopsies can be successfully used for a study objective, we need to improve on this prior to exposing patients to these procedures. Having said that, devoted studies to address these issues are highly needed.

While we are still facing many obstacles on the road to organoid-based clinical decision making, we foresee a great potential for the use of organoids in preclinical research and drug discovery. The distinctive biology of organoids and their resemblance to the original tumor are likely to improve our understanding of drug sensitivity, and preclinical findings may become more translatable. As a research tool, organoids also provide unique opportunities for omic disciplines and fundamental research. Beside the traditional focus of genomics and recent accomplishments of genome-wide screens in tumor organoids, the combination of proteomics and tumor organoids in the field of immunotherapy holds great promise.

**Acknowledgements:** Figures were created with BioRender.com.

**Declaration of interests:** The authors declare no competing interests.



## REFERENCES

- Aref, A.R., Campisi, M., Ivanova, E., Portell, A., Larios, D., Piel, B.P., Mathur, N., Zhou, C., Coakley, R.V., Bartels, A., et al. (2018). 3D microfluidic ex vivo culture of organotypic tumor spheroids to model immune checkpoint blockade. *Lab. Chip* 18, 3129–3143.
- Bartfeld, S., and Clevers, H. (2015). Organoids as model for infectious diseases: culture of human and murine stomach organoids and microinjection of *Helicobacter pylori*. *J. Vis. Exp.* 12, 53359. <https://doi.org/10.3791/53359>.
- Berkers, G., van Mourik, P., Vonk, A.M., Kruisselbrink, E., Dekkers, J.F., de Winter-de Groot, K.M., Arets, H.G.M., Marck-van der Wilt, R.E.P., Dijkema, J.S., Vanderschuren, M.M., et al. (2019). Rectal organoids enable personalized treatment of cystic fibrosis. *Cell Rep.* 26, 1701–17008 e3.
- Bian, S., Repic, M., Guo, Z., Kavirayani, A., Burkard, T., Bagley, J.A., Krauditsch, C., and Knoblich, J.A. (2018). Genetically engineered cerebral organoids model brain tumor formation. *Nat. Methods* 15, 631–639.
- Blokzijl, F., de Ligt, J., Jager, M., Sasselli, V., Roerink, S., Sasaki, N., Huch, M., Boymans, S., Kuijk, E., Prins, P., et al. (2016). Tissue-specific mutation accumulation in human adult stem cells during life. *Nature* 538, 260–264.
- Boj, S.F., Hwang, C.I., Baker, L.A., Chio, I., Engle, D.D., Corbo, V., Jager, M., Ponz-Sarvise, M., Tiriác, H., Spector, M.S., et al. (2015). Organoid models of human and mouse ductal pancreatic cancer. *Cell* 160, 324–338.
- Broutier, L., Mastrogiovanni, G., Verstegen, M.M., Francies, H.E., Gavarro, L.M., Bradshaw, C.R., Allen, G.E., Arnes-Benito, R., Sidorova, O., Gaspersz, M.P., et al. (2017). Human primary liver cancer-derived organoid cultures for disease modeling and drug screening. *Nat. Med.* 23, 1424–1435.
- Bulik-Sullivan, B., Busby, J., Palmer, C.D., Davis, M.J., Murphy, T., Clark, A., Busby, M., Duke, F., Yang, A., Young, L., et al. (2018). Deep learning using tumor HLA peptide mass spectrometry datasets improves neoantigen identification. *Nat. Biotechnol.* 37, 55–63. <https://doi.org/10.1038/nbt.4313>.
- Cattaneo, C.M., Dijkstra, K.K., Fanchi, L.F., Kelderman, S., Kaing, S., van Rooij, N., van den Brink, S., Schumacher, T.N., and Voest, E.E. (2020). Tumor organoid-T-cell coculture systems. *Nat. Protoc.* 15, 15–39.
- Chalabi, M., Fanchi, L.F., Dijkstra, K.K., Van den Berg, J.G., Aalbers, A.G., Sikorska, K., Lopez-Yurda, M., Grootsholten, C., Beets, G.L., Snaebjornsson, P., et al. (2020). Neoadjuvant immunotherapy leads to pathological responses in MMR-proficient and MMR-deficient early-stage colon cancers. *Nat. Med.* 26, 566–576.
- Chen, J., Zhao, L., Peng, H., Dai, S., Quan, Y., Wang, M., Wang, J., Bi, Z., Zheng, Y., Zhou, S., et al. (2021). An organoid-based drug screening identified a menin-MLL inhibitor for endometrial cancer through regulating the HIF pathway. *Cancer Gene Ther.* 28, 112–125.
- Clevers, H. (2016). Modeling development and disease with organoids. *Cell* 165, 1586–1597.
- Cobain, E.F., Wu, Y.M., Vats, P., Chugh, R., Worden, F., Smith, D.C., Schuetz, S.M., Zalupski, M.M., Sahai, V., Alva, A., et al. (2021). Assessment of clinical benefit of integrative genomic profiling in advanced solid tumors. *JAMA Oncol.* 7, 525–533.

Cristobal, A., van den Toorn, H.W.P., van de Wetering, M., Clevers, H., Heck, A.J.R., and Mohammed, S. (2017). Personalized proteome profiles of healthy and tumor human colon organoids reveal both individual diversity and basic features of colorectal cancer. *Cell Rep.* 18, 263–274.

de Witte, C.J., Espejo Valle-Inclan, J., Hami, N., Lohmussaar, K., Kopper, O., Vreuls, C.P.H., Jonges, G.N., van Diest, P., Nguyen, L., Clevers, H., et al. (2020). Patient-derived ovarian cancer organoids mimic clinical response and exhibit heterogeneous inter- and inpatient drug responses. *Cell Rep.* 31, 107762.

Demmers, L.C., Kretschmar, K., Van Hoeck, A., Bar-Epraim, Y.E., van den Toorn, H.W.P., Koomen, M., van Son, G., van Gorp, J., Pronk, A., Smakman, N., et al. (2020). Single-cell derived tumor organoids display diversity in HLA class I peptide presentation. *Nat. Commun.* 11, 5338.

Dijkstra, K.K., Cattaneo, C.M., Weeber, F., Chalabi, M., van de Haar, J., Fan- chi, L.F., Slagter, M., van der Velden, D.L., Kaing, S., Kelderman, S., et al. (2018). Generation of tumor-reactive T cells by co-culture of peripheral blood lymphocytes and tumor organoids. *Cell* 174, 1586–1598.e12.

Dijkstra, K.K., Monkhorst, K., Schipper, L.J., Hartemink, K.J., Smit, E.F., Kaing, S., de Groot, R., Wolkers, M.C., Clevers, H., Cuppen, E., and Voest, E.E. (2020). Challenges in establishing pure lung cancer organoids limit their utility for personalized medicine. *Cell Rep.* 31, 107588.

Dijkstra, K.K., van den Berg, J.G., Weeber, F., van de Haar, J., Velds, A., Kaing, S., Peters, D.D.G.C., Eskens, F., de Groot, D.A., Tesselaar, M.E.T., and Voest, E.E. (2021). Patient-derived organoid models of human neuroendocrine carcinoma. *Front Endocrinol. (Lausanne)* 12, 627819.

Driehuis, E., van Hoeck, A., Moore, K., Kolders, S., Francies, H.E., Gulerson- mez, M.C., Stigter, E.C.A., Burgering, B., Geurts, V., Gracanin, A., et al. (2019). Pancreatic cancer organoids recapitulate disease and allow personalized drug screening. *Proc. Natl. Acad. Sci. U S A* 116, 26580–26590.

Drost, J., and Clevers, H. (2018). Organoids in cancer research. *Nat. Rev. Cancer* 18, 407–418.

Drost, J., van Jaarsveld, R.H., Ponsioen, B., Zimmerlin, C., van Boxtel, R., Buijs, A., Sachs, N., Overmeer, R.M., Offerhaus, G.J., Begthel, H., et al. (2015). Sequential cancer mutations in cultured human intestinal stem cells. *Nature* 521, 43–47.

Eiraku, M., and Sasai, Y. (2012). Self-formation of layered neural structures in three-dimensional culture of ES cells. *Curr. Opin. Neurobiol.* 22, 768–777.

Ganesh, K., Wu, C., O'Rourke, K.P., Szeglin, B.C., Zheng, Y., Sauve, C.G., Adileh, M., Wasserman, I., Marco, M.R., Kim, A.S., et al. (2019). A rectal cancer organoid platform to study individual responses to chemoradiation. *Nat. Med.* 25, 1607–1614.

Gao, D., Vela, I., Sboner, A., laquinta, P.J., Karthaus, W.R., Gopalan, A., Downing, C., Wanjala, J.N., Undvall, E.A., Arora, V.K., et al. (2014). Organoid cultures derived from patients with advanced prostate cancer. *Cell* 159, 176–187.

Gonneaud, A., Asselin, C., Boudreau, F., and Boisvert, F.M. (2017). Phenotypic analysis of organoids by proteomics. *Proteomics* 17. <https://doi.org/10.1002/ pmic.201700023>.

Gonzalez-Exposito, R., Semiannikova, M., Griffiths, B., Khan, K., Barber, L.J., Woolston, A., Spain, G., von Loga, K., Challoner, B., Patel, R., et al. (2019). CEA expression heterogeneity and plasticity confer resistance to the CEA-targeting bispecific immunotherapy antibody cibisatamab (CEA-TCB) in patient-derived colorectal cancer organoids. *J. Immunother. Cancer* 7, 101.

Han, K., Pierce, S.E., Li, A., Spees, K., Anderson, G.R., Seoane, J.A., Lo, Y.H., Dubreuil, M., Olivas, M., Kamber, R.A., et al. (2020). CRISPR screens in cancer spheroids identify 3D growth-specific vulnerabilities. *Nature* 580, 136–141.

Harel, M., Ortenberg, R., Varanasi, S.K., Mangalaha, K.C., Mardamshina, M., Markovits, E., Baruch, E.N., Tripple, V., Arama-Chayoth, M., Greenberg, E., et al. (2019). Proteomics of melanoma response to immunotherapy reveals mitochondrial dependence. *Cell* 179, 236–250.e18.

Hayes, S.A., Clarke, S., Pavlakis, N., and Howell, V.M. (2018). The role of proteomics in the age of immunotherapies. *Mamm. Genome* 29, 757–769.

Hill, S.J., Decker, B., Roberts, E.A., Horowitz, N.S., Muto, M.G., Worley, M.J., Jr., Feltmate, C.M., Nucci, M.R., Swisher, E.M., Nguyen, H., et al. (2018). Prediction of DNA repair inhibitor response in short-term patient-derived ovarian cancer organoids. *Cancer Discov.* 8, 1404–1421.

Huang, L., Holtzinger, A., Jagan, I., BeGora, M., Lohse, I., Ngai, N., Nostro, C., Wang, R., Muthuswamy, L.B., Crawford, H.C., et al. (2015). Ductal pancreatic cancer modeling and drug screening using human pluripotent stem cell- and patient-derived tumor organoids. *Nat. Med.* 21, 1364–1371.

Isakoff, S.J., Mayer, E.L., He, L., Traina, T.A., Carey, L.A., Krag, K.J., Rugo, H.S., Liu, M.C., Stearns, V., Come, S.E., et al. (2015). TBCRC009: a multicenter phase II clinical trial of platinum monotherapy with biomarker assessment in metastatic triple-negative breast cancer. *J. Clin. Oncol.* 33, 1902–1909.

Jacob, F., Salinas, R.D., Zhang, D.Y., Nguyen, P.T.T., Schnoll, J.G., Wong, S.Z.H., Thokala, R., Sheikh, S., Saxena, D., Prokop, S., et al. (2020). A patient-derived glioblastoma organoid model and biobank recapitulates inter- and intra-tumoral heterogeneity. *Cell* 180, 188–204.e22.

Jain, T., Sharma, P., Are, A.C., Vickers, S.M., and Dudeja, V. (2021). New insights into the cancer-microbiome-immune axis: decrypting a decade of discoveries. *Front. Immunol.* 12, 622064.

Jenkins, R.W., Aref, A.R., Lizotte, P.H., Ivanova, E., Stinson, S., Zhou, C.W., Bowden, M., Deng, J., Liu, H., Miao, D., et al. (2018). Ex vivo profiling of PD-1 blockade using organotypic tumor spheroids. *Cancer Discov.* 8, 196–215.

Joshi, R., Castro De Moura, M., Pineyro, D., Alvarez-Errico, D., Arribas, C., and Esteller, M. (2020). The DNA methylation landscape of human cancer organoids available at the American Type Culture Collection. *Epigenetics* 15, 1167–1177.

Karthaus, W.R., Iaquinia, P.J., Drost, J., Gracanin, A., van Boxtel, R., Wongvipat, J., Dowling, C.M., Gao, D., Begthel, H., Sachs, N., et al. (2014). Identification of multipotent luminal progenitor cells in human prostate organoid cultures. *Cell* 159, 163–175.

Kawasaki, K., Toshimitsu, K., Matano, M., Fujita, M., Fujii, M., Togasaki, K., Ebisudani, T., Shimokawa, M., Takano, A., Takahashi, S., et al. (2020). An organoid biobank of neuroendocrine neoplasms enables genotype-phenotype mapping. *Cell* 183, 1420–1435.e21.

Kelly, R.T. (2020). Single-cell proteomics: progress and prospects. *Mol. Cell Proteomics* 19, 1739–1748.

Kodack, D.P., Farago, A.F., Dastur, A., Held, M.A., Dardaei, L., Friboulet, L., von Flotow, F., Damon, L.J., Lee, D., Parks, M., et al. (2017). Primary patient-derived cancer cells and their potential for personalized cancer patient care. *Cell Rep.* 21, 3298–3309.

Kondo, J., and Inoue, M. (2019). Application of cancer organoid model for drug screening and personalized therapy. *Cells* 8, 470.

Kopper, O., de Witte, C.J., Lohmussaar, K., Valle-Inclan, J.E., Hami, N., Kester, L., Balgobind, A.V., Korving, J., Proost, N., Begthel, H., et al. (2019). An organoid platform for ovarian cancer captures intra- and interpatient heterogeneity. *Nat. Med.* 25, 838–849.

Kretzschmar, K. (2021). Cancer research using organoid technology. *J. Mol. Med. (Berl)* 99, 501–515.

Lancaster, M.A., and Knoblich, J.A. (2014). Organogenesis in a dish: modeling development and disease using organoid technologies. *Science* 345, 1247125.

Li, X., Francies, H.E., Secrier, M., Perner, J., Miremadi, A., Galeano-Dalmau, N., Barendt, W.J., Letchford, L., Leyden, G.M., Goffin, E.K., et al. (2018). Organoid cultures recapitulate esophageal adenocarcinoma heterogeneity providing a model for clonality studies and precision therapeutics. *Nat. Commun.* 9, 2983.

Li, X., Ootani, A., and Kuo, C. (2016). An air-liquid interface culture system for 3D organoid culture of diverse primary gastrointestinal tissues. *Methods Mol. Biol.* 1422, 33–40.

Matano, M., Date, S., Shimokawa, M., Takano, A., Fujii, M., Ohta, Y., Watanabe, T., Kanai, T., and Sato, T. (2015). Modeling colorectal cancer using CRISPR-Cas9-mediated engineering of human intestinal organoids. *Nat. Med.* 21, 256–262.

Mazzocchi, A.R., Rajan, S.A.P., Votanopoulos, K.I., Hall, A.R., and Skardal, A. (2018). In vitro patient-derived 3D mesothelioma tumor organoids facilitate patient-centric therapeutic screening. *Sci. Rep.* 8, 2886.

Mullenders, J., de Jongh, E., Brousalı, A., Roosen, M., Blom, J.P.A., Begthel, H., Korving, J., Jonges, T., Kranenburg, O., Meijer, R., and Clevers, H.C. (2019). Mouse and human urothelial cancer organoids: a tool for bladder cancer research. *Proc. Natl. Acad. Sci. U S A* 116, 4567–4574.

Nadauld, L.D., Garcia, S., Natsoulis, G., Bell, J.M., Miotke, L., Hopmans, E.S., Xu, H., Pai, R.K., Palm, C., Regan, J.F., et al. (2014). Metastatic tumor evolution and organoid modeling implicate *TGFBR2* as a cancer driver in diffuse gastric cancer. *Genome Biol.* 15, 428.

Narasimhan, V., Wright, J.A., Churchill, M., Wang, T., Rosati, R., Lannagan, T.R.M., Vrbanac, L., Richardson, A.B., Kobayashi, H., Price, T., et al. (2020). Medium-throughput drug screening of patient-derived organoids from colorectal peritoneal metastases to direct personalized therapy. *Clin. Cancer Res.* 26, 3662–3670.

Neal, J.T., Li, X., Zhu, J., Giangarra, V., Grzeskowiak, C.L., Ju, J., Liu, I.H., Chiou, S.H., Salahudeen, A.A., Smith, A.R., et al. (2018). Organoid modeling of the tumor immune microenvironment. *Cell* 175, 1972–1988 e16.

Ooft, S.N., Weeber, F., Dijkstra, K.K., McLean, C.M., Kaing, S., van Werkhoven, E., Schipper, L., Hoes, L., Vis, D.J., van de Haar, J., et al. (2019). Patient-derived organoids can predict response to chemotherapy in metastatic colorectal cancer patients. *Sci. Transl. Med.* 11, eaay2574.

Ooft, S.N., Weeber, F., Schipper, L., Dijkstra, K.K., McLean, C.M., Kaing, S., van de Haar, J., Prevoo, W., van Werkhoven, E., Snaebjornsson, P., et al. (2021). Prospective experimental treatment of colorectal cancer patients based on organoid drug responses. *ESMO Open* 6, 100103.

Pauli, C., Hopkins, B.D., Prandi, D., Shaw, R., Fedrizzi, T., Sboner, A., Sailer, V., Augello, M., Puca, L., Rosati, R., et al. (2017). Personalized in vitro and in vivo cancer models to guide precision medicine. *Cancer Discov.* 7, 462–477.

Phan, N., Hong, J.J., Tofig, B., Mapua, M., Elashoff, D., Moatamed, N.A., Huang, J., Memarzadeh, S., Damoiseaux, R., and Soragni, A. (2019). A simple high-throughput approach identifies actionable drug sensitivities in patient- derived tumor organoids. *Commun. Biol.* 2, 78.

Planas-Paz, L., Sun, T., Pikiolek, M., Cochran, N.R., Bergling, S., Orsini, V., Yang, Z., Sigoillot, F., Jetzer, J., Syed, M., et al. (2019). YAP, but not RSPO- LGR4/5, signaling in biliary epithelial cells promotes a ductular reaction in response to liver injury. *Cell Stem Cell* 25, 39–53 e10.

Pleguezuelos-Manzano, C., Puschhof, J., Rosendahl Huber, A., van Hoeck, A., Wood, H.M., Nomburg, J., Gurjao, C., Manders, F., Dalmaso, G., Stege, P.B., et al. (2020). Mutational signature in colorectal cancer caused by genotoxic pks(+) *E. coli*. *Nature* 580, 269–273.

Ponsioen, B., Post, J.B., Buissant des Amorie, J.R., Laskaris, D., van Ineveld, R.L., Kersten, S., Bertotti, A., Sassi, F., Sipieter, F., Cappe, B., et al. (2021). Quantifying single-cell ERK dynamics in colorectal cancer organoids reveals EGFR as an amplifier of oncogenic MAPK pathway signalling. *Nat. Cell Biol* 23, 377–390.

Puca, L., Bareja, R., Prandi, D., Shaw, R., Benelli, M., Karthaus, W.R., Hess, J., Sigouros, M., Donoghue, A., Kossai, M., et al. (2018). Patient derived organo- ids to model rare prostate cancer phenotypes. *Nat. Commun.* 9, 2404.

Ribas, A., Lawrence, D., Atkinson, V., Agarwal, S., Miller, W.H., Jr., Carlino, M.S., Fisher, R., Long, G.V., Hodi, F.S., Tsoi, J., et al. (2019). Combined BRAF and MEK inhibition with PD-1 blockade immunotherapy in BRAF-mutant melanoma. *Nat. Med.* 25, 936–940.

Ringel, T., Frey, N., Ringnalda, F., Janjuha, S., Cherkaoui, S., Butz, S., Srivatsa, S., Pirkl, M., Russo, G., Villiger, L., et al. (2020). Genome-scale CRISPR screening in human intestinal organoids identifies drivers of TGF-beta resis- tance. *Cell Stem Cell* 26, 431–440 e8.

Sachs, N., and Clevers, H. (2014). Organoid cultures for the analysis of cancer phenotypes. *Curr. Opin. Genet. Dev.* 24, 68–73.

Sachs, N., de Ligt, J., Kopper, O., Gogola, E., Bounova, G., Weeber, F., Balgo- bind, A.V., Wind, K., Gracanin, A., Begthel, H., et al. (2018). A living biobank of breast cancer organoids captures disease heterogeneity. *Cell* 172, 373– 386 e10.

Sachs, N., Papaspyropoulos, A., Zomer-van Ommen, D.D., Heo, I., Bottinger, L., Klay, D., Weeber, F., Huelsz-Prince, G., Iakobachvili, N., Amatngalim, G.D., et al. (2019). Long-term expanding human airway organoids for disease modeling. *EMBO J.* 38, e100300.

Sato, T., Stange, D.E., Ferrante, M., Vries, R.G., Van Es, J.H., Van den Brink, S., Van Houdt, W.J., Pronk, A., Van Gorp, J., Siersema, P.D., and Clevers, H. (2011). Long-term expansion of epithelial organoids from human colon, ad- enoma, adenocarcinoma, and Barrett's epithelium. *Gastroenterology* 141, 1762– 1772.

Schnalzger, T.E., de Groot, M.H., Zhang, C., Mosa, M.H., Michels, B.E., Roder, J., Darvishi, T., Wels, W.S., and Farin, H.F. (2019). 3D model for CAR-mediated cytotoxicity using patient-derived colorectal cancer organoids. *EMBO J.* 38, e100928.

Schutte, M., Risch, T., Abdavi-Azar, N., Boehnke, K., Schumacher, D., Keil, M., Yildiriman, R., Jandrasits, C., Borodina, T., Amstislavskiy, V., et al. (2017). Mo- lecular dissection of colorectal cancer in pre-clinical models identifies bio- markers predicting sensitivity to EGFR inhibitors. *Nat. Commun.* 8, 14262.

Sebrell, T.A., Hashimi, M., Sidar, B., Wilkinson, R.A., Kirpotina, L., Quinn, M.T., Malkoc, Z., Taylor, P.J., Wilking, J.N., and Bimczok, D. (2019). A novel gastric spheroid co-culture model reveals chemokine-dependent recruitment of human dendritic cells to the gastric epithelium. *Cell Mol. Gastroenterol. Hepatol.* 8, 157–171 e3.

Seino, T., Kawasaki, S., Shimokawa, M., Tamagawa, H., Toshimitsu, K., Fujii, M., Ohta, Y., Matano, M., Nanki, K., Kawasaki, K., et al. (2018). Human pancreatic tumor organoids reveal loss of stem cell niche factor dependence during disease progression. *Cell Stem Cell* 22, 454–467 e6.

Steele, N.G., Chakrabarti, J., Wang, J., Biesiada, J., Holokai, L., Chang, J., Nowacki, L.M., Hawkins, J., Mahe, M., Sundaram, N., et al. (2019). An organoid-based preclinical model of human gastric cancer. *Cell Mol. Gastroenterol. Hepatol.* 7, 161–184.

Takeda, H., Kataoka, S., Nakayama, M., Ali, M.A.E., Oshima, H., Yamamoto, D., Park, J.W., Takegami, Y., An, T., Jenkins, N.A., et al. (2019). CRISPR-Cas9-mediated gene knockout in intestinal tumor organoids provides functional validation for colorectal cancer driver genes. *Proc. Natl. Acad. Sci. U S A* 116, 15635–15644.

Teriyapirom, I., Batista-Rocha, A.S., and Koo, B.K. (2021). Genetic engineering in organoids. *J. Mol. Med. (Berl)* 99, 555–568.

Tiriac, H., Belleau, P., Engle, D.D., Plenker, D., Deschenes, A., Somerville, T.D.D., Froeling, F.E.M., Burkhart, R.A., Denroche, R.E., Jang, G.H., et al. (2018). Organoid profiling identifies common responders to chemotherapy in pancreatic cancer. *Cancer Discov.* 8, 1112–1129.

Tsai, S., McOlash, L., Palen, K., Johnson, B., Duris, C., Yang, Q., Dwinell, M.B., Hunt, B., Evans, D.B., Gershon, J., and James, M.A. (2018). Development of primary human pancreatic cancer organoids, matched stromal and immune cells and 3D tumor microenvironment models. *BMC Cancer* 18, 335.

Turco, M.Y., Gardner, L., Hughes, J., Cindrova-Davies, T., Gomez, M.J., Farrell, L., Hollinshead, M., Marsh, S.G.E., Brosens, J.J., Critchley, H.O., et al. (2017). Long-term, hormone-responsive organoid cultures of human endometrium in a chemically defined medium. *Nat. Cell Biol* 19, 568–577.

van de Wetering, M., Francies, H.E., Francis, J.M., Bounova, G., Iorio, F., Pronk, A., van Houdt, W., van Gorp, J., Taylor-Weiner, A., Kester, L., et al. (2015). Prospective derivation of a living organoid biobank of colorectal cancer patients. *Cell* 161, 933–945.

Vlachogiannis, G., Hedayat, S., Vatsiou, A., Jamin, Y., Fernandez-Mateos, J., Khan, K., Lampis, A., Eason, K., Huntingford, I., Burke, R., et al. (2018). Patient-derived organoids model treatment response of metastatic gastrointestinal cancers. *Science* 359, 920–926.

Wang, Z., Cortes-Sanchez, E., Yang, C.-H., Nelson, D., Delubac, D., Hsu, S.D., Welm, A., and Shen, X. (2021). Micro-organospheres: an automated patient-derived model platform for rapid drug screening of breast cancer. *J. Clin. Oncol.* 39, e12628.

Weeber, F., van de Wetering, M., Hoogstraat, M., Dijkstra, K.K., Krijgsman, O., Kuilman, T., Gadellaa-van Hooijdonk, C.G., van der Velden, D.L., Peeper, D.S., Cuppen, E.P., et al. (2015). Preserved genetic diversity in organoids cultured from biopsies of human colorectal cancer metastases. *Proc. Natl. Acad. Sci. U S A* 112, 13308–13311.

Wong, C.H., Siah, K.W., and Lo, A.W. (2019). Estimation of clinical trial success rates and related parameters. *Biostatistics* 20, 273–286.

Yan, H.H.N., Siu, H.C., Law, S., Ho, S.L., Yue, S.S.K., Tsui, W.Y., Chan, D., Chan, A.S., Ma, S., Lam, K.O., et al. (2018). A comprehensive human gastric cancer organoid biobank captures tumor subtype heterogeneity and enables therapeutic screening. *Cell Stem Cell* 23, 882–897 e11.

Yao, Y., Xu, X., Yang, L., Zhu, J., Wan, J., Shen, L., Xia, F., Fu, G., Deng, Y., Pan, M., et al. (2020). Patient-derived organoids predict chemoradiation responses of locally advanced rectal cancer. *Cell Stem Cell* 26, 17–26 e6.

Yost, K.E., Satpathy, A.T., Wells, D.K., Qi, Y., Wang, C., Kageyama, R., McNamara, K.L., Granja, J.M., Sarin, K.Y., Brown, R.A., et al. (2019). Clonal replacement of tumor-specific T cells following PD-1 blockade. *Nat. Med.* 25, 1251–1259.

Yuki, K., Cheng, N., Nakano, M., and Kuo, C.J. (2020). Organoid models of tumor immunology. *Trends Immunol.* 41, 652–664.

Zitvogel, L., Apetoh, L., Ghiringhelli, F., and Kroemer, G. (2008). Immunological aspects of cancer chemotherapy. *Nat. Rev. Immunol.* 8, 59–73.





The important distinction is not between theists and naturalists; it's about people who care enough about the universe to make a good-faith effort to understand it, and those who fit it into a predetermined box or simply take it for granted. The universe is much bigger than you or me, and the quest to figure it out united people with a spectrum of substantive beliefs. It's us against the mysteries of the universe; if we care about understanding, we're on the same side.

Sean Carroll, *The Big Picture: On the Origins of Life, Meaning, and the Universe Itself*

# Whole genome CRISPR screen of patient-derived tumor organoids to identify mediators of autologous CD8<sup>+</sup> T cell killing

3

Gabriele Picco<sup>1,\*</sup>, **Vivien Veninga**<sup>2,3,\*</sup>, Sara F. Viera<sup>1</sup>, Sarah Consonni<sup>1</sup>, Chiara M. Cattaneo<sup>4</sup>, Alex Wattson<sup>1</sup>, Samantha Walker<sup>1</sup>, Emre Karakoc<sup>1</sup>, Matthew A. Coelho<sup>1</sup>, Thomas Battaglia<sup>2,3</sup>, Iris Mimpfen<sup>2,3</sup>, Allard W.J. van Renterghem<sup>2,3</sup>, Leon Potgeter<sup>5</sup>, Krijn Dijkstra<sup>2,3</sup>, Xuhui Ma<sup>2,3</sup>, Shriram Bhosle<sup>1</sup>, Mathew J. Garnett<sup>1,#</sup>, Emile E. Voest<sup>2,3,#</sup>

<sup>1</sup>Wellcome Sanger Institute, Wellcome Genome Campus, Cambridge, UK

<sup>2</sup>Department of Molecular Oncology and Immunology, Netherlands Cancer Institute, Amsterdam, The Netherlands.

<sup>3</sup>Oncode Institute, Utrecht, The Netherlands.

<sup>4</sup>Experimental Hematology Unit, IRCCS Ospedale San Raffaele Scientific Institute, Milan, Italy

<sup>5</sup>Department of Oncology UNIL-CHUV, Ludwig Institute for Cancer Research Lausanne, Lausanne University Hospital and University of Lausanne, Lausanne, Switzerland

\*These authors contributed equally: Vivien Veninga, Gabriele de Picco

#These authors contributed equally: Mathew Garnett, Emile E. Voest



## ABSTRACT

T cell-mediated killing of cancer cells largely determines the success of immune checkpoint blockade (ICB) treatment. Hence, understanding a cancer cell's susceptibility to the cytotoxic function of CD8<sup>+</sup> T cells is fundamental to improve current treatment options further or developing novel cancer immunotherapies. While many screens on T cells and cancer cells have been performed to advance our understanding, utilizing a fully autologous patient-derived model system has remained challenging. Here, we present whole-genome CRISPR Cas9 in vitro screens on patient-derived colorectal cancer organoids utilizing tumor-reactive autologous CD8<sup>+</sup> T cells. As the importance of IFN $\gamma$  in tumor killing is well described, we additionally performed IFN $\gamma$  sensitivity screens using the same patient-derived tumor organoids. We confirmed that alterations in the IFN $\gamma$  signaling pathway act as a conserved escape mechanism across tumor organoid samples. Moreover, from these screens we discovered proteoglycan synthesis related genes to be associated with modulation of T cell killing and identified galactosyltransferase B4GALT7 as a novel resistance mediating gene. Overall, our study confirms common dominators of tumor escape mechanisms, highlights personalized regulators of a tumor's susceptibility to T cell cytotoxicity and elaborates on the feasibility of fully autologous whole genome CRISPR Cas9 screens.

## INTRODUCTION

The majority of cancer patients unfortunately does not respond to immunotherapies<sup>1</sup>. Because T cells are fundamental to a successful immune response of treatment approaches such as immune checkpoint blockade (ICB)<sup>2</sup>, an advanced understanding of the interaction between T cells and cancer cells and identification of underlying sensitizing and resistance mediating mechanisms to T cell cytotoxicity can improve current immunotherapies. As a patient's T cell repertoire and the genomic make up of their tumor are unique entities, one challenge is to identify T cell tumor interactions that are shared or distinct across tumors and contribute to a patient's T cell tumor response.

3 Tumor organoids offer an opportunity to analyze autologous immune responses on a personalized level<sup>3</sup>. They reflect a patient's tumors geno- and phenotype, have a high establishment rate from colorectal cancer and are susceptible to genetic editing. This makes the model system a perfect candidate to capture personalized tumor responses to T cell pressure<sup>3,4,5</sup>. The model system exceeds conventional cancer cell lines in their recapitulation of human physiology and ability to represent individual tumors, while offering easier handling and laboratory requirements than in vivo models<sup>6</sup>. Nevertheless, organoid culturing includes growth in an extracellular matrix (ECM) and specialized medium supplemented with growth factors. While less relevant for small scale experiments, this makes large scale efforts challenging. Such challenges have hampered whole genome CRISPR screens using patient-derived tumor organoids (PDTOs) and only recently led to genome-scale screening efforts<sup>7,8</sup>, whereas whole genome screens are routinely performed in cell lines<sup>9,10,11</sup>. Recent technological improvements, such as a reduced CRISPR Cas9 library size or suspension techniques that reduce costs by minimizing use of ECM and easier handling, facilitate the feasibility of whole genome screen in tumor organoids<sup>12,13</sup>.

On the other side, large-scale CRISPR screens in (primary) T cells have been successfully performed and significantly improved our understanding on regulators of immune function and drivers of T cell exhaustion<sup>14,15,16</sup>. While most large-scale genome screens may integrate primary T cells or tumor organoids, a fully autologous approach has, to our knowledge, not been performed. We hypothesized that this

would allow the identification of shared and tumor specific regulators of T cell mediated killing that can be further explored as immunotherapy targets.

Here, we report on whole genome screens using two mismatch repair deficient colorectal cancer (MMR-d CRC) tumor organoid lines and autologous tumor reactive CD8<sup>+</sup> T cells. To systematically characterize shared and personalized regulators of T cell cytotoxicity, we perform T cell killing screens and IFN $\gamma$  cytokine screens, as well as a TNF $\alpha$  screen for one tumor organoid T cell pair. Both cytokines are secreted by immune cells and can cause cancer cell death<sup>17</sup>. Defects of TNF and IFN $\gamma$  sensing pathways have been associated with tumor evasion and resistance mechanisms to ICB<sup>18,19,20,21</sup>. Identifying hits of cytokine and T cell killing screens allowed us to identify IFN $\gamma$  and TNF $\alpha$  dependent and independent regulators of susceptibility to T cell antitumor activity. Our data indicates that tumor killing is largely mediated by IFN $\gamma$  and identifies galactosyltransferase B4GALT7 as novel resistance mediator in one of the two model systems. Furthermore, we elaborate on the encountered challenges and technical improvements that allowed for a fully autologous whole genome screen.

## RESULTS

Establishment of an autologous model system and media optimization.

To perform a whole genome CRISPR Cas9 screen in a fully autologous model system, we made use of two established mismatch repair deficient colorectal cancer (MMR-d CRC) organoid and peripheral mononuclear cell (PBMC) pairs (Fig. 1a, Extended Data Fig. 1a). Cytotoxicity of autologous PBMCs in co-culture with tumor organoids, CRC-09 and CRC-12, has previously been described<sup>22</sup>. After generation of tumor-reactive T cells during a 2-week co-culture, T cells were expanded to allow for whole genome screening efforts. Reactivity towards tumor organoids after expansion was confirmed by CD137<sup>+</sup> reactivity assay before further use of the T cell product for evaluation of killing capacity and screens (Fig. 1a). Both tumor organoids, CRC-09 and CRC-12, expressed baseline level of major histocompatibility complex (MHC) class I, which was increased upon IFN $\gamma$  pre-stimulation. MHC class II was not expressed and immune checkpoint inhibitor PD-L1 only after stimulation with IFN $\gamma$  (Fig. 1b). CD8<sup>+</sup> T cells of both model systems showed increased CD137<sup>+</sup> expression when co-cultured with their respective tumor organoids for 24h. Especially CRC-09 exhibits a strong T cell response with around 50% CD137<sup>+</sup> CD8<sup>+</sup> T cells compared to 18% CD137<sup>+</sup> of CRC-12 (Fig. 1c, d). After the generation of sufficient autologous tumor reactive T cells, tumor organoids were transduced with a Cas9 construct and stable expression was in > 85% of cells confirmed (Extended Data Fig. 1c). During tumor organoid and PBMC co-cultures as well as for reactivity assays, T cell culture medium was used to ensure high viability of T cells<sup>22,23</sup>. Tumor organoids, however, generally suffer in T cell culture medium which impacts their viability. We indeed observed reduced viability of CRC-09 after 72h culturing in T cell culture medium compared to organoid medium (Extended Data Fig. 1d). Complete CRC organoid medium is supplemented with nicotinamide to facilitate long term growth of organoid cultures, however, as previously described, this can negatively affect immune cell tumor responses<sup>24</sup>. Depleting nicotinamide from complete CRC organoid medium only mildly interfered with tumor organoid growth over the time course of 3 days and improved their viability over one week when compared to culturing in T cell medium

(Extended Data Fig. 1e). Importantly, organoid medium without nicotinamide did not interfere with T cell killing capacity of CRC-09 (Extended Data Fig. 1f). Therefore, all screens were performed with organoid medium depleted of nicotinamide to ensure viability of tumor organoids and optimal T cell function.

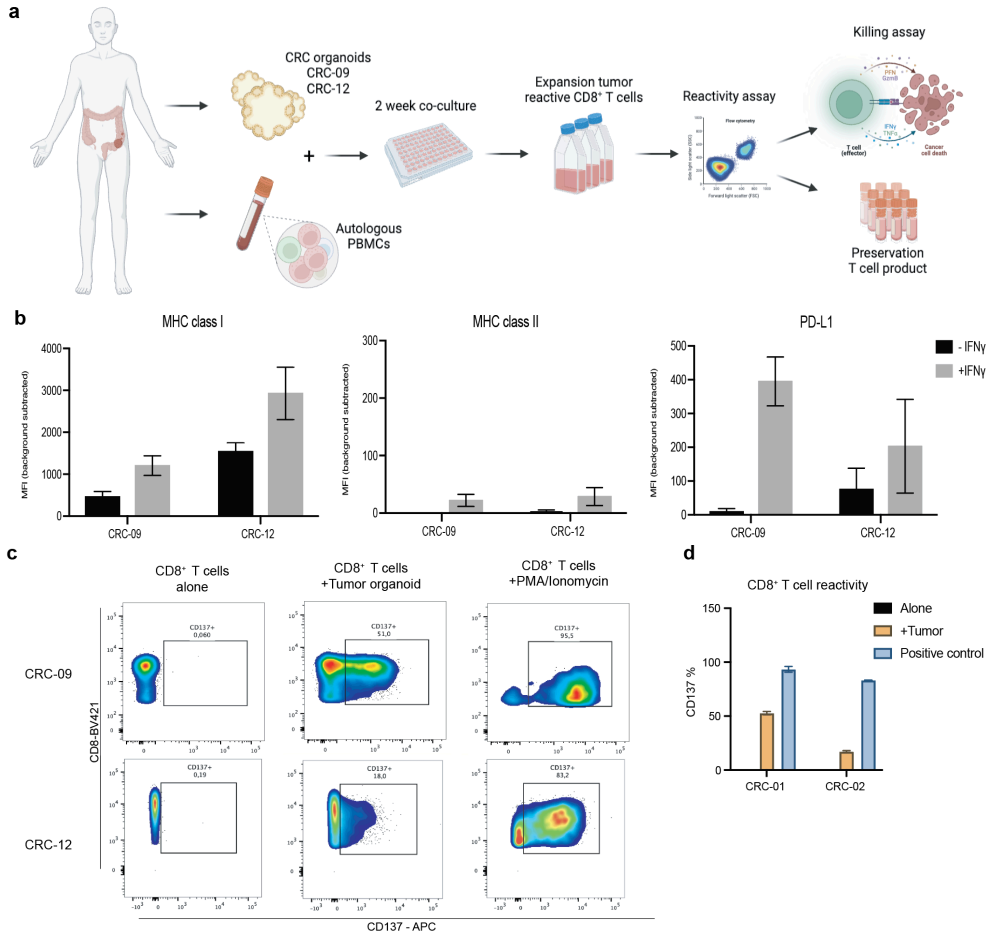


Figure 1: Generation of autologous tumor reactive T cells.

**a.** Graphical overview of the production of autologous tumor reactive T cells from PBMCs and CRC organoids. CRC-09 and CRC-12 tumor organoids and PBMCs were co-culture for 2 weeks and expanded before tumor reactivity of T cells was evaluated. **b.** Bar graphs indicating surface expression of MHC class I/II and PD-L1 of CRC-09 and CRC-12 at baseline or after 24h IFN $\gamma$  pre-stimulation. Error bars indicate SEM of at least three independent experiments (n=3). **c.** Representative flow cytometry dot plots of CD8<sup>+</sup> T cells unstimulated (alone), stimulated with tumor organoids (+tumor organoid) and positive control (+PMA/Ionomycin) for CRC-09 (top) and CRC-12 (bottom) indicating CD137 expression. **d.** Bar graph of CD8<sup>+</sup> T cell reactivity unstimulated



(alone, black), after stimulation with tumor organoids (+tumor, yellow) and positive control (+PMA/ Ionomycin, blue). Error bars indicate SEM of two independent experiments (n=2).

Whole genome screen in tumor organoids confirms JAK1/2 and IFN $\gamma$ R1/2 as shared resistance genes to IFN $\gamma$  stimulation.

We set up two independent screens to better characterize IFN $\gamma$ -dependent and independent regulators of T cell killing. For CRC-09 we additionally performed a whole-genome cytokine screen using TNF $\alpha$  to analyze the response thereof (Fig. 2a). Tumor organoids were transduced with a genome-wide CRISPR knockout pooled library at 200x coverage with two single-guide RNAs (sgRNAs) per gene (MinLibCas9<sup>13</sup>). Library coverage was assessed by each sample's total read counts, zero read counts, and read count distribution. Read count distribution indicates higher quality coverage of CRC-09 than CRC-12 but was overall deemed sufficient (Extended Data Fig. 2a, b, c). Tumor organoids were then stimulated with IFN $\gamma$ , TNF $\alpha$  or left unstimulated as negative control for 9-10 days. Biological replicates before and after stimulation of all conditions were sequenced, analyzed and (Fig. 2a). Clustering of all samples confirmed good correlation (Extended Data Fig. 2d). Enriched hits in CRC-09 or CRC-12 tumor organoids after cytokine stimulation, compared to control samples, indicated resistance genes to IFN $\gamma$  or TNF $\alpha$ , whereas depleted hits indicated sensitizing genes (Fig. 2b, c; Extended Data Fig. 3b). CRC-09 TNF $\alpha$  screen identified TNF receptor superfamily member 1a (TNFRSF1A) as top hit (Extended Data Fig. 3b). Based on the results of the IFN $\gamma$  screens of CRC-09 and CRC-12, JAK1, JAK2, IFN $\gamma$ R1 and IFN $\gamma$ R2 were identified as shared resistance hits of both screens (Extended Data Fig. 3a). Overall, whole-genome cytokine screens of tumor organoids were successful and depicted known regulators of IFN $\gamma$  and TNF $\alpha$  resistance<sup>17,32</sup>.

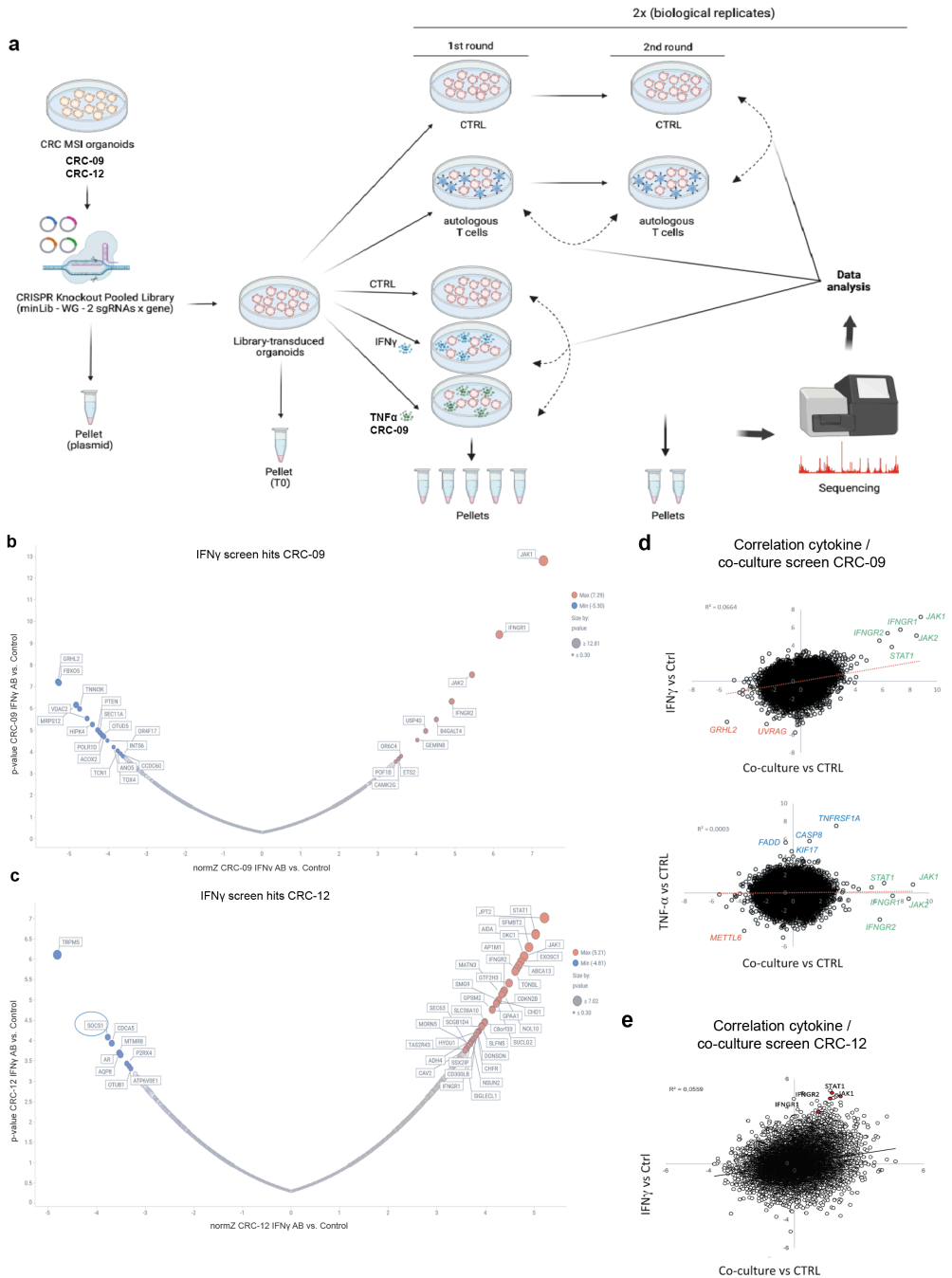


Figure 2: Whole genome screen set up and cytokine screens. **a**. Graphical overview of experimental set up. Starting with CRISPR Cas9 pooled library introduction of MMR-d CRC tumor organoids, CRC-09 and CRC-12. Bottom row indicated pellets taken for sequencing of all conditions. Library-transduced organoids were further



used for i. T cell co-culture screens (top) and ii. cytokine screens (bottom). Co-culture screens with autologous T cells were performed in two rounds of T cell stimulation. All samples were sequenced and analyzed. b. Plot indicating significantly enriched (red) or depleted (blue) hits for IFN $\gamma$  screen of CRC-09 comparing two biological replicates with unstimulated control sample. c. Plot indicating significantly enriched (red) or depleted (blue) hits for IFN $\gamma$  screen of CRC-12 comparing two biological replicates with unstimulated control sample. d. Correlation plot of CRC-09 cytokine screen with IFN $\gamma$  (top) or TNF $\alpha$  (bottom) and T cell co-culture screen showing overlay of identified resistance (green), neutral (blue) and sensitizing (red) hits. e. Correlation plot of CRC-12 cytokine screen with IFN $\gamma$  and T cell co-culture screen showing overlay of identified resistance (red, labelled) hits.

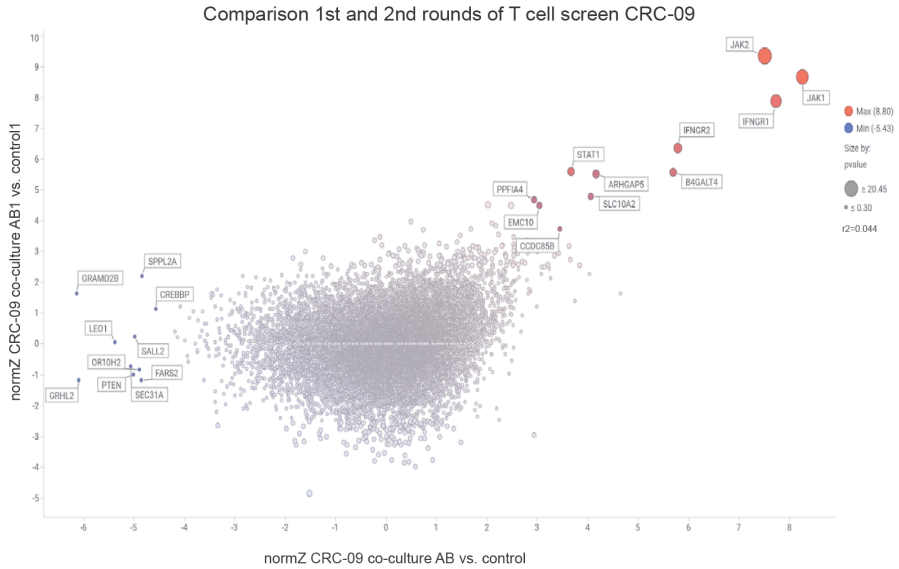
### Fully autologous model system reveals potential IFN $\gamma$ dependent and independent resistance mediators and sensitizers to T cell killing.

3

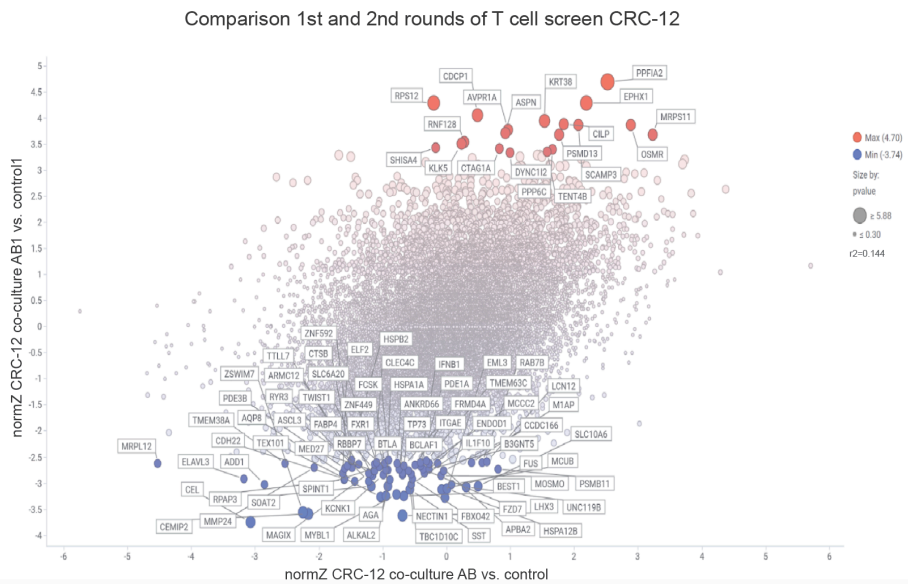
Next, we performed whole genome knockout screens in an autologous setting using expanded tumor reactive CD8<sup>+</sup> T cells and MMR-d CRC organoids. To facilitate better hit selection, tumor organoids were exposed to T cells in two rounds (Fig. 2a). For the killing assay we aimed at 50% killing of tumor organoids to enable us to identify genes associated to resistance or sensitization. Thus, CRC-09 was co-cultured with T cells at an optimized target:effector ratio of 1:1 and CRC-12 at 1:4 in accordance with higher tumor reactivity of CRC-09 (Fig. 1c, d). After first and second T cell exposure CRC-09 showed strong correlation, whereas CRC-12 samples less strongly correlated (Fig. 3a, b). Biological replicates (termed A and B) correlated well for both screens (Extended Data Fig. 2e, f). For CRC-09 and CRC-12 particularly positively selected hits highly correlated in both replicates. Negatively selected hits displayed discordant correlation (Extended Data Fig. 2e, f). Next, we compared our results of the T cell screens with cytokine screens of each sample identify IFN $\gamma$  dependent and independent mechanisms. For the screen of CRC-09 tumor organoids, gene knockouts conferring resistance to T cell killing equally conferred resistance to IFN $\gamma$ , but not to TNF $\alpha$  (Fig. 2d). Indicating killing of CRC-09 tumor organoids by autologous CD8<sup>+</sup> T cells seemed to be largely mediated by IFN $\gamma$  secretion. CRC-12 co-culture screens showed some overlap in resistance to IFN $\gamma$  signaling related hits, however less strong than CRC-09 (Fig. 2e). To identify shared resistance and sensitizing hits, we compared both co-culture T cell screens with each other (Extended Data Fig. 3c). Little overlap of significantly enriched or depleted hits, besides hits associated to IFN $\gamma$

mediated killing, was observed. Suggesting that T cell killing is dependent on IFN $\gamma$  cytotoxicity in both screens, whereas other mediators may be unique to each model system. Based on better T cell availability and enhanced killing, we decided to focus on results of CRC-09 screen to identify IFN $\gamma$  independent regulators of T cell killing. Consequently, for hit selection we excluded significantly enriched or depleted hits that were selected as hits of the IFN $\gamma$  screen. Furthermore, we compared our hits to published data of in vivo and in vitro screens on immune evasion to preferentially include hits reported in other screens<sup>25,26</sup>. Pathway enrichment analysis indicated proteoglycan processes to be associated of top hits (Extended Data Fig. 3d). After evaluation based on enrichment significance, correlation to other screens and association to proteoglycan synthesis, we selected 9 putative resistance genes, including B2M and JAK1 as controls, and 11 putative sensitizer genes to validate their proposed resistance or sensitizer effect (Fig. 3c).  $\gamma$

**a**



**b**



**c**

Gene ID of Sensitizer	Gene ID of Resistor
B3GALT4	B3GALT6
BRD4	B3GALT7
CD40LG	ITGA4
KLK1	NDST2
LGALS12	PRG4
SIGLEC6	TNFRSF17
TARM1	UBE2Q1
TNFRSF18	B2M (control)
GRHL2	JAK1 (control)
PTEN	
PTRP	

Figure 3: Sensitizer and resistance hit selection of whole genome autologous T cell killing screen.

**a.** Plot showing comparison of first and second round enriched or depleted hits of T cell screen of CRC-09. Correlated data is normalized to control samples. Overlapping resistance (red) and sensitizer (blue) hits are indicated by significance according to their diameter. **b.** Plot showing comparison of first and second round enriched or depleted hits of T cell screen of CRC12. Correlated data is normalized to control samples. Overlapping resistance (red) and sensitizer (blue) hits are indicated by significance according to their diameter. **c.** Top hit selection of CRC-09 T cell screen. Tables show putative sensitizing (left) and resistance (right) hits which may act independent of IFN $\gamma$ .

### B4GALT7 identified as novel resistance mediator of T cell killing for CRC-09

To evaluate putative sensitizer and resistance genes, two sgRNAs per hit were selected for CRISPR Cas9 knockout of CRC-09 mCherry<sup>+</sup> tumor organoids. T cell killing was performed at a 1:1 target:effector ratio for resistance hits to achieve 50% killing and at 1:3 for sensitizers. All 9 knockouts of putative resistance genes and 11 putative sensitizer genes were assessed for their interference with CD8<sup>+</sup> T cell cytotoxicity by imaging for mCherry and flow cytometry analysis. All resistance controls, B2M, JAK1 and MHC class I blocking antibody, lead to resistance to T cell killing. While putative sensitizing gene knockouts did not change viability upon T cell exposure, especially one putative resistance genes increased tumor organoid viability (Fig. 4a). B4GALT7 knockout strongly increased viability of CRC-09 tumor organoids normalized to control confirming its role as a mediator of resistance to T cell killing in this model system (Fig. 4b).

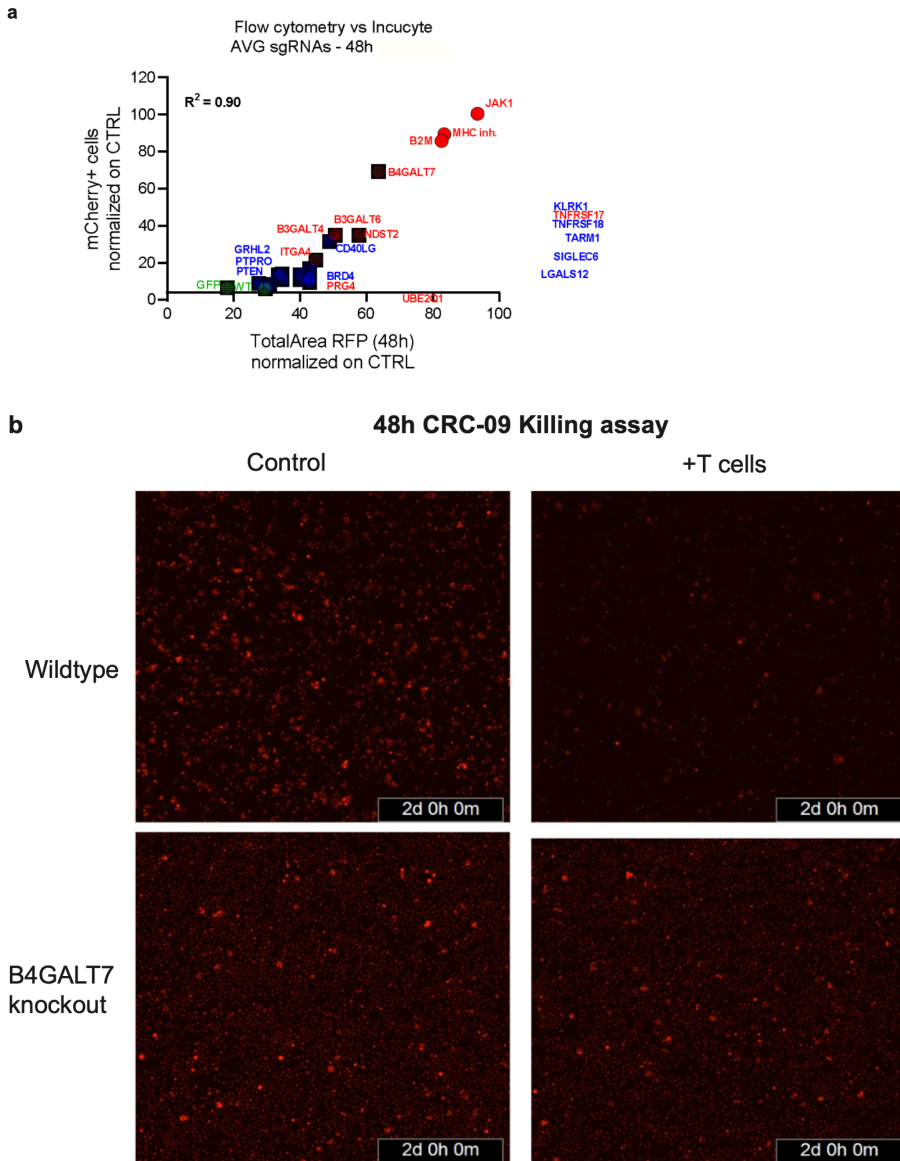


Figure 4: Validation of putative sensitizer and resistance genes to T cell killing.

**a.** Graph showing combined analysis of flow cytometry and Incucyte imaging of average sgRNA knockouts of 7 putative resistance and 11 putative sensitizer genes CRC-09. Flow cytometry readout on mCherry<sup>+</sup> cells normalized to control is plotted against total area red fluorescent protein (RFP) after 48h killing assay normalized to control indicating viability of CRC-09 tumor organoids with respective knockout. CRC-09 gene knockouts of putative sensitizer are depicted in blue, putative resistance mediating hits in red and wildtype in green. **b.** Incucyte imaging of 48h killing assay of wildtype or B4GALT7 knockout CRC-09 mCherry<sup>+</sup> tumor organoids in presence of tumor reactive T cells (+T cells) or absence (control).

## DISCUSSION

Here, we report on whole genome CRISPR Cas9 screens using MMR-d CRC patient-derived tumor organoids and autologous tumor-reactive CD8<sup>+</sup> T cells. Together with specific cytokine screens, we aimed to systematically unveil IFN $\gamma$ -dependent and independent sensitizing and resistance genes of T cell killing. Our efforts confirmed an important role of IFN $\gamma$ -mediated T cell cytotoxicity and defects in IFN $\gamma$  sensing pathways as resistance thereof. Additionally, we identified that knockout of galactosyltransferase B4GALT7 leads to tumor organoid resistance to T cell killing in our model system.

The important role of IFN $\gamma$  signaling has been extensively studied in respect to antitumor T cell responses and resistance to ICB<sup>1,18,19,20,30,31,32</sup>. Both of our cytokine screens with tumor organoids CRC-09 and CRC-12 tumor confirmed key genes of IFN $\gamma$  sensing pathways, such as JAK1/2 and IFN $\gamma$ R1/2. This provided reassurance that whole genome screening using sgRNAs of the MinLibCas9 was feasible for both tumor organoid models. Comparison of cytokine screens and T cell screens of CRC-09 demonstrated that T cell killing in this model system was largely driven by an IFN $\gamma$  response.

While hits of the IFN $\gamma$  screens largely correlated with other screening efforts<sup>32</sup>, performing both cytokine and T cell killing screens on the same tumor organoids, allowed us to identify regulators independent of IFN $\gamma$  signaling. For CRC-09, hits related to proteoglycan synthesis were among top hits of the T cell killing screen. Validation by killing assay of B4GALT7 knockout CRC-09 tumor organoids confirmed this hit as a resistance gene. Besides the functions of proteoglycans in ECM remodeling and some speculation on their role in antitumor immune responses, little is known about a potential involvement of proteoglycans in resistance to T cell cytotoxicity<sup>33</sup>. To our knowledge B4GALT7 has not been described as a resistance gene of T cell mediated antitumor responses. Further evaluation is needed to understand whether this mechanism is unique for the model system of this patient, or if interference with B4GALT7 could overcome resistance to T cells in other tumors. Whole genome screens of CRC-12 did not identify B4GALT7. However, T cell



cytotoxicity of CRC-12 was lower than CRC-09, plus T cell fitness can deviate between autologous T cells. Such differences of the T cell product may influence mediators of T cell killing, aside from the genetic profile of tumor organoids.

That said, our screens in autologous T cell tumor organoid co-cultures also have limitations. As mentioned, screening results may have been impacted by a less functional T cell product. In general, T cells after expansion and culturing deviate in their phenotype compared to the original state. This needs to be taken into account and addressed with appropriate model systems or in combination with clinical data to validate the results. Also, tumor organoids can differ in their sensitivity to suspension cultures or to transduction, which makes not every tumor organoid equally suitable for such screens. Considering those limitations, the differences in overlap between T cell screens of CRC-12 and CRC-09 could be interpreted as a reflection of the complexity of anti-tumor immune responses but could also be a consequence of the model system itself. Further studies are needed to increase the robustness of the model and performing more screens on other tumor organoid pairs, will be crucial to better understand the deviation between patient-derived model systems.

Furthermore, we observed that resistance hits were generally stronger hits than sensitizers. Particularly validation assays demonstrated an influence of putative resistance genes on tumor organoid viability, whereas this was not the case for putative sensitizer genes. One potential explanation is that the model system, CRC-09, already allows for ideal T cell killing which is difficult to further sensitize to.

Lastly, it should be noted that genes associated to antigen presenting machinery, such as B2M, were not strongly enriched in T cell screens although TCR mediated tumor recognition relies on such protein interaction. This could indicate bystander killing or unspecific cell death of tumor organoids. Therefore, we would like to emphasize that validation of identified hits is of high importance.

In conclusion, here we describe a unique genome-wide autologous T cell tumor organoid co-culture screen that may contribute to a better understanding of T cell mediated, individual anti-tumor responses.

## REFERENCES

1. Sharma, P., S. Hu-Lieskovan, J. A. Wargo and A. Ribas (2017). "Primary, Adaptive, and Acquired Resistance to Cancer Immunotherapy." *Cell* 168(4): 707-723.
2. Tumeah, P. C., C. L. Harview, J. H. Yearley, I. P. Shintaku, E. J. Taylor, L. Robert, B. Chmielowski, M. Spasic, G. Henry, V. Ciobanu, A. N. West, M. Carmona, C. Kivork, E. Seja, G. Cherry, A. J. Gutierrez, T. R. Grogan, C. Mateus, G. Tomasic, J. A. Glaspy, R. O. Emerson, H. Robins, R. H. Pierce, D. A. Elashoff, C. Robert and A. Ribas (2014). "PD-1 blockade induces responses by inhibiting adaptive immune resistance." *Nature* 515(7528): 568-571.
3. Veninga, V. and E. E. Voest (2021). "Tumor organoids: Opportunities and challenges to guide precision medicine." *Cancer Cell* 39(9): 1190-1201.
4. Drost, J. and H. Clevers (2018). "Organoids in cancer research." *Nat Rev Cancer* 18(7): 407-418.
5. van de Wetering, M., H. E. Francies, J. M. Francis, G. Bounova, F. Iorio, A. Pronk, W. van Houdt, J. van Gorp, A. Taylor-Weiner, L. Kester, A. McLaren-Douglas, J. Blokker, S. Jaksani, S. Bartfeld, R. Volckman, P. van Sluis, V. S. Li, S. Seepo, C. Sekhar Pedamallu, K. Cibulskis, S. L. Carter, A. McKenna, M. S. Lawrence, L. Lichtenstein, C. Stewart, J. Koster, R. Versteeg, A. van Oudenaarden, J. Saez-Rodriguez, R. G. Vries, G. Getz, L. Wessels, M. R. Stratton, U. McDermott, M. Meyerson, M. J. Garnett and H. Clevers (2015). "Prospective derivation of a living organoid biobank of colorectal cancer patients." *Cell* 161(4): 933-945.
6. Kim, J., B. K. Koo and J. A. Knoblich (2020). "Human organoids: model systems for human biology and medicine." *Nat Rev Mol Cell Biol* 21(10): 571-584.
7. Ringel, T., N. Frey, F. Ringnalda, S. Janjuha, S. Cherkaoui, S. Butz, S. Srivatsa, M. Pirkl, G. Russo, L. Villiger, G. Rogler, H. Clevers, N. Beerenwinkel, N. Zamboni, T. Baubec and G. Schwank (2020). "Genome-Scale CRISPR Screening in Human Intestinal Organoids Identifies Drivers of TGF-beta Resistance." *Cell Stem Cell* 26(3): 431-440 e438.
8. Ungricht, R., L. Guibbal, M. C. Lasbennes, V. Orsini, M. Beibel, A. Waldt, R. Cuttat, W. Carbone, A. Basler, G. Roma, F. Nigsch, J. S. Tchorz, D. Hoepfner and P. S. Hoppe (2022). "Genome-wide screening in human kidney organoids identifies developmental and disease-related aspects of nephrogenesis." *Cell Stem Cell* 29(1): 160-175 e167.
9. Gilbert, L. A., M. A. Horlbeck, B. Adamson, J. E. Villalta, Y. Chen, E. H. Whitehead, C. Guimaraes, B. Panning, H. L. Ploegh, M. C. Bassik, L. S. Qi, M. Kampmann and J. S. Weissman (2014). "Genome-Scale CRISPR-Mediated Control of Gene Repression and Activation." *Cell* 159(3): 647-661.
10. Shalem, O., N. E. Sanjana, E. Hartenian, X. Shi, D. A. Scott, T. Mikkelsen, D. Heckl, B. L. Ebert, D. E. Root, J. G. Doench and F. Zhang (2014). "Genome-scale CRISPR-Cas9 knockout screening in human cells." *Science* 343(6166): 84-87.
11. Wang, T., J. J. Wei, D. M. Sabatini and E. S. Lander (2014). "Genetic screens in human cells using the CRISPR-Cas9 system." *Science* 343(6166): 80-84.
12. Price, S., S. Bhosle, E. Goncalves, X. Li, D. P. McClurg, S. Barthorpe, A. Beck, C. Hall, H. Lightfoot, L. Farrow, R. Ansari, D. A. Jackson, L. Allen, K. Roberts, C. Beaver, H. E. Francies and M. J. Garnett (2022). "A suspension technique for efficient large-scale cancer organoid culturing and perturbation screens." *Sci Rep* 12(1): 5571.
13. Goncalves, E., M. Thomas, F. M. Behan, G. Picco, C. Pacini, F. Allen, A. Vinceti, M. Sharma, D. A. Jackson, S. Price, C. M. Beaver, O. Dovey, D. Parry-Smith, F. Iorio, L. Parts, K. Yusa and M. J. Garnett (2021). "Minimal genome-wide human CRISPR-Cas9 library." *Genome Biol* 22(1): 40.
14. Shifrut, E., J. Carnevale, V. Tobin, T. L. Roth, J. M. Woo, C. T. Bui, P. J. Li, M. E. Diolaiti, A. Ashworth and A. Marson (2018). "Genome-wide CRISPR Screens in Primary Human T Cells Reveal Key Regulators of Immune Function." *Cell* 175(7): 1958-1971 e1915.

15. Dong, M. B., G. Wang, R. D. Chow, L. Ye, L. Zhu, X. Dai, J. J. Park, H. R. Kim, Y. Errami, C. D. Guzman, X. Zhou, K. Y. Chen, P. A. Renauer, Y. Du, J. Shen, S. Z. Lam, J. J. Zhou, D. R. Lannin, R. S. Herbst and S. Chen (2019). "Systematic Immunotherapy Target Discovery Using Genome-Scale In Vivo CRISPR Screens in CD8 T Cells." *Cell* 178(5): 1189-1204 e1123.
16. Belk, J. A., W. Yao, N. Ly, K. A. Freitas, Y. T. Chen, Q. Shi, A. M. Valencia, E. Shifrut, N. Kale, K. E. Yost, C. V. Duffy, B. Daniel, M. A. Hwee, Z. Miao, A. Ashworth, C. L. Mackall, A. Marson, J. Carnevale, S. A. Vardhana and A. T. Satpathy (2022). "Genome-wide CRISPR screens of T cell exhaustion identify chromatin remodeling factors that limit T cell persistence." *Cancer Cell* 40(7): 768-786 e767.
17. Barth, R. J., Jr., J. J. Mule, P. J. Spiess and S. A. Rosenberg (1991). "Interferon gamma and tumor necrosis factor have a role in tumor regressions mediated by murine CD8+ tumor-infiltrating lymphocytes." *J Exp Med* 173(3): 647-658.
18. Zaretsky, J. M., A. Garcia-Diaz, D. S. Shin, H. Escuin-Ordinas, W. Hugo, S. Hu-Lieskovan, D. Y. Torrejon, G. Abril-Rodriguez, S. Sandoval, L. Barthly, J. Saco, B. Hornet Moreno, R. Mezzadra, B. Chmielowski, K. Ruchalski, I. P. Shintaku, P. J. Sanchez, C. Puig-Saus, G. Cherry, E. Seja, X. Kong, J. Pang, B. Berent-Maoz, B. Comin-Anduix, T. G. Graeber, P. C. Tumeh, T. N. Schumacher, R. S. Lo and A. Ribas (2016). "Mutations Associated with Acquired Resistance to PD-1 Blockade in Melanoma." *N Engl J Med* 375(9): 819-829.
19. Shin, D. S., J. M. Zaretsky, H. Escuin-Ordinas, A. Garcia-Diaz, S. Hu-Lieskovan, A. Kalbasi, C. S. Grasso, W. Hugo, S. Sandoval, D. Y. Torrejon, N. Palaskas, G. A. Rodriguez, G. Parisi, A. Azhdam, B. Chmielowski, G. Cherry, E. Seja, B. Berent-Maoz, I. P. Shintaku, D. T. Le, D. M. Pardoll, L. A. Diaz, Jr., P. C. Tumeh, T. G. Graeber, R. S. Lo, B. Comin-Anduix and A. Ribas (2017). "Primary Resistance to PD-1 Blockade Mediated by JAK1/2 Mutations." *Cancer Discov* 7(2): 188-201.
20. Gao, J., L. Z. Shi, H. Zhao, J. Chen, L. Xiong, Q. He, T. Chen, J. Roszik, C. Bernatchez, S. E. Woodman, P. L. Chen, P. Hwu, J. P. Allison, A. Futreal, J. A. Wargo and P. Sharma (2016). "Loss of IFN-gamma Pathway Genes in Tumor Cells as a Mechanism of Resistance to Anti-CTLA-4 Therapy." *Cell* 167(2): 397-404 e399.
21. Kearney, C. J., S. J. Vervoort, S. J. Hogg, K. M. Ramsbottom, A. J. Freeman, N. Lalaoui, L. Pijpers, J. Michie, K. K. Brown, D. A. Knight, V. Sutton, P. A. Beavis, I. Voskoboinik, P. K. Darcy, J. Silke, J. A. Trapani, R. W. Johnstone and J. Orlaro (2018). "Tumor immune evasion arises through loss of TNF sensitivity." *Sci Immunol* 3(23).
22. Dijkstra, K. K., C. M. Cattaneo, F. Weeber, M. Chalabi, J. van de Haar, L. F. Fanchi, M. Slagter, D. L. van der Velden, S. Kaing, S. Kelderman, N. van Rooij, M. E. van Leerdam, A. Depla, E. F. Smit, K. J. Hartemink, R. de Groot, M. C. Wolkers, N. Sachs, P. Snaebjornsson, K. Monkhorst, J. Haanen, H. Clevers, T. N. Schumacher and E. E. Voest (2018). "Generation of Tumor-Reactive T Cells by Co-culture of Peripheral Blood Lymphocytes and Tumor Organoids." *Cell* 174(6): 1586-1598 e1512.
23. Cattaneo, C. M., K. K. Dijkstra, L. F. Fanchi, S. Kelderman, S. Kaing, N. van Rooij, S. van den Brink, T. N. Schumacher and E. E. Voest (2020). "Tumor organoid-T-cell coculture systems." *Nat Protoc* 15(1): 15-39.
24. Schnalzger, T. E., M. H. de Groot, C. Zhang, M. H. Mosa, B. E. Michels, J. Roder, T. Darvishi, W. S. Wels and H. F. Farin (2019). "3D model for CAR-mediated cytotoxicity using patient-derived colorectal cancer organoids." *EMBO J* 38(12).
25. Dubrot, J., P. P. Du, S. K. Lane-Reticker, E. A. Kessler, A. J. Muscato, A. Mehta, S. S. Freeman, P. M. Allen, K. E. Olander, K. M. Ockerman, C. H. Wolfe, F. Wiesmann, N. H. Knudsen, H. W. Tsao, A. Iracheta-Velvet, E. M. Schneider, A. N. Rivera-Rosario, I. C. Kohnle, H. W. Pope, A. Ayer, G. Mishra, M. D. Zimmer, S. Y. Kim, A. Mahapatra, H. Ebrahimi-Nik, D. T. Frederick, G. M. Boland, W. N. Haining, D. E. Root, J. G. Doench, N. Hacohen, K. B. Yates and R. T.

- Manguso (2022). "In vivo CRISPR screens reveal the landscape of immune evasion pathways across cancer." *Nat Immunol* 23(10): 1495-1506.
26. Lawson, K. A., C. M. Sousa, X. Zhang, E. Kim, R. Akthar, J. J. Caumanns, Y. Yao, N. Mikolajewicz, C. Ross, K. R. Brown, A. A. Zid, Z. P. Fan, S. Hui, J. A. Krall, D. M. Simons, C. J. Slater, V. De Jesus, L. Tang, R. Singh, J. E. Goldford, S. Martin, Q. Huang, E. A. Francis, A. Habsid, R. Climie, D. Tieu, J. Wei, R. Li, A. H. Y. Tong, M. Aregger, K. S. Chan, H. Han, X. Wang, P. Mero, J. H. Brumell, A. Finelli, L. Ailles, G. Bader, G. A. Smolen, G. A. Kingsbury, T. Hart, C. Kung and J. Moffat (2020). "Functional genomic landscape of cancer-intrinsic evasion of killing by T cells." *Nature* 586(7827): 120-126.
  27. Li, W., H. Xu, T. Xiao, L. Cong, M. I. Love, F. Zhang, R. A. Irizarry, J. S. Liu, M. Brown and X. S. Liu (2014). "MAGeCK enables robust identification of essential genes from genome-scale CRISPR/Cas9 knockout screens." *Genome Biol* 15(12): 554.
  28. Colic, M., G. Wang, M. Zimmermann, K. Mascall, M. McLaughlin, L. Bertolet, W. F. Lenoir, J. Moffat, S. Angers, D. Durocher and T. Hart (2019). "Identifying chemogenetic interactions from CRISPR screens with drugZ." *Genome Med* 11(1): 52.
  29. Behan, F. M., F. Iorio, G. Picco, E. Goncalves, C. M. Beaver, G. Migliardi, R. Santos, Y. Rao, F. Sassi, M. Pinnelli, R. Ansari, S. Harper, D. A. Jackson, R. McRae, R. Pooley, P. Wilkinson, D. van der Meer, D. Dow, C. Buser-Doepner, A. Bertotti, L. Trusolino, E. A. Stronach, J. Saez-Rodriguez, K. Yusa and M. J. Garnett (2019). "Prioritization of cancer therapeutic targets using CRISPR-Cas9 screens." *Nature* 568(7753): 511-516.
  30. Kaplan, D. H., V. Shankaran, A. S. Dighe, E. Stockert, M. Aguet, L. J. Old and R. D. Schreiber (1998). "Demonstration of an interferon gamma-dependent tumor surveillance system in immunocompetent mice." *Proc Natl Acad Sci U S A* 95(13): 7556-7561.
  31. Sucker, A., F. Zhao, N. Pieper, C. Heeke, R. Maltaner, N. Stadler, B. Real, N. Bielefeld, S. Howe, B. Weide, R. Gutzmer, J. Utikal, C. Loquai, H. Gogas, L. Klein-Hitpass, M. Zeschknig, A. M. Westendorf, M. Trilling, S. Horn, B. Schilling, D. Schadendorf, K. G. Griewank and A. Paschen (2017). "Acquired IFN $\gamma$  resistance impairs anti-tumor immunity and gives rise to T-cell-resistant melanoma lesions." *Nat Commun* 8: 15440.
  32. Coelho, M. A., S. Cooper, M. E. Strauss, E. Karakoc, S. Bhosle, E. Goncalves, G. Picco, T. Burgold, C. M. Cattaneo, V. Veninga, S. Consonni, C. Dincer, S. F. Vieira, F. Gibson, S. Barthorpe, C. Hardy, J. Rein, M. Thomas, J. Marioni, E. E. Voest, A. Bassett and M. J. Garnett (2023). "Base editing screens map mutations affecting interferon-gamma signaling in cancer." *Cancer Cell* 41(2): 288-303 e286.
  33. Tzanakakis, G., M. Neagu, A. Tsatsakis and D. Nikitovic (2019). "Proteoglycans and Immunobiology of Cancer-Therapeutic Implications." *Front Immunol* 10: 875.

## METHODS

### Organoid culture

Establishment of the respective organoid lines from tumor material was performed as previously reported<sup>19,20</sup>. In brief, tumor tissue was mechanically dissociated and digested with 1.5 mg ml<sup>-1</sup> of collagenase II (Sigma-Aldrich), 10 µg ml<sup>-1</sup> of hyaluronidase type IV (Sigma-Aldrich) and 10 µM Y-27632 (Sigma-Aldrich). Cells were embedded in Cultrex RGF BME type 2 (3533-005-02, R&D systems) and placed into a 37 °C incubator for 20 min. Human CRC organoid medium is composed of Ad-DF++ (Advanced DMEM/F12 (GIBCO) supplemented with 2 mM Ultraglutamine I (Lonza), 10 mM HEPES (GIBCO), 100 U ml<sup>-1</sup> of each penicillin and streptomycin (GIBCO), 10% noggin-conditioned medium, 20% R-spondin1-conditioned medium, 1× B27 supplement without vitamin A (GIBCO), 1.25 mM N-acetylcysteine (Sigma-Aldrich), 10 mM nicotinamide (Sigma-Aldrich), 50 ng ml<sup>-1</sup> human recombinant EGF (Peprotech), 500 nM A83-01 (Tocris), 3 µM SB202190 (Cayman Chemicals) and 10 nM prostaglandin E2 (Cayman Chemicals). Organoids were passaged depending on growth every 1–2 weeks by incubating in TrypLE Express (Gibco) for 5–10 min followed by embedding in BME. Organoids were authenticated by SNP array or STR analysis and were regularly tested for Mycoplasma using Mycoplasma PCR43 and the MycoAlert Mycoplasma Detection Kit (LT07-318). In the first two weeks of organoid culture, 1× Primocin (Invivogen) was added to prevent microbial contamination. Procedures performed with patient samples were approved by the Medical Ethical Committee of the Netherlands Cancer Institute–Antoni van Leeuwenhoek hospital (NL48824.031.14) and written informed consent was obtained from all of the patients. Mismatch repair status was assessed using a standard protocol for the Ventana automated immunostainer for MLH1 clone M1 (Roche), MSH2 clone G219-1129 (Roche), MSH6 clone EP49 (Abcam) and PMS2 clone EP51 (Agilent Technologies).

### Phenotyping tumor organoids

For organoid surface expression stainings, tumor organoids were dissociated into single cells using TrypLE Express (Gibco), washed twice in cold FACS buffer (PBS, 5

mM EDTA, 1% bovine serum antigen), and stained with anti-HLA-A/B/C-PE (1:20, W6/32, BD Biosciences), anti-HLA-DR/DP/DQ-FITC (1:20, Tü39, Biolegend), anti-PD-L1-APC (1:200, MIH1, eBioscience) and 1:2,000 near-infrared (NIR) viability dye (Life Technologies), or isotype controls (1:20 FITC; 1:20, PE; or 1:200, APC) mouse IgG1 kappa (BD Biosciences). Tumor cells were incubated for 30 min at 4 °C in the dark and washed twice with FACS buffer. All samples were recorded with the BD LSR Fortessa Cell Analyzer SORP flow cytometer using FACSDiVa (v.8.0.2; BD Biosciences). Data were analysed using FlowJo (v.10.6.1; BD) and presented using GraphPad Prism (v.9.0.0; GraphPad).

### Co-culture and T cell expansion

To generate tumor reactive T cells, tumor organoid and autologous PBMC co-cultures were performed as described before<sup>34,37</sup>. In short, tumor organoids were isolated from BME by washing with cold PBS 2 days before addition of the PBMCs. After washing CRC organoids were resuspended in culture medium in the presence of 10 μM Y27632. A day before coculture, organoids were stimulated with 200 ng/mL of IFN $\gamma$  (Peprotech). On the same day frozen PBMCs, which were beforehand isolated from peripheral blood using Ficoll-Paque, were thawed and cultured overnight in T cell culture medium (RPMI 1640 (Thermo Fisher Scientific) supplemented with 1% Pen Strep and 10% human serum (Sigma Aldrich)) with 150 U/mL IL-2 (Peprotech). Organoids were dissociated into single cells and plated at a 1:20 target:effector ratio with autologous PBMCs, in an anti-CD28 coated (clone CD28.2, eBioscience), 96-well, Ubottomed plate, in the presence of 150 U/mL of IL2 (Proleukin) and 20 μg/mL of anti-PD1 (Merus). Half of the medium was refreshed every 2–3 d with addition of new IL2 and anti-PD1. Tumor reactivity was measured after 2 weeks of co-culture by intracellular staining of IFN $\gamma$  and CD107a. If co-culture was successful and tumor reactivity confirmed T cells were expanded using a rapid expansion protocol. To facilitate enrichment of tumor reactive T cells, CD137<sup>+</sup> T cells were enriched using a CD137 microbead kit (Miltenyi Biotec) according to manufacturers protocol. T cells were then resuspended at 1\*10<sup>4</sup> cells/mL in T cell culture medium and 1:1 mixed with irradiated feeder cells at 2\*10<sup>6</sup> cells/mL in AIM-V medium (Thermo Fisher Scientific).

Feeder cells were derived from PBMCs of three independent healthy donors. Cells were supplemented with 30 ng/mL anti-CD3 (Thermo Fisher Scientific) and 3000 U/mL IL-2 before one week incubation. From day 7-14 medium was replenished or cells 1:1 expanded depending on density and supplemented with 3000 U/mL IL-2. After two weeks of expansion cells were resuspended in low dose (150 U/mL) IL-2 T cell culture medium for 2-3 days before freezing in FBS 10% DMSO.

### Intracellular staining IFN $\gamma$ and CD107a staining

Evaluation of tumor reactivity was performed as described previously<sup>13,19,20</sup>. Two days before the experiment, organoids were isolated from BME by washing with cold PBS before being resuspended in CRC organoid medium with 10  $\mu$ M Y-27632 (Sigma-Aldrich). The organoids were stimulated with 200 ng/mL IFN $\gamma$  (Peprotech) 24 h before the experiment. For the recognition assay and intracellular staining, tumor organoids were dissociated into single cells and plated in 96-well U-bottom plates with PBMCs at a 1:2 target:effector ratio. As a positive control, PBMCs were stimulated with 50 ng/mL of phorbol-12-myristate-13-acetate (PMA) (Sigma-Aldrich) and 1  $\mu$ g/mL of ionomycin (Sigma-Aldrich). As a negative control (alone), T cell culture medium was added to PBMCs. Cells were stained with anti-CD107a-PE (1:50, Biolegend). After 1 h of incubation at 37 °C, GolgiSTOP (BD Biosciences, 1:1500) and GolgiPlug (BD Biosciences, 1:1000) were added. After 4 h of incubation at 37 °C, PBMCs were washed twice in cold FACS buffer (PBS, 5 mM EDTA, 1% bovine serum antigen) and stained with anti-CD3-PerCP-Cy5.5 (1:20, BD Biosciences), anti-CD4-FITC (1:20, BD Bioscience), anti-CD8-BV421 (1:200, BD Biosciences) and 1:2000 near-infrared (NIR) viability dye (Life Technologies) for 30 min at 4 °C. Cells were washed, fixed, using the Cytofix/Cytoperm Kit (BD Biosciences), and stained with 1:40 anti-IFN $\gamma$ -APC (1:40, BD Biosciences) for 30 min at 4 °C. After two washing steps, cells were resuspended in 50mL FACS buffer and recorded with the BD LSR Fortessa Cell Analyzer SORP flow cytometer using FACSDiVa software (v.8.0.2; BD Biosciences). Data were analysed using FlowJo (v.10.6.1, BD) and presented using GraphPad Prism (v.9.0.0, GraphPad).

### CD137 reactivity assay

Analysis of CD137 expression by T cells was evaluated as previously described<sup>22,23</sup>. Two days before the experiment, organoids were isolated from BME by washing with cold PBS before being resuspended in CRC organoid medium with 10  $\mu$ M Y-27632. The organoids were stimulated with 200 ng/mL IFN $\gamma$  24 h before the experiment. T cells were resuspended at  $1 \times 10^5$  cells/mL in T cell culture medium and resuspended with tumor organoids at 2:1 effector:target ratio. Tumor organoids were beforehand dissociated to single cells. T cells were culture only in T cell culture medium as negative control and supplemented with 50 ng/mL of phorbol-12-myristate-13-acetate (PMA) and 1  $\mu$ g/mL of ionomycin as positive control. Cells were then plated in anti-CD28 coated 96-well U-bottom plate in presence of anti-PD1 for 24 hours. The following day cells were washed twice with FACS buffer and stained with anti-CD3-PerCP-Cy5.5 (1:20, BD Biosciences), anti-CD137 (1:30, BD Biosciences) anti-CD4-FITC (1:20, BD Bioscience), anti-CD8-BV421 (1:200, BD Biosciences) and 1:2000 near-infrared (NIR) for 30min in the dark at 4 degrees. After two washing steps with cold FACS buffer, cells were recorded with the BD LSR Fortessa Cell Analyzer SORP flow cytometer using FACSDiVa software (v.8.0.2; BD Biosciences). Data were analysed using FlowJo (v.10.6.1, BD) and presented using GraphPad Prism (v.9.0.0, GraphPad).

### Killing assay

Assessment of tumor organoid killing by T cells was evaluated as previously described<sup>22,23</sup>. First, flat-bottom non-tissue culture plates were coated with 5 mg/mL anti-CD28 at kept at 4 degrees overnight. The plate was washed twice with PBS immediately prior to plating of the cells. Two days before the experiment, organoids were isolated from BME by washing with cold PBS before being resuspended in CRC organoid medium with 10  $\mu$ M Y-27632. The organoids were stimulated with 200 ng/mL IFN $\gamma$  24 h before the experiment. Single cell equivalent number of tumor organoids was determined by dissociation of a sample of tumor organoids. Tumor organoids were resuspended in T cell culture medium or organoid medium depleted of nicotinamide, which was used for the whole genome screen. T cells were and tumor organoids were plated in triplicates at a suitable effector:target ratio depending



on experimental needs. For the whole genome T cell screen cells were plated at 1:1 ratio for CRC-09 and 4:1 for CRC-12. Evaluation of resistance genes was performed at 1:1 and 3:1 for resistance genes. For MHC class I blocking, tumor organoids were beforehand pre-incubated with 50 mg/mL MHC class I blocking antibody (W6/32, BD Biosciences). Cells were cultured for 72h before readout using Incucyte imaging of mCherry signal.

### Whole genome CRISPR Cas9 screen

Similarly, to our previously described method<sup>13</sup>, to express Cas9, tumoral organoids were dissociated into single cells and incubated overnight in suspension and complete media supplemented with pKLV2-EF1a-BsdCas9-W lentiviral particles and polybrene (8 µg ml<sup>-1</sup>). The day after, cells were seeded in BME and grown as organoids. Blasticidin selection (20 mg/ml) commenced 48 h after transduction and maintained until the end of the experiment. All the organoid lines displayed Cas9 activity over 80%. Single-guide RNAs of the minimal genome-wide human CRISPR-Cas9 library (MinLibCas9) were used. Briefly, tumour organoids were dissociated into single cells and a total of  $3.3 \times 10^7$  cells were transduced overnight, in suspension, with an appropriate volume of the lentiviral-packaged whole-genome sgRNA library to achieve 30% transduction efficiency ( $\times 100$  library coverage) and polybrene (8 µg ml<sup>-1</sup>). To achieve high cell numbers, tumor organoids were cultured with 5% extracellular matrix (ECM) in suspension as recently described<sup>12</sup>. After 48 h organoids were selected with puromycin (2 mg/ml). After 14 days, approximately  $2 \times 10^7$  cells were collected as pellets and stored at  $-80^\circ\text{C}$  for DNA extraction. Further cell pellets were taken before exposure to cytokines or T cells (T0), after cytokine exposure (200 ng/mL IFN $\gamma$  or 100 ng/mL TNF $\alpha$ ) and after first and second round of T cell killing. Genomic DNA was extracted using the Qiagen, Blood & Cell Culture DNA Maxi Kit, 13362 as per the manufacturer's instructions. PCR amplification, Illumina sequencing (19-bp single-end sequencing with custom primers on the HiSeq2000 v.4 platform) and sgRNA counting were performed as described previously.

## Computational analysis

In our CRISPR-Cas9 screening methodology, guide RNAs (gRNAs) exhibiting zero read counts in the control samples were excluded. The log<sub>2</sub> fold changes (L2FC) were determined using normalized read counts, where we calculated normalized reads per million by dividing gRNA reads by the total reads in the sample, then multiplying by 1,000,000 and adding a pseudocount of 1 to avoid division by zero error. Finally, the average fold-change for each gene was determined by calculating the mean of the fold-changes for all sgRNAs targeting that gene. To combine the data from replicates, we averaged these gene-level fold-changes. For the MAGeCK analysis<sup>27</sup>, we employed the default settings with one modification: the normalization parameter was set to 'none'. This adjustment was made since the input corrected counts had already undergone normalization.

Moreover, we used DrugZ<sup>28</sup> to calculate gene-level normalized Z-scores and FDR values. To perform gene-set enrichment analysis (GSEA), we utilized the GSEA software obtained from the Broad Institute GSEA portal (<http://software.broadinstitute.org/gsea/index.jsp>). We conducted a pre-ranked GSEA using DrugZ normZ values applying the default parameters. To estimate the significance of enrichment, we used 1,000 gene permutations.

## Author contribution

G.P., V.V., S.V., and C.M.C designed, performed, analyzed and interpreted experiments. A.W. and S.W. performed validation experiments. I.M., A.W.J.R. and X.M. worked on strategic hit selection. E.K. analyzed sequencing data of screens. V.V., G.P., M.J.G and E.E.V wrote the manuscript. All authors reviewed the manuscript.

## Acknowledgements

We thank Martijn van Baalen, Anita Pfauth, Frank van Diepen and Guido de Roo for assistance in flow cytometry at the NKI. We would like to acknowledge the Hartwig Medical Foundation for authentication of tumor organoids. We would like to thank Merus for supply of anti-PD1. The Graphical Abstract was created with [BioRender.com](https://BioRender.com). This work was funded by Open Targets grant for Identification of

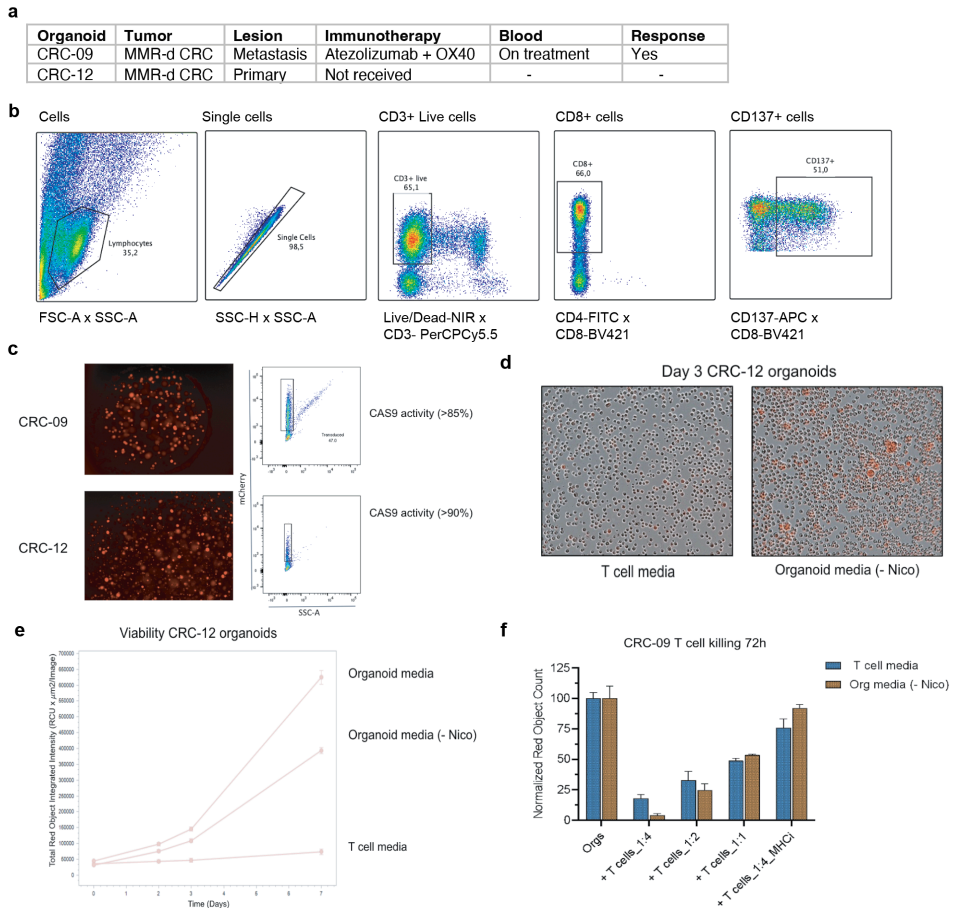
targets modulating lymphocyte-mediated tumour cell killing (iFuncOnc, E.E.V and M.J.G)

### **Competing Interests**

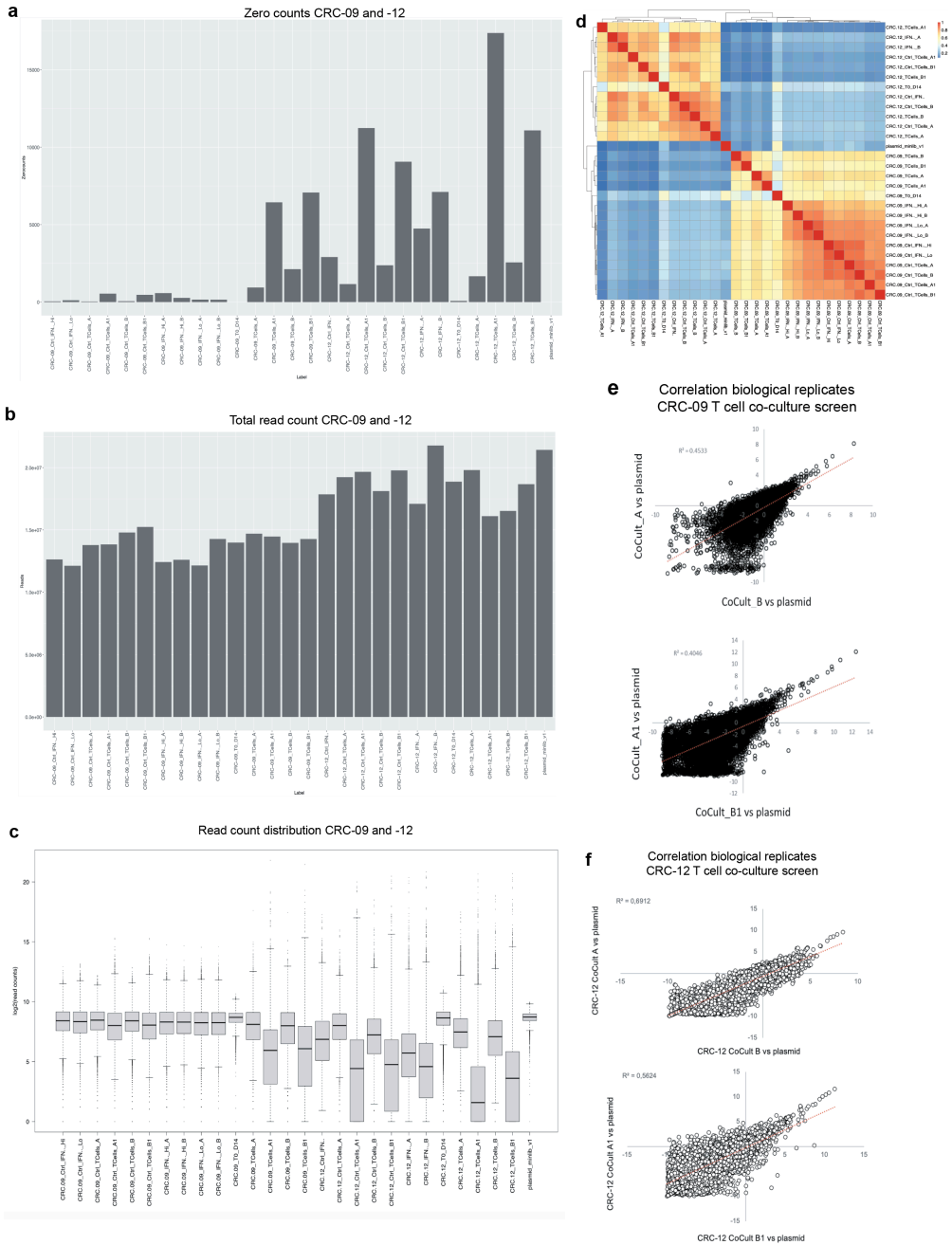
M.J.G. has received research funding from GlaxoSmithKline, Astex Pharmaceuticals and AstraZeneca, and is co-Founder and Chief Scientific Officer for Mosaic Therapeutics. M.J.G., S.P. and H.F. hold a patent application related to this study (GB2009808.3). All other authors declare no competing interests. E.E.V. reports institutional research funding from BMS, GSK, Pfizer, Roche, Clovis, MSD, Astrazeneca, Bayer, Lilly, Eisai, outside the current work, and is co-founder of Mosaic Therapeutics. All other authors declare no competing interests.

3

## SUPPLEMENTAL FIGURES



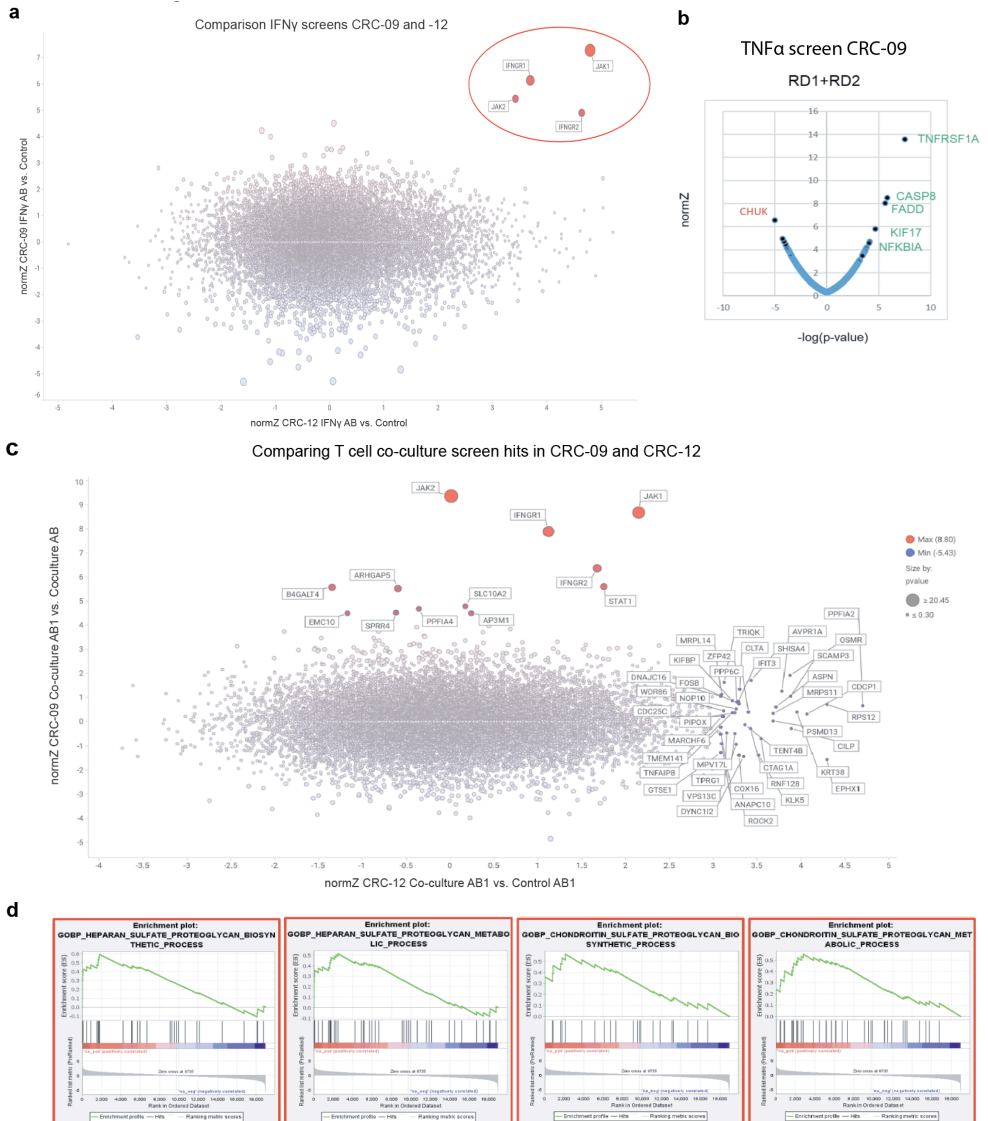
Extended Data Figure 1: Establishment model system and optimizations for screens. **a**. Table summarizing characteristics of model system CRC-09 and CRC-12. **b**. Flow cytometry dot plots showing gating strategy of CD137 reactivity assay of PBMCs. **c**. Incucyte image of mCherry expression of Cas9 transduced tumor organoids CRC-09 and -12 (left). Flow cytometry analysis of mCherry expression in tumor organoids showing >85% mCherry positive cells for CRC-09 and >90% positive cells for CRC-12 (right). **d**. Light and fluorescent microscopy image of CRC-09 showing tumor organoids and mCherry expression (red) when cultured in T cell medium (left) and organoid medium depleted of nicotinamide (right). **e**. Time course depicting viability of CRC-12 organoids over 7 days measured in total red object integrated intensity by Incucyte live cell imaging. Viability is shown for CRC-12 cultured in T cell medium, organoid medium depleted of nicotinamide (Organoid medium -Nico) and complete organoid medium. **f**. Bar graphs indicating CRC-09 viability of killing assay with tumor reactive T cells at target:effector ratio 1:4, 1:2 and 1:1. Viability of tumor organoids alone is shown as reference and MHC I block + T cells 1:4 as control to interfere with CD8<sup>+</sup> T cell cytotoxicity. Effect of culturing in T cell medium (blue) compared to organoid medium depleted of nico (brown) is shown for all samples.



Extended Data Figure 2: Quality control of library transduction and processed samples.

**a.** Bar graphs showing zero counts of each processed sample of CRC-09 and CRC-12. **b.** Bar graphs showing total read count for each processed sample of CRC-09 and CRC-12 **c.** Graph indicating read count

distribution per processed sample of CRC-09 and CRC-12 in log<sub>2</sub>(read counts). **d.** Heatmap showing clustering of each processed sample of CRC-09 and CRC-12. **e.** Plot indicating correlation of both biological replicates of CRC-09 co-culture screen correlated against plasmid, replicate A with B (top) and replicate A1 with B1 (bottom). **f.** Plot indicating correlation of both biological replicates of CRC-12 co-culture screen correlated against plasmid, replicate A with B (top) and replicate A1 with B1 (bottom).



3

See next page for caption

Extended Data Figure 3: Comparison of CRC-09 and CRC-12 and gene pathway enrichment analysis.

**a.** Plot comparing normalized CRC-12 IFN $\gamma$  screen to normalized CRC-09 IFN $\gamma$  screen. Highlighting shared significantly enriched (red) or depleted (blue, none depicted) genes. Size of dots indicated significance. **b.** Plot showing enriched (green) or depleted genes (red) of TNF $\alpha$  cytokine screen for combined biological replicates of CRC-09. **c.** Plot comparing normalized CRC-12 T cell screen to normalized CRC-09 T cell screen. Highlighting shared significantly enriched (red) or depleted (blue) genes. Size of dots indicated significance. **d.** Gene pathway enrichment analysis of top selected hits of CRC-09 T cell screen independent of IFN $\gamma$  mediated cytotoxicity associate proteoglycan biosynthesis or metabolism processes related to hit selection.





A penny for your thoughts, a dollar for your dreams

Mac Miller

# T cell dynamics in patient-derived tumor organoid co-cultures

4

**Vivien Veninga**<sup>1,2</sup>, Luca Braccioli<sup>3</sup>, Moreno Martinovic<sup>3</sup>,  
Leon Potgeter<sup>4</sup>, Elzo de Wit<sup>3</sup>, Emile E. Voest<sup>1,2</sup>

<sup>1</sup> Department of Molecular Oncology and Immunology, Netherlands Cancer Institute, Amsterdam, The Netherlands.

<sup>2</sup> Oncode Institute, Utrecht, The Netherlands.

<sup>3</sup> Division of Gene Regulation, Netherlands Cancer Institute

<sup>4</sup> Department of Oncology UNIL-CHUV, Ludwig Institute for Cancer Research Lausanne, Lausanne University Hospital and University of Lausanne, Lausanne, Switzerland



## ABSTRACT

In depth characterization of T cell reactivity triggered by tumors has been fueled by advances of single cell technologies. A fundamental understanding of which T cell subsets drive an anti-tumor response and how their behavior changes over time can help to overcome current limitations of T cell therapies. While an enormous collection of immune cell profiling datasets on tumor infiltrating lymphocytes has been generated over the past years, fewer studies have looked at the precise moment when autologous T cells interact with cancer cells for the first time. In a fully autologous peripheral blood mononuclear cell (PBMC) and patient-derived tumor organoid co-culture system, we aimed to track T cell subsets over time. We used transposase-accessible chromatin (ATAC) sequencing to allow for an unbiased identification of cell type specific regulatory elements. By combining ATAC sequencing with our co-culture model we aimed to identify gene regulatory factors of T cells that play an essential role in tumor reactivity. Here, we summarize our initial attempts and findings, and propose experimental improvements for future experiments.

## INTRODUCTION

4

T cells are instrumental in orchestrating anti-tumor immunity and play a pivotal role in diverse cancer immunotherapeutic strategies. These strategies, ranging from adoptive T cell transfer (ATC) and the infusion of tumor-infiltrating lymphocytes (TIL) to the utilization of TCR-engineered T cells, synthetic chimeric antigen receptors (CARs) T cells, immune checkpoint therapy, and cancer vaccines, collectively hinge upon the remarkable ability of T cells to selectively recognize and eliminate malignant cells<sup>1</sup>. Especially, immune checkpoint inhibitor (ICI) therapies have revolutionized the treatment of cancer patients by unleashing breaks on T cells and allowing a patient's own immune system to efficiently kill cancer cells. Treatments that target immune checkpoints CTLA-4 and PD-(L)1 have led to impressive clinical results for many cancers<sup>2,3,4</sup>. Despite great success of ICI, there are limitations. When considering metastatic melanoma, as a posterchild of ICI, still 40% of the patients do not respond to combined treatment of anti-PD1 and anti-CTLA4<sup>5</sup>. So far, for example, TMB and MMR-d have been identified to correlate with treatment response, but we are still far from understanding the full mechanism to precisely predict a patient's response to ICI<sup>6</sup>. In order to improve response to ICI and other T cell therapies, it is crucial to identify limitations of anti-tumor T cell reactivity. Better understanding of T cell behavior and T cell exhaustion before and during treatment or also which T cell states kill the tumor, will likely allow us to improve current treatments.

The pursuit to answer such questions benefitted immensely from technological advances in single cell analysis. In the past years, many datasets of transcriptomic profiles of tumor infiltrating lymphocytes have been generated<sup>7</sup>. The outcome of these analyses has expanded our knowledge on the proposed mechanism of PD-(L)1 blockade response. It was suggested that responses to PD-(L)1 blockade would mainly act via reinvigoration of intratumoral pre-existing T cell clones<sup>8,9</sup>, however it was also reported that expansion of T cell clones upon treatment, derived from clonotypes that may have just recently entered the tumor but were not detected in pre-existing tumor infiltrating T cells<sup>10</sup>. This suggested that T cell response to PD-1 blockade may rely on peripheral T cell recruitment as well<sup>11</sup>. Such findings are in line with previous data showing that loss of T cell migration inhibits an effective anti-tumor

T cell response<sup>12</sup> and that the epigenetically stable state of exhausted T cells is difficult to reinvigorate<sup>13,14</sup>.

Next to single cell transcriptomics, epigenomic profiling using assay for transposase-accessible chromatin sequencing (ATACseq) is a powerful tool to dissect immune responses as it allows for an unbiased identification of DNA regulatory elements, deconvolution of all cells in a tissue and marker free reconstruction of cell developmental trajectories. As an example, performing scATACseq on PBMCs and basal cell carcinoma tissue reconstructed B cell trajectories and, besides others, identified regulatory elements of CD8<sup>+</sup> T cell exhaustion and CD4<sup>+</sup> helper T cell development associated with ICB response<sup>15</sup>. Epigenetic changes determine the fate of a T cells behavior and, with that, dysfunctionality during tumor response<sup>16</sup>. Next to the identification of tumor specific TCR or CAR T cell targets, which has been a major undertaking of the field of cancer immunotherapy, the goal to circumvent exhaustion and reprogram T cells to improve their fitness has gained popularity. This was demonstrated by the discovery that alteration of a chromatin remodeling complex, specifically Arid1a, improved anti-tumor immunity<sup>17</sup> or more recently how depletion of chromatin remodeling complex PBAF in CD8<sup>+</sup> T cells increases their anti-tumor response<sup>18</sup>. Tackling T cell exhaustion will likely be a game-changer for improving ATC therapies, ICI response or the discovery of novel cancer immunotherapies.

Besides overcoming T cell exhaustion, one other challenge is to track T cell changes upon tumor interaction over time to identify key T cell subsets of anti-tumor responses. Recently a time sensitive murine in vivo single cell transcriptomics technology, named Zman-seq, has been established and reportedly using time stamps into immune cells which allows to track them in tissue over days<sup>19</sup>. However, the challenge to track human autologous T cells and tumor interaction remains. To our knowledge, TILs and PBMCs of patients have been mostly analyzed separately and few attempts have been made to in depth characterize peripheral blood T cell responses to cancer cells from patient's tumors over time. We therefore embarked on an analysis of open chromatin assessment of autologous T cells co-cultured with patient-derived tumor organoids (PDTOs) in order to identify key T cell states and regulatory elements of anti-tumor T cell responses. Here, we present out initial findings and highlight the future direction of this project.

## RESULTS

4

To obtain chromatin profiles of autologous PBMCs at baseline (day 0) and after a two-week co-culture (day 14) with MMR-d colorectal cancer PDOs, we first generated tumor reactive T cells according to our previously published protocol<sup>20</sup>. In order to maximize the chance to observe differences between day 0 and day 14 and having a reference of a highly tumor reactive CD8<sup>+</sup> T cell population, we used a pair of tumor organoids and PBMCs that elicited high CD8<sup>+</sup> T cell cytotoxicity (Fig. 1c). Autologous PBMCs of PDO-01 were derived from an ICI responder (Extended Data Fig. 1b) which at baseline (day 0) showed increased CD8<sup>+</sup> T cell expression of IFN $\gamma$  and CD107a upon stimulation with PDO-01 compared to an unstimulated control (Fig. 1c). After a two-week co-culture, ~45% of CD8<sup>+</sup> T cells expressed IFN $\gamma$ <sup>+</sup> upon PDO-01 stimulation (Fig. 1c). During the co-culture, the CD4<sup>+</sup> T cell population was largely diminished and remaining cells did not show reactivity towards PDO-01 (Extended Data Fig. 1a). The fraction of CD8<sup>+</sup> T cells increased from 48 % at day 0 to 74% of CD3<sup>+</sup> T cells at day 14 (Fig. 1d). PDO-01 MMR-d CRC organoids expressed MHC class I at baseline, which increased after IFN $\gamma$  stimulation. MHC class II and PD-L1 expression were observed after IFN $\gamma$  stimulation (Fig. 1e).

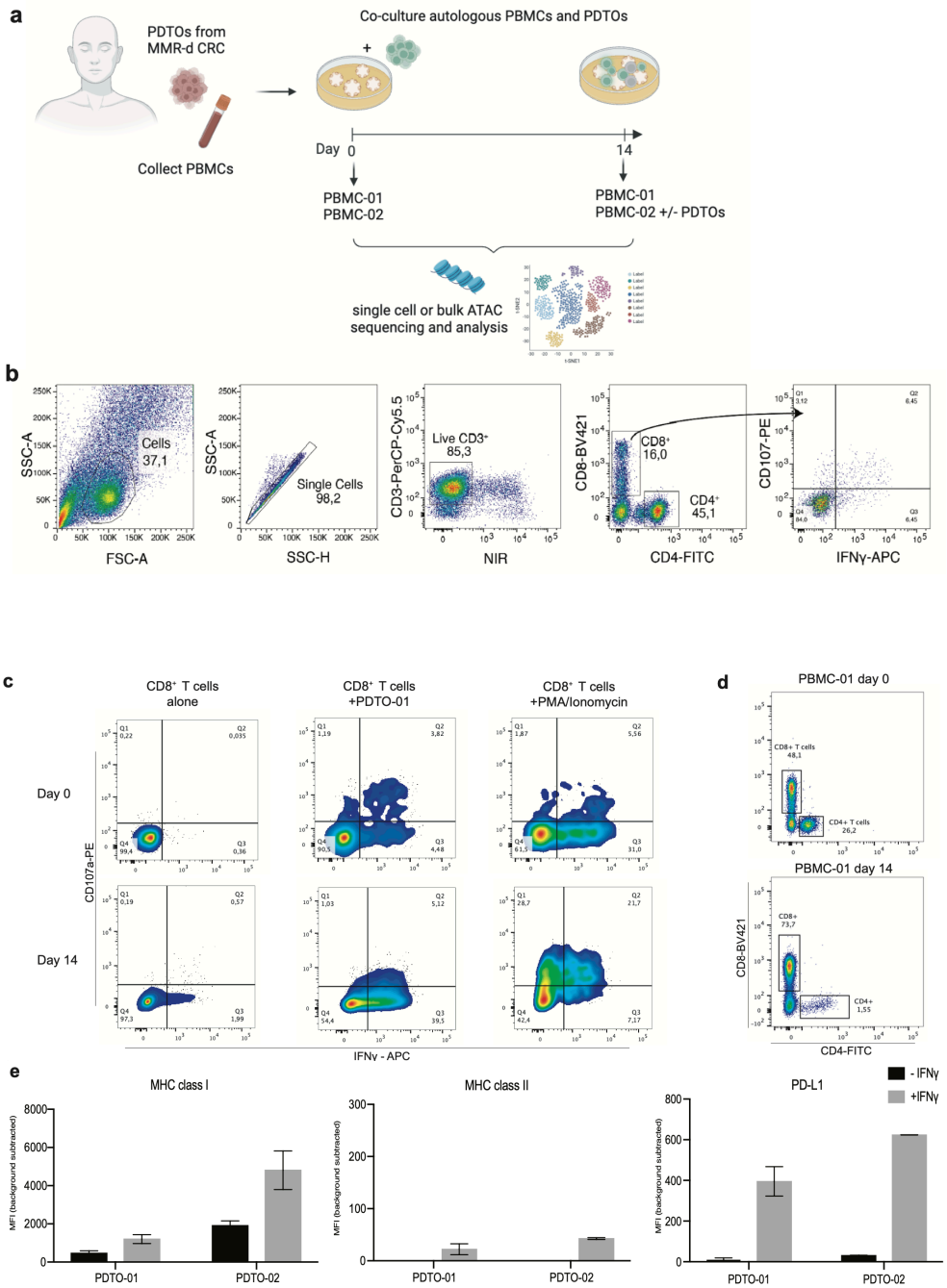




**Figure 1: Establishment of tumor reactive T cells from co-culture of PDTO-01 for scATAC sequencing.**

**a.** Schematic overview of experimental set up. Tumor organoids were established from MMR-d CRC tumors and PBMCs frozen from blood samples. At baseline, day 0, and after two-week co-culture, day 14, PBMCs of co-cultures with autologous PBMCs and PDTO-01 and -02 were frozen down. Additionally, a sample of PBMC-02 not co-cultured with PDTO-02 was taken at day 14. Samples were then further processed for scATAC (PDTO-01) and bulk ATAC (PDTO-02). **b.** Flow cytometry gating strategy of PBMCs to determine intracellular expression of IFN $\gamma$  and CD107a for reactivity assay. **c.** Representative dot plots of CD8<sup>+</sup> T cells unstimulated (alone), stimulated with tumor organoids (+PDTO-01) and positive control (+PMA/Ionomycin) at day 0 (top) and day 14 (bottom) indicating IFN $\gamma$  and CD107a expression. **d.** Flow cytometry dot plots of CD4<sup>+</sup> and CD8<sup>+</sup> T cell distribution of CD3<sup>+</sup> cells of PBMC-01 at day 0 and after co-culture at day 14. **e.** Bar graphs indicating surface expression of MHC class III and PD-L1 of PDTO-01 and -02 at baseline or after 24h IFN $\gamma$  pre-stimulation. Error bars indicate SEM of two independent experiments (n=2).

After tumor reactive CD8<sup>+</sup> T cells were generated and samples were taken at day 0 and day 14 of the co-culture, samples were processed for scATAC sequencing (Fig. 1a). Quality controls of scATAC data showed that a large fraction of the 120M total reads, with valid barcodes, consisted of PCR duplicates. Removal of the duplicates resulted in a reduction of the library complexity to 13M unique reads with median of 5000 reads per cell (Extended Data Fig. 1c, d, f). A total of 1600 cells was sequenced, 509 for day 0 and 1304 for day 14 (Extended Data Fig. 1e). UMAP embedding by time of sample collection showed distinct clustering of day 0 and day 14 with some overlap. In total five clusters were identified across both samples with a majority of day 14 cells in cluster 3, whereas the majority of day 0 cells was spread across cluster 1 and 2. Cluster 4 was exclusively found in day 14 sample (Fig. 2a, b). Genome coverage plots indicated that the CD8A locus is generally accessible in all clusters, while CD4 locus was not clearly depicted (Fig. 2a, c). Overall, this was in line with flow cytometry data of PBMC-01 samples from day 0 and 14 confirming CD8<sup>+</sup> T cells as most abundant cells (Fig. 1d). IL7R locus, a specific promoter for naïve T cells, was accessible in cluster 1 and 5 which overlaps with day 0 clustering (Fig. 2a, c). After analysis of DNA accessibility to identify T cell subsets and differentially open chromatin loci, we next looked at transcription factor DNA binding motif accessibility (Fig. 2e). Significantly variable motifs between day 0 and day 14 cells included mostly JUN and FOS as well as BACH2 and BATF transcription factors (Fig. 2d, f). FLI1 was showed differential accessibility as well (Fig. 2f).

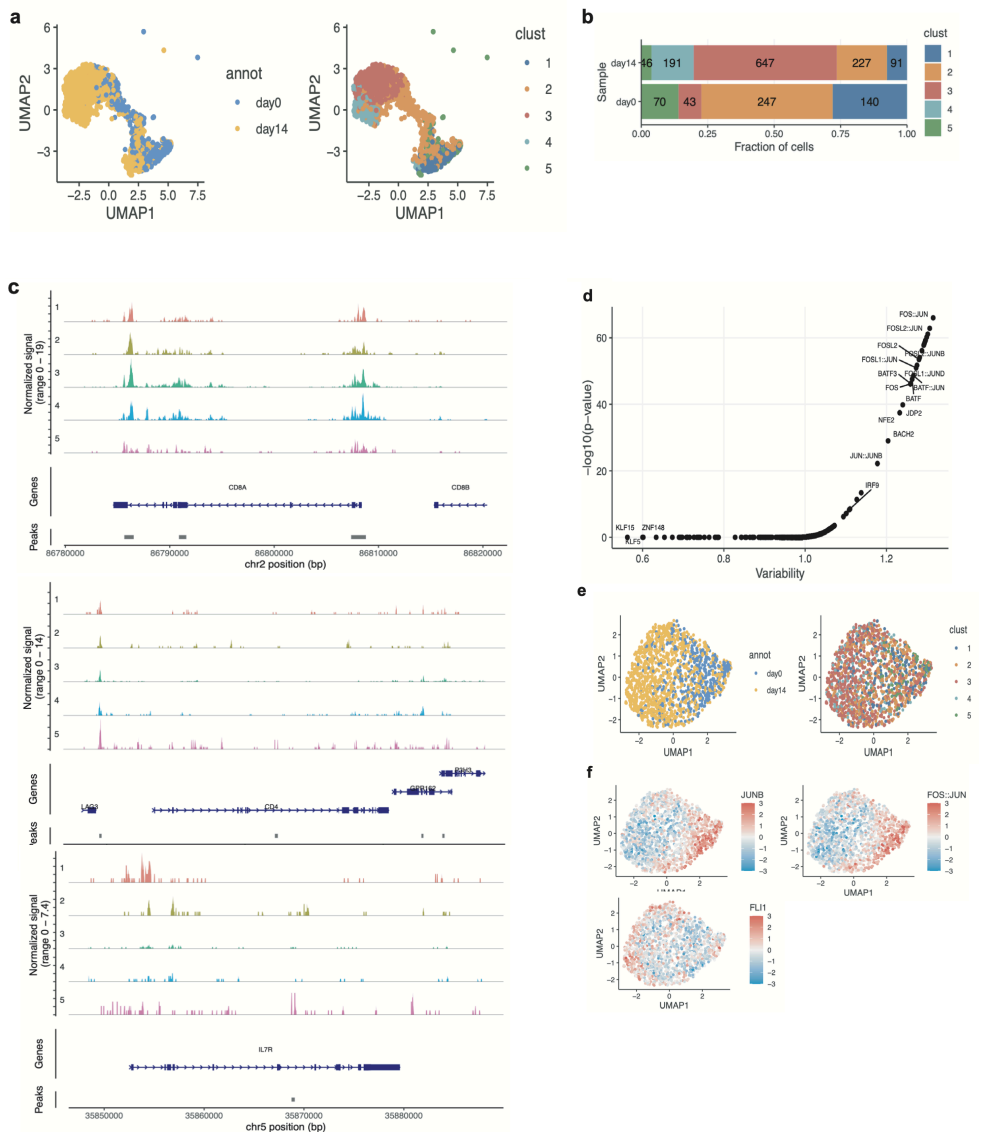
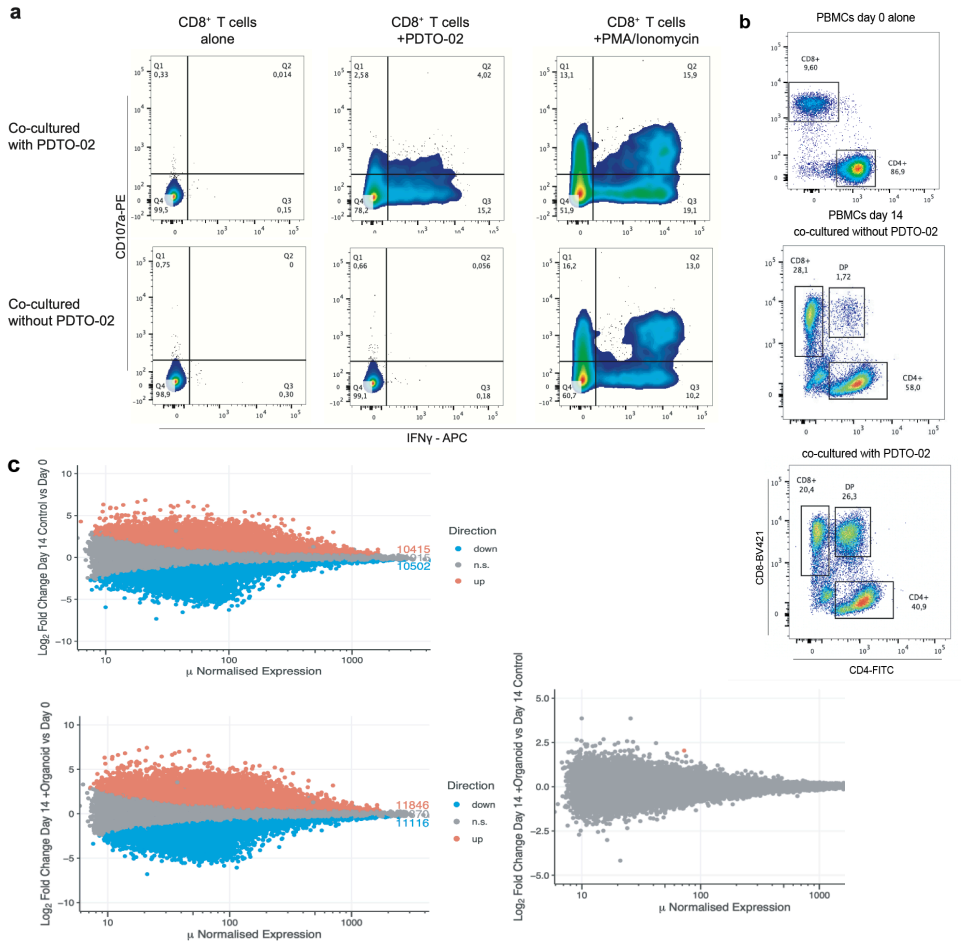


Figure 2: scATAC sequencing of PBMC samples at baseline and after two-week co-culture with MMR-d CRC PDTO-01. **a**. Left: UMAP embedding of single cells colored by the time of collection day 0 (blue) and day 14 (yellow). Right: UMAP embedding of the same single cells colored by five cell clusters. **b**. Fraction of cell count for each cell cluster sample collected at day 0 and day 14. **c**. Gene coverage plots indicating normalized open chromatin of loci CD8, CD4 and ILR7 (top to bottom) for all five clusters. **d**. Graph showing significantly variable motifs identified based on transcription factor motif accessibility comparing day 0 and day 14 samples. **e**. Left: UMAP embedding based on transcription factor motif accessibility of single cells colored

by the time of collection day 0 (blue) and Day 14 (yellow). Right: UMAP embedding based on transcription factor motif accessibility of the same single cells colored by five cell clusters. **f.** UMAP embedding based on transcription factor motif accessibility colored by JUNB, FOS:JUN and FLI1 motifs.

Because processing of fragile co-cultured PBMCs and ensuring sufficient high quality cell input was technically challenging, we next aimed to determine the feasibility of bulk ATAC analysis. To test whether observed differences between day 0 and day 14 were due to culture conditions or tumor organoid stimulation, we included a day 14 sample which was cultured under the same conditions but without tumor organoids stimulation for bulk ATAC. Moreover, we used a different co-culture pair of tumor organoids and autologous PBMCs (PBMC-/PDTO-02) which elicits less tumor reactive T cells compared to PDTO-01 (Fig. 1c, 3a) to determine if it is possible to detect smaller cell populations using bulk ATAC. PDTO-02 organoids were also derived from an ICI responding MMR-d CRC tumor (Extended Data Fig, 1b) with a similar surface expression profile as PDTO-01. MHC class I was expressed at baseline and increased upon IFN $\gamma$  pre-stimulation, whereas MHC class II and PD-L1 was only expressed after IFN $\gamma$  pre-stimulation (Fig. 1e). Co-culture of PDTO-02 with autologous PBMCs elicited tumor reactive CD8<sup>+</sup> T cells as observed by increased IFN $\gamma$  and CD107a expression at day 14 when stimulated with PDTO-02 compared to unstimulated PBMCs. No tumor reactivity was observed by flow cytometry analysis when PBMCs were cultured for two weeks without presence of tumor organoids and then stimulated with PDTO-02 (Fig. 3a). Interestingly, after two-weeks of co-culture a CD4<sup>+</sup> CD8<sup>+</sup> double positive (DP) T cell population was observed, which was not present at baseline or when cultured in absence of tumor organoids (Fig. 3b). DP T cells did not show increased IFN $\gamma$  and CD107a expression upon PDTO-02 stimulation and PMA/Ionomycin stimulation nearly exclusively increased CD107a expression. CD4<sup>+</sup> T cells showed minor IFN $\gamma$  increase upon PDTO-02 stimulation (Extended Data Fig. 1a). After collection of samples at day 0 and day 14 with and without co-culture of PDTO-02, bulk ATAC was performed on biological replicates. Analysis confirmed a high-quality library and well-defined peaks of, for example, locus CD8 could be observed (Extended Data Fig. 1g). An increase of accessible CD8A locus can be depicted in day 14 samples compared to day 0 samples, in line with a CD8<sup>+</sup> T cell increase during co-culture as shown by flow cytometry analysis (Fig. 3b, Extended

Data Fig. 1g). To compare differences between PBMCs cultured with or without tumor organoids, we analyzed the amount of differential accessible regions (DAR) between all conditions. While around 20k different peaks are observed between condition day 0 and day 14, nearly no differences were detected between day 14 with and without co-culture of PDO-02 (Fig. 3c). Comparing our bulk ATAC data to publicly available data<sup>21</sup> on activated T cells showed correlation to an activated T cell signature (Extended Data 1h). Taken together, we demonstrated how co-culture product of tumor organoids and autologous T cells can be used to analyze the regulatory landscape of tumor reactive T cells. Although technical challenges need to be further improved to validate our results, using scATACseq we identified JUNB, FOS:JUN, and FLI1 motifs to be differentially expressed between T cell samples as day 0 and day 14. The addition of bulk ATAC sequencing provided relevant information which will help to improve time point selection for future experiments.



**Figure 3: Bulk ATAC sequencing of PDTO-02 co-culture samples at day 0 and day 14.**

**a.** Representative flow cytometry plots of CD8<sup>+</sup> T cells after two-week (co)-culture with (top) or without (bottom) PDTO-02. Plots show IFN $\gamma$  and CD107a expression of CD8<sup>+</sup> T cells unstimulated (alone), stimulated (+PDTO-02) or simulated with positive control (+PMA/Ionomycin). **b.** Flow cytometry dot plots indicating fractions of CD4<sup>+</sup>, CD8<sup>+</sup> and DP T cells of autologous PBMCs at day 0 (top), day 14 after (co)-culture with (middle) or without (bottom) PDTO-02 presence. **c.** Volcano plots indicating differential accessible regions in sample day 14 without PDTO-02 presence during co-culture (day 14 control) compared to day 0 (top left), day 14 with PDTO-02 presence during co-culture (day 14 + organoid) compared to day 0 (bottom left) and day 14 with compared to without presence or PDTO-02 during co-culture (bottom right).

## DISCUSSION AND OUTLOOK

Advances in single cell technologies have accelerated research that aims to understand anti-tumor immunity. Here, we leveraged our autologous PBMC and PDO co-culture system to compare the regulatory landscape of CD8<sup>+</sup> T cells before and after interaction with tumor organoids.

We used two co-culture pairs of PBMCs and MMR-d CRC PDOs derived from responding patients to ICI and successfully generated tumor reactive CD8<sup>+</sup> T cells. For both models an increase of the CD8<sup>+</sup> T cell population and a decrease of the CD4<sup>+</sup> T cell population could be observed by flow cytometry analysis day 14 compared to day 0 of the co-culture. We were successful in showing that CD8<sup>+</sup> were the dominating cell population using scATAC and bulk ATAC analysis. Notably, analysis of the CD8A locus, using bulk ATAC data of PDO-02, clearly demonstrated an increase of CD8<sup>+</sup> T cells at day 14 but also allowed the detection of CD8<sup>+</sup> T cell population at day 0 which only made up around 10% of total CD3<sup>+</sup> T cells. Clustering of scATAC data of PDO-01 samples indicated two distinct populations based on time points day 0 and day 14 implying changes of the regulatory landscape over time. Also, some overlap was observed between the time points and, based on open chromatin assessment, five clusters were identified. Our data suggests the presence of naive T cells in two clusters (cluster 1 and 5) which may overlap with samples from day 0. To better understand the value of this approach, other tumor organoid and PBMC pairs need to be tested to replicate the identified clusters and then better characterize each cluster for their cell populations.

Furthermore, scATACseq identified FOS:JUN and BATF as significantly differential accessible transcription factor DNA binding motif at the two time points. Those genes have been described as markers for T cell exhaustion<sup>17</sup>. Given a high tumor reactivity in PDO-01 throughout the co-culture it is likely that T cells enter an exhausted state. Surprisingly though, FOS:JUN and BAT seem more accessible in day 1 which would mean reinvigoration of a less exhausted state during co-culture conditions. Additional experiments are required to elaborate those findings. The genetic deletion of another significantly differential accessible transcription factor motif, FLI1, has recently been shown to increase T cell effector function<sup>22</sup>. Thus, providing evidence that scATAC

sequencing of co-cultured autologous T cells may be used to identify T cell exhaustion markers and relevant regulatory elements to interfere with such.

However, it has to be noted that the library complexity of the scATAC sequencing data was suboptimal and additional experiments are necessary to confirm our results. The technical challenging part of the performed single cell experiment seems to be the fragile state of PBMCs which resulted in an overall low cell input. Insufficient coverage of accessible sites per cell, make it challenging to resolve subsets of T cells as they share the majority of accessible sites. Therefore, technical variations between cells may be larger than actual biological difference between cells. To improve our readout in future experiments we aim to use a droplet-based readout instead of single nuclei sorting into plates as this likely facilitates less harsh treatment of fragile PBMCs. For example, our bulk ATAC experiments did not include a cell sorting step and we were able to produce a high-quality library in those experiments.

Using bulk ATAC analysis of samples from PDTO-02 at day 0 and day 14 improved data quality compared to scATAC and showed that major regulatory landscape changes of T cells after two weeks of (co-)culture are likely due to culture conditions but not stimulation of PDTOs. However, flow cytometry analysis confirmed the presence of reactive CD8<sup>+</sup> T cells upon PDTO-02 stimulation only after co-culture in presence of PDTO-02. No reactive CD8<sup>+</sup> T cells were generated upon culture of PBMCs in absence of PDTO-02 and likewise a CD4<sup>+</sup>/CD8<sup>+</sup> double positive T cell population is not present without PDTO-02. Hence, although samples with and without co-culture of tumor organoids showed distinct T cell populations, bulk ATAC analysis failed to identify those smaller sub-populations. It may be that such populations were too small to detect or open chromatin changes were not distinct enough compared to a much broader influence by cell culture conditions.

Moreover, bulk ATAC data suggests that earlier time points may help to detect T cell changes due to tumor organoid stimulation and to lesser extent as a results of culturing conditions. Therefore, we aim to include samples taken at baseline and over the first hours of co-culture for future experiments. After selection of optimal time points, that reflect changes based on T cell and tumor organoid interaction, we plan to include a larger sample size of tumor organoids and autologous PBMCs for scATAC analysis to identify T cell states and regulatory elements that are relevant in

tumor organoid responses. Lastly, we would like to investigate whether interference with identified regulatory elements influences anti-tumor responses to potentially improve such.

Overall, our results provide the basis to further pursue a combination of analyzing single cell chromatin landscapes with a model system that can track autologous T cell tumor responses over time.

## REFERENCES

1. Waldman, A. D., J. M. Fritz and M. J. Lenardo (2020). "A guide to cancer immunotherapy: from T cell basic science to clinical practice." *Nat Rev Immunol* 20(11): 651-668.
2. Hodi, F. S., S. J. O'Day, D. F. McDermott, R. W. Weber, J. A. Sosman, J. B. Haanen, R. Gonzalez, C. Robert, D. Schadendorf, J. C. Hassel, W. Akerley, A. J. van den Eertwegh, J. Lutzky, P. Lorigan, J. M. Vaubel, G. P. Linette, D. Hogg, C. H. Ottensmeier, C. Lebbe, C. Peschel, I. Quirt, J. I. Clark, J. D. Wolchok, J. S. Weber, J. Tian, M. J. Yellin, G. M. Nichol, A. Hoos and W. J. Urba (2010). "Improved survival with ipilimumab in patients with metastatic melanoma." *N Engl J Med* 363(8): 711-723.
3. Topalian, S. L., F. S. Hodi, J. R. Brahmer, S. N. Gettinger, D. C. Smith, D. F. McDermott, J. D. Powderly, R. D. Carvajal, J. A. Sosman, M. B. Atkins, P. D. Leming, D. R. Spigel, S. J. Antonia, L. Horn, C. G. Drake, D. M. Pardoll, L. Chen, W. H. Sharfman, R. A. Anders, J. M. Taube, T. L. McMiller, H. Xu, A. J. Korman, M. Jure-Kunkel, S. Agrawal, D. McDonald, G. D. Kollia, A. Gupta, J. M. Wigginton and M. Sznol (2012). "Safety, activity, and immune correlates of anti-PD-1 antibody in cancer." *N Engl J Med* 366(26): 2443-2454.
4. Ribas, A. and J. D. Wolchok (2018). "Cancer immunotherapy using checkpoint blockade." *Science* 359(6382): 1350-1355.
5. Larkin, J., V. Chiarion-Sileni, R. Gonzalez, J. J. Grob, P. Rutkowski, C. D. Lao, C. L. Cowey, D. Schadendorf, J. Wagstaff, R. Dummer, P. F. Ferrucci, M. Smylie, D. Hogg, A. Hill, I. Marquez-Rodas, J. Haanen, M. Guidoboni, M. Maio, P. Schöffski, M. S. Carlino, C. Lebbe, G. McArthur, P. A. Ascierto, G. A. Daniels, G. V. Long, L. Bastholt, J. I. Rizzo, A. Balogh, A. Moshyk, F. S. Hodi and J. D. Wolchok (2019). "Five-Year Survival with Combined Nivolumab and Ipilimumab in Advanced Melanoma." *N Engl J Med* 381(16): 1535-1546.
6. Li, H., P. A. van der Merwe and S. Sivakumar (2022). "Biomarkers of response to PD-1 pathway blockade." *Br J Cancer* 126(12): 1663-1675.
7. Zheng, L., S. Qin, W. Si, A. Wang, B. Xing, R. Gao, X. Ren, L. Wang, X. Wu, J. Zhang, N. Wu, N. Zhang, H. Zheng, H. Ouyang, K. Chen, Z. Bu, X. Hu, J. Ji and Z. Zhang (2021). "Pan-cancer single-cell landscape of tumor-infiltrating T cells." *Science* 374(6574): abe6474.
8. Tume, P. C., C. L. Harview, J. H. Yearley, I. P. Shintaku, E. J. Taylor, L. Robert, B. Chmielowski, M. Spasic, G. Henry, V. Ciobanu, A. N. West, M. Carmona, C. Kivork, E. Seja, G. Cherry, A. J. Gutierrez, T. R. Grogan, C. Mateus, G. Tomasic, J. A. Glaspy, R. O. Emerson, H. Robins, R. H. Pierce, D. A. Elashoff, C. Robert and A. Ribas (2014). "PD-1 blockade induces responses by inhibiting adaptive immune resistance." *Nature* 515(7528): 568-571.
9. Ribas, A. and J. D. Wolchok (2018). "Cancer immunotherapy using checkpoint blockade." *Science* 359(6382): 1350-1355.
10. Yost, K. E., A. T. Satpathy, D. K. Wells, Y. Qi, C. Wang, R. Kageyama, K. L. McNamara, J. M. Granja, K. Y. Sarin, R. A. Brown, R. K. Gupta, C. Curtis, S. L. Bucktrout, M. M. Davis, A. L. S.



- Chang and H. Y. Chang (2019). "Clonal replacement of tumor-specific T cells following PD-1 blockade." *Nat Med* 25(8): 1251-1259.
11. Yost, K. E., H. Y. Chang and A. T. Satpathy (2021). "Recruiting T cells in cancer immunotherapy." *Science* 372(6538): 130-131.
  12. Spitzer, M. H., Y. Carmi, N. E. Reticker-Flynn, S. S. Kwek, D. Madhiredy, M. M. Martins, P. F. Gherardini, T. R. Prestwood, J. Chabon, S. C. Bendall, L. Fong, G. P. Nolan and E. G. Engleman (2017). "Systemic Immunity Is Required for Effective Cancer Immunotherapy." *Cell* 168(3): 487-502 e415.
  13. Pauken, K. E., M. A. Sammons, P. M. Odorizzi, S. Manne, J. Godec, O. Khan, A. M. Drake, Z. Chen, D. R. Sen, M. Kurachi, R. A. Barnitz, C. Bartman, B. Bengsch, A. C. Huang, J. M. Schenkel, G. Vahedi, W. N. Haining, S. L. Berger and E. J. Wherry (2016). "Epigenetic stability of exhausted T cells limits durability of reinvigoration by PD-1 blockade." *Science* 354(6316): 1160-1165.
  14. Scott, A. C., F. Dunder, P. Zumbo, S. S. Chandran, C. A. Klebanoff, M. Shakiba, P. Trivedi, L. Menocal, H. Appleby, S. Camara, D. Zamarin, T. Walther, A. Snyder, M. R. Femia, E. A. Comen, H. Y. Wen, M. D. Hellmann, N. Anandasabapathy, Y. Liu, N. K. Altorki, P. Lauer, O. Levy, M. S. Glickman, J. Kaye, D. Betel, M. Philip and A. Schietinger (2019). "TOX is a critical regulator of tumour-specific T cell differentiation." *Nature* 571(7764): 270-274.
  15. Satpathy, A. T., J. M. Granja, K. E. Yost, Y. Qi, F. Meschi, G. P. McDermott, B. N. Olsen, M. R. Mumbach, S. E. Pierce, M. R. Corces, P. Shah, J. C. Bell, D. Jhutti, C. M. Nemecek, J. Wang, L. Wang, Y. Yin, P. G. Giresi, A. L. S. Chang, G. X. Y. Zheng, W. J. Greenleaf and H. Y. Chang (2019). "Massively parallel single-cell chromatin landscapes of human immune cell development and intratumoral T cell exhaustion." *Nat Biotechnol* 37(8): 925-936.
  16. Philip, M., L. Fairchild, L. Sun, E. L. Horste, S. Camara, M. Shakiba, A. C. Scott, A. Viale, P. Lauer, T. Merghoub, M. D. Hellmann, J. D. Wolchok, C. S. Leslie and A. Schietinger (2017). "Chromatin states define tumour-specific T cell dysfunction and reprogramming." *Nature* 545(7655): 452-456.
  17. Belk, J. A., W. Yao, N. Ly, K. A. Freitas, Y. T. Chen, Q. Shi, A. M. Valencia, E. Shifrut, N. Kale, K. E. Yost, C. V. Duffy, B. Daniel, M. A. Hwee, Z. Miao, A. Ashworth, C. L. Mackall, A. Marson, J. Carnevale, S. A. Vardhana and A. T. Satpathy (2022). "Genome-wide CRISPR screens of T cell exhaustion identify chromatin remodeling factors that limit T cell persistence." *Cancer Cell* 40(7): 768-786 e767.
  18. Baxter, A. E., H. Huang, J. R. Giles, Z. Chen, J. E. Wu, S. Drury, K. Dalton, S. L. Park, L. Torres, B. W. Simone, M. Klapholz, S. F. Ngiow, E. Freilich, S. Manne, V. Alcalde, V. Ekshyyan, S. L. Berger, J. Shi, M. S. Jordan and E. J. Wherry (2023). "The SWI/SNF chromatin remodeling complexes BAF and PBAF differentially regulate epigenetic transitions in exhausted CD8(+) T cells." *Immunity* 56(6): 1320-1340 e1310.
  19. Kirschenbaum, D., K. Xie, F. Ingelfinger, Y. Katzenelenbogen, K. Abadie, T. Look, F. Sheban, T. S. Phan, B. Li, P. Zwicky, I. Yofe, E. David, K. Mazuz, J. Hou, Y. Chen, H. Shaim, M. Shanley, S. Becker, J. Qian, M. Colonna, F. Ginhoux, K. Rezvani, F. J. Theis, N. Yosef, T. Weiss, A. Weiner and I. Amit (2023). "Time-resolved single-cell transcriptomics defines immune trajectories in glioblastoma." *Cell*.
  20. Cattaneo, C. M., K. K. Dijkstra, L. F. Fanchi, S. Kelderman, S. Kaing, N. van Rooij, S. van den Brink, T. N. Schumacher and E. E. Voest (2020). "Tumor organoid-T-cell coculture systems." *Nat Protoc* 15(1): 15-39.
  21. Bediaga, N. G., H. D. Coughlan, T. M. Johanson, A. L. Garnham, G. Naselli, J. Schroder, L. G. Fearnley, E. Bandala-Sanchez, R. S. Allan, G. K. Smyth and L. C. Harrison (2021). "Multi-level remodelling of chromatin underlying activation of human T cells." *Sci Rep* 11(1): 528.
  22. Chen, Z., E. Arai, O. Khan, Z. Zhang, S. F. Ngiow, Y. He, H. Huang, S. Manne, Z. Cao, A. E. Baxter, Z. Cai, E. Freilich, M. A. Ali, J. R. Giles, J. E. Wu, A. R. Greenplate, M. A. Hakeem, Q. Chen, M. Kurachi, K. Nzingha, V. Ekshyyan, D. Mathew, Z. Wen, N. A. Speck, A. Battle, S. L.

Berger, E. J. Wherry and J. Shi (2021). "In vivo CD8(+) T cell CRISPR screening reveals control by Fli1 in infection and cancer." *Cell* 184(5): 1262-1280 e1222

## METHODS

### Organoid culture

Tumor organoids were derived from two MMR-d CRC tumors, PDTO-01 and PDTO-02. Establishment of the respective organoid lines from tumor material was performed as previously reported<sup>1,2</sup>. In brief, tumor tissue was mechanically dissociated and digested with 1.5 mg ml<sup>-1</sup> of collagenase II (Sigma-Aldrich), 10 µg ml<sup>-1</sup> of hyaluronidase type IV (Sigma-Aldrich) and 10 µM Y-27632 (Sigma-Aldrich). Cells were embedded in Cultrex RGF BME type 2 (3533-005-02, R&D systems) and placed into a 37 °C incubator for 20 min. Human CRC organoid medium is composed of Ad-DF+++ (Advanced DMEM/F12 (GIBCO) supplemented with 2 mM Ultraglutamine I (Lonza), 10 mM HEPES (GIBCO), 100 U ml<sup>-1</sup> of each penicillin and streptomycin (GIBCO), 10% noggin-conditioned medium, 20% R-spondin1-conditioned medium, 1× B27 supplement without vitamin A (GIBCO), 1.25 mM N-acetylcysteine (Sigma-Aldrich), 10 mM nicotinamide (Sigma-Aldrich), 50 ng ml<sup>-1</sup> human recombinant EGF (Peprotech), 500 nM A83-01 (Tocris), 3 µM SB202190 (Cayman Chemicals) and 10 nM prostaglandin E2 (Cayman Chemicals). Organoids were passaged depending on growth every 1–2 weeks by incubating in TrypLE Express (Gibco) for 5–10 min followed by embedding in BME. Organoids were authenticated by SNP array or STR analysis and were regularly tested for Mycoplasma using Mycoplasma PCR43 and the MycoAlert Mycoplasma Detection Kit (LT07-318). In the first two weeks of organoid culture, 1× Primocin (Invivogen) was added to prevent microbial contamination. Procedures performed with patient samples were approved by the Medical Ethical Committee of the Netherlands Cancer Institute–Antoni van Leeuwenhoek hospital (NL48824.031.14) and written informed consent was obtained from all of the patients. Mismatch repair status was assessed using a standard protocol for the Ventana automated immunostainer for MLH1 clone M1 (Roche), MSH2 clone G219-1129 (Roche), MSH6 clone EP49 (Abcam) and PMS2 clone EP51 (Agilent Technologies).

## Phenotyping tumor organoids

For organoid surface expression stainings, tumor organoids were dissociated into single cells using TrypLE Express (Gibco), washed twice in cold FACS buffer (PBS, 5 mM EDTA, 1% bovine serum antigen), and stained with anti-HLA-A/B/C-PE (1:20, W6/32, BD Biosciences), anti-HLA-DR/DP/DQ-FITC (1:20, Tü39, Biolegend), anti-PD-L1-APC (1:200, MIH1, eBioscience) and 1:2,000 near-infrared (NIR) viability dye (Life Technologies), or isotype controls (1:20 FITC; 1:20, PE; or 1:200, APC) mouse IgG1 kappa (BD Biosciences). Tumor cells were incubated for 30 min at 4 °C in the dark and washed twice with FACS buffer. All samples were recorded with the BD LSR Fortessa Cell Analyzer SORP flow cytometer using FACSDiVa (v.8.0.2; BD Biosciences). Data were analysed using FlowJo (v.10.6.1; BD) and presented using GraphPad Prism (v.9.0.0; GraphPad).

## Co-culture

To generate PBMC samples of both autologous co-culture pairs and freeze samples at baseline (day 0) and after two-weeks in presence or absence of tumor organoids (day 14), the co-culture was performed as described before<sup>1,2,3</sup>. In short, tumor organoids were isolated from BME by washing with cold PBS 2 days before addition of the PBMCs. After washing CRC organoids were resuspended in culture medium in the presence of 10  $\mu$ M Y27632. A day before coculture, organoids were stimulated with 200 ng/mL of IFN $\gamma$  (Peprotech). On the same day frozen PBMCs, which were beforehand isolated from peripheral blood using Ficoll-Paque, were thawed and cultured overnight in T cell culture medium (RPMI 1640 (Thermo Fisher Scientific) supplemented with 1% Pen Strep and 10% human serum (Sigma Aldrich)) with 150 U/mL IL-2 (Peprotech). Before start of the co-culture at day 0, 500k cells of PBMCs were cryopreserved as baseline sample for later use. Organoids were dissociated into single cells and plated at a 1:20 target:effector ratio with autologous PBMCs, in an anti-CD28 coated (clone CD28.2, eBioscience), 96well, Ubottomed plate, in the presence of 150 U/mL of IL2 (Proleukin) and 20  $\mu$ g/mL of anti-PD1/nivolumab (Opdivo). Half of the medium was refreshed every 2–3 d with addition of new IL2 and anti-PD1. PBMCs were collected and restimulated as above after 1 week of co-

culture. A second sample of 500k cells was cryopreserved at day 14. Tumor reactivity was measured after 2 weeks of co-culture.

#### Tumor reactivity assay

Evaluation of tumor reactivity towards PDTO-01 and PDTO-02 was performed as described previously<sup>1,2</sup>. Two days before the experiment, organoids were isolated from BME by washing with cold PBS before being resuspended in CRC organoid medium with 10  $\mu$ M Y-27632 (Sigma-Aldrich). The organoids were stimulated with 200 ng/mL IFN $\gamma$  (Peprotech) 24 h before the experiment. For the recognition assay and intracellular staining, tumor organoids were dissociated into single cells and plated in 96-well U-bottom plates with PBMCs at a 1:2 target:effector ratio. As a positive control, PBMCs were stimulated with 50 ng/mL of phorbol-12-myristate-13-acetate (PMA) (Sigma-Aldrich) and 1  $\mu$ g/mL of ionomycin (Sigma-Aldrich). As a negative control (alone), T cell culture medium was added to PBMCs. Cells were stained with anti-CD107a-PE (1:50, Biolegend). After 1 h of incubation at 37 °C, GolgiSTOP (BD Biosciences, 1:1500) and GolgiPlug (BD Biosciences, 1:1000) were added. After 4 h of incubation at 37 °C, PBMCs were washed twice in cold FACS buffer (PBS, 5 mM EDTA, 1% bovine serum antigen) and stained with anti-CD3-PerCP-Cy5.5 (1:20, BD Biosciences), anti-CD4-FITC (1:20, BD Bioscience), anti-CD8-BV421 (1:200, BD Biosciences) and 1:2000 near-infrared (NIR) viability dye (Life Technologies) for 30 min at 4 °C. Cells were washed, fixed, using the Cytotfix/Cytoperm Kit (BD Biosciences), and stained with 1:40 anti-IFN $\gamma$ -APC (1:40, BD Biosciences) for 30 min at 4 °C. After two washing steps, cells were resuspended in 50mL FACS buffer and recorded with the BD LSR Fortessa Cell Analyzer SORP flow cytometer using FACSDiVa software (v.8.0.2; BD Biosciences). Data were analysed using FlowJo (v.10.6.1, BD) and presented using GraphPad Prism (v.9.0.0, GraphPad).

#### scATAC

sciATACseq was performed as previously described<sup>4</sup>. In brief, 2-5 $\times$ 10<sup>5</sup> cells were lysed for 3min in 500 $\mu$ L of RSB buffer (Tris-HCl pH 7.5 10mM, NaCl 10mM, MgCl<sub>2</sub> 3mM, NP40 0.1%, Tween-20 0.1%, digitonin 0.01%) in presence of cComplete

4

protease inhibitor cocktail (Roche). Next, cells were resuspended 3 times and washed in 10 mL of RSBT buffer (Tris-HCl pH 7.5 10mM, NaCl 10mM, MgCl<sub>2</sub> 3mM, Tween-20 0.1% and protease inhibitor cocktail) by inverting the tube 3 times and spinning at 500g for 10min at 4°C. Next, the buffer was removed and 2500 nuclei were resuspended in 7.6µL of cold PBS and pipetted in a well of a 96-well plate with 1µL of i7 and i5 transposons and 10.4µL of transposition mix containing 10µL of 2xTD buffer (20 mM Tris, 10 mM MgCl<sub>2</sub>, 20% dimethylformamide, pH adjusted to 7.6), 0.2µL digitonin 1% and 0.2µL Tween 10%. The tagmentation was carried at 55°C for 30min, nuclei were pooled and stained with 3µM 4',6-diamidino-2-phenylindole (DAPI). The reaction was stopped by incubation at 37°C for 15 min with 20µL 40 mM EDTA supplemented with spermidine 1mM. Next, 25 nuclei were sorted into either one or four 96 well plates (see run details) containing 11µL of EB buffer (Qiagen) and 1µL of Proteinase K 10 mg/ml (Roche). Decrosslinking was carried overnight at 65°C and PCR was performed by adding 25µL of KAPA HiFi HotStart ReadyMix (Roche), 5µL of P5 and P7 primers (see oligonucleotides list), 1µL of BSA 10mg/mL and 2 µL H<sub>2</sub>O. The thermocycler was set up as follows: 72°C for 3min, 98°C for 30s, 21 cycles of 98°C for 10s, 63°C for 30s, 72°C for 1min and finally 72°C for 5min. Next, all PCR reactions were pooled and 1mL of the solution was purified using DNA clean & concentrator 5 (Zymo Research) following manufacturer instructions. Next, the library was size selected by 1x and 0.55x selection steps using AMPure XP beads (Beckman Coulter), followed by purification with QIAquick PCR purification kit (Qiagen). Finally, libraries were sequenced with a NextSeq 550 system (Illumina) using a customized protocol<sup>5</sup> (genomic DNA read 1 (cycles 1–51), index 1 (transposon i7, cycles 52–59, followed by 27 dark cycles, and PCR i7, cycles 60–67), index 2 (PCR i5, cycles 68–75, followed by 21 dark cycles, and transposon i5, cycles 76–83), and genomic DNA read 2 (cycles 84–134).

#### Bulk ATAC

Bulk ATAC was performed as previously described<sup>4</sup>. In brief, 50,000 cells were collected in cold PBS and lysed with a 2x lysis buffer (Tris-HCl pH7.5 1M, NaCl 5M, MgCl<sub>2</sub> 1M, 10% IGEPAL). Next, cells were pelleted and incubated with 2xTD buffer and 2 µL transposon mix. Next, PCR amplification was carried twice by KAPA HiFi

HotStart ReadyMix using P5 and P7 indexed primers (see oligonucleotide list). Fragments between 200 and 700 bp were purified using AMPure XP beads. Quality control was performed by Bioanalyzer High Sensitivity DNA analysis (Agilent).

#### Data analysis

##### Data preparation

Data was prepared as previously described<sup>4</sup>. Fastq files from single cell combinatorial indexing ATACseq were edited such that the combination of i5, i7, P5 and P7 barcodes (further referred to as 'barcode') from fastq comments were prepended with the 'BC:Z:' tag to allow transfer of barcodes to alignment files. Edited fastq files were mapped to the GRCh38 reference genome with the bwa program version 0.7.17-r118 using the command 'bwa mem -MC'<sup>6</sup>. Mapped reads were filtered with samtools version 1.10 using 'samtools view -h -b -q 10'<sup>7</sup>. Paired-end alignments were further processed to apply the +4, -5 Tn5 shift to proper pairs, deduplicated and matched to valid experimental barcodes, and resulting fragments were written to tabix files, using a custom R script. Fragments were considered duplicates when they matched chromosome, start and end positions, strand of the first mate and barcode. For the bulk data, reads were aligned to the GRCh38 human reference genome using bwa mem<sup>23</sup>. Using samtools, reads mapped as proper pairs (-f 3) and with mapping quality > 10 (-q 10) were retained. MACS2 was used to call peaks with the arguments "-g hs --nomodel" and for each sample count reads overlapping peaks using the 'genomics range' package<sup>24</sup>. DESeq2<sup>25</sup> was used to normalize the counts and identify differentially accessible sites.

##### Quality control

Data quality control was performed as previously described<sup>4</sup>. Barcodes were considered to represent cells when at least 2,000 unique nuclear fragments were represented by that barcode and the TSS score for that barcode exceeded 4. TSS scores were calculated by taking 100 basepairs centred at the transcription start site of UCSC's known genes<sup>8</sup>, along with 1000 basepair upstream and downstream flanks. The number of overlapping fragments were determined for these TSSs and flanks, and divided by the 100 and 1000 basepair widths of the regions. The TSS

score is then the ratio between the number for TSSs and the number for flanks. The fragments of included cells were then used to call peaks using MACS2 callpeak version 2.2.7.1<sup>9</sup> with the arguments '-g mm -f BED -nomodel -extsize 200 -shift -100 -keep-duplicates=all'. A count matrix was constructed by quantifying the number of overlapping fragments in each cell with the peaks. Doublets were called with the scDbfFinder<sup>10</sup> R package with the arguments 'aggregateFeatures = TRUE, nfeatures = 25, processing = "normFeatures"', which is their recommended setting for single cell ATACseq. We further excluded cells that had less than 2,000 fragments in peaks. In addition, we inspected banding scores<sup>11</sup>, duplication rates, fraction of reads mapping to mitochondria, cell-wise GC bias, fragment length distributions and fraction of reads in peaks, but none of these were used as criteria for including or excluding cells.

#### Dimensionality reduction

Dimensionality reduction was performed as previously described<sup>4</sup>. From the binarized count matrix, peaks were excluded where fragments were observed in less than 2% of cells. Moreover, we excluded peaks that were within 1.5kb of a TSS<sup>12</sup> (exclude promoter bit). Term frequency – inverse document frequency (TF-IDF) with a log transformation on the TF<sup>11</sup>, term was used as a weighting scheme for the binarized count matrix. The irlba package<sup>13</sup> was used to perform partial singular value decomposition of the scaled and centered TF-IDF matrix for the first 100 left and right singular vectors. The diagonal matrix was multiplied by the left singular vectors to obtain principal components. The mutual nearest neighbor method, per the 'reducedMNN' function in the batchelor R package<sup>14</sup>, was used on the principal components to integrate cells from different batches. The 2<sup>nd</sup>-50<sup>th</sup> corrected principal components were used to compute UMAPs using the uwot R package<sup>15</sup> with the arguments 'metric = "cosine", init = "agspectral"'.

#### Clustering and marker detection

For single cell ATAC analysis was performed as previously described with minor changes in marker peak detection<sup>4</sup>. Clustering of cells was performed using the Leiden algorithm on a shared nearest neighbor (SNN) graph computed on the batch-

integrated principal components. The SNN graph was computed using the 'makeSNNGraph' function from the bluster R/Bioconductor package<sup>16</sup> with the argument 'k = 15'. The 'cluster\_leiden' function from the igraph<sup>17</sup> R package was used for clustering, with the 'resolution\_parameter = 0.1' argument. Marker genes were detected using the 'find all markers' from the Seurat package<sup>18</sup>. 20% of cells in each cluster were randomly combined to form a reference level for the cluster membership variable. In this regression, when the cluster membership had a significant log-odds ratio as determined by a Wald test after adjusting for false discovery rate, the peak was considered a marker peak for the tested cluster.

#### DNA binding motif analysis

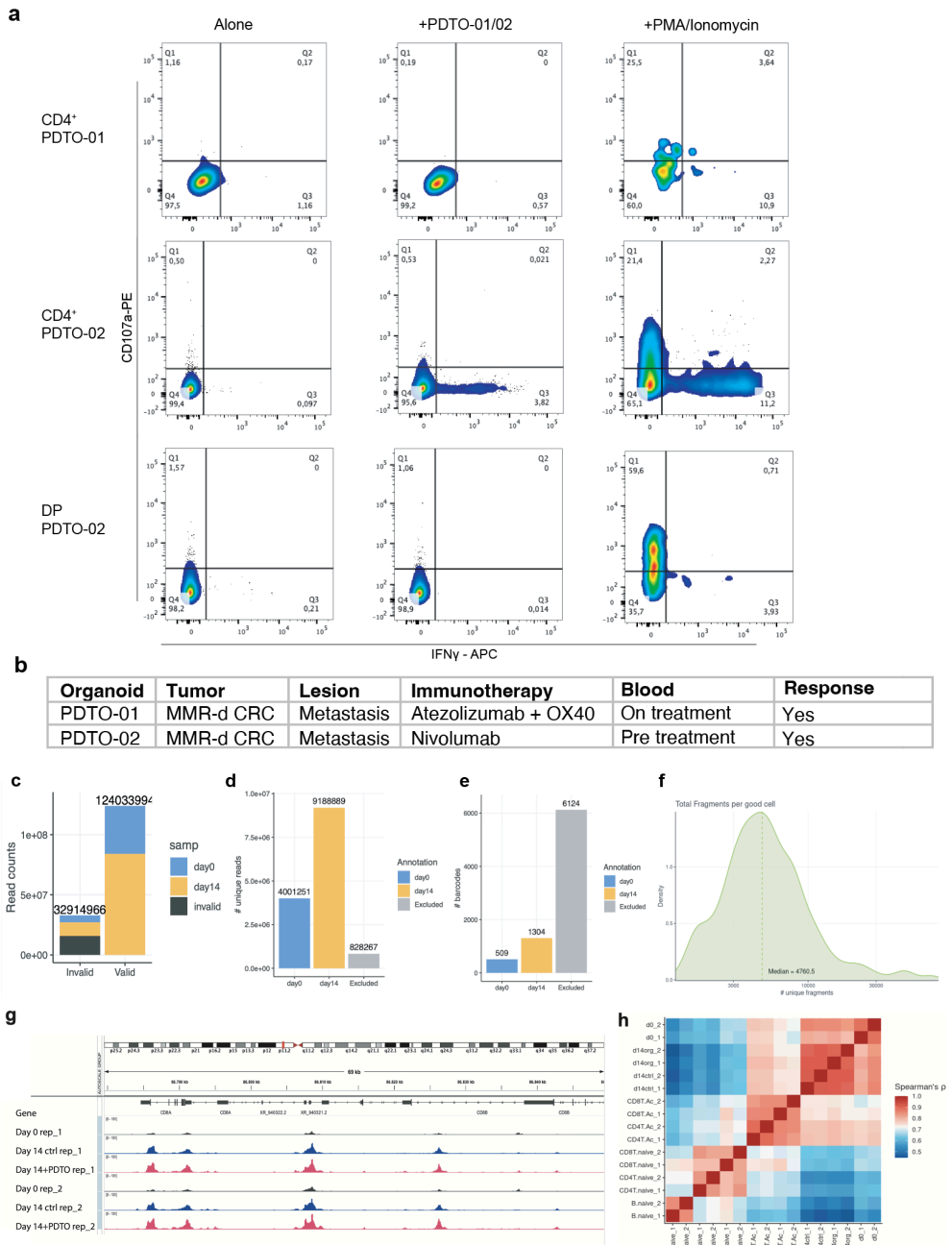
Motif analysis was performed as previously described with minor changes for bulk ATAC<sup>4</sup>. Position frequency matrices of motifs were obtained with the<sup>19</sup> R/Bioconductor package from the vertebrate's taxonomical group and core collection. For analyzing motifs, we looked at the DNA content of peaks where cluster membership was a significant factor according to a likelihood ratio test, comparing the logistic regression model described above against a reduced model where cluster membership was omitted from the predictor variables. Peaks were then scanned for motif matches using the 'matchMotifs' function from the motifmatchr<sup>20,21</sup> R/Bioconductor package. Motif Z-scores stabilized for GC bias were then computed using the chromVAR R/Bioconductor<sup>22</sup> package. For bulk ATAC motif analysis, motif position weight matrices were obtained from the JASPAR 2020 core vertebrate dataset as provided in the JAPSPAR2020 R package<sup>26</sup>. Then 'motifmatchr'<sup>27</sup> was used to scan for presence of TF motifs in each peak. Finally, Fisher's test was performed with FDR correction to assess the degree of enrichment of each motif in differentially accessible sites. For functional enrichment of differentially accessible sites, 'GREAT'<sup>28</sup> was used with default settings. For comparisons with Bediaga et al. 2021 T cell dataset<sup>29</sup>, their ATAC peaks were obtained from the GEO accession based on their reports and reads in these peaks were re-counted. Then DESeq2<sup>25</sup> was used to normalize all the data together. Finally, principal components were computed and pairwise Pearson's correlation coefficients using the variance stabilized counts from DESeq2 were generated.



## REFERENCES METHODS

1. Dijkstra, K. K., C. M. Cattaneo, F. Weeber, M. Chalabi, J. van de Haar, L. F. Fanchi, M. Slagter, D. L. van der Velden, S. Kaing, S. Kelderman, N. van Rooij, M. E. van Leerdam, A. Depla, E. F. Smit, K. J. Hartemink, R. de Groot, M. C. Wolkers, N. Sachs, P. Snaebjornsson, K. Monkhorst, J. Haanen, H. Clevers, T. N. Schumacher and E. E. Voest (2018). "Generation of Tumor-Reactive T Cells by Co-culture of Peripheral Blood Lymphocytes and Tumor Organoids." *Cell* 174(6): 1586-1598 e1512.
2. Cattaneo, C. M., K. K. Dijkstra, L. F. Fanchi, S. Kelderman, S. Kaing, N. van Rooij, S. van den Brink, T. N. Schumacher and E. E. Voest (2020). "Tumor organoid-T-cell coculture systems." *Nat Protoc* 15(1): 15-39.
3. Chalabi, M., L. F. Fanchi, K. K. Dijkstra, J. G. Van den Berg, A. G. Aalbers, K. Sikorska, M. Lopez-Yurda, C. Grootsholten, G. L. Beets, P. Snaebjornsson, M. Maas, M. Mertz, V. Veninga, G. Bounova, A. Broeks, R. G. Beets-Tan, T. R. de Wijkerslooth, A. U. van Lent, H. A. Marsman, E. Nuijten, N. F. Kok, M. Kuiper, W. H. Verbeek, M. Kok, M. E. Van Leerdam, T. N. Schumacher, E. E. Voest and J. B. Haanen (2020). "Neoadjuvant immunotherapy leads to pathological responses in MMR-proficient and MMR-deficient early-stage colon cancers." *Nat Med* 26(4): 566-576.
4. Braccioli, L., T. v. d. Brand, N. A. Saiz, C. Fountas, P. H. N. Celie, J. Kazokaitė-Adomaitienė and E. d. Wit (2022). "Identifying cross-lineage dependencies of cell-type specific regulators in gastruloids." *bioRxiv*: 2022.2011.2001.514697.
5. Christiansen, L., S. Amini, F. Zhang, M. Ronaghi, K. L. Gunderson and F. J. Steemers (2017). "Contiguity-Preserving Transposition Sequencing (CPT-Seq) for Genome-Wide Haplotyping, Assembly, and Single-Cell ATAC-Seq." *Methods Mol Biol* 1551: 207-221.
6. Li, H. (2013). Aligning sequence reads, clone sequences and assembly contigs with BWA-MEM. *arXiv preprint arXiv:1303.3997*.
7. Li, H., B. Handsaker, A. Wysoker, T. Fennell, J. Ruan, N. Homer, G. Marth, G. Abecasis, R. Durbin and S. Genome Project Data Processing (2009). "The Sequence Alignment/Map format and SAMtools." *Bioinformatics* 25(16): 2078-2079.
8. Hsu, F., W. J. Kent, H. Clawson, R. M. Kuhn, M. Diekhans and D. Haussler (2006). "The UCSC Known Genes." *Bioinformatics* 22(9): 1036-1046.
9. Zhang, Y., T. Liu, C. A. Meyer, J. Eeckhoutte, D. S. Johnson, B. E. Bernstein, C. Nusbaum, R. M. Myers, M. Brown, W. Li and X. S. Liu (2008). "Model-based analysis of ChIP-Seq (MACS)." *Genome Biol* 9(9): R137.
10. Germain, P.L., Robinson, M.D., Lun, A., Garcia Meixide, C., and Macnair, W. (2022). Doublet identification in single-cell sequencing data using scDblFinder. *F1000Research* 2022 10979 10, 979. doi:10.12688/f1000research.73600.2.
11. Cusanovich, D. A., A. J. Hill, D. Aghamirzaie, R. M. Daza, H. A. Pliner, J. B. Berletch, G. N. Filippova, X. Huang, L. Christiansen, W. S. DeWitt, C. Lee, S. G. Regalado, D. F. Read, F. J. Steemers, C. M. Disteché, C. Trapnell and J. Shendure (2018). "A Single-Cell Atlas of In Vivo Mammalian Chromatin Accessibility." *Cell* 174(5): 1309-1324 e1318.
12. Chung, C. Y., Z. Ma, C. Dravis, S. Preissl, O. Poirion, G. Luna, X. Hou, R. R. Girardi, B. Ren and G. M. Wahl (2019). "Single-Cell Chromatin Analysis of Mammary Gland Development Reveals Cell-State Transcriptional Regulators and Lineage Relationships." *Cell Rep* 29(2): 495-510 e496.
13. Baglama, J., and Reichel, L. (2006). Augmented Implicitly Restarted Lanczos Bidiagonalization *Methods*. <https://doi.org/10.1137/04060593X> 27, 19-42. doi:10.1137/04060593X.
14. Haghverdi, L., M. Buttner, F. A. Wolf, F. Büttner and F. J. Theis (2016). "Diffusion pseudotime robustly reconstructs lineage branching." *Nat Methods* 13(10): 845-848.

15. uwot: The Uniform Manifold Approximation and Projection (UMAP) Method for Dimensionality Reduction version 0.1.14 from CRAN <https://rdrr.io/cran/uwot/>.
16. Bioconductor - bluster <https://bioconductor.org/packages/release/bioc/html/bluster.html>.
17. Csárdi, G., Nepusz, T., Horvát, S., Traag, V., Zanini, F., and Noom, D. (2022). igraph. doi:10.5281/ZENODO.7199219.
18. Hao et al. Dictionary learning for integrative, multimodal and scalable single-cell analysis. *Nature Biotechnology* (2023)
19. Fornes, O., J. A. Castro-Mondragon, A. Khan, R. van der Lee, X. Zhang, P. A. Richmond, B. P. Modi, S. Correard, M. Gheorghe, D. Baranasic, W. Santana-Garcia, G. Tan, J. Cheneby, B. Ballester, F. Parcy, A. Sandelin, B. Lenhard, W. W. Wasserman and A. Mathelier (2020). "JASPAR 2020: update of the open-access database of transcription factor binding profiles." *Nucleic Acids Res* 48(D1): D87-D92.
20. Bioconductor - motifmatchr <https://bioconductor.org/packages/release/bioc/html/motifmatchr.html>.
21. Korhonen, J. H., K. Palin, J. Taipale and E. Ukkonen (2017). "Fast motif matching revisited: high-order PWMs, SNPs and indels." *Bioinformatics* 33(4): 514-521.
22. Schep, A. N., B. Wu, J. D. Buenrostro and W. J. Greenleaf (2017). "chromVAR: inferring transcription-factor-associated accessibility from single-cell epigenomic data." *Nat Methods* 14(10): 975-978.
23. Li H. and Durbin R. (2009) Fast and accurate short read alignment with Burrows-Wheeler Transform. *Bioinformatics*, 25:1754-60.
24. Lawrence M, Huber W, Pagès H, Aboyoun P, Carlson M, Gentleman R, Morgan M, Carey V (2013). "Software for Computing and Annotating Genomic Ranges." *PLoS Computational Biology*
25. Love MI, Huber W, Anders S (2014). "Moderated estimation of fold change and dispersion for RNA-seq data with DESeq2." *Genome Biology*, 15, 550
26. Baranasic D (2022). JASPAR2020: Data package for JASPAR database (version 2020). R package version 0.99.8
27. Schep A (2023). motifmatchr: Fast Motif Matching in R. doi:10.18129/B9.bioc.motifmatchr, R package version 1.24.0
28. Cory Y McLean, Dave Bristor, Michael Hiller, Shoa L Clarke, Bruce T Schaar, Craig B Lowe, Aaron M Wenger, and Gill Bejerano. "GREAT improves functional interpretation of cis-regulatory regions". *Nat. Biotechnol.* 28(5):495-501, 2010
29. Bediaga, N. G., H. D. Coughlan, T. M. Johanson, A. L. Garnham, G. Naselli, J. Schroder, L. G. Fearnley, E. Bandala-Sanchez, R. S. Allan, G. K. Smyth and L. C. Harrison (2021). "Multi-level remodelling of chromatin underlying activation of human T cells." *Sci Rep* 11(1): 528.



Extended Data Figure 1: Flow plots of CD4<sup>+</sup> and DP T cells and quality controls for single cell and bulk ATAC experiments. **a**. Representative flow cytometry plots of CD4<sup>+</sup> T cells after two-week (co)-culture with PDTO-01 (top), with PDTO-02 (middle) or of DP T cells with PDTO-02 co-culture (bottom). Plots show IFN $\gamma$  and

CD107a expression of CD4<sup>+</sup> or DP T cells unstimulated (alone), stimulated (+PDTO-02) or simulated with positive control (+PMA/Ionomycin). **b.** Table summarizing patient-derived tumor organoid data of PDTO-01 and PDTO-02. **c.** Barcode quality control of scATAC experiment indicating initial total valid read count of samples generated at day 0 (blue) and day 14 (yellow). **d.** Quality control analysis of unique reads after removing of PCR duplicates for samples generated at day 0 (blue) and day 14 (yellow). **e.** Quality control analysis of barcodes per sample generated at day 0 (blue), day 14 (yellow) and excluded (grey). **f.** Graph presenting the reads per cell distribution. **g.** Bulk ATAC genomic track showing gene coverage plot at the CD8A locus for all processed samples including replicates. **h.** Heatmap indicating Spearman's correlation of our ATAC data to published activated T cell ATAC data<sup>35</sup>.

But he was able to understand one thing: making a decision was only the beginning of things. When someone makes a decision, he is really diving into a strong current that will carry him to places he had never dreamed of when he first made the decision.

Paulo Coelho, *The Alchemist*

# $\gamma\delta$ T cells are effectors of immune checkpoint blockade in mismatch repair-deficient colon cancers with antigen presentation defects

5

Natasja L. de Vries<sup>1,2,13</sup>, Joris van de Haar<sup>3,4,5,13</sup>,  
**Vivien Veninga**<sup>3,4,13</sup>, Myriam Chalabi<sup>3,6,7,13</sup>, Marieke E.  
Ijsselsteijn<sup>1</sup>, Manon van der Ploeg<sup>1</sup>,  
Jitske van den Bulk<sup>1</sup>, Dina Ruano<sup>1</sup>,  
Jose G. van den Berg<sup>8</sup>, John B. Haanen<sup>3,7</sup>, Laurien J.  
Zeverijn<sup>3,4</sup>, Birgit S. Geurts<sup>3,4</sup>, Gijs F. de Wit<sup>3,4</sup>,  
Thomas W. Battaglia<sup>3,4</sup>, Hans Gelderblo<sup>9</sup>, Henk M. W.  
Verheul<sup>10</sup>, Ton N. Schumacher<sup>3,4,11</sup>, Lodewyk F. A.  
Wessels<sup>4,5,12</sup>, Frits Koning<sup>2,14</sup>,  
Noel F.C.C de Miranda<sup>1,14</sup> & Emile E. Voest<sup>3,4,14</sup>

<sup>13</sup>Co-first author

<sup>1</sup>Department of Pathology, Leiden University Medical Center, Leiden, The Netherlands.  
<sup>2</sup>Department of Immunology, Leiden University Medical Center, Leiden, The Netherlands.  
<sup>3</sup>Department of Molecular Oncology and Immunology, Netherlands Cancer Institute, Amsterdam, The Netherlands. <sup>4</sup>Oncode Institute, Utrecht, The Netherlands. <sup>5</sup>Division of Molecular Carcinogenesis, Netherlands Cancer Institute, Amsterdam, The Netherlands.  
<sup>6</sup>Gastrointestinal Oncology, Netherlands Cancer Institute, Amsterdam, The Netherlands.  
<sup>7</sup>Medical Oncology, Netherlands Cancer Institute, Amsterdam, The Netherlands.  
<sup>8</sup>Department of Pathology, Netherlands Cancer Institute, Amsterdam, The Netherlands.  
<sup>9</sup>Department of Medical Oncology, Leiden University Medical Center, Leiden, The Netherlands. <sup>10</sup>Department of Medical Oncology, Erasmus MC, Rotterdam, The Netherlands. <sup>11</sup>Department of Hematology, Leiden University Medical Center, Leiden, The Netherlands. <sup>12</sup>Faculty of EEMCS, Delft University of Technology, Delft, The Netherlands.  
<sup>13</sup>These authors contributed equally <sup>14</sup>These authors jointly supervised this work



## ABSTRACT

DNA mismatch repair-deficient (MMR-d) cancers present an abundance of neoantigens that is thought to explain their exceptional responsiveness to immune checkpoint blockade (ICB)<sup>1,2</sup>. Here, in contrast to other cancer types<sup>3,4,5</sup> we observed that 20 out of 21 (95%) MMR-d cancers with genomic inactivation of  $\beta$ 2-microglobulin (encoded by *B2M*) retained responsiveness to ICB, suggesting the involvement of immune effector cells other than CD8+ T cells in this context. We next identified a strong association between *B2M* inactivation and increased infiltration by  $\gamma\delta$  T cells in MMR-d cancers. These  $\gamma\delta$  T cells mainly comprised the V $\delta$ 1 and V $\delta$ 3 subsets, and expressed high levels of PD-1, other activation markers, including cytotoxic molecules, and a broad repertoire of killer-cell immunoglobulin-like receptors. In vitro, PD-1+  $\gamma\delta$  T cells that were isolated from MMR-d colon cancers exhibited enhanced reactivity to human leukocyte antigen (HLA)-class-I-negative MMR-d colon cancer cell lines and *B2M*-knockout patient-derived tumour organoids compared with antigen-presentation-proficient cells. By comparing paired tumour samples from patients with MMR-d colon cancer that were obtained before and after dual PD-1 and CTLA-4 blockade, we found that immune checkpoint blockade substantially increased the frequency of  $\gamma\delta$  T cells in *B2M*-deficient cancers. Taken together, these data indicate that  $\gamma\delta$  T cells contribute to the response to immune checkpoint blockade in patients with HLA-class-I-negative MMR-d colon cancers, and underline the potential of  $\gamma\delta$  T cells in cancer immunotherapy.



## INTRODUCTION

ICB targeting the PD-1–PD-L1 and/or CTLA-4 axes provides durable clinical benefits to patients who have cancers with MMR-d and high microsatellite instability<sup>6,7,8,9</sup>. The exceptional responses of cancers with MMR-d and high microsatellite instability to ICB is thought to be explained by their substantial burden of putative neoantigens, which originate from the extensive accumulation of mutations in their genomes<sup>1,2</sup>. This is consistent with the current view that PD-1 blockade mainly boosts endogenous antitumour immunity driven by CD8<sup>+</sup> T cells, which recognize HLA-class-I-bound neopeptides on cancer cells<sup>10,11,12</sup>. However, MMR-d colon cancers frequently lose HLA-class-I-mediated antigen presentation due to silencing of HLA class I genes, inactivating mutations in  $\beta$ 2-microglobulin (encoded by B2M) or other defects in the antigen processing machinery<sup>13,14,15,16</sup>, which can render these tumours resistant to CD8<sup>+</sup> T-cell-mediated immunity<sup>3,4,5,17</sup>. Notably, early evidence has indicated that B2M-deficient, MMR-d cancers can obtain durable responses to PD-1 blockade<sup>18</sup>, suggesting that immune cell subsets other than CD8<sup>+</sup> T cells contribute to these responses.

5 HLA-class-I-unrestricted immune cell subsets, which have the ability to kill tumour cells, include natural killer (NK) cells and  $\gamma\delta$  T cells.  $\gamma\delta$  T cells share many characteristics with their  $\alpha\beta$  T cell counterpart, such as cytotoxic effector functions, but express a distinct TCR that is composed of a  $\gamma$  and a  $\delta$  chain. Different subsets of  $\gamma\delta$  T cells are defined by their TCR  $\delta$  chain use, of which those expressing V $\delta$ 1 and V $\delta$ 3 are primarily ‘tissue-resident’ at mucosal sites, whereas those expressing V $\delta$ 2 are mainly found in blood<sup>19</sup>. Both adaptive and innate mechanisms of activation—for example, through stimulation of their  $\gamma\delta$  TCR or innate receptors such as NKG2D, DNAM-1, NKp30 or NKp44—have been described for  $\gamma\delta$  T cells<sup>20</sup>. Killer-cell immunoglobulin-like receptors (KIRs) are expressed by  $\gamma\delta$  T cells and regulate their activity depending on HLA class I expression in target cells<sup>21</sup>. Furthermore,  $\gamma\delta$  T cells were found to express high levels of PD-1 in MMR-d colorectal cancers (CRCs)<sup>22</sup>, suggesting that these cells may be targeted by PD-1 blockade.

Here, we applied a combination of transcriptomic and imaging approaches for an in-depth analysis of ICB-naive and ICB-treated MMR-d colon cancers, as well as in vitro functional assays, and found evidence indicating that  $\gamma\delta$  T cells mediate responses to HLA-class-I-negative MMR-d tumours during treatment with ICB.

## RESULTS

### ICB is effective in B2M MUT MMR-d cancers

We evaluated responses to PD-1 blockade therapy in a cohort of 71 patients with MMR-d cancers from various anatomical sites treated in the Drug Rediscovery Protocol (DRUP)<sup>23</sup> in relation to their B2M status (Fig. 1a, Extended Data Fig. 1a-c and Supplementary Table 1). A clinical benefit (CB; defined as at least 4 months of disease control; the primary outcome of the DRUP) was observed in 20 out of 21 (95%) of patients with tumours with mutant or deleted B2M (B2MMUT) tumours versus 31 out of 50 (62%) of patients with tumours with wild-type B2M (B2MWT) (two-sided Fisher's exact test,  $P = 0.0038$ ; logistic regression,  $P = 0.022$  and  $P = 0.027$ , adjusted for tumour mutational burden (TMB), and TMB plus tumour type, respectively; Fig. 1b). Among patients with B2MMUT tumours, 3 out of 21 (14%) individuals experienced a complete response (according to RECIST1.1 criteria), 12 (57%) experienced a partial response, 5 (24%) experienced a durable stable disease and 1 (4.8%) experienced progressive disease as the best overall response. All 44 B2M alterations across 21 patients were clonal (Methods), consistent with previous observations in MMR-d cancers<sup>18</sup>. A total of 13 out of 21 (62%) patients with B2MMUT tumours had biallelic B2M alterations, 4 (19%) had potentially biallelic alterations and 4 (19%) had non-biallelic alterations (Fig. 1c and Methods). Non-biallelic alterations have also been associated with complete loss of B2M protein expression in MMR-d tumours<sup>18</sup>. Thus, B2M alterations are associated with a high clinical benefit rate of PD-1 blockade in patients with MMR-d cancers.

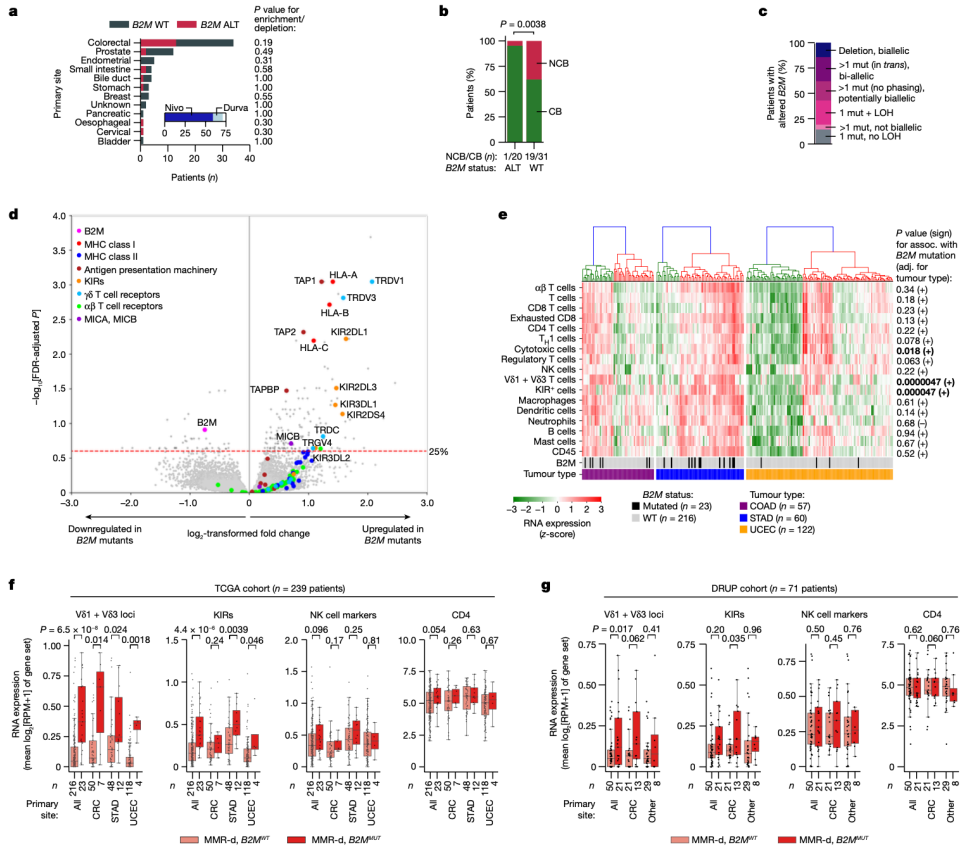


Fig. 1: In MMR-d cancers, B2M defects are positively associated with ICB responsiveness and infiltration by Vδ1 and Vδ3 T cells and KIR-expressing cells.

a, Tumour type distribution in the DRUP cohort (n = 71 patients). The colours denote patients' B2M status; grey, WT; red, altered (ALT). P values for the enrichment/depletion of B2M-altered tumours per primary site were calculated using two-sided Fisher's exact tests. The inset denotes the ICB treatment; dark blue, nivolumab (Nivo); light blue, durvalumab (Durva). b, B2M status (x axis) versus clinical benefit (green, CB; red, no clinical benefit (NCB)) of ICB treatment in the DRUP cohort. The P value was calculated using a two-sided Fisher's exact test. c, The allelic status of B2M alterations in the DRUP cohort. Mut, mutation. d, Differential gene expression between B2MMUT and B2MWT MMR-d cancers in the TCGA COAD (colon adenocarcinoma; n = 57 patients), STAD (stomach adenocarcinoma; n = 60 patients) and UCEC (uterus corpus endometrial carcinoma; n = 122 patients) cohorts. The results were adjusted (adj.) for tumour type and multiple-hypothesis testing (Methods). e, Immune marker gene set expression in MMR-d cancers of the COAD, STAD and UCEC cohorts of the TCGA. The bottom two bars indicate B2M status and cancer type. The association (assoc.) between gene set expression and B2M status was tested using ordinary least squares linear regression (adjusted for tumour type; Methods), of which two-sided P values and the association sign are shown on the right. Cancers were ranked on the basis of hierarchical clustering (top dendrograms). P values less than 0.05 are in bold. f, Immune marker gene set expression in B2MWT (pink) and B2MMUT (red) MMR-d

cancers in the TCGA COAD, STAD and UCEC cohorts separately or combined (all). Boxes, whiskers and dots indicate the quartiles, 1.5 $\times$  the interquartile range (IQR) and individual data points, respectively. P values were calculated using two-sided Wilcoxon rank-sum tests. g, Immune marker gene set expression in B2MWT (pink) and B2MMUT (red) as described in f, but for MMR-d cancers in the DRUP cohort. Results are shown for all cancers combined, only CRC or all non-CRC cancers (other). Two-sided P values were calculated using linear regression, adjusting for biopsy site and tumour type (Methods).

### **V $\delta$ 1 and V $\delta$ 3 TCRs are overexpressed in B2M MUT cancers**

To gain insights into the immune cell subsets that are involved in immune responses to HLA-class-I-negative MMR-d cancers, we used data of The Cancer Genome Atlas (TCGA) and studied the transcriptomic changes associated with the genomic loss of B2M in three cohorts of individuals with MMR-d cancer in colon adenocarcinoma (COAD; n = 50 (B2MWT), n = 7 (B2MMUT)), stomach adenocarcinoma (STAD; n = 48 (B2MWT) and n = 12 (B2MMUT)), and endometrium carcinoma (UCEC; n = 118 (B2MWT) and n = 4 (B2MMUT)). We found that B2M was among the most significantly downregulated genes in B2MMUT cancers (two-sided limma-voom-based regression,  $P = 3.5 \times 10^{-4}$ , Benjamini–Hochberg false-discovery rate (FDR)-adjusted  $P = 0.12$ , adjusted for tumour type; Fig.1d). Genes encoding components of the HLA class I antigen presentation machinery other than B2M were highly upregulated in B2MMUT tumours, which may reflect reduced evolutionary pressure on somatic inactivation of these genes in the B2MMUT context<sup>18</sup> (Fig.1d). Notably, we found TRDV1 and TRDV3, which encode the variable regions of the  $\delta$ 1 and  $\delta$ 3 chains of the  $\gamma\delta$  T cell receptor (TCR), among the most significantly upregulated loci in B2MMUT tumours (TRDV1, two-sided limma-voom-based regression, FDR-adjusted  $P = 0.00090$ , adjusted for tumour type; TRDV3, two-sided limma-voom-based regression, FDR-adjusted  $P = 0.0015$ , adjusted for tumour type; Fig. 1d), regardless of the allelic status of the B2M alteration (Extended Data Fig. 1d). Consistent with this, the expression levels of TRDV1 and TRDV3 were higher in B2MMUT compared with in B2MWT MMR-d cancers (two-sided Wilcoxon rank-sum test,  $P = 6.5 \times 10^{-8}$  for all of the cohorts combined; two-sided linear regression,  $P = 4.7 \times 10^{-6}$ , adjusted for tumour type; Fig.1d-f). Moreover, B2MMUT tumours showed overexpression of multiple KIRs (Fig.1d), which clustered together with TRDV1 and TRDV3 on the basis of hierarchical clustering (Extended Data Fig.1e). The expression level of different KIRs (Supplementary Table 2)

was higher in B2MMUT tumours compared with in B2MWT MMR-d tumours (two-sided Wilcoxon rank-sum test,  $P = 4.4 \times 10^{-6}$  for all cohorts combined; two-sided linear regression,  $P = 4.7 \times 10^{-5}$ , adjusted for tumour type; Fig.1d-f). Together, these results suggest that ICB-naive B2MMUT MMR-d cancers show increased levels of V $\delta$ 1 and V $\delta$ 3 T cells as well as increased numbers of these or other immune cells expressing KIRs—a potential mechanism of recognition of HLA class I loss.

We used marker gene sets (modified from ref.24; Methods and Supplementary Table 2) to estimate the abundance of a broad set of other immune cell types on the basis of the RNA expression data of the TCGA cohorts. Hierarchical clustering identified a high- and a low-infiltrated cluster in each of the three tumour types (Fig. 1e). Compared with the V $\delta$ 1 and V $\delta$ 3 T cell and KIR gene sets, the other marker gene sets showed no or only weak association between expression level and B2M status, indicating that our findings were not solely driven by a generally more inflamed state of B2MMUT tumours (Fig.1e,f and Extended Data Fig. 1f).

5 We next revisited the DRUP cohort and specifically applied the marker gene sets to RNA expression data. Despite the low patient numbers and high heterogeneity regarding tumour types and biopsy locations of this cohort, we confirmed increased TRDV1 and TRDV3 expression in B2MMUT tumours pan-cancer (two-sided linear regression,  $P = 0.017$ , adjusted for tumour type and biopsy site; Fig. 1g, Extended Data Fig.1g and Methods). KIR expression was significantly associated with B2M status only in CRC (Fig. 1g). Across mismatch repair-proficient (MMR-p) metastatic cancers in the Hartwig database<sup>25</sup>, 36 out of 2,256 (1.6%) cancers had a clonal B2M alteration, which was frequently accompanied by loss of heterozygosity (LOH) (Extended Data Fig.1h and Supplementary Table 3). Although rare, B2M alterations were also significantly associated with increased expression of TRDV1/TRDV3 loci in this context (two-sided linear regression,  $P = 2.2 \times 10^{-17}$ , adjusted for tumour type; Extended Data Fig. 1i and Methods). Taken together, B2M defects are positively associated with clinical benefits of ICB treatment, as well as infiltration by V $\delta$ 1 and V $\delta$ 3 T cells and expression of KIRs.

## V $\delta$ 1 and V $\delta$ 3 T cells are activated in MMR-d CRC

To investigate which  $\gamma\delta$  T cell subsets are present in MMR-d colon cancers and to determine their functional characteristics, we performed single-cell RNA-sequencing (scRNA-seq) analysis of  $\gamma\delta$  T cells isolated from five MMR-d colon cancers (Extended Data Figs. 2 and 3 and Supplementary Table 4). Three distinct V $\delta$  subsets were identified (Fig. 2a)— V $\delta$ 1 T cells were the most prevalent (43% of  $\gamma\delta$  T cells), followed by V $\delta$ 2 (19%) and V $\delta$ 3 T cells (11%) (Fig. 2b). PDCD1 (encoding PD-1) was predominantly expressed by V $\delta$ 1 and V $\delta$ 3 T cells, whereas V $\delta$ 1 cells expressed high levels of genes that encode activation markers such as CD39 (ENTPD1) and CD38 (Fig. 2c and Extended Data Fig. 2b). Furthermore, proliferating  $\gamma\delta$  T cells (expressing MKI67) were especially observed in the V $\delta$ 1 and V $\delta$ 3 subsets (Fig. 2c). Other distinguishing features of the V $\delta$ 1 and V $\delta$ 3 T cell subsets included the expression of genes encoding activating receptors NKp46 (encoded by NCR1), NKG2C (encoded by KLRC2) and NKG2D (encoded by KLRK1) (Fig. 2c). Notably, the expression of several KIRs was also higher in the V $\delta$ 1 and V $\delta$ 3 subsets as compared to V $\delta$ 2 T cells (Fig. 2c). Almost all  $\gamma\delta$  T cells displayed expression of the genes encoding granzyme B (GZMB), perforin (PRF1) and granulysin (GNLY) (Fig. 2c). Together, these data support a role for  $\gamma\delta$  T cells in mediating natural cytotoxic antitumour responses in HLA-class-I-negative MMR-d colon cancers.

Next, we applied imaging mass cytometry (IMC) analysis to a cohort of 17 individuals with ICB-naive MMR-d colon cancers (Supplementary Table 4). High levels of  $\gamma\delta$  T cell infiltration were observed in cancers with B2M defects as compared to B2M-proficient cancers, albeit this difference was not significant (Fig. 2d). The levels of other immune cells, including NK cells, CD4<sup>+</sup> T cells and CD8<sup>+</sup> T cells, were similar between B2M-deficient and B2M-proficient tumours (Fig. 2d). In B2M-deficient cancers,  $\gamma\delta$  T cells showed frequent intraepithelial localization and expression of CD103 (tissue-residency), CD39 (activation), granzyme B (cytotoxicity) and Ki-67 (proliferation), as well as PD-1 (Fig. 2d–f and Extended Data Fig. 2c), consistent with the scRNA-seq data. Notably,  $\gamma\delta$  T cells in B2M-deficient cancers showed co-

expression of CD103 and CD39 (Extended Data Fig. 2d), which has been reported to identify tumour-reactive CD8<sup>+</sup>  $\alpha\beta$  T cells in a variety of cancers<sup>26</sup>.

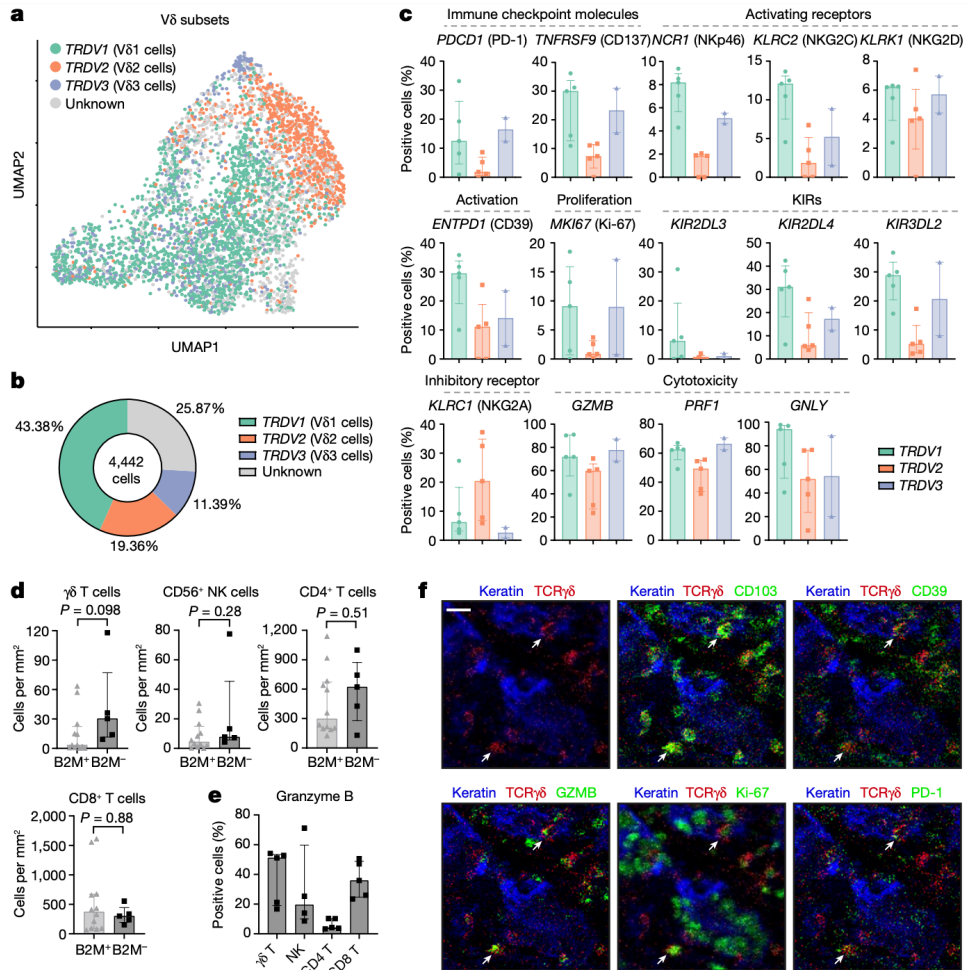


**Fig. 2 | Tumour-infiltrating V $\delta$ 1 and V $\delta$ 3 T cell subsets display hallmarks of cytotoxic activity in MMR-d colon cancers.** a, UMAP embedding showing the clustering of  $\gamma\delta$  T cells (n = 4,442) isolated from MMR-d colon cancers (n = 5) analysed using scRNA-seq. The colours represent the TCR V $\delta$  chain usage. The functionally distinct  $\gamma\delta$  T cell clusters are shown in Extended Data Fig. 3. Dots represent single cells. b, The frequencies of TCR V $\delta$  chain use of the  $\gamma\delta$  T cells (n = 4,442) analysed using scRNA-seq as a percentage of total  $\gamma\delta$  T cells. c, The frequencies of positive cells for selected genes across V $\delta$ 1 (n = 1,927), V $\delta$ 2 (n = 860) and V $\delta$ 3 (n = 506) cells as the percentage of total  $\gamma\delta$  T cells from each MMR-d colon tumour (n = 5) analysed using scRNA-seq. V $\delta$ 3 cells were present in two out of five colon cancers. Data are median  $\pm$  IQR, with

individual samples (dots). d, The frequencies of  $\gamma\delta$  T cells, CD56<sup>+</sup> NK cells, CD4<sup>+</sup> T cells and CD8<sup>+</sup> T cells in treatment-naive B2M<sup>+</sup> (n = 12) and B2M<sup>-</sup> (n = 5) MMR-d colon cancers. Data are median  $\pm$  IQR, with individual samples (dots). P values were calculated using two-sided Wilcoxon rank-sum tests. e, The frequencies of granzyme-B-positive  $\gamma\delta$  T cells, CD56<sup>+</sup> NK cells, CD4<sup>+</sup> T cells and CD8<sup>+</sup> T cells in treatment-naive B2M<sup>-</sup> (n = 5) MMR-d colon cancers. CD56<sup>+</sup> NK cells were present in four out of five B2M<sup>-</sup> cancer samples. Data are median  $\pm$  IQR, with individual samples (dots). f, Representative images of the detection of tissue-resident (CD103<sup>+</sup>), activated (CD39<sup>+</sup>), cytotoxic (granzyme B<sup>+</sup>), proliferating (Ki-67<sup>+</sup>) and PD-1<sup>+</sup>  $\gamma\delta$  T cells (white arrows) by IMC analysis of a treatment-naive MMR-d colon cancer with B2M defects. Scale bar, 20  $\mu$ m.

### PD-1<sup>+</sup> V $\delta$ 1 and V $\delta$ 3 T cells kill HLA-class-I<sup>-</sup> CRC cells

We next sought to determine whether tumour-infiltrating  $\gamma\delta$  T cells can recognize and kill CRC cells. We isolated and expanded PD-1<sup>-</sup> and PD-1<sup>+</sup>  $\gamma\delta$  T cells from five MMR-d colon cancers (Extended Data Fig. 4-c and Supplementary Table 4). Consistent with the scRNA-seq data, expanded PD-1<sup>+</sup>  $\gamma\delta$  T cell populations lacked V $\delta$ 2<sup>+</sup> cells and comprised the V $\delta$ 1<sup>+</sup> or V $\delta$ 3<sup>+</sup> subsets, whereas the PD-1<sup>-</sup> fractions contained V $\delta$ 2<sup>+</sup> or a mixture of V $\delta$ 1<sup>+</sup>, V $\delta$ 2<sup>+</sup> and V $\delta$ 3<sup>+</sup> populations (Fig. 3a and Extended Data Fig. 4d). Detailed immunophenotyping of the expanded  $\gamma\delta$  T cells (Fig. 3a and Extended Data Fig. 5a) showed that all of the subsets expressed the activating receptor NKG2D, whereas the surface expression of natural cytotoxicity receptors (NCRs) and KIRs was most frequent on PD-1<sup>+</sup>  $\gamma\delta$  T cells (V $\delta$ 1 or V $\delta$ 3<sup>+</sup>), consistent with the scRNA-seq results of unexpanded populations. We measured the reactivity of the expanded  $\gamma\delta$  T cell populations to HLA-class-I-negative and HLA-class-I-positive cancer cell lines (Fig. 3b and Extended Data Fig. 4b). After co-culture with the different cancer cell lines, reactivity (assessed by expression of activation markers and secretion of IFN $\gamma$ ) was largely restricted to PD-1<sup>+</sup>  $\gamma\delta$  T cells (V $\delta$ 1 or V $\delta$ 3<sup>+</sup>), whereas activation of PD-1<sup>-</sup>  $\gamma\delta$  T cells (V $\delta$ 2<sup>+</sup>) was generally not detected (Fig. 3c and Extended Data Fig. 4). PD-1<sup>+</sup>  $\gamma\delta$  T cell (V $\delta$ 1 or V $\delta$ 3<sup>+</sup>) reactivity was variable and was observed against both HLA-class-I-negative and HLA-class-I-positive cell lines (Fig. 3c and Extended Data Fig. 4). To quantify and visualize the differences in the killing of CRC cell lines by PD-1<sup>+</sup> and PD-1<sup>-</sup>  $\gamma\delta$  T cells, we co-cultured the  $\gamma\delta$  T cell populations with three CRC cell lines (HCT-15, LoVo, HT-29) in the presence of a fluorescent cleaved-caspase-3/7 reporter to measure cancer cell apoptosis over time (Fig. 3d,e). We found pronounced cancer cell apoptosis after co-culture with PD-1<sup>+</sup>  $\gamma\delta$  T cells (V $\delta$ 1 or V $\delta$ 3<sup>+</sup>) compared with PD-1<sup>-</sup> cells; cancer cell death was



more pronounced in HLA-class-I-negative HCT-15 cells (Fig. 3e and Supplementary Videos 1 and 2). Reintroduction of B2M in the B2M-deficient HCT-15 and LoVo cells diminished their killing by PD-1+  $\gamma\delta$  T cells (V $\delta$ 1 or V $\delta$ 3+) cells (Extended Data Fig. 6), suggesting that B2M loss increases the sensitivity to  $\gamma\delta$  T cells.

Next, we established two parental patient-derived tumour organoid lines (PDTOs; Supplementary Table 5) of MMR-d CRC and generated isogenic B2MKO lines using CRISPR. Genomic knockout of B2M effectively abrogated cell surface expression of HLA class I (Extended Data Fig. 7). We exposed two B2MKO lines and their parental B2MWT lines to the expanded  $\gamma\delta$  T cell subsets, and quantified  $\gamma\delta$  T cell activation by determination of IFN $\gamma$  expression. Similar to our cell line data,  $\gamma\delta$  T cells displayed increased reactivity to B2MKO PDTOs in comparison to the B2MWT PDTOs (Fig. 3f,g). Furthermore,  $\gamma\delta$  T cell reactivity to B2MKO tumour organoids was preferentially contained within the PD-1+ population of  $\gamma\delta$  T cells (Fig. 3g). Thus, a lack of HLA class I antigen presentation in MMR-d tumour cells can be effectively sensed by  $\gamma\delta$  T cells and stimulates their antitumour response.

5 Expression of NKG2D on  $\gamma\delta$  T cells decreased during co-culture with target cells (Extended Data Fig. 8a,b), suggesting the involvement of the NKG2D receptor in  $\gamma\delta$  T cell activity. The NKG2D ligands MICA/B and ULBPs were expressed by the cancer cell lines (Fig. 3b) and the MMR-d CRC PDTOs, irrespective of their B2M status (Extended Data Fig. 7). To examine which receptor–ligand interactions might regulate the activity of PD-1+  $\gamma\delta$  T cells, we performed blocking experiments focused on (1) NKG2D, (2) DNAM-1 and (3)  $\gamma\delta$  TCR signaling. Of these candidates, the only consistent inhibitory effect was observed for NKG2D ligand blocking on cancer cells, which decreased the activation and killing ability of most PD-1+  $\gamma\delta$  T cells (Fig. 3h and Extended Data Fig. 8c,d), confirming the mechanistic involvement of the NKG2D receptor in  $\gamma\delta$  T cell activation in this context. Moreover, blocking NKG2D ligands on MMR-d CRC PDTOs reduced the PDTO-directed tumour reactivity of  $\gamma\delta$  T cells from CRC94 and CRC134 (Fig. 3i). Together, these results show that  $\gamma\delta$  T cell reactivity to MMR-d tumours is partly dependent on NKG2D/NKG2D-ligand interactions.

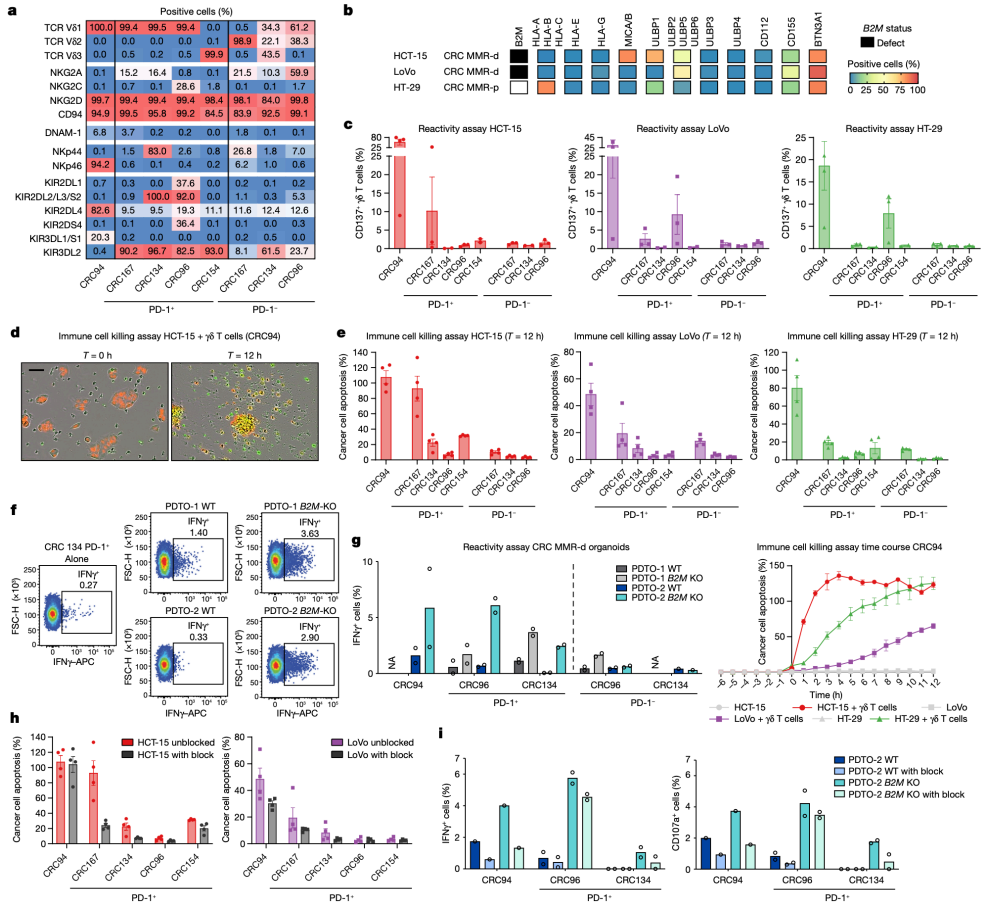


**Fig. 3:**  $\gamma\delta$  T cells from MMR-d colon cancers show preferential reactivity to HLA-class-I-negative cancer cell lines and organoids. **a**, The percentage of positive cells for the indicated markers on expanded  $\gamma\delta$  T cells from MMR-d colon cancers ( $n = 5$ ). **b**, Diagram showing the B2M status and surface expression of HLA class I, NKG2D ligands, DNAM-1 ligands and butyrophilin on CRC cell lines. MMR-p, MMR proficient. **c**, CD137 expression on  $\gamma\delta$  T cells after co-culture with CRC cell lines. Data are mean  $\pm$  s.e.m. from at least two independent experiments. **d**, Representative images showing the killing of NuclightRed-transduced HCT-15 cells by  $\gamma\delta$  T cells in the presence of a green fluorescent caspase-3/7 reagent. Cancer cell apoptosis is visualized in yellow. Scale bar, 50  $\mu$ m. **e**, Quantification of the killing of CRC cell lines after co-culture with  $\gamma\delta$  T cells as described in **d**. Data are mean  $\pm$  s.e.m. of two wells with two images per well. A representative time course of cancer cell apoptosis is shown at the bottom right. **f**, Representative flow cytometry plots showing IFN $\gamma$  expression in  $\gamma\delta$  T cells unstimulated (alone) and after stimulation with two B2MWT and B2MKO CRC MMR-d organoids. **g**, IFN $\gamma$  expression in  $\gamma\delta$  T cells after stimulation with two B2MWT and B2MKO CRC MMR-d organoids, shown as the difference compared with the unstimulated  $\gamma\delta$  T cell sample. Data are from two biological replicates, except for a single biological replicate of CRC134 PD-1 $^{-}$ . NA, not available. **h**, The killing of CRC cell lines after 12 h co-culture with  $\gamma\delta$  T cells with or without NKG2D ligand blocking. Data are mean  $\pm$  s.e.m. of two wells with two images per well. **i**, IFN $\gamma$  (left) and CD107a (right) expression in  $\gamma\delta$  T cells after

stimulation with B2MWT PDTO-2 or B2MKO PDTO-2, with or without NKG2D ligand blocking and subtracted background signal. Data are from two biological replicates, except for a single biological replicate of CRC94.

### ICB boosts V $\delta$ 1 and V $\delta$ 3 T cells in B2M MUT CRC

We subsequently studied how ICB influences  $\gamma\delta$  T cell infiltration and activation in MMR-d colon cancers in the therapeutic context. For this purpose, we analysed pre- and post-treatment samples of the NICHE trial<sup>9</sup>, in which patients with colon cancer were treated with neoadjuvant PD-1 plus CTLA-4 blockade. Consistent with our observations in the DRUP cohort, 4 out of 5 (80%) individuals with B2MMUT cancers in the NICHE trial showed a complete pathologic clinical response. Immunohistochemical analysis confirmed the loss of B2M protein expression on tumour cells in all mutated cases (Extended Data Fig. 9). Whereas expression of immune marker gene sets in the pretreatment samples was similar between 5 B2MMUT versus 13 B2MWT cancers, ICB induced a clear immunological divergence between these two groups (Fig. 4a). The B2MMUT subgroup was most significantly associated with higher post-treatment expression of TRDV1 and TRDV3 (two-sided Wilcoxon rank-sum test,  $P = 0.0067$ ; Fig. 4a), followed by higher expression of the general immune cell marker CD45, NK-cell-related markers, KIRs and  $\alpha\beta$ TCRs (two-sided Wilcoxon rank-sum test,  $P = 0.016$ ,  $P = 0.016$ ,  $P = 0.027$  and  $P = 0.043$ , respectively; Fig. 4a and Extended Data Fig. 10a). The set of KIRs upregulated after ICB in B2MMUT cancers (Extended Data Fig. 10b) was consistent with the sets of KIRs upregulated in B2MMUT MMR-d cancers in TCGA (Fig. 1e), and those expressed by MMR-d tumour-infiltrating  $\gamma\delta$  T cells (Fig. 2c). Pre- and post-ICB gene expression levels related to CD4 and CD8 infiltration were not associated with B2M status (Fig. 4a and Extended Data Fig. 10a). To quantify and investigate the differences in immune profiles after ICB treatment, we used IMC to analyse tissues derived from five B2MMUT HLA-class-I-negative and five B2MWT HLA-class-I-positive cancers before and after ICB treatment. In the ICB-naive setting, B2MMUT MMR-d colon cancers showed higher  $\gamma\delta$  T cell infiltration compared with B2MWT MMR-d colon cancers (two-sided Wilcoxon rank-sum test,  $P = 0.032$ ; Fig. 4b and Extended Data Fig. 10c).

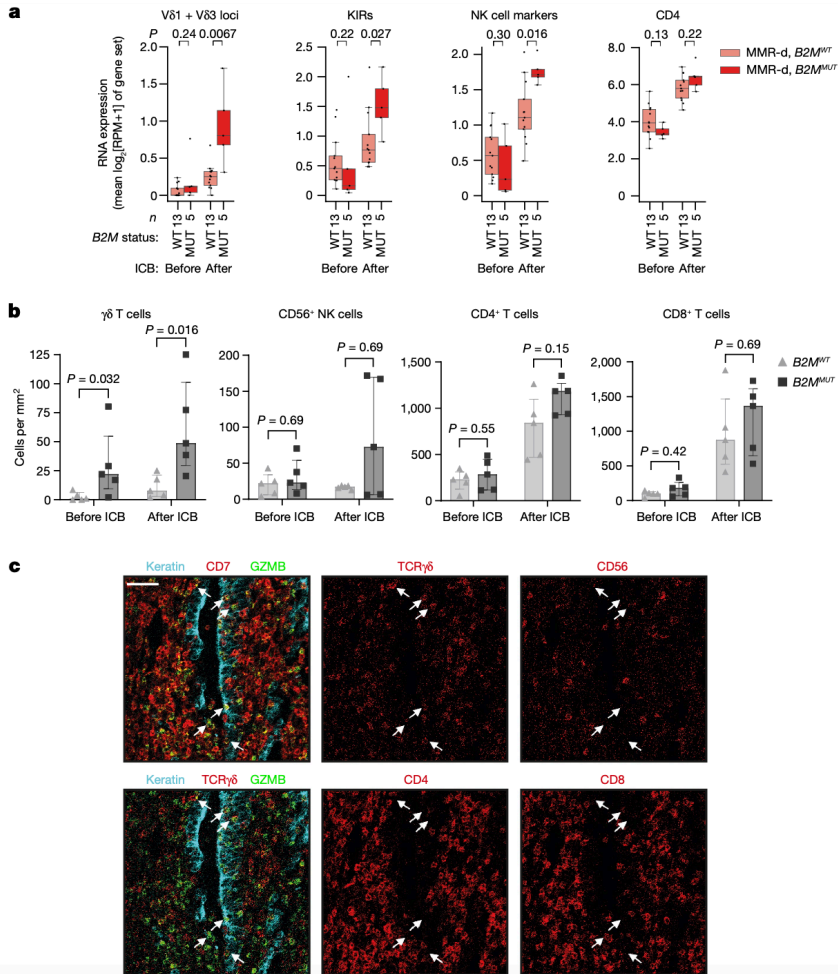


**Fig. 4: ICB induces substantial infiltration of  $\gamma\delta$  T cells into MMR-d colon cancers with defects in antigen presentation.** a, The RNA expression of different immune marker gene sets in MMR-d B2M<sup>WT</sup> (pink) and MMR-d B2M<sup>MUT</sup> (red) cancers before (left) and after (right) neoadjuvant ICB in the NICHE study. The boxes, whiskers and dots indicate quartiles, 1.5  $\times$  IQR and individual data points, respectively. P values were calculated using two-sided Wilcoxon rank-sum tests comparing MMR-d B2M<sup>WT</sup> versus MMR-d B2M<sup>MUT</sup> cancers. b, The frequencies of  $\gamma\delta$  T cells, CD56<sup>+</sup> NK cells, CD4<sup>+</sup> T cells and CD8<sup>+</sup> T cells in B2M<sup>WT</sup> (n = 5) and B2M<sup>MUT</sup> (n = 5) MMR-d colon cancers before and after ICB treatment. Data are median  $\pm$  IQR, with individual samples (dots). P values were calculated using two-sided Wilcoxon rank-sum tests. c, Representative images of granzyme-B-positive  $\gamma\delta$  T cells infiltrating the tumour epithelium (white arrows) by IMC analysis of a B2M<sup>MUT</sup> MMR-d colon cancer after ICB treatment. Scale bar, 50  $\mu$ m.

Importantly, a large proportion of these  $\gamma\delta$  T cells showed an intraepithelial localization in B2MMUT MMR-d colon cancers compared with the B2MWT samples (two-sided Wilcoxon rank-sum test,  $P = 0.0079$ ; Extended Data Fig. 10d). No significant differences were observed in the infiltration of other immune cells, such as NK cells, CD4+ T cells and CD8+ T cells, in ICB-naive B2MMUT versus B2MWT MMR-d colon cancers (Fig. 4b). ICB treatment resulted in major pathologic clinical responses, and residual cancer cells were absent in most post-ICB samples. All post-ICB tissues showed a profound infiltration of different types of immune cells (Extended Data Fig. 10e), of which  $\gamma\delta$  T cells were the only immune subset that was significantly higher in ICB-treated B2MMUT compared with B2MWT MMR-d colon cancers (two-sided Wilcoxon rank-sum test,  $P = 0.016$ ; Fig. 4b and Extended Data Fig. 10c). In the sole B2MMUT case that still contained cancer cells after treatment with ICB, the majority of granzyme B+ immune cells infiltrating the tumour epithelium were  $\gamma\delta$  T cells (Fig. 4c). These  $\gamma\delta$  T cells displayed co-expression of CD103, CD39, Ki-67 and PD-1 (Extended Data Fig. 10f-h). Taken together, these results show that ICB treatment of MMR-d colon cancer increases the presence of activated, cytotoxic and proliferating  $\gamma\delta$  T cells at the tumour site, especially when these cancers are B2M-deficient, highlighting  $\gamma\delta$  T cells as effectors of ICB treatment within this context.

## DISCUSSION

CD8+  $\alpha\beta$  T cells are major effectors of ICB<sup>11,12,27</sup> and rely on HLA class I antigen presentation of target cells. We confirm and shed light on the paradox that patients with HLA class I defects in MMR-d cancers retain the clinical benefit of ICB, suggesting that other immune effector cells are involved in compensating for the lack of conventional CD8+ T cell immunity in this setting. We show that genomic inactivation of B2M in MMR-d colon cancers was associated with: (1) an elevated frequency of activated  $\gamma\delta$  T cells in ICB-naive tumours; (2) an increased presence of tumour-infiltrating  $\gamma\delta$  T cells after ICB treatment; (3) in vitro activation of tumour-infiltrating  $\gamma\delta$  T cells by CRC cell lines and PDTOs; and (4) killing of tumour cell lines by  $\gamma\delta$  T cells, in particular by V $\delta$ 1 and V $\delta$ 3 subsets expressing PD-1.

Different subsets of  $\gamma\delta$  T cells exhibit substantially diverse functions that, in the context of cancer, range from tumour-promoting to tumouricidal effects<sup>20,28,29</sup>. Thus, it is of interest to determine what defines antitumour reactivity of  $\gamma\delta$  T cells. Here we isolated V $\delta$ 1/3-expressing PD-1+ T cells as well as V $\delta$ 2-expressing PD-1- T cells from MMR-d tumour tissues. Our data suggest that especially tumour-infiltrating V $\delta$ 1 and V $\delta$ 3 T cells can recognize and kill HLA-class-I-negative MMR-d tumours, whereas V $\gamma$ 9V $\delta$ 2 cells, the most studied and main subset of  $\gamma\delta$  T cells in the blood, appear to be less relevant within this context. This is consistent with other studies showing that the cytotoxic ability of V $\delta$ 1 cells generally outperforms their V $\delta$ 2 counterparts<sup>30-34</sup>. Notably, reports of the cytotoxicity of tumour-infiltrating V $\delta$ 3 cells have been lacking. Furthermore, the observation that PD-1+  $\gamma\delta$  T cells (V $\delta$ 1 and V $\delta$ 3 phenotype) demonstrated clearly higher levels of antitumour reactivity compared with their PD-1- counterparts (V $\delta$ 2 phenotype) suggests that, as for CD8+  $\alpha\beta$  T cells<sup>35</sup>, PD-1 expression may be a marker of antitumour reactivity in  $\gamma\delta$  T cells.

The mechanisms of activation of  $\gamma\delta$  T cells are notoriously complex and diverse<sup>20</sup>. Specifically, for V $\delta$ 1+ cells, NKG2D has been described to be involved in tumour recognition, which is dependent on tumour cell expression of NKG2D ligands MICA/B and ULBPs<sup>36,37,38</sup>. Here, MICA/B and ULBPs were highly expressed by the MMR-d CRC cell lines and tumour organoids, and blocking these ligands reduced  $\gamma\delta$  T cell activation and cytotoxicity. This suggests a role for the activating receptor NKG2D in  $\gamma\delta$  T cell immunity to MMR-d tumours. Future research should address the outstanding question of how  $\gamma\delta$  T cells accumulate in B2M-deficient tumours, and whether the lack of CD8+ T cell activity might contribute to the establishment of an attractive niche for  $\gamma\delta$  T cells and other immune effector cells. Potential mechanisms for the recognition of HLA-class-I-negative phenotypes may include KIR-, NKG2A- and LILRB1-mediated interactions with target cancer cells. Notably, we found that the expression of KIRs was most pronounced on PD-1+  $\gamma\delta$  T cells (V $\delta$ 1 or V $\delta$ 3+ subsets), which demonstrated anti-tumour activity. Whether the lack of KIR-mediated signaling promotes the survival of  $\gamma\delta$  T cells and their intratumoural proliferation remains to be studied.

Our findings have broad implications for cancer immunotherapy. First, our findings strengthen the rationale for combining PD-1 blockade with immunotherapeutic approaches to further enhance  $\gamma\delta$  T-cell-based antitumour immunity. Second, the

presence or absence in tumours of specific  $\gamma\delta$  T cell subsets (such as V $\delta$ 1 or V $\delta$ 3) may help to define patients who are responsive or unresponsive to ICB, respectively, especially in the case of MMR-d cancers and other malignancies with frequent HLA class I defects, such as stomach adenocarcinoma<sup>39</sup> and Hodgkin's lymphoma<sup>40</sup>. Third, our results suggest that MMR-d cancers and other tumours with HLA class I defects may be particularly attractive targets for V $\delta$ 1 or V $\delta$ 3 T-cell-based cellular therapies.

Although we have provided detailed and multidimensional analyses, it is probable that  $\gamma\delta$  T cells are not the only factor driving ICB responses in HLA-class-I-negative MMR-d CRC tumours. In this context, other HLA-class-I-independent immune subsets, such as NK cells and neoantigen-specific CD4+ T cells may also contribute. The latter were shown to have an important role in the response to ICB (as reported in mouse B2M-deficient MMR-d cancer models<sup>41</sup>), and may also support  $\gamma\delta$  T-cell-driven responses. Notably, no subset equivalent to V $\delta$ 1 or V $\delta$ 3 T cells has been identified in mice, which complicates their investigation in *in vivo* models. In conclusion, our results provide strong evidence that  $\gamma\delta$  T cells are cytotoxic effector cells of ICB treatment in HLA-class-I-negative MMR-d colon cancers, with implications for further exploitation of  $\gamma\delta$  T cells in cancer immunotherapy.

## Online content

Any methods, additional references, Nature Portfolio reporting summaries, source data, extended data, supplementary information, acknowledgements, peer review information; details of author contributions and competing interests; and statements of data and code availability are available at <https://doi.org/10.1038/s41586-022-05593-1>.

## REFERENCES

1. Ionov, Y., Peinado, M. A., Malkhosyan, S., Shibata, D. & Perucho, M. Ubiquitous somatic mutations in simple repeated sequences reveal a new mechanism for colonic carcinogenesis. *Nature* 363, 558–561 (1993).
2. Germano, G. et al. Inactivation of DNA repair triggers neoantigen generation and impairs tumour growth. *Nature* 552, 116–120 (2017).

3. Zaretsky, J. M. et al. Mutations associated with acquired resistance to PD-1 blockade in melanoma. *N. Engl. J. Med.* 375, 819–829 (2016).
4. Gettinger, S. et al. Impaired HLA class I antigen processing and presentation as a mechanism of acquired resistance to immune checkpoint inhibitors in lung cancer. *Cancer Discov.* 7, 1420–1435 (2017).
5. Sade-Feldman, M. et al. Resistance to checkpoint blockade therapy through inactivation of antigen presentation. *Nat. Commun.* 8, 1136 (2017).
6. Le, D. T. et al. Mismatch repair deficiency predicts response of solid tumors to PD-1 blockade. *Science* 357, 409–413 (2017).
7. Overman, M. J. et al. Nivolumab in patients with metastatic DNA mismatch repair-deficient or microsatellite instability-high colorectal cancer (CheckMate 142): an open-label, multicentre, phase 2 study. *Lancet. Oncol.* 18, 1182–1191 (2017).
8. Overman, M. J. et al. Durable clinical benefit with nivolumab plus ipilimumab in DNA mismatch repair-deficient/microsatellite instability-high metastatic colorectal cancer. *J. Clin. Oncol.* 36, 773–779 (2018).
9. Chalabi, M. et al. Neoadjuvant immunotherapy leads to pathological responses in MMR-proficient and MMR-deficient early-stage colon cancers. *Nat. Med.* 26, 566–576 (2020).
10. Dolcetti, R. et al. High prevalence of activated intraepithelial cytotoxic T lymphocytes and increased neoplastic cell apoptosis in colorectal carcinomas with microsatellite instability. *Am. J. Pathol.* 154, 1805–1813 (1999).
11. Tumei, P. C. et al. PD-1 blockade induces responses by inhibiting adaptive immune resistance. *Nature* 515, 568–571 (2014).
12. Taube, J. M. et al. Association of PD-1, PD-1 ligands, and other features of the tumor immune microenvironment with response to anti-PD-1 therapy. *Clin. Cancer Res.* 20, 5064–5074 (2014).
13. Bicknell, D. C., Kaklamanis, L., Hampson, R., Bodmer, W. F. & Karran, P. Selection for  $\beta_2$ -microglobulin mutation in mismatch repair-defective colorectal carcinomas. *Curr. Biol.* 6, 1695–1697 (1996).
14. Kloor, M. et al. Immunoselective pressure and human leukocyte antigen class I antigen machinery defects in microsatellite unstable colorectal cancers. *Cancer Res.* 65, 6418–6424 (2005).
15. Dierssen, J. W. et al. HNPCC versus sporadic microsatellite-unstable colon cancers follow different routes toward loss of HLA class I expression. *BMC Cancer* 7, 33 (2007).
16. Ijsselstein, M. E. et al. Revisiting immune escape in colorectal cancer in the era of immunotherapy. *Br. J. Cancer* 120, 815–818 (2019).
17. Hughes, E. A., Hammond, C. & Cresswell, P. Misfolded major histocompatibility complex class I heavy chains are translocated into the cytoplasm and degraded by the proteasome. *Proc. Natl Acad. Sci. USA* 94, 1896–1901 (1997).
18. Middha, S. et al. Majority of B2M-mutant and -deficient colorectal carcinomas achieve clinical benefit from immune checkpoint inhibitor therapy and are microsatellite instability-high. *JCO Precis. Oncol.* 3, 1–14 (2019).



19. Groh, V. et al. Human lymphocytes bearing T cell receptor  $\gamma\delta$  are phenotypically diverse and evenly distributed throughout the lymphoid system. *J. Exp. Med.* 169, 1277–1294 (1989).
20. Silva-Santos, B., Mensurado, S. & Coffelt, S. B.  $\gamma\delta$  T cells: pleiotropic immune effectors with therapeutic potential in cancer. *Nat. Rev. Cancer* 19, 392–404 (2019).
21. Halary, F. et al. Control of self-reactive cytotoxic T lymphocytes expressing  $\gamma\delta$  T cell receptors by natural killer inhibitory receptors. *Eur. J. Immunol.* 27, 2812–2821 (1997).
22. de Vries, N. L. et al. High-dimensional cytometric analysis of colorectal cancer reveals novel mediators of antitumour immunity. *Gut* 69, 691–703 (2020).
23. van der Velden, D. L. et al. The Drug Rediscovery protocol facilitates the expanded use of existing anticancer drugs. *Nature* 574, 127–131 (2019).
24. Danaher, P. et al. Gene expression markers of tumor infiltrating leukocytes. *J. Immunother. Cancer* 5, 18 (2017).
25. Priestley, P. et al. Pan-cancer whole-genome analyses of metastatic solid tumours. *Nature* 575, 210–216 (2019).
26. Duhén, T. et al. Co-expression of CD39 and CD103 identifies tumor-reactive CD8 T cells in human solid tumors. *Nat. Commun.* 9, 2724 (2018).
27. Kwon, M. et al. Determinants of response and intrinsic resistance to PD-1 blockade in microsatellite instability-high gastric cancer. *Cancer Discov.* 11, 2168–2185 (2021).
28. Wu, Y. et al. An innate-like  $V\delta 1^+$   $\gamma\delta$  T cell compartment in the human breast is associated with remission in triple-negative breast cancer. *Sci. Transl. Med.* 11, eaax9364 (2019).
29. Wu, Y. et al. A local human  $V\delta 1$  T cell population is associated with survival in nonsmall-cell lung cancer. *Nat. Cancer* 3, 696–709 (2022).
30. Mæurer, M. J. et al. Human intestinal  $V\delta 1^+$  lymphocytes recognize tumor cells of epithelial origin. *J. Exp. Med.* 183, 1681–1696 (1996).
31. Siegers, G. M., Ribot, E. J., Keating, A. & Foster, P. J. Extensive expansion of primary human gamma delta T cells generates cytotoxic effector memory cells that can be labeled with feraheme for cellular MRI. *Cancer Immunol. Immunother.* 62, 571–583 (2013).
32. Wu, D. et al. Ex vivo expanded human circulating  $V\delta 1$   $\gamma\delta$ T cells exhibit favorable therapeutic potential for colon cancer. *Oncoimmunology* 4, e992749 (2015).
33. Almeida, A. R. et al. Delta one T cells for immunotherapy of chronic lymphocytic leukemia: clinical-grade expansion/differentiation and preclinical proof of concept. *Clin. Cancer Res.* 22, 5795–5804 (2016).
34. Mikulak, J. et al. NKp46-expressing human gut-resident intraepithelial  $V\delta 1$  T cell subpopulation exhibits high antitumor activity against colorectal cancer. *JCI Insight* 4, e125884 (2019).
35. van der Leun, A. M., Thommen, D. S. & Schumacher, T. N.  $CD8^+$  T cell states in human cancer: insights from single-cell analysis. *Nat. Rev. Cancer* 20, 218–232 (2020).

36. Groh, V., Steinle, A., Bauer, S. & Spies, T. Recognition of stress-induced MHC molecules by intestinal epithelial  $\gamma\delta$  T cells. *Science* 279, 1737–1740 (1998).
37. Groh, V. et al. Broad tumor-associated expression and recognition by tumor-derived  $\gamma\delta$  T cells of MICA and MICB. *Proc. Natl Acad. Sci. USA* 96, 6879–6884 (1999).
38. Poggi, A. et al. V $\delta$ 1 T lymphocytes from B-CLL patients recognize ULBP3 expressed on leukemic B cells and up-regulated by trans-retinoic acid. *Cancer Res.* 64, 9172–9179 (2004).
39. Hause, R. J., Pritchard, C. C., Shendure, J. & Salipante, S. J. Classification and characterization of microsatellite instability across 18 cancer types. *Nat. Med.* 22, 1342–1350 (2016).
40. Cader, F. Z. et al. A peripheral immune signature of responsiveness to PD-1 blockade in patients with classical Hodgkin lymphoma. *Nat. Med.* 26, 1468–1479 (2020).
41. Germano, G. et al. CD4 T cell-dependent rejection of beta-2 microglobulin null mismatch repair-deficient tumors. *Cancer Discov.* 11, 1844–1859 (2021).
42. Carter, S. L. et al. Absolute quantification of somatic DNA alterations in human cancer. *Nat. Biotechnol.* 30, 413–421 (2012).
43. Taylor, A. M. et al. Genomic and functional approaches to understanding cancer aneuploidy. *Cancer Cell* 33, 676–689 (2018).
44. Thorsson, V. et al. The immune landscape of cancer. *Immunity* 51, 411–412 (2019).
45. Huang, M. N. et al. MSIsq: software for assessing microsatellite instability from catalogs of somatic mutations. *Sci. Rep.* 5, 13321 (2015).
46. Dobin, A. et al. STAR: ultrafast universal RNA-seq aligner. *Bioinformatics* 29, 15–21 (2013).
47. Shale, C. et al. Unscrambling cancer genomes via integrated analysis of structural variation and copy number. *Cell Genomics* 2, 100112 (2022).
48. Robinson, J. T. et al. Integrative genomics viewer. *Nat. Biotechnol.* 29, 24–26 (2011).
49. Virtanen, P. et al. SciPy 1.0: fundamental algorithms for scientific computing in Python. *Nat. Methods* 17, 261–272 (2020).
50. Robinson, M. D., McCarthy, D. J. & Smyth, G. K. edgeR: a Bioconductor package for differential expression analysis of digital gene expression data. *Bioinformatics* 26, 139–140 (2010).
51. Ritchie, M. E. et al. limma powers differential expression analyses for RNA-sequencing and microarray studies. *Nucleic Acids Res.* 43, e47 (2015).
52. Law, C. W., Chen, Y., Shi, W. & Smyth, G. K. voom: precision weights unlock linear model analysis tools for RNA-seq read counts. *Genome Biol.* 15, R29 (2014).
53. Hall, G. et al. Immunohistochemistry for PMS2 and MSH6 alone can replace a four antibody panel for mismatch repair deficiency screening in colorectal adenocarcinoma. *Pathology* 42, 409–413 (2010).
54. Stoeckius, M. et al. Simultaneous epitope and transcriptome measurement in single cells. *Nat. Methods* 14, 865–868 (2017).
55. Stuart, T. et al. Comprehensive integration of single-cell data. *Cell* 177, 1888–1902 (2019).

56. McGinnis, C. S. et al. MULTI-seq: sample multiplexing for single-cell RNA sequencing using lipid-tagged indices. *Nat. Methods* 16, 619–626 (2019).
57. Haghverdi, L., Lun, A. T. L., Morgan, M. D. & Marioni, J. C. Batch effects in single-cell RNA-sequencing data are corrected by matching mutual nearest neighbors. *Nat. Biotechnol.* 36, 421–427 (2018).
58. McInnes, L., Healy, J. & Melville, J. UMAP: uniform manifold approximation and projection for dimension reduction. Preprint at arXiv <https://arxiv.org/abs/1802.03426> (2018).
59. Ijsselsteijn, M. E., van der Breggen, R., Farina Sarasqueta, A., Koning, F. & de Miranda, N. F. C. A 40-marker panel for high dimensional characterization of cancer immune microenvironments by imaging mass cytometry. *Front. Immunol.* 10, 2534–2534 (2019).
60. Berg, S. et al. ilastik: interactive machine learning for (bio)image analysis. *Nat. Methods* 16, 1226–1232 (2019).
61. Ijsselsteijn, M. E., Somarakis, A., Lelieveldt, B. P. F., Höllt, T. & de Miranda, N. Semi-automated background removal limits data loss and normalises imaging mass cytometry data. *Cytometry A* 99, 1187–1197 (2021).
62. Carpenter, A. E. et al. CellProfiler: image analysis software for identifying and quantifying cell phenotypes. *Genome Biol.* 7, R100 (2006).
63. Somarakis, A., Van Unen, V., Koning, F., Lelieveldt, B. P. F. & Holtt, T. ImaCytE: visual exploration of cellular microenvironments for imaging mass cytometry data. *IEEE Trans. Vis. Comp. Graph.* 27, 98–110 (2019).
64. van der Maaten, L. J. P. & Hinton, G. E. Visualizing high-dimensional data using t-SNE. *J. Mach. Learn. Res.* 9, 2579–2605 (2008).
65. Höllt, T. et al. Cytosplore: interactive immune cell phenotyping for large single-cell datasets. *Comput. Graph. Forum* 35, 171–180 (2016).
66. Dijkstra, K. K. et al. Generation of tumor-reactive T cells by co-culture of peripheral blood lymphocytes and tumor organoids. *Cell* 174, 1586–1598 (2018).
67. Cattaneo, C. M. et al. Tumor organoid-T-cell coculture systems. *Nat. Protoc.* 15, 15–39(2020).
68. Dutta, I., Postovit, L. M. & Siegers, G. M. Apoptosis induced via gamma delta T cell antigen receptor “blocking” antibodies: a cautionary tale. *Front. Immunol.* 8, 776 (2017).

## METHODS

### TCGA data

RNA expression data (raw counts) of the colon adenocarcinoma (COAD), stomach adenocarcinoma (STAD) and Uterus Corpus Endometrium Carcinoma (UCEC) cohorts of The Cancer Genome Atlas (TCGA) Research Network were downloaded through the GDC data portal (<https://portal.gdc.cancer.gov>) on 10 April 2019. Of these cohorts, mutation, copy number, purity and ploidy data were downloaded from the GDC on 11 November 2021, as the controlled access ABSOLUTE-annotated<sup>42</sup> MAF file (mutations), SNP6 white-listed copy number segments file (copy numbers) and ABSOLUTE purity/ploidy file of the TCGA

PanCanAtlas project<sup>43</sup>. Mismatch-repair-deficiency status was obtained from ref. 44 (TCGA subtype = GI.HM-indel or UCEC.MSI).

#### DRUP data

A detailed description of the DRUP, including details on patient accrual, study design, oversight and end points was published previously<sup>23</sup>. In brief, the DRUP is a national, non-randomized multidrug and multitumour study in the Netherlands, in which patients receive off-label drugs registered for other treatment indications. These patients had advanced or metastatic solid tumours and had exhausted standard-treatment options, they were required to be at least 18 years of age, with acceptable organ function and performance status (Eastern Cooperative Oncology Group (ECOG) score  $\leq 2$ ), and have an objectively evaluable disease of which a fresh baseline tumour biopsy could safely be obtained. We analysed 71 patients with MMR-d cancers recruited and treated with PD-1 blockade in 22 Dutch hospitals participating in the DRUP<sup>23</sup> between 2016 and 2021. Patients included in this analysis had (1) a clinical follow-up  $\geq 16$  weeks after start of PD-1 blockade treatment; (2) WGS data passing standard quality controls (as defined previously, including a sequencing-based tumour purity of  $\geq 20\%$ )<sup>25</sup>; and (3) available RNA-seq data (Supplementary Table 1). MMR-d status was determined using routine diagnostics at the hospital of patient accrual and was confirmed by WGS, on the basis of an MSIseq (v.1.0.0)<sup>45</sup> score of  $>4$ , which represents a predefined threshold<sup>25</sup>. Consistent with the study protocol of the DRUP<sup>23</sup>, the primary outcome measure for our analysis was clinical benefit, defined as disease control of  $\geq 16$  weeks, and the secondary outcome measure was best overall response, all assessed according to the RECIST 1.1 guidelines by the local treatment team at the site of accrual. As determined in the study protocol, these outcome measures were considered to be evaluable in patients who received at least two cycles of intravenous study medication, and for whom the response was radiologically or clinically evaluable (at the treating physician's discretion). For genomics and transcriptomics analyses, fresh frozen tumour biopsies were obtained at the baseline (that is, before PD-1 blockade). WGS analysis (median depths,  $\sim 100\times$  and  $\sim 40\times$  for tumour and normal, respectively) and bioinformatics analyses were performed as previously described<sup>23,25</sup>, with an optimized pipeline based on open-source tools that is freely available at GitHub (<https://github.com/hartwigmedical/pipeline5>). The TMB per Mb was determined by counting the genome-wide number of mutations (SNVs, MNVs and indels) and dividing this number by the number of megabases sequenced. For RNA-seq analysis, we extracted total RNA using the QIAGEN QIAasympphony RNA kit (931636). Samples with approximately 100 ng total RNA were prepared using KAPA RNA Hyper + RiboErase HMR (8098131702) and the RNA libraries were paired-end sequenced on the Illumina NextSeq550 platform ( $2 \times 75$  bp) or the Illumina NovaSeq6000 platform ( $2 \times 150$  bp). Raw RNA reads (FASTA files) were aligned to the human reference genome (GRCh38) using STAR<sup>46</sup>, (v.2.7.7a) using the default settings in two-pass mode.

#### Hartwig data

We analysed 2,256 metastatic tumours included in the freely available Hartwig database<sup>25</sup> that (1) were MMR-p (WGS-based MSIseq<sup>45</sup> score  $\leq 4$ ); (2) had available WGS data passing standard quality controls (as defined before, including a sequencing-based tumour purity  $\geq 20\%$ )<sup>25</sup>; (3) and had available RNA-seq data. We excluded 89 tumours from rare primary tumour locations, defined as locations with less than  $<20$

patients in our selection. When individual patients had data available of biopsies obtained at different timepoints, we included data of only the first biopsy. Sequencing and bioinformatics were performed identically to the procedures used for the generation of the DRUP dataset (see above). Details of this cohort are provided in Supplementary Table 3.

#### NICHE study data

Raw RNA reads (FASTA files) of our recently published NICHE study<sup>9</sup> (ClinicalTrials.gov: [NCT03026140](https://clinicaltrials.gov/ct2/show/study/NCT03026140)) were generated as described in the original publication and aligned to the human reference genome (GRCh38) with STAR<sup>46</sup> (v.2.7.7a) using the default settings in two-pass mode. For gene expression quantification, we used the gencode.v35.annotation.gtf annotation file. Somatic mutation data were obtained from DNA-seq of pretreatment tumour biopsies and matched germline DNA, as described in the original publication<sup>9</sup>.

#### B2M status

Consistent with the notion that both biallelic and monoallelic non-synonymous B2M mutations are strongly associated with tumour-specific loss of B2M protein expression<sup>18</sup>, we considered all tumours with at least one somatic, non-synonymous B2M mutation to be a B2M mutant. As none of the B2M mutant tumours in TCGA had B2M copy number gains or losses, LOH of B2M could easily be assessed by a simple calculation estimating the mutation's copy number:

$$\text{Mut}_{\text{CN}} = \text{round}\left(2 \times \frac{\text{VAF}}{\text{purity}}\right)$$

A MutCN equal to 2 was considered to be consistent with LOH, as the most parsimonious explanation of such a result is the scenario in which all tumour-derived reads spanning the region of

the B2M mutation contain the mutation and none of the tumour-derived reads are WT. In analyses of patients in the DRUP and Hartwig datasets, LOH of B2M mutations was determined as an integrated functionality of PURPLE (v.2.34)<sup>47</sup>. When multiple B2M mutations were present within a sample, we manually phased the mutations through inspection of the B2M-aligned reads using the Integrative Genomics Viewer (IGV)<sup>48</sup>. Here mutations were phased in case single reads were observed spanning the genomic locations of both mutations. We divided patients with multiple B2M mutations into three subgroups: (1) Biallelic, if (a) the multiple mutations were in trans AND the integer sum of the mutation copy numbers equalled (or exceeded) the integer copy number of the B2M gene (for mutations in cis, only one of these mutations was considered in the calculation); or (b) at least one of the mutations showed LOH. (2) Potentially biallelic, if the multiple mutations affected genomic locations too distant to be phased and the (integer) sum of the mutation copy numbers equalled (or exceeded) the integer copy number of the B2M gene (for mutations in cis, only one of these mutations was considered in the calculation) and none of the mutations showed LOH. (3) Not bi-allelic, if the integer sum of the mutation copy numbers was smaller than the integer copy number of the B2M gene (for mutations in cis, only one of these mutations was considered in the calculation) and none of the mutations showed LOH. In these analyses, mutations were considered to be subclonal in the case in which the probability of subclonality was  $>0.5$  (the situation in which a mutation is more likely subclonal than clonal), as determined using PURPLE (v.2.34)<sup>47</sup>.

#### Association of B2M status with outcome and tumour characteristics

To test whether somatic B2M alterations were associated with the clinical benefit rate of patients with MMR-d tumours treated with ICB in the DRUP, we used a Fisher's exact test (using the Python package Scipy<sup>49</sup> (v.1.3.1)) for unadjusted analyses and logistic regression (as implemented by the Python package Statsmodels (<https://pypi.org/project/statsmodels/>; v.0.10.1) for analyses adjusted for the continuous TMB per Mb and/or the primary site of the tumour. The association of B2M status with TMB was tested using Scipy's Wilcoxon rank-sum test. Associations of B2M status with the primary site of the tumour or the biopsy location were tested using Scipy's Fisher's exact test.

#### Association of TMB with ICB treatment outcome

For the DRUP cohort, the association of clinical benefit with TMB was tested using Statsmodels' Wilcoxon rank-sum test.

#### Differential gene expression analysis

Differential RNA expression of genes was tested in R using EdgeR<sup>50</sup> (v.3.28.1) and Limma<sup>51</sup> (including Voom<sup>52</sup>) (v.3.42.2). Raw read counts were filtered by removing low-expressed genes. Normalization factors were calculated using EdgeR to transform the raw counts to  $\log_2$ [counts per million reads (CPM)] and calculate residuals using Voom. Voom was then used to fit a smoothed curve to the  $\sqrt{(\text{residual standard deviation})}$  by average gene expression, which was then plotted for visual inspection to confirm that the appropriate threshold was used for filtering of low-expressed genes (defined as the minimal amount of filtering necessary to overcome a dipping mean-variance trend at low counts). Next, Limma was used to calculate the differential expression of genes on the basis of a linear model fit, considering the smoothed curve for sample weights, and empirical Bayes smoothing of standard errors. FDR-adjusted P values were calculated using Benjamini–Hochberg correction of the obtained P values.

#### TCGA

Using TCGA data, we calculated the differential expression between tumours with and without mutations in B2M, adjusting for tumour type, using the following design formula:  $\text{expression} \propto \text{Primary\_Site} + \text{B2M\_status}$  (+ intercept by default), for which Primary\_Site was a three-levelled factor (COAD, STAD, or UCEC) and B2M\_status was a two-levelled factor (mutated, or wildtype).

#### NICHE study

Using NICHE study data, we calculated differential expression between pre- and post-ICB treatment. To respect the paired nature of these data, we used the following design formula:  $\text{expression} \propto \text{Patient} + \text{ICB}$  + intercept, where Patient is a factor for each individual patient and ICB is a two-levelled factor (ICB-treated, yes/no).

### Immune marker gene set expression analysis

To use RNA-seq data to obtain a relative estimate of the infiltration of specific immune cell types within tumours, we calculated the average  $\log_2[\text{RPM} + 1]$  expression of marker genes that are specifically expressed in the immune cell types of interest. To this end, we used the previously published marker gene sets<sup>24</sup>, and extended this by (1) CD4 as a CD4+ T cell marker gene; (2) TRDV1 and TRDV3 as  $\gamma\delta 1/3T$  cell marker genes; and (3) a killer-cell Ig-like receptor (KIR) gene set (comprising all genes of which the name starts with KIR and of which the name contains DL or DS). We excluded the gene set 'NK CD56dim cells' of ref.<sup>24</sup> (comprising IL21R, KIR2DL3, KIR3DL1 and KIR3DL2) from our analyses, as three out of four genes within this set were KIRs and this set therefore showed high collinearity/redundancy to our full KIR gene set. As XLC1 and XLC2 are highly expressed by tumour-infiltrating  $\gamma\delta$  T cells, these genes were removed from the NK cell marker gene set and replaced by KLRF1, which encodes the well-established NK cell marker NKp80. The resulting gene set consisted of NCR1 and KLRF1, encoding the well-established NK cell markers NKp46 and NKp80, respectively. Finally, we reduced the 'cytotoxic cells' marker gene set of ref. 24 to those genes in the set encoding cytotoxic molecules (GZMA, GZMB, GZMH, PRF1, GNLY, CTSW). A list of the final collection of our marker gene sets is provided in Supplementary Table 2.

Association of immune cell marker gene set expression with B2M alteration status (alteration yes/no) was calculated as follows:

1. For TCGA-study-based analyses, we used (i) the Wilcoxon rank-sum test (for unadjusted analyses) and (ii) ordinary least squares linear regression (for analyses adjusted for tumour type; as implemented by the Python package 'Statsmodels'), using a similar design formula as for the differential gene expression analysis. 2. For DRUP-cohort-based analyses, we used a linear mixed effects model (as implemented by the lmer function of the R package Lme4 (v.1.1.26)), adjusting for tumour type and biopsy site as random effects, using the following design formula:  $\text{expression} \sim \text{B2M\_status} + (1|\text{tumour\_type}) + (1|\text{biopsy\_site}) + \text{intercept}$ . In subgroup analysis of CRC, we omitted tumour type in this formula:  $\text{expression} \sim \text{B2M\_status} + (1|\text{biopsy\_site}) + \text{intercept}$ . 3. Hartwig data-based analyses, we used ordinary least squares linear regression (as implemented by the Python package Statsmodels) adjusting for tumour type, using the following design formula:  $\text{expression} \sim \text{Primary\_Site} + \text{B2M\_status} + \text{intercept}$ . 4. For NICHE-study-based analyses, we used the Wilcoxon rank-sum test (as implemented by the Python package Scipy).

### Hierarchical clustering

Hierarchical clustering of expression profiles of individual genes or immune marker gene sets of TCGA cohorts was performed on Z-score-transformed  $\log_2[\text{RPM} + 1]$  expression values, using the Python package Scipy<sup>49</sup>, with Euclidean distance as the distance metric and using the Ward variance minimization algorithm. Here, we used the default settings with one exception—for visualization purposes, the colour threshold was halved in the TCGA-based clustering of individual genes.

### Patient samples

The DRUP study and the generation of the Hartwig database were initiated and conducted on behalf of the Center for Personalized Cancer Treatment (CPCT; ClinicalTrials.gov: [NCT02925234](https://clinicaltrials.gov/ct2/show/study/NCT02925234), [NCT01855477](https://clinicaltrials.gov/ct2/show/study/NCT01855477)). These studies were approved by the Medical Ethical Committee of the Netherlands Cancer Institute in Amsterdam and the University Medical Center Utrecht, respectively, and were conducted in accordance with good clinical practice guidelines and the Declaration of Helsinki's ethical principles for medical research. Written informed consent was obtained from all of the study participants. Moreover, primary colon cancer tissues from a total of 17 patients with colon cancer who underwent surgical resection of their tumour at the Leiden University Medical Center (LUMC, The Netherlands; Supplementary Table 4) were used for scRNA-seq, IMC and functional assays. No patient with a previous history of inflammatory bowel disease was included. This study was approved by the Medical Ethical Committee of the Leiden University Medical Center (protocol P15.282), and patients provided written informed consent. Finally, primary colon cancer tissues from ten patients with colon cancer included in the NICHE study ([NCT03026140](https://clinicaltrials.gov/ct2/show/study/NCT03026140))<sup>9</sup> carried out at the Netherlands Cancer Institute (NKI, The Netherlands) were used for this study. All samples were anonymized and handled according to the ethical guidelines described in the Code for Proper Secondary Use of Human Tissue in the Netherlands of the Dutch Federation of Medical Scientific Societies.

#### Processing of colon cancer tissues

Details on the processing of colon cancer tissues have been described previously<sup>22</sup>. In brief, macroscopic sectioning from the lumen to the most invasive area of the tumour was performed. Tissues were collected in IMDM + GlutaMax medium (Gibco) complemented with 20% fetal calf serum (FCS) (Sigma-Aldrich), 1% penicillin–streptomycin (Gibco) and fungizone (Gibco), and 0.1% ciprofloxacin (provided by apothecary LUMC) and gentamicin (Invitrogen), and immediately cut into small fragments in a Petri dish. Enzymatic digestion was performed using 1 mg ml<sup>-1</sup> collagenase D (Roche Diagnostics) and 50 µg ml<sup>-1</sup> DNase I (Roche Diagnostics) in 5 ml of IMDM + GlutaMax medium for 30 min at 37 °C in gentleMACS C tubes (Miltenyi Biotec). During and after incubation, cell suspensions were dissociated mechanically on the gentleMACS Dissociator (Miltenyi Biotec). Cell suspensions were filtered through a 70 µm cell strainer (Corning), washed in IMDM + GlutaMax medium with 20% FCS, 1% penicillin–streptomycin and 0.1% fungizone, and the cell count and viability were determined using the Muse Count & Viability Kit (Merck) on the Muse Cell Analyser (Merck). On the basis of the number of viable cells, cells in IMDM + GlutaMax medium were cryopreserved in liquid nitrogen until time of analysis complemented 1:1 with 80% FCS and 20% dimethyl sulfoxide (Merck).

#### Immunohistochemical detection of MMR, B2M and HLA class I proteins

For the tumour tissue samples from the LUMC, tumour MMR status was determined by immunohistochemical detection of PMS2 (anti-PMS2 antibodies; EP51, DAKO) and MSH6 (anti-MSH6 antibodies; EPR3945, Abcam) proteins<sup>53</sup>. MMR-deficiency was defined as the lack of expression of at least one of the MMR-proteins in the presence of an internal positive control. Tumour B2M status was determined by immunohistochemical detection of B2M (anti-B2M antibodies; EP2978Y, Abcam). Immunohistochemical detection of HLA class I expression on tumour cells was performed with HCA2 and HC10 monoclonal antibodies (Nordic-MUbio), and tumours were classified as HLA class I positive, weak or loss, as described previously<sup>16</sup>. For the tumour samples from the NICHE study, immunohistochemistry



analysis of the formalin-fixed paraffin-embedded (FFPE) tissue was performed on the BenchMark Ultra autostainer (Ventana Medical Systems). In brief, paraffin sections were cut at 3  $\mu\text{m}$ , heated at 75 °C for 28 min and deparaffinized in the instrument using EZ prep solution (Ventana Medical Systems). Heat-induced antigen retrieval was performed using Cell Conditioning 1 (CC1, Ventana Medical Systems) for 32 min at 95 °C (HC10) or 64 min at 95 °C (B2M and HCA2). HLA class I heavy chain expression was detected using clone HCA2 (1:5,000, 60 min at room temperature; Nordic-Mubio) and clone HC10 (1:20,000, 32 min at 37 °C; Nordic-Mubio). B2M was detected using clone D8P1H (1:1,500, 60 min at room temperature; Cell Signaling). Bound antibodies were detected using the OptiView DAB Detection Kit (Ventana Medical Systems). Slides were counterstained with haematoxylin and Bluing Reagent (Ventana Medical Systems). A PANNORAMIC 1000 scanner from 3DHISTECH was used to scan the slides at  $\times 40$  magnification.

#### Sorting of $\gamma\delta$ T cells from colon cancers and scRNA-seq

scRNA-seq was performed on sorted  $\gamma\delta$  T cells from colon cancers (MMR-d) of five patients from the LUMC in the presence of hashtag oligos (HTOs) for sample ID and antibody-derived tags (ADTs) for CD45RA and CD45RO protein expression by CITE-seq<sup>54</sup>. Cells were thawed, rested at 37 °C in IMDM (Lonza)/20% FCS for 1 h, and then incubated with human Fc receptor block (BioLegend) for 10 min at 4 °C. Cells were then stained with cell surface antibodies (anti-CD3-PE (1:50, SK7, BD Biosciences), anti-CD45-PerCP-Cy5.5 (1:160, 2D1, eBioscience), anti-CD7-APC (1:200, 124-1D1, eBioscience), anti-EPCAM-FITC (1:60, HEA-125, Miltenyi), anti-TCR $\gamma\delta$ -BV421 (1:80, 11F2, BD Biosciences); and a 1:1,000 near-infrared viability dye (Life Technologies)), 1  $\mu\text{g}$  of TotalSeq-C anti-CD45RA (HI100, BioLegend, 2  $\mu\text{l}$  per sample) and 1  $\mu\text{g}$  of TotalSeq-C anti-CD45RO (UCHL1, BioLegend, 2  $\mu\text{l}$  per sample) antibodies, and 0.5  $\mu\text{g}$  of a unique TotalSeq-C CD298/B2M hashtag antibody (LNH-94/2M2, BioLegend, 1  $\mu\text{l}$  per sample) for 30 min at 4 °C. Cells were washed three times in FACS buffer (PBS (Fresenius Kabi)/1% FCS) and kept under cold and dark conditions until cell sorting. Compensation was performed using CompBeads (BD Biosciences) and ArC reactive beads (Life Technologies). Single, live CD45+EPCAM-CD3+TCR $\gamma\delta$ + cells were sorted on the FACS Aria III 4L (BD Biosciences) system. After sorting, the samples were pooled.

scRNA-seq libraries were prepared using the Chromium Single Cell 5' Reagent Kit v1 chemistry (10x Genomics) according to the manufacturer's instructions. The construction of 5' gene expression libraries enabled the identification of  $\gamma\delta$  T cell subsets according to V $\delta$  and V $\gamma$  usage. Libraries were sequenced on the HiSeq X Ten using paired-end 2  $\times$  150 bp sequencing (Illumina). Reads were aligned to the human reference genome (GRCh38) and quantified using Cell Ranger (v.3.1.0). Downstream analysis was performed using Seurat (v.3.1.5) according to the author's instructions<sup>55</sup>. In brief, cells that had less than 200 detected genes and genes that were expressed in less than six cells were excluded. The resulting 5,669 cells were demultiplexed on the basis of HTO enrichment using the MULTISEQDemux algorithm<sup>56</sup>. Next, cells with a mitochondrial gene content of greater than 10% and cells with outlying numbers of expressed genes (>3,000) were filtered out from the analysis, resulting in a final dataset of 4,442 cells, derived from HTO1 (n = 332), HTO6 (n = 105), HTO7 (n = 1,100), HTO8 (n = 1,842) and HTO9 (n = 1,063). Data were normalized using the LogNormalize function of Seurat with a scale factor of 10,000. Variable features were identified using the FindVariableFeatures function of Seurat returning 2,000 features. We next applied the RunFastMNN function of SeuratWrappers split by sample ID to adjust for potential batch-

derived effects across the samples<sup>57</sup>. Uniform manifold approximation and projection (UMAP)<sup>58</sup> was used to visualize the cells in a two-dimensional space, followed by the FindNeighbors and FindClusters functions of Seurat. Data were scaled, and heterogeneity associated with mitochondrial contamination was regressed out. Cell clusters were identified by performing differentially expressed gene analysis using the FindAllMarkers function, with min.pct and logfc.threshold at 0.25. The number of TRDV1+ (V $\delta$ 1, n = 1,927), TRDV2+ (V $\delta$ 2, n = 860) or TRDV3+ (V $\delta$ 3, n = 506) cells was determined as the percentage of all cells with an expression level of >1, with <1 for the other TCR V $\delta$  chains. CRC96, 134 and 167 had less than ten TRDV3+ cells, and were not included in the V $\delta$ 3 analysis. Transcripts of V $\delta$ 4 (TRDV4), V $\delta$ 5 (TRDV5) and V $\delta$ 8 (TRDV8) cells were not detected. The percentage of cells positive for a certain gene was determined as all cells with an expression level of >1.

### IMC staining and analysis

IMC analysis was performed on ICB-naive colon cancer tissues (MMR-d) of 17 patients from the LUMC; 5 of these colon cancer tissues had B2M defects and the remainder were B2M-positive (Supplementary Table 4). Moreover, IMC was performed on ICB-naive and ICB-treated colon cancer tissues (MMR-d) of ten patients from the NICHE study; five of these colon cancer tissues were B2MWT and five were B2MMUT. Antibody conjugation and immunodetection were performed according to previously published methodology<sup>59</sup>. FFPE tissue (thickness, 4  $\mu$ m) was incubated with 41 antibodies in four steps. First, sections were incubated overnight at room temperature with anti-CD4 and anti-TCR $\delta$  antibodies, which were subsequently detected using metal-conjugated secondary antibodies (1  $\mu$ g ml<sup>-1</sup>, donkey anti-rabbit IgG and goat anti-mouse IgG, respectively; Abcam). Second, the sections were incubated with 20 antibodies (Supplementary Table 6) for five hours at room temperature. Third, the sections were incubated overnight at 4 °C with the remaining 19 antibodies (Supplementary Table 6). Fourth, the sections were incubated with 0.125  $\mu$ M Cell-ID intercalator-Ir (Fluidigm) to detect the DNA, and stored dry until measurement. For each sample, six 1,000  $\mu$ m  $\times$  1,000  $\mu$ m regions (two to three for pretreatment NICHE biopsies due to the small tissue size) were selected on the basis of consecutive haematoxylin and eosin stains and ablated using the Hyperion Imaging system (Fluidigm). Data were acquired using the CyTOF Software (v.7.0) and exported using MCD Viewer (v.1.0.5). Data were normalized using semi-automated background removal in ilastik<sup>60</sup> (v.1.3.3), to control for variations in the signal-to-noise ratio between FFPE sections as described previously<sup>61</sup>. Next, the phenotype data were normalized at the pixel level. Cell segmentation masks were created for all cells in ilastik and CellProfiler<sup>62</sup> (v.2.2.0). In ImaCytE<sup>63</sup> (v.1.1.4), cell segmentation masks and normalized images were combined to generate single-cell FCS files containing the relative frequency of positive pixels for each marker per cell. Cells forming visual neighbourhoods in a t-distributed stochastic neighbour embedding<sup>64</sup> in Cytosplore<sup>65</sup> (v.2.3.0) were grouped and exported as separate FCS files. The resulting subsets were imported back into ImaCytE and visualized on the segmentation masks. Expression of immunomodulatory markers was determined as all cells with a relative frequency of at least 0.2 positive pixels per cell. Differences in cells per mm<sup>2</sup> were calculated using Mann-Whitney tests in GraphPad Prism (v.9.0.1). Image acquisition and analysis were performed blinded to group allocation.

### Sorting of $\gamma\delta$ T cells from colon cancers and cell culturing

$\gamma\delta$  T cells from colon cancers (MMR-d) of five patients from the LUMC were sorted for cell culture. Cells were thawed and rested at 37 °C in IMDM (Lonza)/10% nHS for 1 h. Next, cells were incubated with human Fc receptor block (BioLegend) and stained with cell surface antibodies (anti-CD3-Am Cyan (1:20, SK7, BD Biosciences), anti-TCR $\gamma\delta$ -BV421 (1:80, 11F2, BD Biosciences) and anti-PD-1-PE (1:30, MIH4, eBioscience)) for 45 min at 4 °C together with different additional antibodies for immunophenotyping (anti-CD103-FITC (1:10, Ber-ACT8, BD Biosciences), anti-CD38-PE-Cy7 (1:200, HIT2, eBioscience); anti-CD39-APC (1:60, A1, BioLegend), anti-CD45RA-PE-Dazzle594 (1:20, HI100, Sony), anti-CD45RO-PerCP-Cy5.5 (1:20, UCHL1, Sony), anti-TCR $\alpha\beta$ -PE-Cy7 (1:40, IP26, BioLegend), anti-TCRV $\delta$ 1-FITC (1:50, TS8.2, Invitrogen) or anti-TCRV $\delta$ 2-PerCP-Cy5.5 (1:200' B6, BioLegend). A 1:1,000 live/dead fixable near-infrared viability dye (Life Technologies) was included in each staining. Cells were washed three times in FACS buffer (PBS/1% FCS) and kept under cold and dark conditions until cell sorting. Compensation was performed using CompBeads (BD Biosciences) and ArC reactive beads (Life Technologies). Single, live CD3+TCR $\gamma\delta$ +PD-1+ and PD-1- cells were sorted on the FACS Aria III 4L (BD Biosciences) system. For CRC94, all  $\gamma\delta$  T cells were sorted owing to the low number of PD-1+ cells.  $\gamma\delta$  T cells were sorted in medium containing feeder cells (1 × 10<sup>6</sup> per ml), PHA (1 µg ml<sup>-1</sup>; Thermo Fisher Scientific), IL-2 (1,000 IU ml<sup>-1</sup>; Novartis), IL-15 (10 ng ml<sup>-1</sup>; R&D Systems), gentamicin (50 µg ml<sup>-1</sup>) and fungizone (0.5 µg ml<sup>-1</sup>). Sorted  $\gamma\delta$  T cells were expanded in the presence of 1,000 IU ml<sup>-1</sup> IL-2 and 10 ng ml<sup>-1</sup> IL-15 for 3–4 weeks. The purity and phenotype of  $\gamma\delta$  T cells were assessed using flow cytometry. We obtained a >170,000-fold increase in 3–4 weeks of expansion of  $\gamma\delta$  T cells (Extended Data Fig. 4c).

#### Immunophenotyping of expanded $\gamma\delta$ T cells by flow cytometry

Expanded  $\gamma\delta$  T cells from colon tumours were analysed by flow cytometry for the expression of TCR V $\delta$  chains, NKG2 receptors, NCRs, KIRs, tissue-residency/activation markers, cytotoxic molecules, immune checkpoint molecules, cytokine receptors and Fc receptors. In brief, cells were incubated with human Fc receptor block (BioLegend) and stained with cell surface antibodies (Supplementary Table 7) for 45 min at 4 °C, followed by three wash steps in FACS buffer (PBS/1% FCS). Granzyme B and perforin were detected intracellularly using fixation buffer and intracellular staining permeabilization wash buffer (BioLegend). Compensation was performed using CompBeads (BD Biosciences) and ArC reactive beads (Life Technologies). Cells were acquired on the FACS LSR Fortessa 4L (BD Biosciences) system running FACSDiva software (v.9.0; BD Biosciences). Data were analysed using FlowJo (v.10.6.1; Tree Star).

#### Cancer cell line models and culture

Human colorectal adenocarcinoma cell lines HCT-15 (MMR-d), LoVo (MMR-d), HT-29 (MMR-p), SW403 (MMR-p) and SK-CO-1 (MMR-p), as well as HLA-class-I-deficient human leukaemia cell line K-562 and Burkitt lymphoma cell line Daudi were used as targets for reactivity and immune cell killing assays. All of the cell lines were obtained from the ATCC. The cell lines were authenticated by STR profiling and tested for mycoplasma. HCT-15, LoVo, HT-29, K-562 and Daudi cells were maintained in RPMI (Gibco)/10% FCS. SW403 and SK-CO-1 were maintained in DMEM/F12 (Gibco)/10% FCS. All adherent cell lines were trypsinized before passaging. The B2M-knockin HCT-15 and LoVo cell lines were generated using the B2M plasmid (pLV[Exp]-EF1A>hB2M[NM\_004048.4](ns):T2A:Puro), produced in lentivirus according to

standard methodology. Cells were selected using puromycin and then FACS-sorted on the basis of HLA-A/B/C expression using 1:100 anti-HLA-A/B/C-FITC (W6/32, eBioscience).

#### Organoid models and culture

Tumour organoids were derived from MMR-d CRC tumours of two patients through resection from the colon (tumour organoid 1) or peritoneal biopsy (tumour organoid 2) (Supplementary Table 5). Establishment of the respective organoid lines from tumour material was performed as previously reported<sup>66,67</sup>. In brief, tumour tissue was mechanically dissociated and digested with 1.5 mg ml<sup>-1</sup> of collagenase II (Sigma-Aldrich), 10  $\mu$ g ml<sup>-1</sup> of hyaluronidase type IV (Sigma-Aldrich) and 10  $\mu$ M Y-27632 (Sigma-Aldrich). Cells were embedded in Cultrex RGF BME type 2 (3533-005-02, R&D systems) and placed into a 37 °C incubator for 20 min. Human CRC organoid medium is composed of Ad-DF+++ (Advanced DMEM/F12 (GIBCO) supplemented with 2 mM Ultraglutamine I (Lonza), 10 mM HEPES (GIBCO), 100 U ml<sup>-1</sup> of each penicillin and streptomycin (GIBCO), 10% noggin-conditioned medium, 20% R-spondin1-conditioned medium, 1 $\times$  B27 supplement without vitamin A (GIBCO), 1.25 mM N-acetylcysteine (Sigma-Aldrich), 10 mM nicotinamide (Sigma-Aldrich), 50 ng ml<sup>-1</sup> human recombinant EGF (Peprotech), 500 nM A83-01 (Tocris), 3  $\mu$ M SB202190 (Cayman Chemicals) and 10 nM prostaglandin E2 (Cayman Chemicals). Organoids were passaged depending on growth every 1–2 weeks by incubating in TrypLE Express (Gibco) for 5–10 min followed by embedding in BME. Organoids were authenticated by SNP array or STR analysis and were regularly tested for Mycoplasma using Mycoplasma PCR43 and the MycoAlert Mycoplasma Detection Kit (LT07-318). In the first two weeks of organoid culture, 1 $\times$  Primocin (Invivogen) was added to prevent microbial contamination. Procedures performed with patient samples were approved by the Medical Ethical Committee of the Netherlands Cancer Institute–Antoni van Leeuwenhoek hospital (NL48824.031.14) and written informed consent was obtained from all of the patients. Mismatch repair status was assessed using a standard protocol for the Ventana automated immunostainer for MLH1 clone M1 (Roche), MSH2 clone G219-1129 (Roche), MSH6 clone EP49 (Abcam) and PMS2 clone EP51 (Agilent Technologies). The B2MKO tumour organoid lines were generated using sgRNA targeting B2M (GGCCGAGATGTCTCGCTCCG), cloned into LentiCRISPR v2 plasmid. The virus was produced using a standard method.

#### Screening of cancer cell lines and tumour organoids by flow cytometry

The cancer cell lines used in the reactivity and killing assays were screened for the expression of B2M, HLA class I molecules, NKG2D ligands, DNAM-1 ligands and butyrophilin using flow cytometry. In brief, cells were incubated with human Fc receptor block (BioLegend) and stained with the cell surface antibodies in different experiments (anti-CD112-PE (1:10, R2.525, BD Biosciences), anti-CD155-PE (1:10, 300907, R&D Systems), anti-CD277/BTN3A1-PE (1:50, BT3.1, Miltenyi), anti-B2M-PE (1:100, 2M2, BioLegend), anti-HLA-A/B/C-FITC (1:100, W6/32, eBioscience), anti-HLA-A/B/C-AF647 (1:160, W6/32, BioLegend), anti-HLA-E-BV421 (1:20, 3D12, BioLegend), anti-HLA-G-APC (1:20, 87G, BioLegend), anti-MICA/B-PE (1:300, 6D4, BioLegend), anti-ULBP1-PE (1:10, 170818, R&D Systems), anti-ULBP2/5/6-PE (1:20, 165903, R&D Systems), anti-ULBP3-PE (1:20, 166510, R&D Systems) or anti-ULBP4-PE (1:20, 709116, R&D Systems)) for 45 min at 4 °C. A 1:1,000 live/dead fixable near-infrared viability dye (Life Technologies) was included in each staining. Cells were washed three times in FACS buffer (PBS/1% FCS). Compensation was performed

using CompBeads (BD Biosciences) and ArC reactive beads (Life Technologies). Cells were acquired on the FACS Canto II 3L or FACS LSR Fortessa 4L (BD Biosciences) system running FACSDiva software (v.9.0; BD Biosciences). Isotype or FMO controls were included to determine the percentage of positive cancer cells. Data were analysed using FlowJo v.10.6.1 (Tree Star).

For organoid surface staining, tumour organoids were dissociated into single cells using TrypLE Express (Gibco), washed twice in cold FACS buffer (PBS, 5 mM EDTA, 1% bovine serum antigen), and stained with anti-HLA-A/B/C-PE (1:20, W6/32, BD Biosciences), anti-B2M-FITC (1:100, 2M2, BioLegend), anti-PD-L1-APC (1:200, MIH1, eBioscience) and 1:2,000 near-infrared (NIR) viability dye (Life Technologies), or isotype controls (1:1,000 FITC; 1:20, PE; or 1:200, APC) mouse IgG1 kappa (BD Biosciences). For NKG2D ligand expression analysis, cells were stained with anti-MICA/MICB (1:300), anti-ULBP1 (1:10), anti-ULBP2/5/6 (1:20), anti-ULBP3 (1:20), anti-ULBP4 (1:20) and 1:2,000 near-infrared (NIR) viability dye (Life Technologies). Tumour cells were incubated for 30 min at 4 °C in the dark and washed twice with FACS buffer. All of the samples were recorded with the BD LSR Fortessa Cell Analyzer SORP flow cytometer using FACSDiVa (v.8.0.2; BD Biosciences). Data were analysed using FlowJo (v.10.6.1; BD) and presented using GraphPad Prism (v.9.0.0; GraphPad).

#### Reactivity assay of $\gamma\delta$ T cells

The reactivity of  $\gamma\delta$  T cells to the different cancer cell lines was assessed by a co-culture reactivity assay.  $\gamma\delta$  T cells were thawed and cultured in IMDM + GlutaMax (Gibco)/8% nHS medium with penicillin (100 IU ml<sup>-1</sup>) and streptomycin (100 µg ml<sup>-1</sup>) in the presence of low-dose IL-2 (25 IU ml<sup>-1</sup>) and IL-15 (5 ng ml<sup>-1</sup>) overnight at 37 °C. Cancer cell lines were counted, adjusted to a concentration of 0.5 × 10<sup>5</sup> cells per ml in IMDM + GlutaMax/10% FCS medium with penicillin (100 IU ml<sup>-1</sup>) and streptomycin (100 µg ml<sup>-1</sup>), and seeded (100 µl per well) in coated 96-well flat-bottom microplates (Greiner CellStar) (for 5,000 cells per well) overnight at 37 °C. The next day,  $\gamma\delta$  T cells were collected, counted and adjusted to a concentration of 1.2 × 10<sup>6</sup> cells per ml in IMDM + GlutaMax/10% FCS medium. The  $\gamma\delta$  T cells were added in 50 µl (for 60,000 cells per well) and co-cultured (12:1 effector:target ratio) at 37 °C for 18 h in biological triplicates. The medium (without cancer cells) was used as a negative control and PMA (20 ng ml<sup>-1</sup>)/ionomycin (1 µg ml<sup>-1</sup>) was used as a positive control. After co-culture, the supernatant was collected to detect IFN $\gamma$  secretion by enzyme-linked immunosorbent assay (Mabtech) according to the manufacturer's instructions. Moreover, cells were collected, incubated with human Fc receptor block (BioLegend) and stained with cell surface antibodies (anti-CD137-APC (1:100, 4B4-1, BD Biosciences), anti-CD226/DNAM-1-BV510 (1:150, DX11, BD Biosciences), anti-CD3-AF700 (1:400, UCHT1, BD Biosciences), anti-CD39-APC (1:80, A1, BioLegend), anti-CD40L-PE (1:10, TRAP1, BD Biosciences), or anti-PD-1-PE (1:30, MIH4, eBioscience), anti-TCR $\gamma\delta$ -BV650 (1:40, 11F2, BD Biosciences), anti-NKG2D-PE-Cy7 (1:300, 1D11, BD Biosciences) and anti-OX40-FITC (1:20, ACT35, BioLegend)) for 45 min at 4 °C. A 1:1,000 live/dead fixable near-infrared viability dye (Life Technologies) was included in each staining. Cells were washed three times in FACS buffer (PBS/1% FCS). Compensation was performed using CompBeads (BD Biosciences) and ArC reactive beads (Life Technologies). Cells were acquired on the FACS LSR Fortessa X-20 4L (BD Biosciences) system running FACSDiva software (v.9.0; BD Biosciences). Data were analysed using FlowJo (v.10.6.1; Tree Star). All data are representative of at least two independent experiments.

### Immune cell killing assay $\gamma\delta$ T cells

Killing of the different cancer cell lines by  $\gamma\delta$  T cells was visualized and quantified by a co-culture immune cell killing assay using the IncuCyte S3 Live-Cell Analysis System (Essen Bioscience). HCT-15, LoVo and HT-29 cells were transduced with IncuCyte NuLight Red Lentivirus Reagent (EF-1 $\alpha$ , Puro; Essen BioScience) providing a nuclear-restricted expression of a red (mKate2) fluorescent protein. In brief, HCT-15, LoVo and HT-29 cells were seeded, transduced according to the manufacturer's instructions and stable cell populations were generated using puromycin selection. The B2M-knockin cell lines were created under puromycin selection; therefore, stable NuLight Red-expressing cell populations were generated by sorting for mKate2 (the red fluorescent protein) in the PE Texas Red filter set instead. Cancer cell lines were counted, adjusted to a concentration of  $1 \times 10^5$  cells per ml in IMDM + GlutaMax/10% FCS medium with penicillin (100 IU ml<sup>-1</sup>) and streptomycin (100  $\mu$ g ml<sup>-1</sup>), and seeded (100  $\mu$ l per well) in 96-well flat-bottom clear microplates (Greiner CellStar) (for 10,000 cells per well). The target cell plate was placed in the IncuCyte system at 37 °C to monitor for cell confluency for 3 days. On day 2,  $\gamma\delta$  T cells were thawed and cultured in IMDM + GlutaMax/8% nHS medium with penicillin (100 IU ml<sup>-1</sup>) and streptomycin (100  $\mu$ g ml<sup>-1</sup>) in the presence of low-dose IL-2 (25 IU ml<sup>-1</sup>) and IL-15 (5 ng ml<sup>-1</sup>) overnight at 37 °C. The next day,  $\gamma\delta$  T cells were collected, counted and adjusted to a concentration of  $7.2 \times 10^5$  cells per ml in IMDM + GlutaMax/10% FCS medium. After aspiration of the medium of the target cell plate, 100  $\mu$ l of new medium containing 3.75  $\mu$ M IncuCyte Caspase-3/7 Green Apoptosis Reagent (Essen BioScience) (1.5 $\times$  final assay concentration of 2.5  $\mu$ M) was added together with 50  $\mu$ l of  $\gamma\delta$  T cells (for 36,000 cells per well). They were co-cultured (4:1 effector:target ratio) in the IncuCyte system at 37 °C in biological duplicates. Cancer cells alone and cancer cells alone with caspase-3/7 were used as negative controls. Images (2 images per well) were captured every hour at  $\times 20$  magnification with the phase, green and red channels for up to 4 days.

Analysis was performed using the IncuCyte software (v.2020B) for each cancer cell line separately. The following analysis definitions were applied: a minimum phase area of 200  $\mu$ m<sup>2</sup>, RCU of 2.0, and a GCU of 2.0 (for HCT-15 cells) and 4.0 (for LoVo and HT-29 cells). Cancer cell apoptosis was then quantified in the IncuCyte software by counting the total number of green + red objects per image normalized (by division) to the total number of red objects per image after 12 h co-culture and displayed as a percentage (mean  $\pm$  s.e.m.) of two wells with two images per well. For the comparison of the killing of B2M-knockin HCT-15 and LoVo cell lines versus the WT cell lines, Caspase-3/7 Red Apoptosis Reagent (Essen BioScience) was used. The transfection of the target reporter was not as successful in combination with the B2M-knockin. Thus, apoptosis was quantified by dividing the red area by the phase area and displayed as a percentage (mean  $\pm$  s.e.m.) of two wells with two images per well. The following analysis definitions were applied: a minimum phase area of 100  $\mu$ m<sup>2</sup> and a RCU of 0.5 (for HCT-15 cells) and 0.75 (for LoVo cells).

### Tumour organoid recognition assay

For evaluation of tumour reactivity towards B2MWT and B2MKO organoids and NKG2D ligand blocking conditions, tumour organoids and  $\gamma\delta$  T cells were prepared as described previously<sup>9,66,67</sup>. Two days before the experiment, organoids were isolated from BME by incubation in 2 mg ml<sup>-1</sup> type II dispase (Sigma-Aldrich) for 15 min before addition of 5 mM EDTA and washed with PBS before being resuspended in CRC organoid medium with 10  $\mu$ M Y-27632 (Sigma-Aldrich). The organoids were stimulated with 200 ng

ml<sup>-1</sup> IFN $\gamma$  (Peprotech) 24 h before the experiment. For the recognition assay and intracellular staining, tumour organoids were dissociated into single cells and plated in anti-CD28-coated (CD28.2, eBioscience) 96-well U-bottom plates with  $\gamma\delta$  T cells at a 1:1 target:effector ratio in the presence of 20  $\mu$ g ml<sup>-1</sup> anti-PD-1 (Merus). As a positive control,  $\gamma\delta$  T cells were stimulated with 50 ng ml<sup>-1</sup> of phorbol-12-myristate-13-acetate (Sigma-Aldrich) and 1  $\mu$ g ml<sup>-1</sup> of ionomycin (Sigma-Aldrich). After 1 h of incubation at 37 °C, GolgiSTOP (BD Biosciences, 1:1,500) and GolgiPlug (BD Biosciences, 1:1,000) were added. After 4 h of incubation at 37 °C,  $\gamma\delta$  T cells were washed twice in cold FACS buffer (PBS, 5 mM EDTA, 1% bovine serum antigen) and stained with anti-CD3-PerCP-Cy5.5 (1:20, BD Biosciences), anti-TCR $\gamma\delta$ -PE (1:20, BD Bioscience), anti-CD4-FITC (1:20, BD Bioscience) (not added in experiments with NKG2D ligand blocking), anti-CD8-BV421 (1:200, BD Biosciences) and 1:2,000 near-infrared (NIR) viability dye (Life Technologies) for 30 min at 4 °C. Cells were washed, fixed and stained with 1:40 anti-IFN $\gamma$ -APC (BD Biosciences) for 30 min at 4 °C, using the Cytotfix/Cytoperm Kit (BD Biosciences). After two wash steps, cells were resuspended in FACS buffer and recorded with the BD LSR Fortessa Cell Analyzer SORP flow cytometer using FACSDiVa software (v.8.0.2; BD Biosciences). Data were analysed using FlowJo (v.10.6.1, BD) and presented using GraphPad Prism (v.9.0.0, GraphPad).

Blocking experiments with cancer cell lines and tumour organoids.

The reactivity of and killing by the  $\gamma\delta$  T cells was examined in the presence of different blocking antibodies to investigate which receptor–ligand interactions were involved. For DNAM-1 blocking,  $\gamma\delta$  T cells were incubated with 3  $\mu$ g ml<sup>-1</sup> purified anti-DNAM-1 (DX11, BD Biosciences) for 1 h at 37 °C. For  $\gamma\delta$  TCR blocking,  $\gamma\delta$  T cells were incubated with 3  $\mu$ g ml<sup>-1</sup> purified anti-TCR $\gamma\delta$  (5A6.E9, Invitrogen) for 1 h at 37 °C; the clone that we used was tested to be the best for use in  $\gamma\delta$  TCR blocking assays<sup>68</sup>. NKG2D ligands were blocked on the cancer cell lines and single cells of tumour organoids by incubating the target cells with 12  $\mu$ g ml<sup>-1</sup> anti-MICA/B (6D4, BioLegend), 1  $\mu$ g ml<sup>-1</sup> anti-ULBP1 (170818, R&D Systems), 3  $\mu$ g ml<sup>-1</sup> anti-ULBP2/5/6 (165903, R&D Systems) and 6  $\mu$ g ml<sup>-1</sup> anti-ULBP3 (166510, R&D Systems) for 1 h at 37 °C before plating with  $\gamma\delta$  T cells. After incubation with the blocking antibodies, the  $\gamma\delta$  T cells were added to cancer cell lines HCT-15, LoVo and HT-29 as described above with a minimum of two biological replicates per blocking condition. For organoid experiments, anti-CD107a-FITC (1:50, H4A3, BioLegend) was added during incubation.

As a control for Fc-mediated antibody effector functions,  $\gamma\delta$  T cells alone were incubated with the blocking antibodies in the presence of 2.5  $\mu$ M InCuCyte Caspase-3/7 Green Apoptosis Reagent (Essen BioScience) in the InCuCyte system at 37 °C, and the number of apoptotic  $\gamma\delta$  T cells was quantified over time.

Data analysis and visualization

Bulk DNA-seq and RNA-seq data were analysed using Python (v.3) and R (v.3.6.1) in Jupyter Notebook (v.6.0.1). Numpy (v.1.17.2) and Pandas (v.0.25.1) were used for array and data frame operations, respectively. Data visualization was performed using Matplotlib (v.3.2.1) and Seaborn (v.0.9.0). scRNA-seq data were analysed using Cell Ranger (v.3.1.0), R (v.4.1.0) and Seurat (v.3.1.5). IMC data were analysed

using ilastik (v.1.3.3), CellProfiler (v.2.2.0), ImaCyte (v.1.1.4) and Cytosplore (v.2.3.0). Flow cytometry data were analysed using FlowJo (v.10.6.1). IncuCyte data were analysed using IncuCyte (v.2020B). Data visualization was performed using GraphPad Prism (v.9.0.0 and v.9.0.1).

#### Reporting summary

Further information on research design is available in the [Nature Portfolio Reporting Summary](#) linked to this article.

#### Data availability

The TCGA data used here are publicly available at the National Cancer Institute GDC Data Portal (<https://portal.gdc.cancer.gov>; cohorts COAD, STAD and UCEC). Of the DRUP study participants included in this preliminary analysis across all (complete and incomplete) cohorts of the study, we included all clinical data, genomics data on B2M status and RNA expression data of marker gene sets in Supplementary Table 1. The raw sequencing data of the DRUP and Hartwig cohorts can be accessed through Hartwig Medical Foundation on approval of a research access request (<https://www.hartwigmedicalfoundation.nl/en/data/data-access-request>). As determined in the original publication, NICHE study RNA-seq and DNA-seq data have been deposited into the European Genome-Phenome Archive under accession number [EGAS00001004160](https://www.ebi.ac.uk/ena/browser/view/EGAS00001004160) and are available on reasonable request for academic use and within the limitations of the provided informed consent. The scRNA-seq data have been deposited at the GEO ([GSE216534](https://www.ncbi.nlm.nih.gov/geo/query/acc.cgi?acc=GSE216534)) and are publicly available. All other data are available from the corresponding author on reasonable request. The GRCh38 primary assembly of the human reference genome was downloaded from Gencode ([https://ftp.ebi.ac.uk/pub/databases/gencode/Gencode\\_human/release\\_42/GRCh38.primary\\_assembly.genome.fa.gz](https://ftp.ebi.ac.uk/pub/databases/gencode/Gencode_human/release_42/GRCh38.primary_assembly.genome.fa.gz)) with Gencode's matching v29 annotation file ([https://ftp.ebi.ac.uk/pub/databases/gencode/Gencode\\_human/release\\_29/gencode.v29.annotation.gtf.gz](https://ftp.ebi.ac.uk/pub/databases/gencode/Gencode_human/release_29/gencode.v29.annotation.gtf.gz)) for gene expression quantification.

**Acknowledgements** We thank K. C. M. J. Peeters, M. G. Kallenberg-Lantrua, D. Berends-van der Meer and F. A. Holman for their help in collecting and providing samples from patients with colon cancer; the staff at the Flow Cytometry Core Facility of the Leiden University Medical Center for their help with cell sorting; the staff at the Leiden Genome Technology Center for their help with scRNA-seq; M. Ganesh for help with cell culturing; D. Thommen for discussions; I. S. Rodriguez for the establishment of a B2M-knockout organoid line; L. Hoes for initial clinical findings; the staff at the Flow Cytometry Core Facility at the Netherlands Cancer Institute for their support; X. Kong for providing the lentiCRISPR plasmid for B2M knockout; the staff at Merus for providing anti-PD-1 antibodies for organoid experiments; and the staff at The Cancer Genome Atlas (TCGA) for providing data used in this manuscript. N.F.C.C.d.M. is funded by the European Research Council (ERC) under the European Union's Horizon 2020 Research and Innovation Programme (grant agreement no. 852832). E.E.V. received funding from the Oncode Institute and Open Targets (Identification of targets modulating lymphocyte-mediated tumour cell killing (project ID: OTAR2061); project leaders, M. Garnett and E.E.V.) and the Josephine Nefkens Foundation. F.K. was supported by the collaboration project TIMID (LSHM18057-SGF) financed by the PPP allowance made

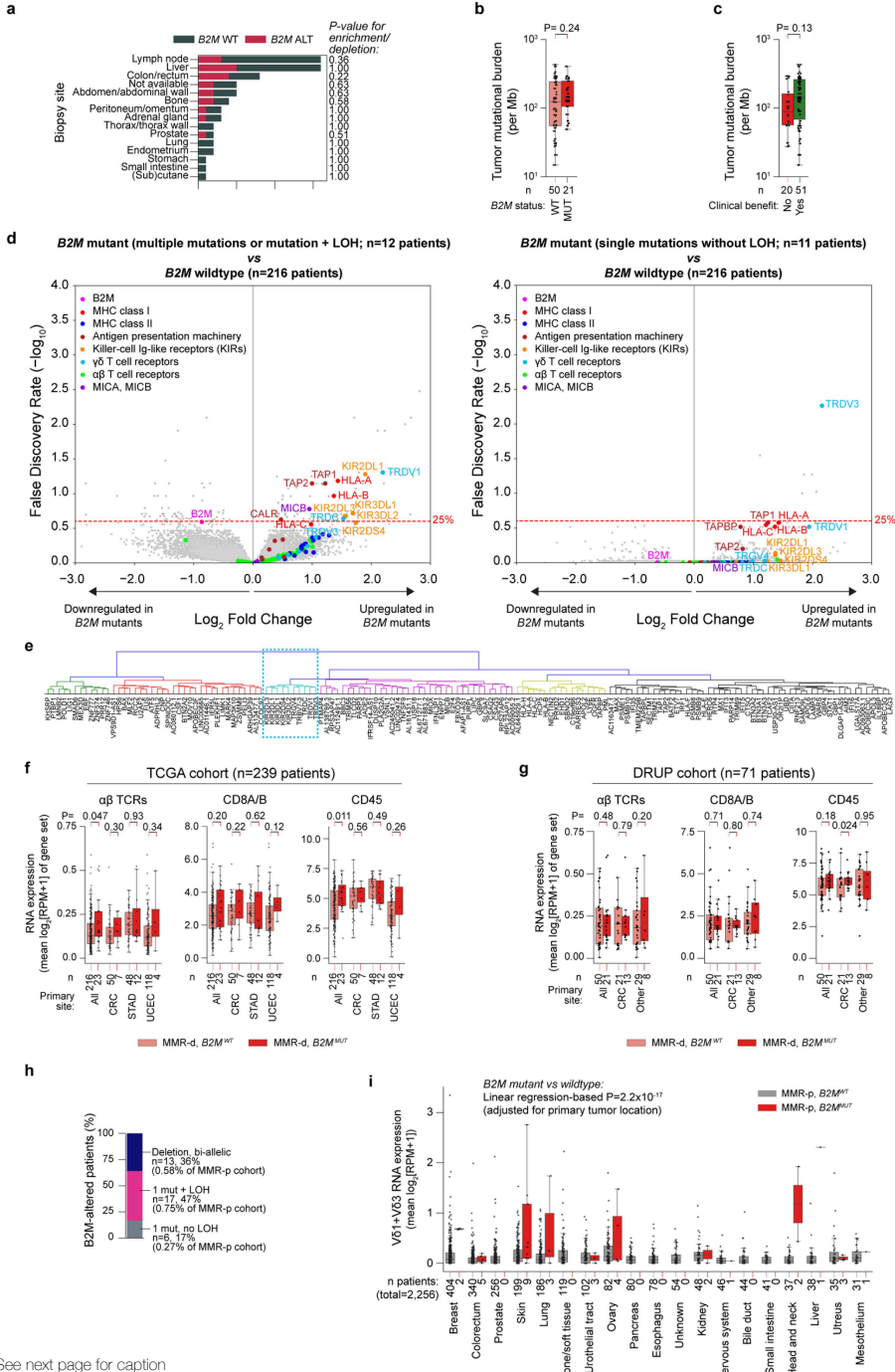


available by Top Sector Life Sciences & Health to Samenwerkende Gezondheidsfondsen (SGF) to stimulate public-private partnerships and co-financing by health foundations that are part of the SGF.

**Author contributions** N.L.d.V., J.v.d.H. and V.V. conceived the study and performed experiments. J.v.d.H. performed genomic and bulk transcriptomic analyses of ICB-naive as well as ICB-treated MMR-d cancers. N.L.d.V. performed scRNA-seq and cell culturing experiments. V.V. performed organoid experiments. N.L.d.V., M.v.d.P. and J.v.d.B. performed cell line reactivity and immune cell killing experiments. N.L.d.V., V.V. and M.v.d.P. performed blocking experiments. M.C. provided tissue sections of patients in the NICHE study, which was designed and coordinated by M.C. under the joint supervision of T.N.S., E.E.V. and J.B.H.; M.E.I. performed IMC experiments. M.E.I., N.F.C.C.d.M., N.L.d.V. and D.R. analysed the IMC data. N.L.d.V. and D.R. analysed the scRNA-seq data. J.G.v.d.B. evaluated histological and immunohistochemical analyses. L.J.Z., B.S.G., G.F.d.W., T.W.B., H.G. and H.M.W.V. designed, coordinated and analysed data from the DRUP study. General scientific coordination was undertaken by J.v.d.H.; L.F.A.W., F.K., N.F.C.C.d.M. and E.E.V. supervised the study; T.N.S. had an advisory role. The manuscript was written by N.L.d.V., J.v.d.H. and V.V. in collaboration with all of the authors. All of the authors commented on and approved the manuscript.

**Competing interests** M.C. has performed an advisory role or offered expert testimony for BMS, MSD and NUMAB; has received honoraria from BMS and Roche; and has received financing of scientific research from Roche, BMS and MSD. J.B.H. has received research funding from BMS; and has performed an advisory role for BMS.

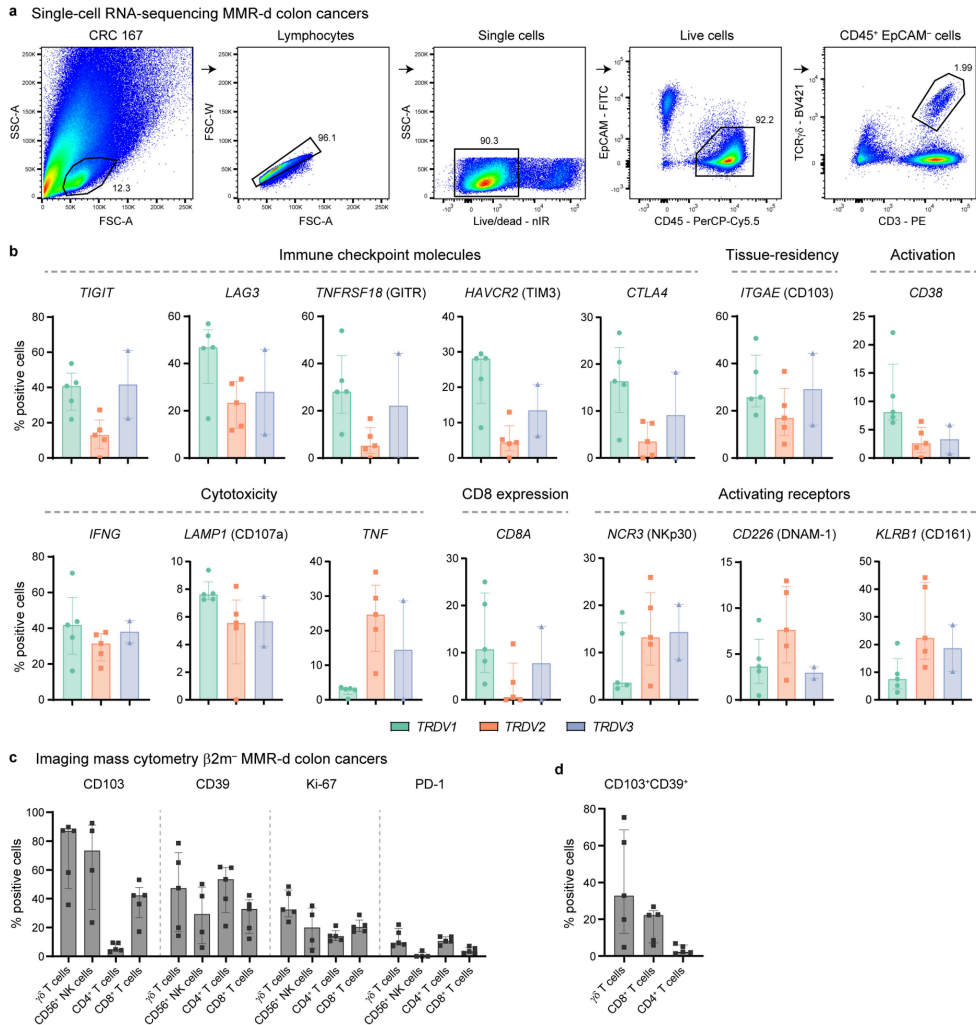
SUPPLEMENTAL FIGURES



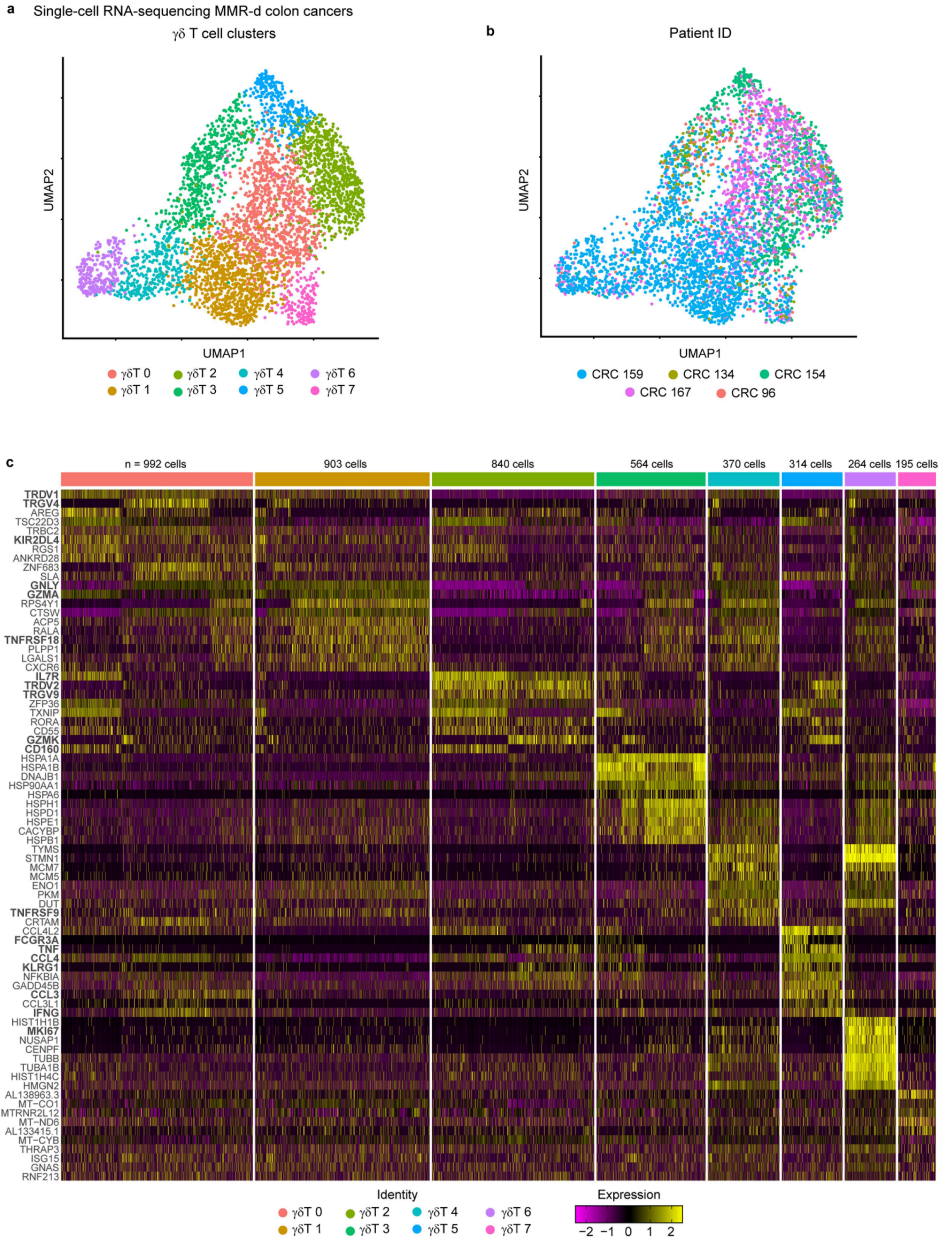
See next page for caption



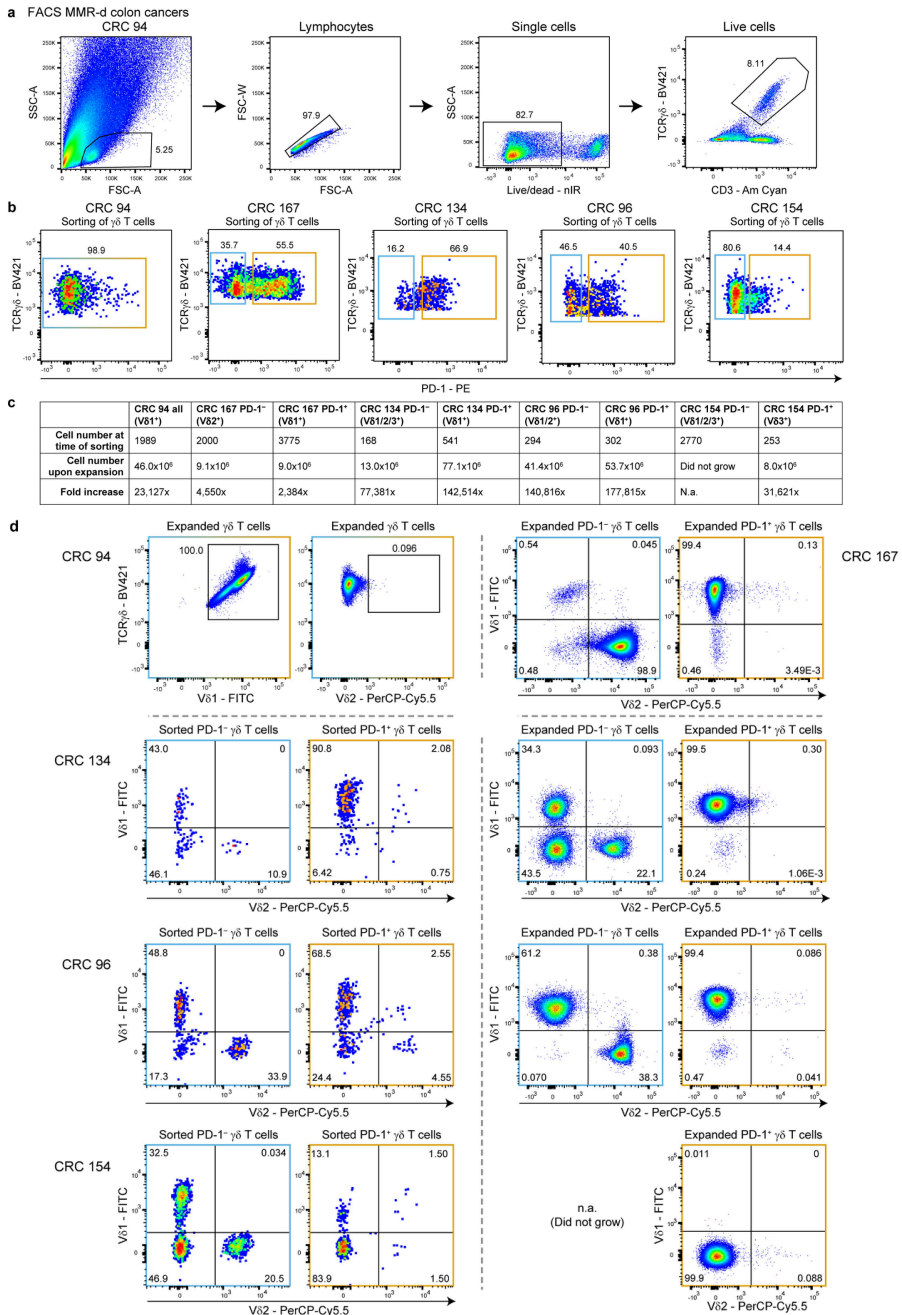
**Extended Data Fig. 1 Association of B2M status to clinical, genomic, and transcriptomic characteristics of MMR-d and MMR-p tumours.** Biopsy site distribution in the DRUP cohort (n = 71 patients). Colours denote patients' B2M status (WT: wildtype,; ALT: altered). Fisher's exact test-based two-sided P-values for enrichment/depletion of B2M altered tumours per biopsy site are shown. b. Tumour mutational burden vs B2M status. Wilcoxon rank sum test-based two-sided P-value is shown. Boxes, whiskers, and dots indicate quartiles, 1.5 interquartile ranges, and individual data points, respectively. c. As b, but for clinical benefit to ICB (x-axis). d. Volcano plots indicating differential gene expression between B2M-based subgroups (see title) of MMR-d cancers in TCGA COAD (colon adenocarcinoma; n = 57 patients), STAD (stomach adenocarcinoma; n = 60 patients) and UCEC (uterus corpus endometrial carcinoma; n = 122 patients) cohorts. Results were adjusted for tumour type and multiple hypothesis testing (Methods). e. Hierarchical clusters of expression of genes significantly (FDR <25%; see Fig. 1D) upregulated in MMR-d B2MMUT vs MMR-d B2MWT cancers in the TCGA COAD/STAD/UCEC cohorts. The blue dashed rectangle denotes the V $\delta$ 1/3 T cell cluster. f. Immune marker gene set expression in B2MWT (pink), and B2MMUT (red) MMR-d cancers in the TCGA COAD/STAD/UCEC cohorts separately or combined (All). Boxes, whiskers, and dots indicate quartiles, 1.5 interquartile ranges, and individual data points, respectively. Wilcoxon rank sum test-based two-sided P-values are shown. g. As f, but for MMR-d cancers in the DRUP cohort, for all cancers combined (All), only colorectal cancer (CRC), or all non-CRC cancers (Other). Two-sided P-values were calculated with linear regression adjusting for biopsy site and tumour type (Methods). h. Allelic alteration status of B2M in the Hartwig cohort of MMR-p cancers. i. RNA expression of V $\delta$ 1+V $\delta$ 3 loci in MMR-p B2MWT (grey), and MMR-p B2MMUT (red) cancers in the Hartwig cohort, stratified per primary tumour location. Boxes, whiskers, and dots indicate quartiles, 1.5 interquartile ranges, and individual data points, respectively. The linear regression-based, two-sided, primary tumour location-adjusted P-value for association of B2M status with V $\delta$ 1+V $\delta$ 3 loci expression is shown.



**Extended Data Fig. 2: Characterization of  $\gamma\delta$  T cells and other immune cell populations infiltrating MMR-d colon cancers.** a. FACS gating strategy for single, live CD45+ EpCAM- CD3+ TCR $\gamma\delta$ + cells from a representative MMR-d colon cancer sample showing sequential gates with percentages. b. Frequencies of positive cells for selected genes across V $\delta$ 1 (n = 1927), V $\delta$ 2 (n = 860), and V $\delta$ 3 (n = 506) cells as percentage of total  $\gamma\delta$  T cells from each MMR-d colon tumour (n = 5) analysed by single-cell RNA-sequencing. V $\delta$ 3 cells were present in two out of five colon cancers. Bars and dots indicate median  $\pm$  IQR and individual samples, respectively. c. Frequencies of marker-positive  $\gamma\delta$  T cells, CD56+ NK cells, CD4+ T cells, and CD8+ T cells in treatment-naive  $\beta 2m^-$  (n = 5) MMR-d colon cancers. CD56+ NK cells were present in four out of five  $\beta 2m^-$ -cancer samples. Bars and dots indicate median  $\pm$  IQR and individual samples, respectively. d. Frequencies of CD103+CD39+  $\gamma\delta$  T cells, CD8+ T cells, and CD4+ T cells in treatment-naive  $\beta 2m^-$  (n = 5) MMR-d colon cancers. Bars indicate median  $\pm$  IQR and individual samples, respectively.



Extended Data Fig. 3: Distinct clusters of  $\gamma\delta$  T cells in MMR-d colon cancers by single-cell RNA-sequencing. a. UMAP embedding showing  $\gamma\delta$  T cells ( $n = 4442$ ) isolated from MMR-d colon cancers ( $n = 5$ ) analysed by single-cell RNA-sequencing. Colours represent the functionally different  $\gamma\delta$  T cell clusters identified by graph-based clustering and non-linear dimensional reduction. Dots represent single cells. b. UMAP embedding of (a) coloured by patient ID. Dots represent single cells. c. Heatmap showing the normalized single-cell gene expression value (z-score, purple-to-yellow scale) for the top 10 differentially expressed genes in each identified  $\gamma\delta$  T cell cluster.

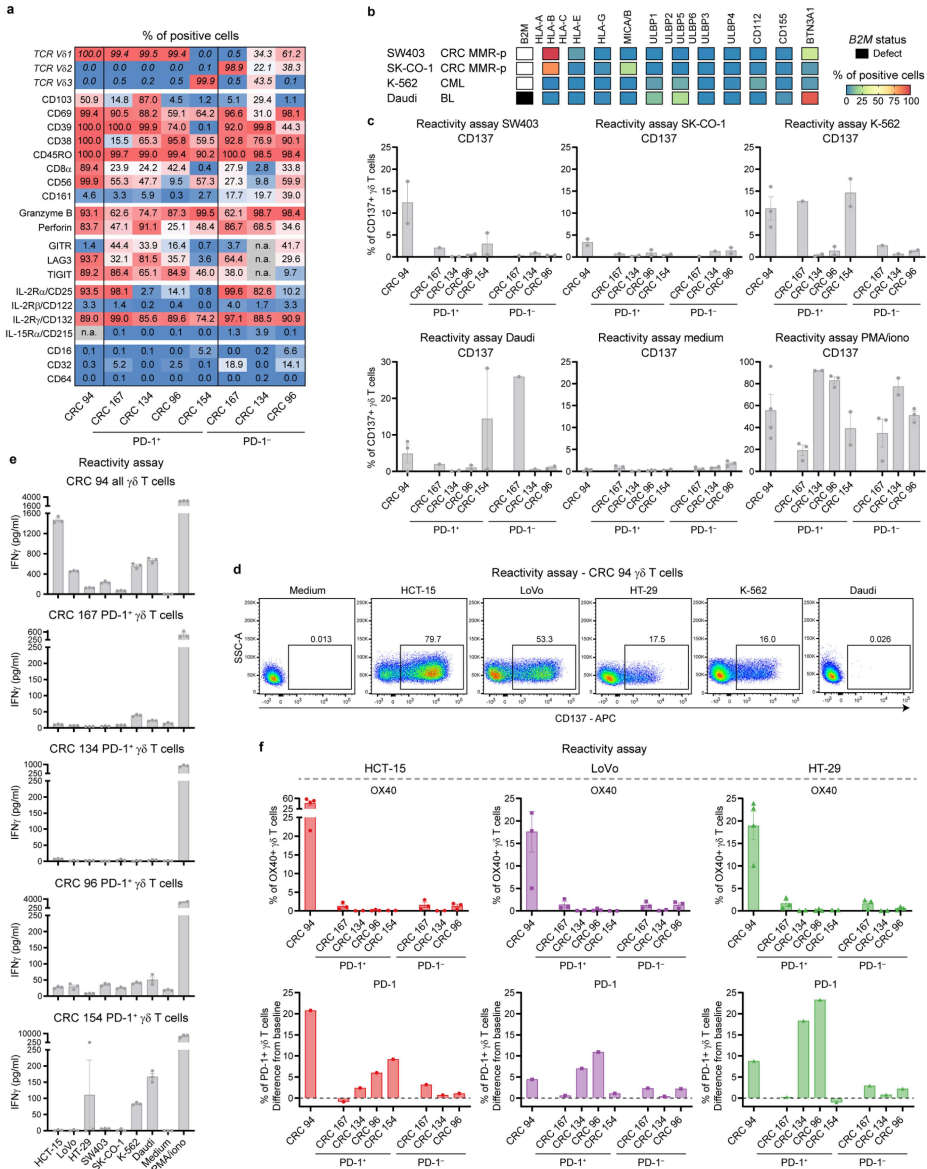


Extended Data Fig. 4 | Sorting and expansion of  $\gamma\delta$  T cells from MMR-d colon cancers.

a. FACS gating strategy for single, live CD3+ TCR $\gamma\delta$ + cells from a representative MMR-d colon cancer sample showing sequential gates with percentages. b. Sorting of all  $\gamma\delta$  T cells from CRC94 (due to the low number of PD-1+ cells), and of PD-1- (blue squares) and PD-1+ (orange squares)  $\gamma\delta$  T cells from CRC167, CRC134,

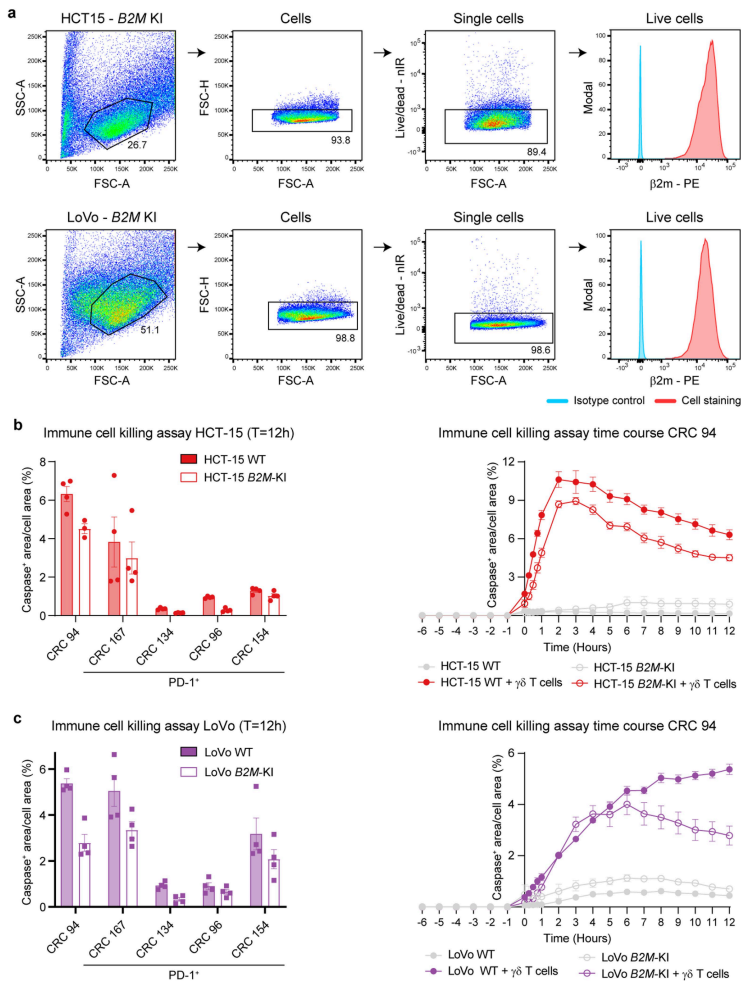


CRC96, and CRC154. Dots represent single cells. c. Table showing the number of  $\gamma\delta$  T cells isolated from MMR-d colon cancers (n = 5) at the time of sorting vs 3-4 weeks after expansion, and the fold increase thereof. d. TCR V $\delta$  chain usage after expansion of  $\gamma\delta$  T cells from CRC94 and CRC167 (first row), and at the time of sorting (left panel) as well as after expansion (right panel) of  $\gamma\delta$  T cells from CRC134, CRC96, and CRC154. PD-1-  $\gamma\delta$  T cells from CRC154 did not expand in culture. Dots represent single cells.



Extended Data Fig. 5: Phenotype and reactivity of  $\gamma\delta$  T cells towards cancer cell lines. a. The percentage of positive cells for the indicated markers on expanded  $\gamma\delta$  T cells from MMR-d colon cancers (n = 5). b. Diagram showing the B2M status and surface expression of HLA class I, NKG2D ligands, DNAM-1 ligands,

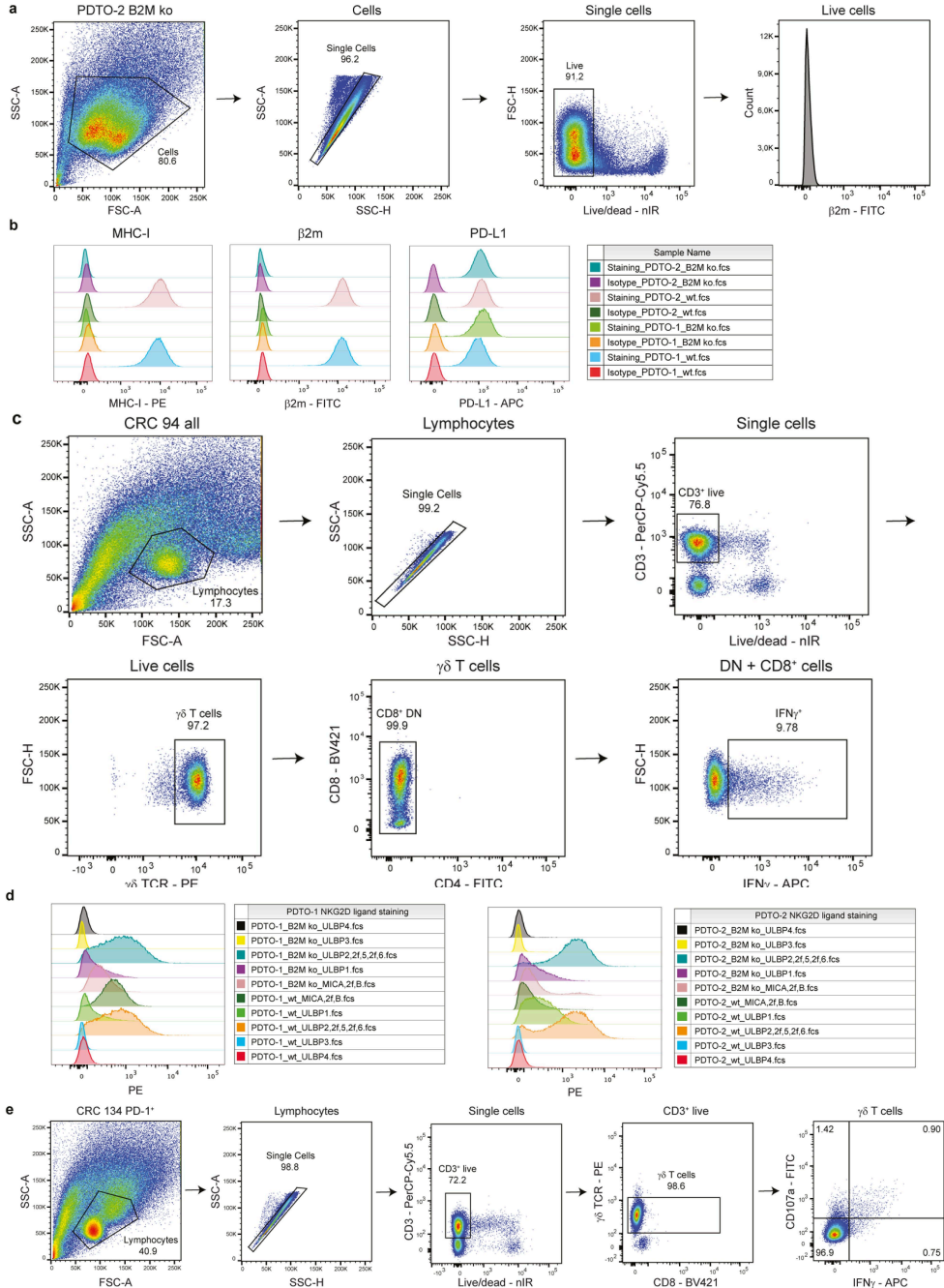
and butyrophilin on cancer cell lines. c. Bar plots showing CD137 expression on  $\gamma\delta$  T cells upon co-culture with cancer cell lines. Medium was used as negative control and PMA/ionomycin as positive control. Bars indicate mean  $\pm$  SEM. Data from at least two independent experiments except for CRC167, depending on availability of  $\gamma\delta$  T cells. d. Representative flow cytometry plots showing CD137 expression on  $\gamma\delta$  T cells from a MMR-d colon cancer upon co-culture with cancer cell lines as compared to medium only. Gates indicate percentage of positive  $\gamma\delta$  T cells. e. Bar plots showing the presence of IFN $\gamma$  in the supernatant upon co-culture of  $\gamma\delta$  T cells from MMR-d colon cancers (n = 5) with cancer cell lines. Medium as negative control and PMA/ionomycin as positive control are included. Bars indicate mean  $\pm$  SEM of triplicates. f. Bar plots showing the expression of OX40 (first row) and PD-1 (second row) on  $\gamma\delta$  T cells upon co-culture of  $\gamma\delta$  T cells with CRC cell lines. PD-1 expression is shown as difference from baseline (medium) condition. Bars indicate mean  $\pm$  SEM. Data from at least two independent experiments.



Extended Data Fig. 6: Reactivity of  $\gamma\delta$  T cells towards B2M-knockin vs -wildtype cancer cell lines. a. Flow cytometry gating strategy to validate  $\beta$ 2m expression on HCT-15 and LoVo B2M-knockin (B2M-KI) cell

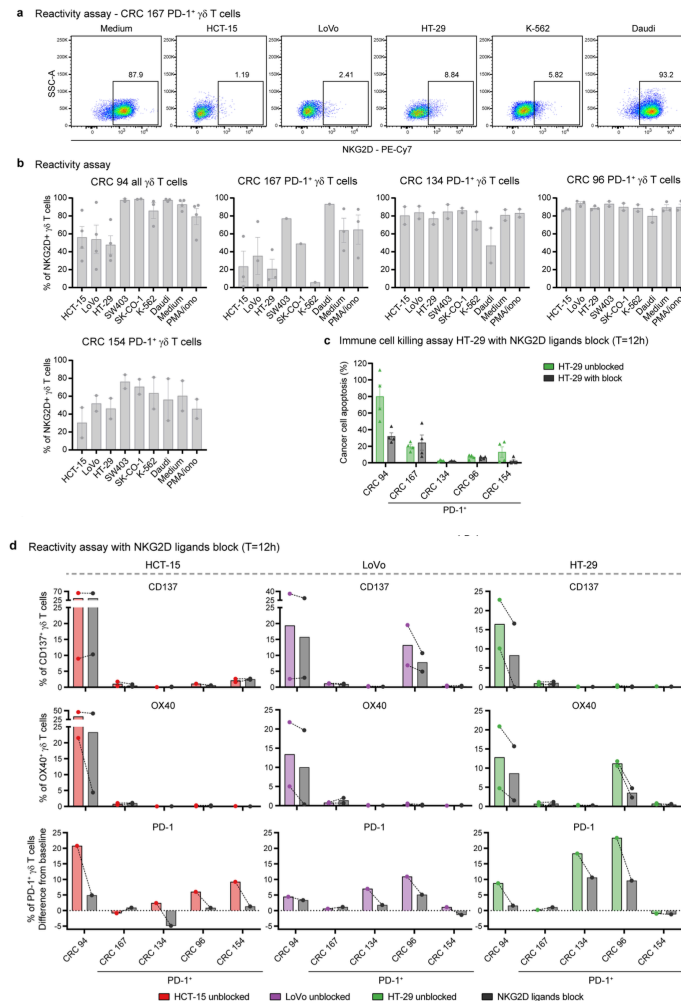


lines. Isotype controls were included as negative control. b. Bar plots showing the quantification of killing of HCT-15 B2M-KI vs wildtype (WT) cells upon co-culture with  $\gamma\delta$  T cells from MMR-d colon cancers (n = 5) in the presence of a red fluorescent caspase-3/7 reagent. Bars indicate mean  $\pm$  SEM of two wells with two images/well. Right panel shows representative time course of apoptosis. c. As b, but for LoVo B2M-KI vs WT cells.



See next page for caption

**Extended Data Fig. 7: Tumour organoid characterization and reactivity assay readout.** Flow cytometry gating strategy on PDO cells for analysis of surface staining. Selected cells were gated on single, live cells before quantification of staining signal. b. Histogram representation and count for surface staining of MHC-I, PD-L1, and  $\beta$ 2m expression on two PDO lines B2M WT and B2M KO after IFN $\gamma$  pre-stimulation. Staining with isotype antibodies for each fluorochrome (PE, APC and FITC) were included as negative control. c. Flow cytometry gating strategy on  $\gamma\delta$  T cell samples for analysis of intracellular staining to test antitumour reactivity upon PDO stimulation. Lymphocyte population was further gated on single cells, live and CD3+ cells,  $\gamma\delta$ TCR+ cells and CD8+ as well as CD8-CD4- cells. Reactivity of the sample was based on IFN $\gamma$ + cells of the selected population. d. Histogram representation and count for surface staining of NKG2D ligands MICA/B, ULBP1, ULBP2/5/6, ULBP3, and ULBP4 on two PDO lines B2M wt and B2M ko after IFN $\gamma$  pre-stimulation. e. Flow cytometry gating strategy on  $\gamma\delta$  T cell samples for analysis of intracellular staining after stimulation with PDOs in the presence of NKG2D ligand blocking. Lymphocyte population was further gated on single cells, live and CD3+ cells, followed by  $\gamma\delta$ TCR+ and CD8+ as well as CD8- cells. Reactivity of final population was based on IFN $\gamma$ + or CD107a+ cells.

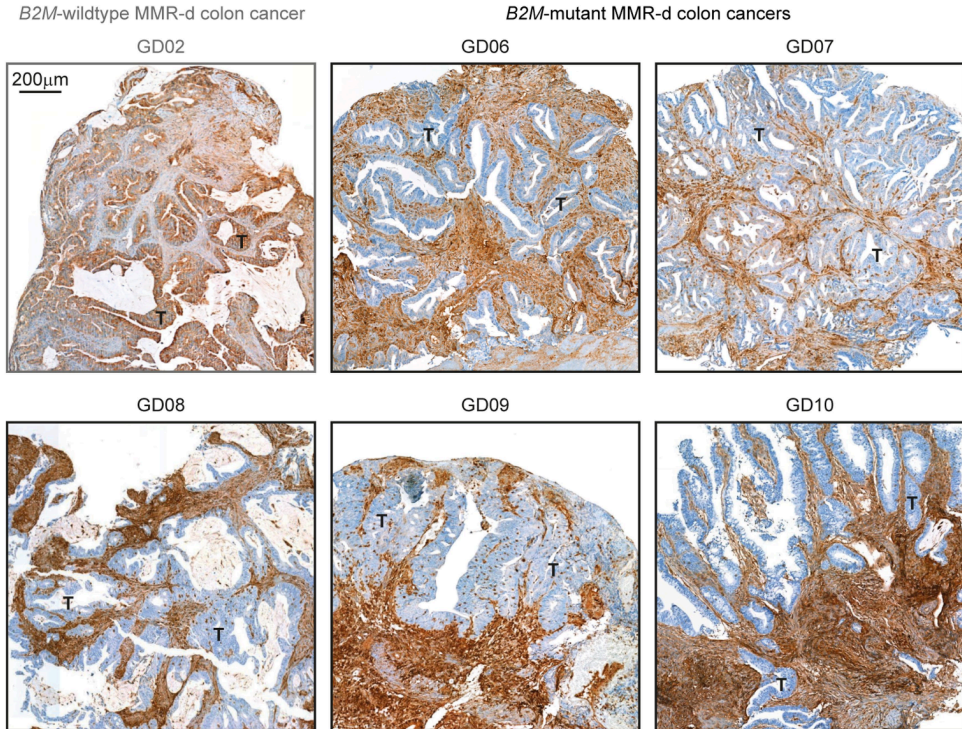


**Extended Data Fig. 8: Reactivity of  $\gamma\delta$  T cells towards cancer cell lines in the presence of NKG2D ligand blocking.**

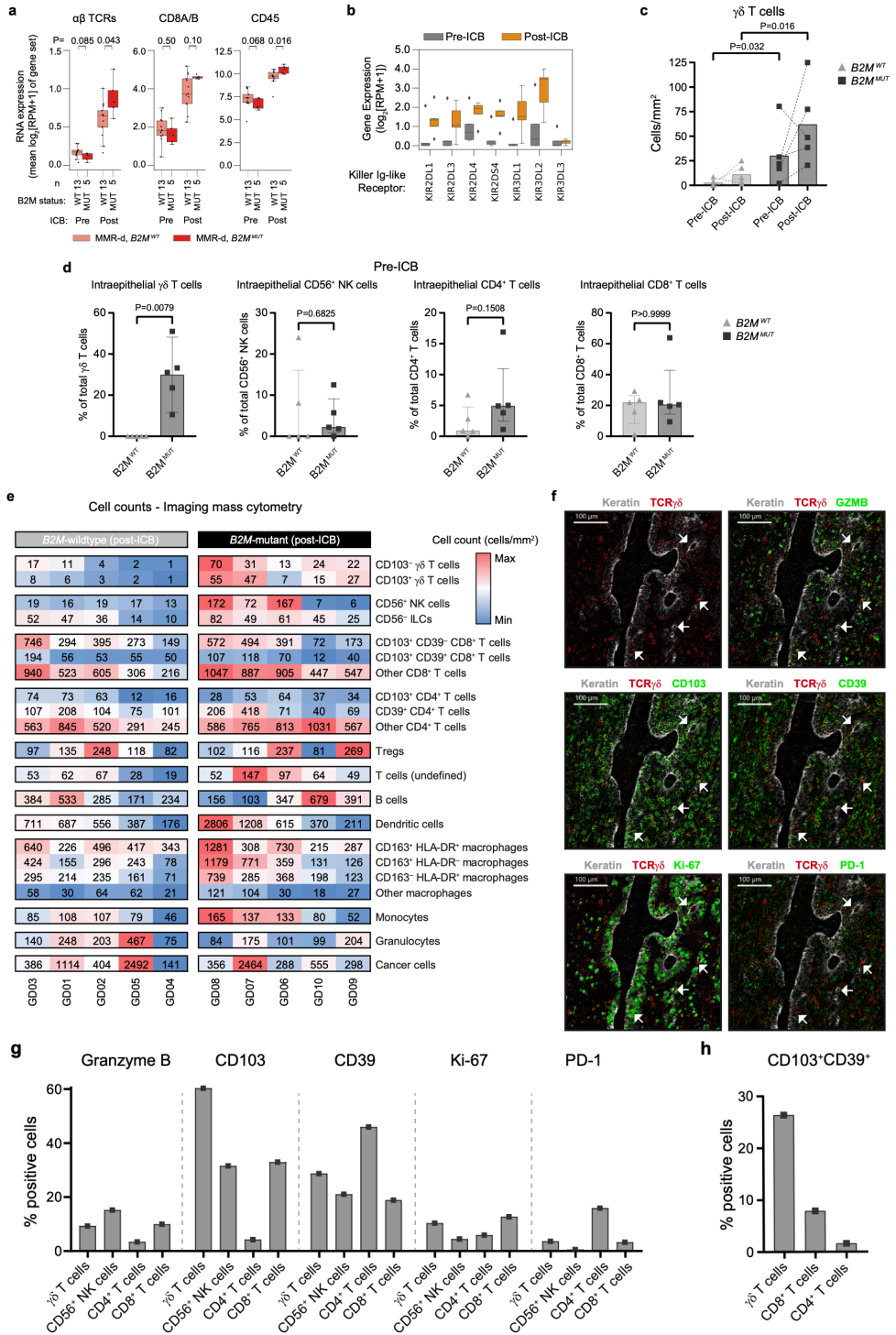
a. Representative flow cytometry plots showing NKG2D expression on  $\gamma\delta$  T cells from a MMR-d colon cancer upon co-culture with cancer cell lines as compared to medium only. Gates indicate percentage of positive  $\gamma\delta$  T cells. b. Bar plots showing NKG2D expression on  $\gamma\delta$  T cells from MMR-d colon cancers (n = 5) upon co-culture with cancer cell lines. Medium as negative control and PMA/ionomycin as positive control are included. Bars indicate mean  $\pm$  SEM. Data from at least two independent experiments except for CRC167 (SW403, SK-CO-1, K-562), depending on availability of  $\gamma\delta$  T cells. c. Bar plots showing the killing



of HT-29 cells upon co-culture with  $\gamma\delta$  T cells with or without NKG2D ligand blocking. Bars indicate mean  $\pm$  SEM of two wells with two images/well. d. Bar plots showing the expression of CD137 (first row), OX40 (second row), and PD-1 (third row) on  $\gamma\delta$  T cells upon co-culture of  $\gamma\delta$  T cells with CRC cell lines with or without NKG2D ligand blocking. PD-1 expression is shown as difference from baseline (medium) condition. Bars and lines indicate mean and similar experiments, respectively. Data from two independent experiments for CD137 and OX40.



**Extended Data Fig. 9: Loss of  $\beta$ 2m protein expression on tumour cells in B2M-mutant MMR-d colon cancers.** Immunohistochemical analysis of  $\beta$ 2m protein expression in FFPE tissue from all five B2M MUT MMR-d colon cancers of the NICHE cohort. A B2M WT case (GD02) staining positive for  $\beta$ 2m is included as control. Details on the staining procedure can be found in Methods.



See next page for caption

**Extended Data Fig. 10: Distribution of immune cell populations in B2M- mutant and B2M-wildtype MMR-d colon cancers pre- and post-ICB treatment in the NICHE trial.** a. Immune marker gene set RNA expression in MMR-d B2M WT (pink), and MMR-d B2M MUT (red) cancers, before (left) and after (right) neoadjuvant ICB. Boxes, whiskers, and dots indicate quartiles, 1.5 interquartile ranges, and individual data points, respectively. Wilcoxon rank sum test-based two-sided P-values are shown. b. Pre- (grey) and post-ICB (orange) RNA expression of KIRs in B2M MUT MMR-d cancers in the NICHE study (n = 5). Boxes, whiskers, and dots indicate quartiles, 1.5 interquartile ranges, and outliers, respectively. Two-sided P-values were calculated by Wilcoxon rank sum test. c. Pre- and post-ICB frequencies of  $\gamma\delta$  T cells by imaging mass cytometry in B2M WT (n = 5) and B2M MUT (n = 5) MMR-d colon cancers (corresponding to Fig. 4b). Lines indicate paired samples, dots represent individual samples. Wilcoxon rank sum test-based two-sided P-values are shown. d. Imaging mass cytometry-based frequencies of intraepithelial  $\gamma\delta$  T cells, CD56+ NK cells, CD4+ T cells, and CD8+ T cells in ICB-naïve B2M WT (n = 5) and B2M MUT (n = 5) MMR-d colon cancers. Bars and dots indicate median  $\pm$  IQR and individual samples, respectively. Wilcoxon rank sum test-based two-sided P-values are shown. e. Cell counts (cells/mm<sup>2</sup>) of immune populations from the imaging mass cytometry of B2M WT (n = 5) and B2M MUT (n = 5) MMR-d colon cancers upon ICB treatment. Colour bar is scaled per immune population. f. Representative images of the detection of cytotoxic (granzyme B+), tissue-resident (CD103+), activated (CD39+), proliferating (Ki-67+), and PD-1+  $\gamma\delta$  T cells by imaging mass cytometry in a B2M MUT MMR-d colon cancer upon ICB treatment. g. Frequencies of marker-positive  $\gamma\delta$  T cells, CD56+ NK cells, CD4+ T cells, and CD8+ T cells in the sole B2M MUT MMR-d colon cancer that contained cancer cells upon ICB treatment. h. Frequencies of CD103+CD39+  $\gamma\delta$  T cells, CD8+ T cells, and CD4+ T cells in the sole B2M MUT MMR-d colon cancer that contained cancer cells upon ICB treatment.



- Extended periods of calm are unnerving to him
- Maniacal sense of urgency is our operating principle

Walter Isaacson, Elon Musk

# Making mismatch repair proficient colorectal cancer visible to $\gamma\delta$ T cells

6

**Vivien Veninga**<sup>1,2, \*</sup>, Paula T. van Royen<sup>1,2, \*</sup>, Mariangela Russo<sup>3</sup>, Sharon Scardellato<sup>3</sup>, Chiara M. Cattaneo<sup>4</sup>, Maarten Breet<sup>5</sup>, Joris van de Haar<sup>1,2</sup>, Noel F.C.C. de Miranda<sup>6</sup>, Alberto Bardelli<sup>3,7,8</sup>, Emile E. Voest<sup>1,2</sup>

<sup>1</sup> Department of Molecular Oncology and Immunology, Netherlands Cancer Institute, Amsterdam, The Netherlands.

<sup>2</sup> Oncode Institute, Utrecht, The Netherlands.

<sup>3</sup> Department of Oncology, University of Torino, 10060 Candiolo, TO, Italy

<sup>4</sup> Experimental Hematology Unit, IRCCS Ospedale San Raffaele Scientific Institute, Milan, Italy

<sup>5</sup> Pathology, Netherlands Cancer Institute, Amsterdam, The Netherlands.

<sup>6</sup> Department of Pathology, Leiden University Medical Center, Leiden, The Netherlands

<sup>7</sup> Candiolo Cancer Institute, FPO - IRCCS, 10060 Candiolo, TO, Italy

<sup>8</sup> IFOM ETS - The AIRC Institute of Molecular Oncology, 20139 Milan, Italy

\*These authors contributed equally: Vivien Veninga, Paula van Royen





## ABSTRACT

Around 95% of metastatic colorectal cancer (CRC) patients have mismatch repair proficient (MMR-p) tumors. Unlike mismatch repair deficient (MMR-d) tumors, MMR-p tumors respond poorly to immune checkpoint blockade (ICB) treatment. It is commonly believed that higher tumor mutational load in MMR-d tumors, and hence increased probability for neoantigens, triggers CD8<sup>+</sup> T cells. This explains part of the success of ICB in MMR-d CRC and the failure of ICB in MMR-p CRC. Recently  $\gamma\delta$  T cells were identified as effectors of ICB in MMR-d CRC with HLA- class I defects. We therefore hypothesized that MMR-p CRC could be made visible to  $\gamma\delta$  T cells by interfering with b-2 microglobulin (B2M), which leads to HLA class I deficiency. Here, we present our initial results how MMR status and B2M knockout, affected  $\gamma\delta$  T cell reactivity. Our data indicates that HLA class I deficiency in MMR-p CRC cells can activate  $\gamma\delta$  T cell reactivity in a similar manner as in MMR-d CRC. Interestingly, we also observed that microsatellite instability, as a result of mismatch repair deficiency, elicited higher  $\gamma\delta$  T cell reactivity compared to microsatellite stable CRC cells. These results suggest that interference with B2M may be exploited as an alternative strategy to elicit  $\gamma\delta$  T cell reactivity in MMR-p CRC and that MMR-d/MSI status can influence  $\gamma\delta$  T cell responses.

## INTRODUCTION

The DNA mismatch repair (MMR) pathway is highly conserved across species and supports genomic stability by recognizing and repairing DNA base-base mismatches that can occur during replication, recombination or DNA damage<sup>1,2</sup>. MuTS homologs (MSH2, MSH3 and MSH6) and MuTL homologs (MLH1, MLH3, hPMS1 and hPMS2) are core proteins of the DNA mismatch repair system in human cells. MSH2 heterodimerizes with MSH3 or MSH6 and initiates recognition of aberrant base mismatches while the heterodimer of MLH1 and hPMS2 acts as endonuclease during mismatch repair<sup>3,4</sup>. A defective mismatch repair system leads to accumulation of mutations in the genome, and is associated to a high tumor mutational burden (TMB) across cancer types and causes microsatellite instability (MSI)<sup>5,6</sup>. Germline mutations of MMR genes, especially of any gene encoding the mentioned core proteins, lead to a hereditary form of colon cancers, also known as Lynch syndrome<sup>7,8,9</sup>. MMR deficiency (MMR-d)/ MSI status of tumors is commonly tested using polymerase chain reaction (PCR) or immunohistochemistry as diagnostic methods<sup>10</sup>.

Even though a dysfunctional MMR system promotes the development of a cancerous cell and increases the mutational load, MMR-d tumors share characteristics that allow for better recognition and elimination by immune cells compared to MMR-p tumors. A higher mutational load increases the probability of neoantigen expression and subsequent recognition by CD8<sup>+</sup> T cells. This currently serves as an explanation for the success of immune checkpoint inhibitors in MMR-d deficient cancers<sup>11</sup>.

Colorectal cancer (CRC) is a good example to compare ICB treatment response in relation to MMR status. Patients with MMR-d CRC generally respond well to ICB<sup>12</sup>. However, the vast majority of metastatic CRC patients has mismatch repair proficient (MMR-p) tumors which remain difficult to treat<sup>11</sup>. Equally in early-stage CRC patients, MMR-d tumors respond better to neoadjuvant ICB treatment than MMR-p tumors<sup>13</sup>.

An important question is what can we learn from the response of MMR-d tumors to ICB treatment and how can we translate this success to MMR-p tumors. One strategy is to create an MMR-d/MSI signature in MMR-p tumors to increase immunogenicity and subsequent response to ICB. Temozolomide, and alkylating agent, has been shown to induce such signatures and increase tumor mutational

burden in mice models as well as in a clinical trial with colorectal cancer patients<sup>14,15</sup>. This method was designed to elicit an adaptive immune response via CD8<sup>+</sup> T cell recognition. Lately, we have shown that  $\gamma\delta$  T cells can act as effectors of ICB response in b-2 microglobulin (B2M) mutant MMR-d tumors, which are invisible to conventional T cells<sup>16</sup>. This conceptually opens up opportunities to nudge MMR-p tumors to a phenotype that is more accessible to certain innate immune cells such as  $\gamma\delta$  T cells. As an immune cell type that bridges adaptive and innate immunity,  $\gamma\delta$  T cells express a  $\gamma\delta$  TCR that acts independent of MHC class I/II peptide presentation, share NK cell like features like NKG2D expression and their role in cancer immunity has been extensively described<sup>17</sup>. Importantly, although infiltration of CD103<sup>+</sup> PD1<sup>+</sup>  $\gamma\delta$  T cells is mostly observed in MMR-d CRC tumors, CD103<sup>+</sup> PD1<sup>-</sup>  $\gamma\delta$  T cells infiltrate MMR-p tumors as well<sup>18</sup>. It is however currently unclear whether the likely more activated CD103<sup>+</sup> PD1<sup>+</sup>  $\gamma\delta$  T cells in MMR-d CRC are a result of the presence of other activated immune cells or whether MMR status does directly affect  $\gamma\delta$  T cells. Moreover, a confirmed presence of  $\gamma\delta$  T cells in MMR-p CRC, provides an opportunity to potentially activate them.

Here, we aim to translate our findings of  $\gamma\delta$  T cell reactivity in B2M mutant MMR-d tumors to MMR-p tumors by depletion of B2M. Furthermore, we will assess whether MMR status has an influence on  $\gamma\delta$  T cells reactivity.

## RESULTS

As a first step we aimed to systematically analyze the influence of MMR/ MSI status on  $\gamma\delta$  T cell reactivity. To do so we used an established model, generated by the Bardelli group, that introduced an MSI signature in an MMR-p/MSS CRC cell line. The MSI/MSS CRC model was established by MLH1 knockout of MMR-p CRC cell line HT29, which over time introduced an MSI signature thus generating isogenic pairs of cells with and without MSI signature<sup>19</sup> (Figure 1a). Confirmed by STR profile, HT29 empty vector (EV) cells remained without MSI signature whereas MLH1 knockout cells presented with an MSI signature at day 841 but not at day 211. Using MSS/MSI signature pairs of HT29, we were able to address the question whether MMR deficiency is critical for  $\gamma\delta$  T cell reactivity.

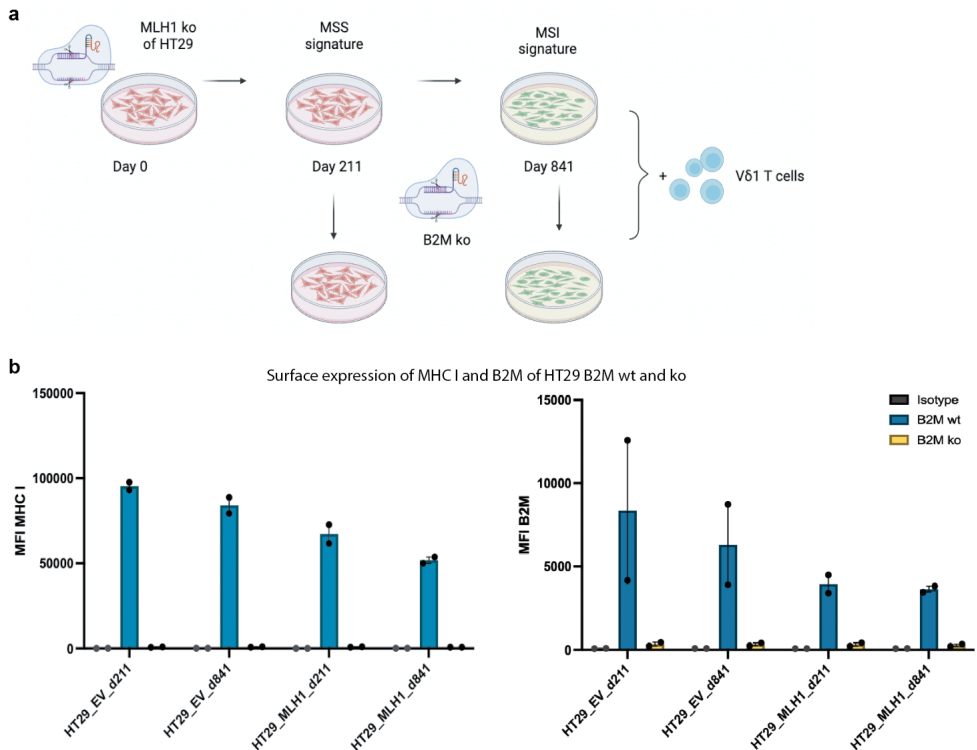
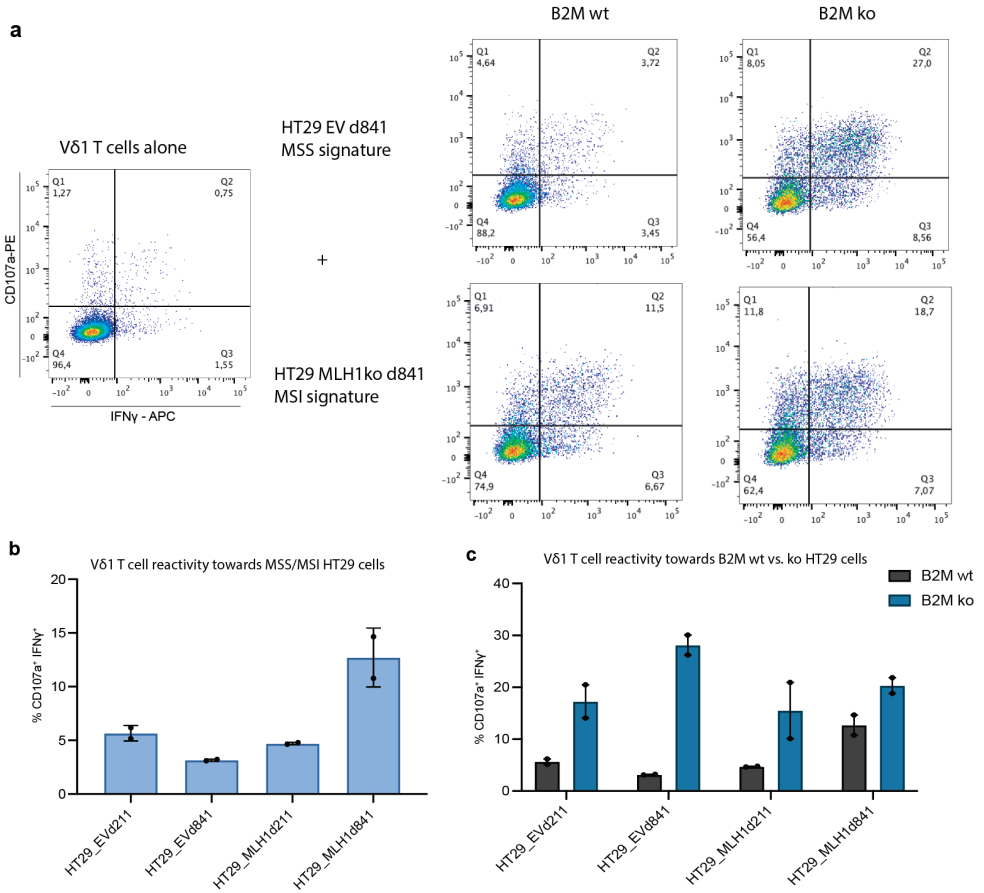


Figure 1: Schematic overview of HT29 model system combining isogenic pairs of MSS/MSI signature and B2M wt/ko including  $\gamma\delta$  T cell reactivity thereof.

a. Schematic overview of establishment of MLH1 knockout of HT29 colorectal adenocarcinoma cell line. Transfection of EV or MLH1 knockout at day 0 and culture until day 211 and day 841. MLH1 knockout lead to a MSI signature at the later time point. B2M knockouts were established of both EV and MLH1 knockout lines at day 211 and 841 before reactivity of  $V\delta 1$  T cells was tested. b. Bar graphs showing MHC I and B2M surface expression on generated HT29 B2M wildtype and knockout pairs (n=2). Whiskers indicate SEM.

After expansion of  $V\delta 1$  T cells from healthy donor peripheral blood mononuclear cells (HD PBMCs), we stimulated  $V\delta 1$  T cells with HT29 cells, with and without MLH1 knockout derived from two time points d211 and d841. HT29 MLH1 knockout d841 elicited highest IFN $\gamma$  and CD107a expression of  $V\delta 1$  T cells compared to HT29 EV cells or MLH1 knockout d211 (Figure 2b). Taken together,  $V\delta 1$  T cells were most reactive towards HT29 cells with an MSI signature.

Next, we introduced CRISPR Cas9 knockouts of B2M in all four HT29 samples (Figure 1b) to test if depletion of B2M, and hence HLA class I deficiency, has a stimulating effect on  $V\delta 1$  T cells in MMR-p CRC as it does in MMR-d CRC. We stimulated  $V\delta 1$  T cells with the isogenic HT29 B2M knockout and wildtype pairs. B2M knockout increased  $V\delta 1$  T cell reactivity in all four samples regardless of MMR/MSI status. Lowest IFN $\gamma$  and CD107a expression was observed in three MSS signature lines without B2M knockout (HT29 EV d211, HT29 EV d841 and HT29 MLH1ko d211), while highest expression was observed in all B2M knockout lines and MSI signature HT29 MLH1ko d841 B2M wildtype (Figure 2a, c). Largest fold change in reactivity was achieved in HT29 EV d841 upon B2M knockout (Figure 2c).



**Figure 2: V $\delta$ 1 T cell reactivity towards generated MSS/MSI HT29 cells and their respective B2M knockouts.**

a. Representative flow cytometry dot plots of healthy donor V $\delta$ 1 T cells unstimulated (alone) or when stimulated with B2M wildtype and knockout of either HT29 EV d841, representing a MSS signature, or HT29 MLH1ko d841, representing a MSI signature. Depicted after intracellular CD107a and IFN $\gamma$  expression. b. Bar graph comparing CD107a and IFN $\gamma$  expression of healthy donor V $\delta$ 1 T cell when stimulated with HT29 MLH1 wildtype (EV) and knockout cells. HT29 MLH1 day 841 developed a MSI signature. Whiskers indicate SEM (n=2). c. Bar graph shows CD107a and IFN $\gamma$  expression of healthy donor V $\delta$ 1 T cells when stimulated with isogenic B2M wildtype and knockout pairs of MLH1 wildtype (EV) and knockout HT29 cells established at day 211 and day 841 (n=2). Whiskers indicate SEM.

## DISCUSSION

There is an unmet need for better treatment options for MMR-p CRC. The success of ICB in MMR-d CRC has fuelled attempts to translate an effective immune response to tumors that are MMR-p, for example by creating an MSI signature to attract CD8<sup>+</sup> T cells<sup>14,15</sup>. Here, we proposed an alternative strategy to overcome low immunogenicity in MMR-p CRC. We aimed to deplete HLA class I expression in order to activate V $\delta$ 1 T cells and circumvent the bottleneck of low TMB in MMR-p tumors.

As a result of immune escape mechanisms to immune surveillance by CD8<sup>+</sup> T cells, HLA class I loss is more frequently observed in MMR-d CRC tumors compared to MMR-p<sup>18,21</sup>.

Based on our previous findings we identified  $\gamma\delta$  T cells as effectors of ICB in B2M mutant MMR-d tumors<sup>16</sup>. Having identified the potential of HLA class I loss to activate specifically V $\delta$ 1 T cells and the consideration that the majority of MMR-p expresses HLA class I, this provides a strategy to render MMR-p CRC sensitive to ICB. Because the mechanism through which V $\delta$ 1 T cells are activated by cancer cells is not fully understood, we aimed to address two major questions. First, does MMR status influence V $\delta$ 1 T cell reactivity and second, is B2M knockout activating V $\delta$ 1 T cell reactivity in MMR-p CRC similar to MMR-d CRC. MMR status influences genomic stability and TMB, therefore likely generating more neoantigens which can be recognized by CD8<sup>+</sup> T cells. Although the immunogenicity of MMR-d tumors may not be solely driven by the number of neoantigens, it is likely to be one of the drivers for ICB response in MMR-d tumors compared to MMR-p tumors. Increased neoantigen presentation by HLA class I, however, should not influence V $\delta$ 1 T cell activation because  $\gamma\delta$  T cells act independent of HLA class I. This leaves the question open if MMR status influences their activation. Interestingly, a MSI signature, established by long term culture of MLH1 knockout cells, increased V $\delta$ 1 T cell reactivity. This is in line with previous findings by the de Miranda lab that showed higher infiltration of CD103<sup>+</sup> PD1<sup>+</sup>  $\gamma\delta$  T cells in MMR-d compared to MMR-p CRC<sup>17</sup>. Future experiments should



aim to analyze the underlying mechanism which makes MMR-d tumors more recognizable to  $V\delta 1$  T cells, which may facilitate the development of treatments that can increase immunogenicity in MMR-p tumors. In addition to the association of MMR deficiency/ MSI signature to  $V\delta 1$  T cell reactivity, our data also provides proof that B2M knockout equally, or perhaps even better, activates  $V\delta 1$  T cells. We hypothesize that HLA class I acts as negative regulator of  $V\delta 1$  T cells but activation likely requires additional stimuli which could explain different fold changes of  $V\delta 1$  T cell reactivity upon B2M knockout in different HT29 cell line samples. However, further experiments are required to validate the results using additional model systems such as patient-derived tumor organoids. Our initial findings support the future direction of interference with HLA class I in MMR-p CRC to activate  $V\delta 1$  T cells. Our study also has limitations. First, we need to confirm this effect in multiple tumor models and for different donor  $V\delta 1$  T cells and second, the role of the MMR/MSI signature on  $V\delta 1$  T cells remains incompletely understood. Once we have a good understanding of the mechanism through which  $V\delta 1$  T cells are activated we may translate these findings into therapeutic strategies that interfere with HLA class I expression and  $V\delta 1$  T cells.

## REFERENCES

1. Modrich, P. and R. Lahue (1996). "Mismatch repair in replication fidelity, genetic recombination, and cancer biology." *Annu Rev Biochem* 65: 101-133.
2. Li, G. M. (2008). "Mechanisms and functions of DNA mismatch repair." *Cell Res* 18(1): 85-98.
3. Kunkel, T. A. and D. A. Erie (2005). "DNA mismatch repair." *Annu Rev Biochem* 74: 681-710.
4. Kadyrova, L. Y. and F. A. Kadyrov (2016). "Endonuclease activities of MutLalpha and its homologs in DNA mismatch repair." *DNA Repair (Amst)* 38: 42-49.
5. Chalmers, Z. R., C. F. Connelly, D. Fabrizio, L. Gay, S. M. Ali, R. Ennis, A. Schrock, B. Campbell, A. Shlien, J. Chmielecki, F. Huang, Y. He, J. Sun, U. Tabori, M. Kennedy, D. S. Lieber, S. Roels, J. White, G. A. Otto, J. S. Ross, L. Garraway, V. A. Miller, P. J. Stephens and G. M. Frampton (2017). "Analysis of 100,000 human cancer genomes reveals the landscape of tumor mutational burden." *Genome Med* 9(1): 34.
6. Boland, C. R. and A. Goel (2010). "Microsatellite instability in colorectal cancer." *Gastroenterology* 138(6): 2073-2087 e2073.
7. Bronner, C. E., S. M. Baker, P. T. Morrison, G. Warren, L. G. Smith, M. K. Lescoe, M. Kane, C. Earabino, J. Lipford, A. Lindblom and et al. (1994). "Mutation in the DNA mismatch repair gene homologue hMLH1 is associated with hereditary non-polyposis colon cancer." *Nature* 368(6468): 258-261.

8. Fishel, R., M. K. Lescoe, M. R. Rao, N. G. Copeland, N. A. Jenkins, J. Garber, M. Kane and R. Kolodner (1993). "The human mutator gene homolog MSH2 and its association with hereditary nonpolyposis colon cancer." *Cell* 75(5): 1027-1038.
9. Papadopoulos, N., N. C. Nicolaides, Y. F. Wei, S. M. Ruben, K. C. Carter, C. A. Rosen, W. A. Haseltine, R. D. Fleischmann, C. M. Fraser, M. D. Adams and et al. (1994). "Mutation of a mutL homolog in hereditary colon cancer." *Science* 263(5153): 1625-1629.
10. Luchini, C., F. Bibeau, M. J. L. Ligtenberg, N. Singh, A. Nottegar, T. Bosse, R. Miller, N. Riaz, J. Y. Douillard, F. Andre and A. Scarpa (2019). "ESMO recommendations on microsatellite instability testing for immunotherapy in cancer, and its relationship with PD-1/PD-L1 expression and Tumor mutational burden: a systematic review-based approach." *Ann Oncol* 30(8): 1232-1243.
11. Le, D. T., J. N. Uram, H. Wang, B. R. Bartlett, H. Kemberling, A. D. Eyring, A. D. Skora, B. S. Lubner, N. S. Azad, D. Laheru, B. Biedrzycki, R. C. Donehower, A. Zaheer, G. A. Fisher, T. S. Crocenzi, J. J. Lee, S. M. Duffy, R. M. Goldberg, A. de la Chapelle, M. Koshiji, F. Bhajjee, T. Huebner, R. H. Hruban, L. D. Wood, N. Cuka, D. M. Pardoll, N. Papadopoulos, K. W. Kinzler, S. Zhou, T. C. Cornish, J. M. Taube, R. A. Anders, J. R. Eshleman, B. Vogelstein and L. A. Diaz, Jr. (2015). "PD-1 Blockade in Tumors with Mismatch-Repair Deficiency." *N Engl J Med* 372(26): 2509-2520.
12. Overman, M. J., S. Lonardi, K. Y. M. Wong, H. J. Lenz, F. Gelsomino, M. Aglietta, M. A. Morse, E. Van Cutsem, R. McDermott, A. Hill, M. B. Sawyer, A. Hendlisz, B. Neyns, M. Svrcek, R. A. Moss, J. M. Ledezne, Z. A. Cao, S. Kamble, S. Kopetz and T. Andre (2018). "Durable Clinical Benefit With Nivolumab Plus Ipilimumab in DNA Mismatch Repair-Deficient/Microsatellite Instability-High Metastatic Colorectal Cancer." *J Clin Oncol* 36(8): 773-779.
13. Chalabi, M., L. F. Fanchi, K. K. Dijkstra, J. G. Van den Berg, A. G. Aalbers, K. Sikorska, M. Lopez-Yurda, C. Grootsholten, G. L. Beets, P. Snaebjornsson, M. Maas, M. Mertz, V. Veninga, G. Bounova, A. Broeks, R. G. Beets-Tan, T. R. de Wijkerslooth, A. U. van Lent, H. A. Marsman, E. Nuijten, N. F. Kok, M. Kuiper, W. H. Verbeek, M. Kok, M. E. Van Leerdam, T. N. Schumacher, E. E. Voest and J. B. Haanen (2020). "Neoadjuvant immunotherapy leads to pathological responses in MMR-proficient and MMR-deficient early-stage colon cancers." *Nat Med* 26(4): 566-576.
14. Germano, G., S. Lamba, G. Rospo, L. Barault, A. Magri, F. Maione, M. Russo, G. Crisafulli, A. Bartolini, G. Lerda, G. Siravegna, B. Mussolin, R. Frapolli, M. Montone, F. Morano, F. de Braud, N. Amirouchene-Angelozzi, S. Marsoni, M. D'Incalci, A. Orlandi, E. Giraudo, A. Sartore-Bianchi, S. Siena, F. Pietrantonio, F. Di Nicolantonio and A. Bardelli (2017). "Inactivation of DNA repair triggers neoantigen generation and impairs Tumor growth." *Nature* 552(7683): 116-120.
15. Crisafulli, G., A. Sartore-Bianchi, L. Lazzari, F. Pietrantonio, A. Amatu, M. Macagno, L. Barault, A. Cassingena, A. Bartolini, P. Luraghi, G. Mauri, P. Battuello, N. Personeni, M. G. Zampino, V. Pessei, P. P. Vitiello, F. Tosi, L. Idotta, F. Morano, E. Valtorta, E. Bonoldi, G. Germano, F. Di Nicolantonio, S. Marsoni, S. Siena and A. Bardelli (2022). "Temozolomide Treatment Alters Mismatch Repair and Boosts Mutational Burden in Tumor and Blood of Colorectal Cancer Patients." *Cancer Discov* 12(7): 1656-1675.
16. De Vries, N. L., J. van de Haar, V. Veninga, M. Chalabi, M. E. Ijsselsteijn, M. van der Ploeg, J. van den Bulk, D. Ruano, J. G. van den Berg, J. B. Haanen, L. J. Zevenijn, B. S. Geurts, G. F. de Wit, T. W. Battaglia, H. Gelderblom, H. M. W. Verheul, T. N. Schumacher, L. F. A. Wessels, F. Koning, N. de Miranda and E. E. Voest (2023). "gammadelta T cells are effectors of immunotherapy in cancers with HLA class I defects." *Nature* 613(7945): 743-750.
17. Silva-Santos, B., K. Serre and H. Norell (2015). "gammadelta T cells in cancer." *Nat Rev Immunol* 15(11): 683-691.
18. Dunn, G. P., L. J. Old and R. D. Schreiber (2004). "The immunobiology of cancer immunosurveillance and immunoediting." *Immunity* 21(2): 137-148.

19. Russo, M., G. Crisafulli, A. Sogari, N. M. Reilly, S. Arena, S. Lamba, A. Bartolini, V. Amodio, A. Magri, L. Novara, I. Sarotto, Z. D. Nagel, C. G. Pielt, A. Amatu, A. Sartore-Bianchi, S. Siena, A. Bertotti, L. Trusolino, M. Corigliano, M. Gherardi, M. C. Lagomarsino, F. Di Nicolantonio and A. Bardelli (2019). "Adaptive mutability of colorectal cancers in response to targeted therapies." *Science* 366(6472): 1473-1480.
20. De Vries, N. L., V. van Unen, M. E. Ijsselsteijn, T. Abdelaal, R. van der Breggen, A. Farina Sarasqueta, A. Mahfouz, K. Peeters, T. Holtt, B. P. F. Lelieveldt, F. Koning and N. de Miranda (2020). "High-dimensional cytometric analysis of colorectal cancer reveals novel mediators of antiTumor immunity." *Gut* 69(4): 691-703.
21. Anderson, P., N. Aptsiauri, F. Ruiz-Cabello and F. Garrido (2021). "HLA class I loss in colorectal cancer: implications for immune escape and immunotherapy." *Cell Mol Immunol* 18(3): 556-565.
22. Dijkstra, K. K., C. M. Cattaneo, F. Weeber, M. Chalabi, J. van de Haar, L. F. Fanchi, M. Slagter, D. L. van der Velden, S. Kaing, S. Kelderman, N. van Rooij, M. E. van Leerdam, A. Depla, E. F. Smit, K. J. Hartemink, R. de Groot, M. C. Wolkers, N. Sachs, P. Snaebjornsson, K. Monkhorst, J. Haanen, H. Clevers, T. N. Schumacher and E. E. Voest (2018). "Generation of Tumor-Reactive T Cells by Co-culture of Peripheral Blood Lymphocytes and Tumor Organoids." *Cell* 174(6): 1586-1598 e1512.
23. Cattaneo, C. M., K. K. Dijkstra, L. F. Fanchi, S. Kelderman, S. Kaing, N. van Rooij, S. van den Brink, T. N. Schumacher and E. E. Voest (2020). "Tumor organoid-T-cell coculture systems." *Nat Protoc* 15(1): 15-39.

## METHODS

### Organoid culture

6

Tumor organoids were derived from MMR-p or MMR-d CRC tumors. Establishment of the respective organoid lines from tumor material was performed as previously reported<sup>22,23</sup>. In brief, tumor tissue was mechanically dissociated and digested with 1.5 mg ml<sup>-1</sup> of collagenase II (Sigma-Aldrich), 10  $\mu$ g ml<sup>-1</sup> of hyaluronidase type IV (Sigma-Aldrich) and 10  $\mu$ M Y-27632 (Sigma-Aldrich). Cells were embedded in Cultrex RGF BME type 2 (3533-005-02, R&D systems) and placed into a 37 °C incubator for 20 min. Human CRC organoid medium is composed of Ad-DF+++ (Advanced DMEM/F12 (GIBCO) supplemented with 2 mM Ultraglutamine I (Lonza), 10 mM HEPES (GIBCO), 100 U ml<sup>-1</sup> of each penicillin and streptomycin (GIBCO), 10% noggin-conditioned medium, 20% R-spondin1-conditioned medium, 1 $\times$  B27 supplement without vitamin A (GIBCO), 1.25 mM N-acetylcysteine (Sigma-Aldrich), 10 mM nicotinamide (Sigma-Aldrich), 50 ng ml<sup>-1</sup> human recombinant EGF (Peprotech), 500 nM A83-01 (Tocris), 3  $\mu$ M SB202190 (Cayman Chemicals) and 10 nM

prostaglandin E2 (Cayman Chemicals). Organoids were passaged depending on growth every 1–2 weeks by incubating in TrypLE Express (Gibco) for 5–10 min followed by embedding in BME. Organoids were authenticated by SNP array or STR analysis and were regularly tested for Mycoplasma using Mycoplasma PCR43 and the MycoAlert Mycoplasma Detection Kit (LT07-318). In the first two weeks of organoid culture, 1× Primocin (Invivogen) was added to prevent microbial contamination. Procedures performed with patient samples were approved by the Medical Ethical Committee of the Netherlands Cancer Institute–Antoni van Leeuwenhoek hospital (NL48824.031.14) and written informed consent was obtained from all of the patients. Mismatch repair status was assessed using a standard protocol for the Ventana automated immunostainer for MLH1 clone M1 (Roche), MSH2 clone G219-1129 (Roche), MSH6 clone EP49 (Abcam) and PMS2 clone EP51 (Agilant Technologies).

#### HT29 model system generation

Colorectal adenocarcinoma cell line HT29 was cultured in RPMI-1640 medium (Gibco) with 10% fetal calf serum (FCS) (Sigma Aldrich) and 1% penicillin and streptomycin (GIBCO). Depending on confluency cells were split twice per week. For generation of a MSI signature, HT29 cells were transfected with a plasmid containing Cas9, MLH1 single guide RNA and puromycin selection to achieve an MLH1 knockout. Empty vector plasmid contained Cas9 and puromycin selection. After transfection with either MLH1 or empty vector plasmid at day 0, HT29 cells were kept in culture and then stored at day 211 and 841 to achieve a full MSI signature. HT29 cells at day 211 resemble a MSS signature while cells at day 841 obtained a full MSI signature which was confirmed by OncoMate® MSI Dx Analysis System (Promega) as previously described<sup>19</sup>. Short tandem repeat (STR) analysis confirmed a 100% match of HT29 EV d211 and HT29 EV d841 with HT29 cell line, whereas HT29 MLH1 ko d211 is a 78.1 % match and HT29 MLH1 ko d841 65.1% indicating increased TMB and MSI signature. Generation of MLH1 knockout HT29 cells was performed in the Bardelli lab at the University of Turin, Italy.

## $\gamma\delta$ T cells generation

$\gamma\delta$  T cells were isolated from frozen healthy donor PBMCs. After a washing step with phosphate-buffered saline (PBS), PBMCs were stained with anti-CD3-PerCPy5.5 (1:20, SK7, BD Biosciences), anti-ab TCR- BV421 (1:40, IP26, Biolegend), anti-Vd1-PECy7 (1:40, TS8.2, Invitrogen), anti-Vd2-FITC (1:100, B6, Biolegend), anti-PD1-AF647 (1:40, MIH4, BD Biosciences) and 1:2,000 near-infrared (NIR) viability dye (Life Technologies) for 30min in the dark at 4 degrees. Following two washing steps with PBS and resuspension in 0.1% PBSA (Sigma-Aldrich), cells were sorted with a BD LSR Fortessa Cell Analyzer SORP using FACSDiVa (v.8.0.2; BD Biosciences). Sorted  $\gamma\delta$ 1 cells were expanded over three to four weeks in presence of feeder cells ( $2 \times 10^6$  per ml), PHA ( $1 \mu\text{g ml}^{-1}$ ; Thermo Fisher Scientific), IL-2 ( $1,000 \text{ IU ml}^{-1}$ ; PeproTech), IL-15 ( $10 \text{ ng ml}^{-1}$ ; PeproTech).

## B2M CRISPR Cas9 knockout of tumor organoids and HT29 cells

The B2M<sup>KO</sup> tumor organoid and HT29 cell lines were generated using sgRNA targeting B2M (GGCCGAGATGTCTCGCTCCG), cloned into LentiCRISPR v2 plasmid. The virus was produced using a standard method. Tumor organoids and cell lines were dissociated to single cells and resuspended at  $1 \times 10^6$  cells/mL in AD+++ or RPMI-1640 10% FCS respectively. Undiluted viral suspension was added 1:1 to tumor organoids or HT29 cells plus 1:1000 protamine sulfate (Sigma-Aldrich).  $10 \mu\text{M}$  Y-27632 was added to tumor organoids to prevent anoikis. Spinfection was performed in 48-well plates for 1h at room temperature before cells were incubated overnight at 37 degrees. Next day cells were resuspended in their respective culture medium and plated as usual. Puromycin was added as selection after 2 days. B2M knockout was confirmed by flow cytometry analysis of surface expression of B2M and MHC class I.

## Surface expression analysis

For organoid surface staining, tumor organoids were dissociated into single cells using TrypLE Express (Gibco), washed twice in cold FACS buffer (PBS, 5 mM EDTA, 1% bovine serum antigen), and stained with anti-HLA-A/B/C-PE (1:20, W6/32, BD Biosciences), anti-B2M-FITC (1:100, 2M2, BioLegend), anti-PD-L1-APC (1:200, MIH1, eBioscience) and 1:2,000 near-infrared (NIR) viability dye (Life Technologies), or isotype controls (1:1,000 FITC; 1:20, PE; or 1:200, APC) mouse IgG1 kappa (BD Biosciences). For NKG2D ligand expression analysis, cells were stained with anti-MICA/MICB-PECy7 (1:20, 6D4, Biolegend), anti-ULBP1-AF647 (1:20, 170818, R&D), anti-ULBP2/5/6-BV421 (1:20, 165903, BD Biosciences), anti-ULBP3-PE (1:10, 166510, R&D), anti-ULBP4-PE (1:10, 709116, R&D) and 1:2,000 near-infrared (NIR) viability dye (Life Technologies). Tumor cells were incubated for 30 min at 4 °C in the dark and washed twice with FACS buffer. All of the samples were recorded with the BD LSR Fortessa Cell Analyzer SORP flow cytometer using FACSDiVa (v.8.0.2; BD Biosciences). Data were analysed using FlowJo (v.10.6.1; BD) and presented using GraphPad Prism (v.9.0.0; GraphPad).

## Reactivity assay

For evaluation of Tumor reactivity towards B2M<sup>WT</sup> and B2M<sup>KO</sup> organoids and NKG2D ligand blocking conditions, Tumor organoids and  $\gamma\delta$  T cells were prepared as described previously<sup>13,22,23</sup>. Two days before the experiment, organoids were isolated from BME by incubation in 2 mg ml<sup>-1</sup> type II dispase (Sigma-Aldrich) for 15 min before addition of 5 mM EDTA and washed with PBS before being resuspended in CRC organoid medium with 10  $\mu$ M Y-27632 (Sigma-Aldrich). The organoids were stimulated with 200 ng ml<sup>-1</sup> IFN $\gamma$  (Peprotech) 24 h before the experiment. For the recognition assay and intracellular staining, Tumor organoids were dissociated into single cells and plated in anti-CD28-coated (CD28.2, eBioscience) 96-well U-bottom plates with  $\gamma\delta$  T cells at a 1:1 target:effector ratio in the presence of 20  $\mu$ g ml<sup>-1</sup> anti-

PD-1 (Merus). As a positive control,  $\gamma\delta$  T cells were stimulated with 50 ng ml<sup>-1</sup> of phorbol-12-myristate-13-acetate (Sigma-Aldrich) and 1  $\mu$ g ml<sup>-1</sup> of ionomycin (Sigma-Aldrich). After 1 h of incubation at 37 °C, GolgiSTOP (BD Biosciences, 1:1,500) and GolgiPlug (BD Biosciences, 1:1,000) were added. After 4 h of incubation at 37 °C,  $\gamma\delta$  T cells were washed twice in cold FACS buffer (PBS, 5 mM EDTA, 1% bovine serum antigen) and stained with anti-CD3-PerCP-Cy5.5 (1:20, BD Biosciences), anti-TCR $\gamma\delta$ -PE (1:20, BD Bioscience), anti-CD4-FITC (1:20, BD Bioscience) (not added in experiments with NKG2D ligand blocking), anti-CD8-BV421 (1:200, BD Biosciences) and 1:2,000 near-infrared (NIR) viability dye (Life Technologies) for 30 min at 4 °C. Cells were washed, fixed and stained with 1:40 anti-IFN $\gamma$ -APC (BD Biosciences) for 30 min at 4 °C, using the Cytfix/Cytoperm Kit (BD Biosciences). After two wash steps, cells were resuspended in FACS buffer and recorded with the BD LSR Fortessa Cell Analyzer SORP flow cytometer using FACSDiVa software (v.8.0.2; BD Biosciences). Data were analysed using FlowJo (v.10.6.1, BD) and presented using GraphPad Prism (v.9.0.0, GraphPad).





Authentic human interactions become impossible when you lose yourself in a role

Eckhart Tolle: A New Earth

# Unveiling determinants that drive CD34<sup>+</sup> progenitor-derived NK cell reactivity against patient-derived tumor organoids

7

**Vivien Veninga**<sup>1,2,\*</sup>, Steven L.C. Ketelaars<sup>3,\*</sup>, Paul K.J.D. de Jonge<sup>4,#</sup>, Don Schilder<sup>5,#</sup>, Joris van de Haar<sup>1,2</sup>, Yara L. Verschoor<sup>6,7</sup>, Allard W.J. van Renterghem<sup>1,2</sup>, Myriam Chalabi<sup>6,7</sup>, Noel F.C.C. de Miranda<sup>9</sup>, Harry Dolstra<sup>4</sup>, Emile E. Voest<sup>1,2</sup>

<sup>1</sup>Department of Molecular Oncology and Immunology, Netherlands Cancer Institute, Amsterdam, The Netherlands.

<sup>2</sup>Oncode Institute, Utrecht, The Netherlands.

<sup>3</sup>Pathology, Netherlands Cancer Institute, Amsterdam, The Netherlands

<sup>4</sup>Department of Laboratory Medicine - Laboratory of Hematology, Radboud University Nijmegen Medical Center, Nijmegen, the Netherlands

<sup>5</sup>Department of Supramolecular and Biomaterials Chemistry, Leiden Institute of Chemistry, Leiden University, Leiden, The Netherlands

<sup>6</sup>Gastrointestinal Oncology, Netherlands Cancer Institute, Amsterdam, The Netherlands.

<sup>7</sup>Medical Oncology, Netherlands Cancer Institute, Amsterdam, The Netherlands.

<sup>9</sup>Netherlands Cancer Institute, Amsterdam, The Netherlands

<sup>9</sup>Department of Pathology, Leiden University Medical Center, Leiden, The Netherlands.

\*These authors contributed equally: Vivien Veninga, Steven L.C. Ketelaars

#These authors contributed equally: Paul de Jonge, Don Schilder



## ABSTRACT

Natural killer (NK) cells can eliminate cancer cells in a highly effective manner. However, their activation depends on a fine-tuned balance of inhibitory and activating ligands. Here, we used patient-derived tumor organoids (PDTOs) and CD34<sup>+</sup> hematopoietic stem and progenitor cell-derived NK cells (HSPC-NK cells) to capture tumor-specific determinants of NK cell reactivity. Notably, we observed that allogeneic HSPC-NK cells were consistently reactive toward PDTOs compared to autologous patient-derived blood NK cells which showed more heterogeneous responses. Interestingly, we observed reduced HSPC-NK cell reactivity towards tumor organoids derived from tumors exposed to immune checkpoint inhibitor (ICI) compared to their pre-treatment counterparts. Differential gene expression analysis revealed that chondroitin sulfate proteoglycan 4 (CSPG4) was consistently upregulated in these post-ICI tumor samples, potentially reflecting changes in post-ICI tumors associated with reduced susceptibility to NK cell reactivity. Furthermore, IFN $\gamma$  stimulation of tumor organoids decreased HSPC-NK cell reactivity suggesting a context-dependent dual role of IFN $\gamma$  in anti-tumor immune responses. Overall, this study points out relevant drivers of HSPC-NK cell activation, a negative influence of IFN $\gamma$  on HSPC-NK tumor recognition and decreased reactivity towards tumor organoids derived from post-ICI tumors.

## INTRODUCTION

With the clinical success of cellular therapies and immune checkpoint inhibitor (ICI) treatment, T cells have been in the spotlight of cancer immunotherapies. However, common tumor-intrinsic mechanisms of immune escape and resistance to ICI, such as loss of human leukocyte antigen (HLA) class I, aberrations in the antigen presenting machinery or IFN $\gamma$  signaling pathway inactivation, limit an effective T cell response<sup>1,2</sup>. Utilizing the innate immune system might be especially valuable for tumors less susceptible to T cell recognition. For example, gd T cells, a cell type with features of both the innate and adaptive immune system, have recently been identified as effectors of ICI response in cancers with HLA class I deficiency<sup>3</sup>. NK cells have also been reported to be activated and mediate the effect of ICI in in vivo models<sup>4</sup>. Such observations point towards the involvement of innate immune cells in tumor recognition and effective anti-tumor response upon ICI. Importantly, while loss of HLA class I is a common mechanism to prevent tumor recognition by T cells, it conversely enhances the potential of tumors to be recognized by NK cells via the ‘missing self’ principle<sup>5,6</sup>. Likewise IFN $\gamma$  has been shown to lower NK cell anti-tumor reactivity in in vivo models by upregulation of HLA class I<sup>7</sup>, whereas it is associated with increased tumor recognition by T cells and relevant for mediating an ICI response due to upregulation of the antigen processing and presenting machinery<sup>8</sup>. However, the role of IFN $\gamma$  is complex as it can also promote NK cell cytotoxicity by upregulation of ICAM-1 expression which facilitates adhesion of NK cells to cancer cells<sup>9</sup>. Overall suggesting that a better understanding of the influence of IFN $\gamma$  on NK cells responses towards tumors can be valuable to further improve ICB response.

Although NK cells are well known for their capability to exert cytotoxicity and kill cancer cells<sup>10</sup>, several challenges hamper the development of clinically successful NK cell-directed therapies, such as a suppressive tumor microenvironment<sup>11</sup>, low NK cell homing and tumor infiltration<sup>12</sup>, a dysfunctional phenotype<sup>13</sup> and various tumor escape mechanisms. One approach to overcome for example dysfunctional NK cells is the use of highly functional ex vivo-generated NK cells from CD34<sup>+</sup> hematopoietic stem- and progenitor cells (HSPC). A HSPC-NK cell product offers the benefit of off-

the-shelf availability, better expansion potential compared to peripheral blood NK cells and the possibility of optimization by genetic engineering, overcoming a potential dysfunctional state of autologous NK cells<sup>14,15,16</sup>.

Here, we aim to understand the determining factors of tumor recognition by HSPC-NK cells in greater detail by using patient-derived tumor organoids (PDTOs) from colorectal cancer (CRC) and non-small cell lung cancer (NSCLC). Furthermore, we use pairs of pre- and post-ICI colon cancer PDTOs to evaluate changes upon ICI therapy and explore changes in NK cell modulating mechanisms. Finally, we zoom in on the effects of IFN $\gamma$  stimulation of PDTOs in respect to anti-tumor reactivity of HSPC-NK cells.

## RESULTS

### HSPC-NK cell reactivity towards patient-derived tumor organoids.

First, we aimed to compare the reactivity of autologous peripheral blood derived NK cells (PB-NK cells) with HSPC-NK cells to assess whether HSPC-NK cells demonstrate more consistent reactivity towards PDTOs and are suitable for subsequent experiments. Using our established co-culture model system<sup>17,18</sup>, we first tested the reactivity of different populations of autologous peripheral blood-derived NK cells to matching PDTO's (Extended Data Fig. 1a, d). We examined five PDTO's, derived from two mismatch repair deficient colorectal cancers (MMR-d CRC), PDTO-06 and -07 pre, and three non-small cell lung cancers (NSCLC), PDTO-11, -05, -12. We observed differential NK cell reactivity ranging from no to high reactivity, measured by intracellular IFN $\gamma$  expression (Extended Data Fig.1 e, f). The highest and most consistent NK cell reactivity was observed in the CD56<sup>bright</sup> CD16<sup>-</sup> population which, across all samples, represented, on average, 14.5 % ranging from 2.6 – 24.2% of all CD3<sup>-</sup> cells (Extended Data Fig. 1e, f; Extended Data Table 3). Given the potency and high translational efficacy of HSPC-NK cells as previously described<sup>14,15,16</sup>, we next sought to determine their reactivity towards the same set of PDTOs. Reactivity assessment of HSPC-NK cells was generally performed on the CD56<sup>+</sup> Perforin<sup>+</sup> cell population. Notably, when HSPC-NK cells were co-cultured with

PDTOs, we observed a more homogeneous reactivity compared to autologous NK cells as assessed by IFN $\gamma$  expression (Extended Data Fig. 1 b). More consistent tumor reactivity and easier product availability demonstrated advantages of HSPC-NK cells over autologous PB-NK cells, which are difficult to derive from patient's PBMCs at high numbers and seem more heterogenous and less functional in their tumor response.

As a next step, we tested the robustness of our model system using HSPC-NK cells and PDTOs to determine activating and inhibitory mechanisms of tumor reactivity (Fig. 1a). HSPC-NK cells, derived from two independent donors and co-cultured with four different PDTOs, demonstrated reproducible reactivity independent of the donor, measured by expression of IFN $\gamma$  and the degranulation marker CD107a on HSPC-NK cells (Extended Data Fig. 2b). The only difference between independent HSPC-NK cell donors was the magnitude of response, but differential response across targets were very similar. To exclude that such responses were solely based on an allogeneic human leukocyte antigen (HLA) mismatch, we tested three pairs tumor organoids and matched normal organoids from the same patient.

HSPC-NK cell reactivity was significantly lower towards two out of three normal organoids compared to their tumor counterpart (Fig. 1b). Furthermore, we observed a striking cytotoxic activity of HSPC-NK cells towards NSCLC tumor organoids PDTO-03 whereas the matched normal organoids, PDO-03, were not affected (Fig. 1c). Next to normal and tumor pairs, we included two tumor organoids which were derived from two independent colorectal tumors occurring in the same patient. PDTO-10 MMRd was established pre-ICI from a mismatch repair-deficient (MMR-d) tumor and PDTO-10 MMRp was derived post-ICI from a second tumor which retained mismatch repair-proficiency (MMR-p) (Extended Data Table 1). Notably, both tumor organoids expressed similar levels of major histocompatibility complex class I and II (MHC I/II) (Extended Data Fig. 2g), but PDTO-10 MMRd consistently elicited a higher HSPC-NK cell response compared to PDTO-10 MMRp (Fig. 1d, e).

Overall, we using HSPC-NK cells and PDTOs offers an opportunity to understand tumor reactivity of HSPC-NK cells in greater detail and dissect possible mechanisms of resistance.

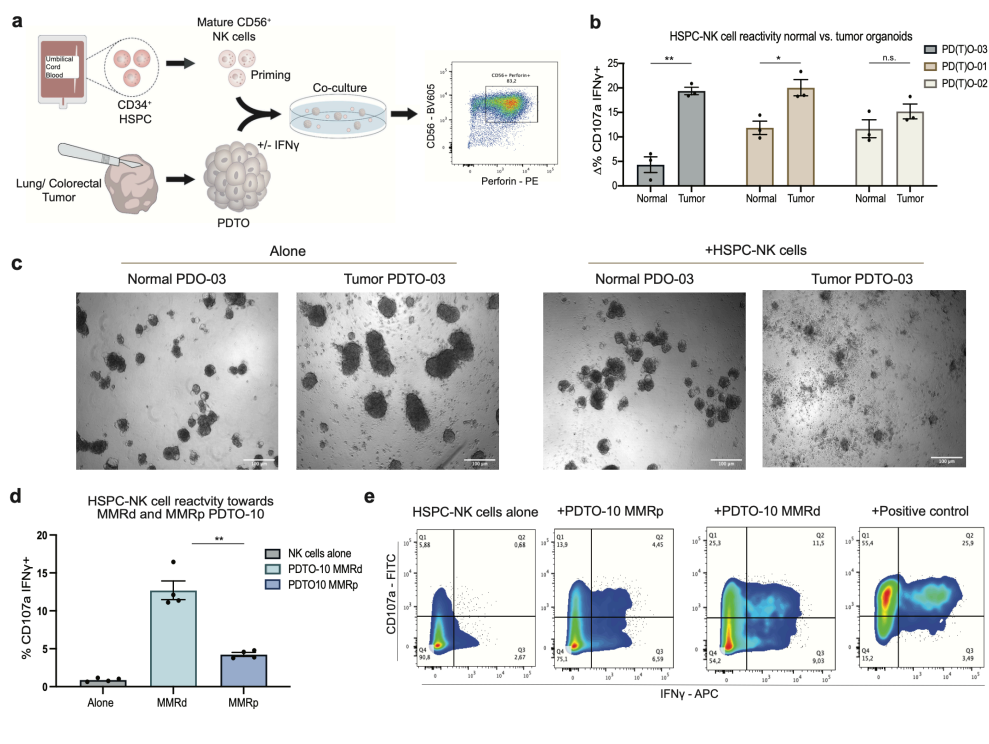


**Figure 1: Utilizing patient derived (tumor) organoids, autologous and HSPC-NK cells to dissect tumor specific immune responses.** **a.** Schematic overview of the experimental set up of HSPC-NK cell reactivity assays. Patient derived (tumor) organoids were established from lung or colorectal tumors, depending on the assay pre-stimulated with IFN $\gamma$  and exposed to NK cells which were primed for one week prior to the readout. **b.** Bar plots showing IFN $\gamma$  and CD107a expression of HSPC-NK cells when stimulated with three pairs of normal and tumor organoids (PD(T)O-03, -01, -02). Background signal of unstimulated NK cells has been subtracted from the respective IFN $\gamma$  and CD107a signal of stimulated NK cells. Data is shown for three biological replicates (n=3) and whiskers indicate SEM. Statistical significance between normal and tumor organoids was tested using Welch's t-test. Not significant (n.s.) p > 0.05; \* p < 0.05; \*\* p < 0.01; \*\*\* p < 0.001. **c.** Representative microscopy images of 48h killing assay comparing HSPC-NK cell killing of tumor (right) and normal (left) organoids (PD(T)O-03). Top images show tumor/normal organoid cultures without NK cells and bottom images show tumor/normal organoid cultures in presence with NK cells. Scale indicates 100 $\mu$ m. **d.** Bar plots showing IFN $\gamma$  and CD107a expression in unstimulated HSPC-NK cells (alone) and upon stimulation with MMR-d and MMR-p PDO-10 tumor organoids derived from two independent tumors of the same patient (n=4). Whiskers indicate SEM. Statistical significance between MMR-p and MMR-d PDO-10 organoids was tested using Welch's t-test and indicated by not significant (n.s.) p > 0.05; \* p < 0.05; \*\* p < 0.01; \*\*\* p < 0.001. **e.** Representative flow cytometry plots of HSPC-NK cells indicating IFN $\gamma$  and CD107a expression in unstimulated condition (NK cells alone), upon stimulation with MMR-p and MMR-d PDO-10 and positive control.



## Determinants of HSPC-NK cell activation and inhibition towards PDTO

We next set out to identify drivers of HSPC-NK cell activation and understand to what degree they followed known modulators of NK cell tumor reactivity. We tested HSPC-NK cell reactivity towards a panel of seven PDTOs and ranked them by their ability to induce a response, as measured by expression of IFN $\gamma$  and CD107a (Fig. 2a). Using flow cytometry, we measured the expression of a panel of 15 known NK cell surface ligands on those seven PDTOs. Highest reactivity of HSPC-NK cells was elicited by PDTO-03 and PDTO-12 resulting in 25.0% and 17.8% CD107a<sup>+</sup> IFN $\gamma$ <sup>+</sup> cells respectively. Lowest reactivity was elicited by PDTO-13 and PDTO-10 MMRp with 5.1% and 4.4% CD107a<sup>+</sup> IFN $\gamma$ <sup>+</sup> cells respectively (Fig. 2a, c).

We specifically focused on NKG2A, NKG2D and DNAM-1 ligands for PDTO phenotyping as the receptors for these ligands were highly expressed on HSPC-NK cells (Extended Data Table 5). In line with previous reports on the relevance of NKG2D ligands for NK cell activation<sup>19</sup>, surface expression levels of activating NK cell ligands, such as MICA/B, ULBP3 and ULBP4, aligned well with the observed HSPC-NK cell reactivity gradient (Fig. 2b). Expression of those ligands was highest on PDTO-03 and PDTO-12 and nearly absent on PDTOs which elicited lower responses (Fig. 2b). In contrast, expression of inhibitory NK cell ligand ULBP2/5/6 was increased on PDTOs that induced lower reactivity. DNAM-1 ligand CD155, a bivalent NK cell ligand with reported activating and inhibitory functions, and Fas, a cell surface receptor involved in apoptosis, both showed higher expression on PDTOs associated with higher HSPC-NK cell reactivity (Fig. 2b, Extended Data Fig. 3b). The significance of MICA/B and ULBP ligands, and the bivalent CD155, was tested by blocking both NKG2D (receptor of MICA/B and ULBPs) and DNAM-1 (receptor of CD155) on five PDTOs using blocking antibodies. For one out of five PDTOs, PDTO-03, HSPC-NK cell reactivity was reduced after blocking of NKG2D and DNAM-1 and two additional lines, PDTO-08 and -09, showed a trend towards reduced reactivity (Extended Data Fig. 2c). Relevance of DNAM-1 expression for HSPC-NK cell reactivity towards ovarian cancer has been previously described<sup>20</sup>.

In line with low KIR expression of HSPC-NK cells<sup>15,21</sup>, neither the expression levels of inhibitory NK cell ligands HLA-C or HLA-E, nor presence or absence of MHC class I/II

was associated with reduced HSPC-NK cell reactivity (Extended Data Fig. 2g, 3b). To challenge this, we tested PDTO-08, derived from a b-2-Microglobulin (B2M) mutant colorectal tumor and thus MHC class I negative (Extended Data Fig. 2g), which induced reactivity similarly to the other four tested MHC I proficient PDTOs (Extended Data Fig. 2c).

In addition to flow cytometry analysis, we performed RNA sequencing on the seven tested PDTOs and identified genes whose expression was linearly associated with the measured HSPC-NK cell reactivity ranking (Extended Data Fig. 5). To identify potential ligands of HSPC-NK cells, we filtered for genes whose product belong to the Gene Ontology terms GO:0009986 ('cell surface') and/or GO:0009897 ('external side of plasma membrane'), meaning gene products that are known to be located on the cell surface. This resulted in 28 genes for which gene expression was significantly linearly associated with HSPC-NK cell reactivity and where the gene product was located on the cell surface (Fig. 2d). Of specific interest were carcinoembryonic antigen-related cell adhesion molecules (CEACAMs) -5 and -6, whose expression was enriched on PDTOs with reduced HSPC-NK cell reactivity. Some members of the CEACAM family, like CEACAM1 and CEACAM5 are already known inhibitory NK cell ligands<sup>22,23</sup>. To further support this finding, we used publicly available gene expression data for 597 colorectal cancer patients from The Cancer Genome Atlas - Colorectal Adenoma and Rectal Adenoma (TCGA-COADREAD) datasets annotated with the abundance (tissue fraction) of activated NK cells per sample as a proxy for NK cell reactivity (Methods). In the TCGA-COADREAD datasets, tumors with a low (below median) abundance of activated NK cells also had a significantly higher expression of CEACAM5 ( $p=0.00096$ ) or CEACAM6 ( $p=0.028$ ), compared to tumors with a high (above median) abundance of activated NK cells (Extended Data Fig. 4f). Collectively, these data indicate that CEACAM-5 and -6 expression seems to be negatively correlated with NK cell reactivity. Overall, these findings highlight the potential of the HSPC-NK cell and PDTOs platform to identify known and novel activating or inhibitory NK cell ligands for further experimental validation.

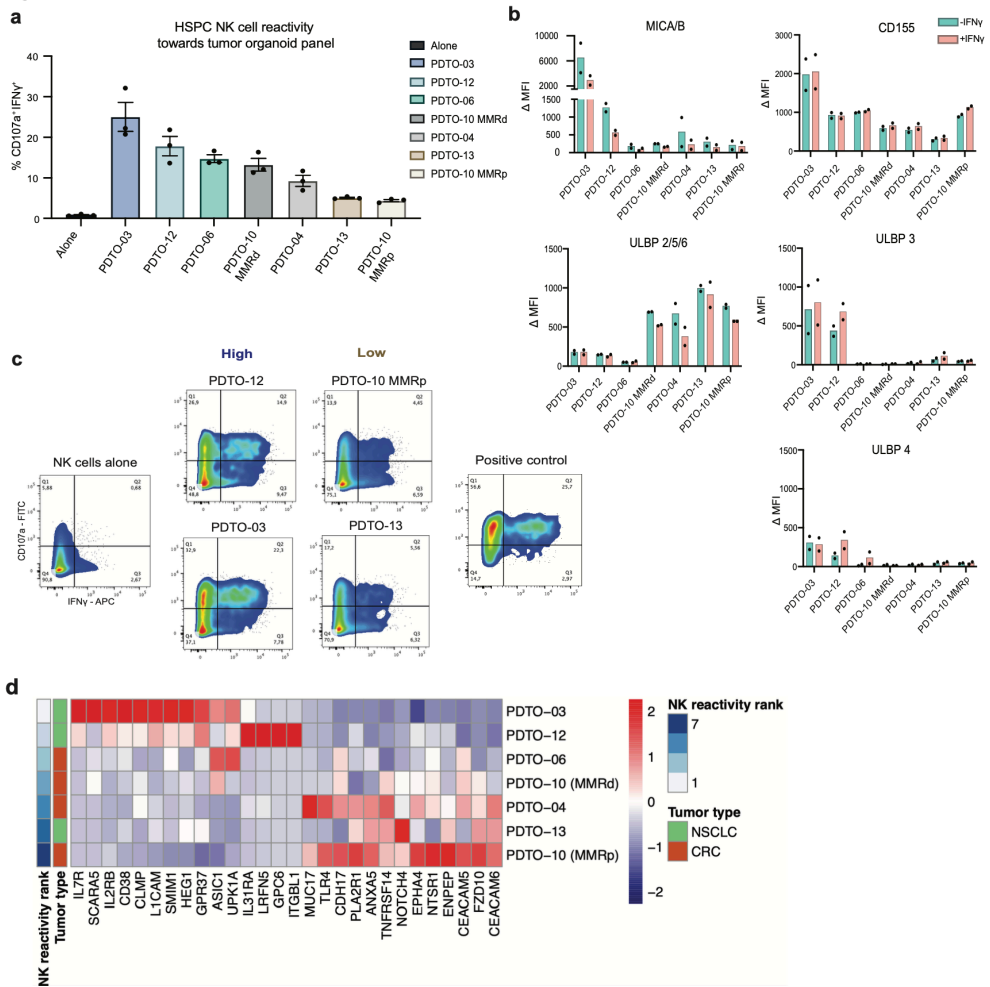


**Figure 2:** HSPC-NK cell tumor organoid specificity and identification of drivers of tumor visibility. **a.** Bar plots of IFN̳ and CD107a expression of unstimulated HSPC-NK cells (alone) and upon stimulation with a panel of seven tumor organoids (PDTO-03, -12, -06, -10 MMRd, -04, -13 and -10 MMRp) ranked from high to low signal. Bars indicate mean  $\pm$  SEM of three biological replicates (n=3). **b.** Five bar plots indicating  $\Delta$  MFI of surface expression of NK cell ligands MICA/B, CD155, ULBP2/5/6, ULBP3 and ULBP4 on tumor organoids ranked from high to low NK cell reactivity, as determined in Fig. 2a. Surface expression analysis was performed on tumor organoids without IFN̳ (mint color) and with IFN̳ pre-stimulation (coral color). Bars show mean of two biological replicates (n=2). **c.** Representative flow cytometry plots of unstimulated HSPC-NK cells (alone), stimulated with tumor organoids eliciting high NK cell responses (left: PDTO-03, -12), stimulated with tumor organoids eliciting low NK cell responses (right: PDTO-10 MMRp, -13) and positive control. **d.** Heatmap of normalized RNA expression (column z-scores) of genes whose expression was linearly associated with the order of HSPC-NK cell reactivity in the tested PDTOs (decreasing from top-to-bottom) per Fig. 2a. The depicted genes encode for proteins expressed on the external side of the plasma membrane.

### ICI treatment makes PDOs less visible to HSPC-NK cells

To elucidate how treatment with ICI affects HSPC-NK cell reactivity towards PDOs, we analyzed HSPC-NK cell reactivity towards four pre- and on/post ICI treatment CRC PDO pairs (Extended Data Table 2).

Interestingly, for three out of four PDO pairs (PDO-02, 07 and 09), co-culture of HSPC-NK cells with tumor organoids derived from patients treated with ICI resulted in reduced reactivity compared to tumor organoids derived from the same tumor, prior to ICI treatment (Fig. 3a, d; Extended Data Fig. 2e). While per pair changes in ligand expression occurred, no ligand seemed to be commonly up- or downregulated across all four pairs (Fig. 3f). To expand on the surface ligand flow cytometry analysis, we performed differential gene expression analysis on the pairs of pre and post/on-ICI PDOs. When focusing the analysis on the three PDO pairs that had decreased HSPC-NK cell reactivity post/on-ICI, we identified, for example, a higher differential expression of UGT1A1, SMOC2 and DRD2 in pre-treatment organoids, while CSPG4 and MELTF had a higher differential expression in post-treatment organoids (Extended Data Fig. 4b, g). The only gene that was consistently upregulated in all four pairs of PDOs post/on-ICI was Chondroitin Sulfate Proteoglycan 4 (CSPG4) (Fig. 3b). To validate our finding, we tested the upregulation of CSPG4 gene expression in a larger patient cohort of 19 pre- and post/on-ICI MMR-d CRC tumor samples from the recently published NICHE study<sup>24</sup>. In line with our PDO data, CSPG4 was significantly upregulated in post-ICI tumors compared to pre-ICI (Fig. 3c). Surface staining of CSPG4 of PDO-07 also confirmed higher surface expression on post-ICI PDOs (Extended Data Fig. 4e). Importantly, in our TCGA-COADREAD dataset, tumors with a low abundance of activated NK cells also had a significantly higher expression of CSPG4 compared to tumors with a high abundance of activated NK cells (Fig. 3e; Extended Data Fig. 4c). Additionally, as determined by Thorsson et al.<sup>35</sup> in the TCGA-COADREAD dataset there was a striking correlation between CSPG4 expression and TGF $\beta$  response gene signature (Extended Data Fig. 4d).

Taken together, our data suggests that clinical treatment with ICI promotes tumor changes that may lead to a decreased PDO mediated activation of HSPC-NK cells. CSPG4 RNA expression, was consistently upregulated in CRC tumors post/on-ICI and this may suggest an involvement in tumor escape from NK cell recognition.

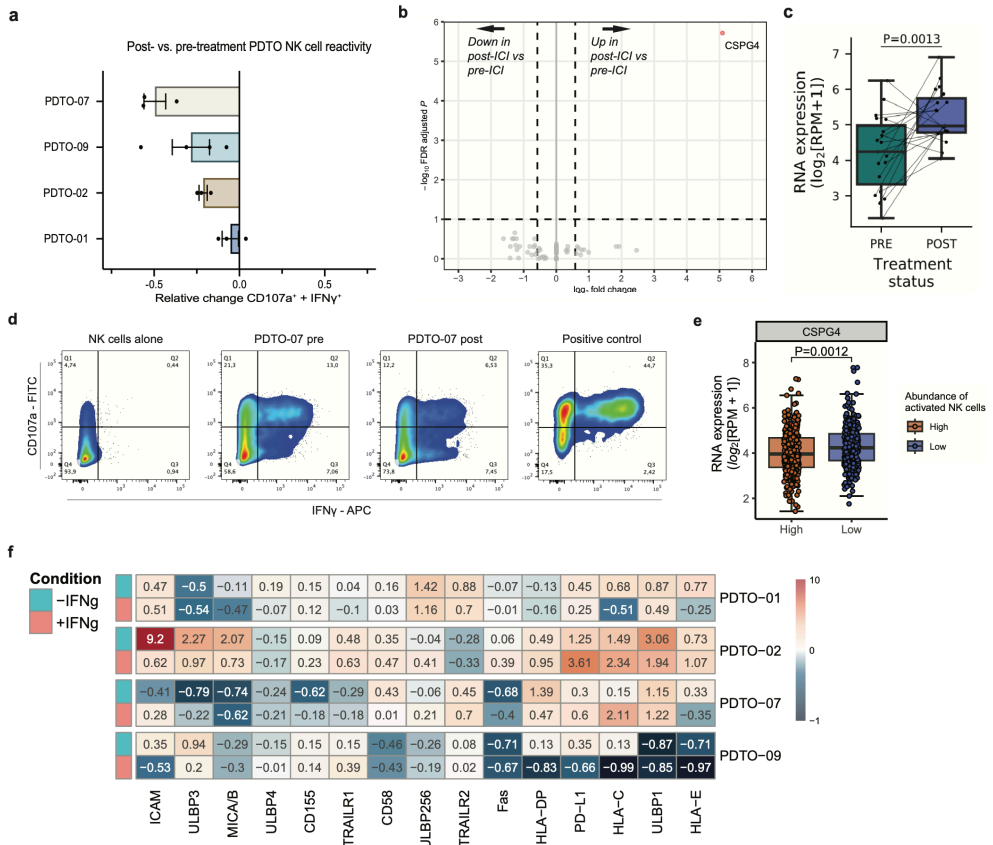


Figure 3: Comparison of HSPC-NK cell reactivity towards patient-derived tumor organoids pre- and post-ICI therapy. **a**. Bar plots indicating the mean relative change of background-subtracted IFN $\gamma$  and CD107a expression of HSPC-NK cells after co-culture with post-ICI therapy derived PTDOs compared to pre-ICI therapy derived PDTOs (n=3; PDTO-09 n=4). Bars pointing to the left indicate reduced HSPC-NK cell reactivity. Whiskers indicate SEM. **b**. Volcano plot indicating differential gene expression between post-ICI and pre-ICI therapy PDTOs (4 pairs). Vertical and horizontal dotted lines indicate absolute 1.5-fold change differential expression threshold and 10% false discovery rate (FDR) threshold, respectively. **c**. Boxplot showing CSPG4 expression of pre and post ICI MSI CRC tumor pairs from NICHE study (n=19 patients). Boxes, whiskers, and dots indicate quartiles, 1.5 interquartile ranges, and individual data points, respectively. Two-sided Wilcoxon rank sum test-based P-value is shown. **d**. Representative flow cytometry plots of HSPC-NK cells indicating IFN $\gamma$  and CD107a expression in unstimulated condition (NK cells alone), upon stimulation with pre-treatment tumor organoids (PDTO-07 pre), post-treatment tumor organoids (PDTO-07 post) and positive control. **e**. CSPG4 expression in TCGA-COADREAD samples with high or low abundance of activated NK cells (n=597). **f**. Heatmap depicting mean fold change of background-subtracted surface expression (DMFI) of the indicated NK cell ligands on post-ICI therapy PDTOs compared to matched pre-ICI therapy PDTOs. PDTOs were pre-incubated with (coral color) or without IFN $\gamma$  (mint color). Red color indicates increased DMFI in post-ICI therapy PDTOs (value > 0), whereas blue indicates decreased DMFI (value < 0).

color indicates decreased DMFI in post-ICI therapy PDTOs compared to pre-ICI therapy PDTOs (value < 0). Box plots indicate the median (line), interquartile range (box), minima and maxima (whiskers). Statistical significance was tested with a two-sided Wilcoxon rank sum test.

### IFN $\gamma$ inhibits HSPC-NK cell PDO recognition

We next sought to determine the effect of IFN $\gamma$  on NK cell reactivity, as this is a master regulator of (ICI-mediated) anti-tumor immune response. To do so CRC and NSCLC tumor organoids were pre-stimulated with or without IFN $\gamma$  24h prior to the NK cell reactivity assays. A trend of decreased HSPC-NK cell reactivity upon IFN $\gamma$  exposure was observed in six out of seven tumor organoids (Fig. 4b, Extended Data Fig. 2d). PDO-10 MMRp showed the opposite effect and induced higher HSPC-NK cell recognition upon IFN $\gamma$  pre-stimulation (Fig. 4b, Extended Figure 2d). Although exploratory, this case is particularly interesting because both tumor organoids, PDO-10 MMRd and MMRp, were derived from the same patient but from two different primary tumors at different time points (Extended Data Table 1). While the NK cell ligand phenotype of both tumor organoids is similar, IFN $\gamma$  stimulation increased HLA-DP and HLA-E to greater extent in PDO-10 MMRd, whereas ICAM-1 expression is dramatically increased in PDO-10 MMRp likely facilitating better adhesion as previously described<sup>9</sup> (Extended Data Fig. 3a, b).

When we tested IFN $\gamma$  stimulation in a panel of 15 tumor organoids, NK cell ligand expression showed a decrease in expression of TRAILR2 and activating ligand MICA/B for the majority of tumor organoids and an increase of ICAM-1 as well as the inhibiting ligands HLA-C and HLA-E, potentially causing reduced HSPC-NK cell activation (Fig. 4a). Notably, HLA-E was one of the most consistently upregulated inhibitory ligand across our tumor organoid panel (Fig. 4a, c, Extended Data Fig. 3b). PD-L1 was also increased upon IFN $\gamma$  stimulation but unlikely relevant because of lack of PD-1 expression on HSPC-NK cells (Extended Data Fig. 1g). Moreover, we observed lowest ICAM-1 increase upon IFN $\gamma$  stimulation and diminished TRAIL-R2 and MICA/B expression in both PDTOs (PDO-03 and -13) that show most notable fold change of decreased HSPC-NK cell activation upon IFN $\gamma$  pre-stimulation (Fig. 4c; Extended Data Fig. 2g).

Taken together, HSPC-NK cell reactivity towards PDOs can be decreased upon IFN $\gamma$  stimulation of tumor organoids. Particularly, protein surface expression of MICA/B and TRAIL-R2 was decreased by IFN $\gamma$  while expression of inhibiting NK cell ligands, especially HLA-E, increased. Most notably is the increase of ICAM-1 which seems to tip the balance to better HSPC-NK cell recognition.

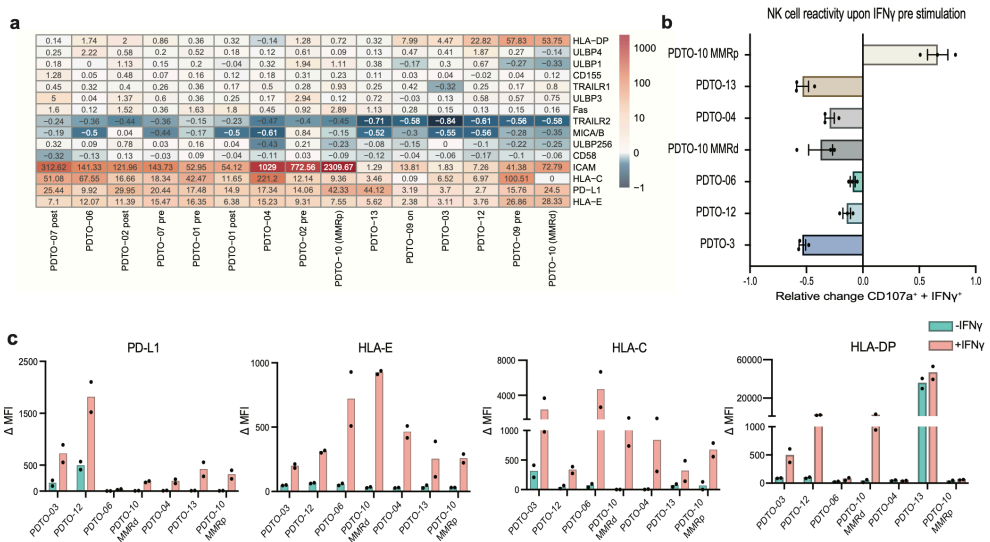


**Figure 4: IFN $\gamma$  pre-stimulation of tumor organoids lowers tumor recognition of HSPC-NK cells changing activating and inhibiting ligands landscape.** **a.** Heatmap depicting mean fold change of background-subtracted surface expression (DMFI) of the indicated NK cell ligands on PDOs after incubation with IFN $\gamma$  versus without IFN $\gamma$ . Red color indicates increased DMFI after incubation with IFN $\gamma$  (value > 0), whereas blue color indicates decreased DMFI after incubation with IFN $\gamma$  (value < 0). **b.** Bar plots indicating the mean relative change of background-subtracted IFN $\gamma$  and CD107a expression of HSPC-NK cells after co-culture with PDOs pre-incubated with IFN $\gamma$  compared to no IFN $\gamma$  pre-incubation (n=3). Bars of PDO-03, -12, -06, -10 MMRd, -04 and -13, pointing to the left, indicate decreased HSPC-NK cell reactivity to IFN $\gamma$  pre-incubated PDOs (value < 0). The bar of PDO-10 MMRp, pointing to the right, indicates increased HSPC-NK cell reactivity to IFN $\gamma$  pre-incubated PDOs (value > 0). Whiskers indicate SEM. **c.** Bar plots indicating the mean background-subtracted surface expression (DMFI) of NK cell ligands PD-L1, HLA-E, HLA-C and HLA-DP on PDOs, ranked from high to low HSPC-NK cell reactivity, per Fig. 2a. Analysis was performed on PDOs pre-incubated with IFN $\gamma$  (coral color) or without IFN $\gamma$  (mint color). Data is shown for two biological replicates (n=2).

7

## DISCUSSION

To advance our understanding of personalized tumor recognition using HSPC-NK cells as potential therapeutic product in ACT, we employed PDTOs established from NSCLC and CRC. Our approach unveiled several key insights: i) allogeneic HSPC-NK cells are more reactive toward PDTOs compared to autologous PB-NK cells, ii) known activating ligands for NK cells also trigger HSPC-NK cell activation by PDTOs; iii) IFN $\gamma$  pre-stimulation of PDTOs can decrease tumor reactivity of HSPC-NK cells; and iv) PDTOs from tumors exposed to ICI treatment exhibited reduced visibility to HSPC-NK cells.

Remarkably, the latter observation indicated that HSPC-NK cells exhibited decreased IFN- and CD107a expression when stimulated with CRC PDTOs derived from post-ICI treated tumors compared to their pre-treated counterparts. This implies a potential active role of NK cells in ICI response, as previously reported in mouse models<sup>4</sup>, and a subsequent tumor escape mechanism from NK cells during ICI treatment. Alternatively, pressure from other immune cells may lead to changes in the tumor that indirectly affecting NK cell recognition. To delve deeper into the role of NK cells during ICI, we propose a detailed phenotyping of tumor-infiltrating NK cells pre- and post-ICI.

Our analysis revealed that the surface proteoglycan CSPG4 was significantly upregulated in post-ICI PDTOs and post-ICI tumors from a patient cohort with 19 matching pre- and post-ICI colon cancer samples. Previously, CSPG4 has been associated with tumor progression and lower immune cell infiltration<sup>25</sup>. Interestingly, using the TCGA-COADREAD dataset, we found that CSPG4 expression correlated with TGF- $\beta$  response, which may be in line with an inhibitory effect on NK cells<sup>26</sup>. Although the full mechanism of how tumors become less visible to HSPC-NK cells remains to be identified, our findings offer a novel perspective on potential escape mechanisms that could be explored to enhance the design of future HSPC-NK cell products.

Similarly, our data underscore a primarily negative role of IFN $\gamma$  in tumor recognition by HSPC-NK cells, which could be considered in future immunotherapies. This underlies a dual role of IFN $\gamma$  signaling for tumor immune responses. IFN $\gamma$  stimulation of the



majority of PDOs resulted in decreased HSPC-NK cell reactivity and was associated with decreased expression of MICA/B and TRAIL-R2 as well as an increased expression activating ligand ICAM-1 and of inhibitory ligands such as HLA-E, PD-L1, or classical MHC class I. Demonstrating the fine-tuned balance of activating and inhibiting ligands that determines NK cell activation. Of note, PD-L1 increase does not interfere with HSPC-NK cell reactivity as they do not express PD-1. Supporting our findings on reduced reactivity upon IFN $\gamma$  stimulation, a recent *in vivo* CRISPR screen on immune evasion mechanisms by Dubrot et al. linked the loss of IFN $\gamma$  signaling to immune sensitization mediated by NK cells and CD8 $^+$  T cells<sup>7</sup>. They also identified HLA-E as one of the most broadly upregulated immune inhibitory checkpoints, leading to CD8 $^+$  T cell inhibition, hence supporting the potential of inhibitory NKG2A antibodies, such as monalizumab, which is currently being tested in clinical studies, as a combination with ICI treatment<sup>27</sup>. Additionally, CRISPR Cas9 knockout of NKG2A in primary NK cells facilitated their cytotoxic potential against multiple myeloma<sup>28</sup>.

Beyond the surface expression of known inhibitory ligands, TCGA-COADREAD and PDO gene expression data of CEACAM-5 and -6 correlated with lower HSPC-NK cell activation by PDOs. An inhibitory effect of CEACAM-1/5 on NK cell reactivity has been reported previously<sup>18,19</sup>, supporting our data and hinting at similar properties for CEACAM-6. Conversely, surface expression of activating ligands like MICA/B and ULBP3/4 positively correlated with HSPC-NK cell reactivity, suggesting these may be targets to enhance immune responses through NK cell activation.

While HSPC-NK cells and PDOs provide a promising model system to understand drivers of NK cell reactivity and differences between pre- and post-ICI treatment samples, translating these findings to intratumoral NK cells should be considered carefully. Although a detailed comparison to patient NK cells is out of scope for our work, our findings suggest that HSPC-NK cell generally outperform autologous derived NK cells from peripheral blood. Though it has to be noted that the autologous NK cells were primed with IL-2 instead of IL-15 and IL-12, an enhanced HSPC-NK cell reactivity could imply possible dysfunction of patient-derived NK cells or generally improved tumor reactivity of HSPC-NK cells.

In summary, our findings contribute to improve the design of future HSPC-NK cell products to overcome tumor escape mechanisms, such as the expression of inhibitory ligands or resistance mechanisms that arise during ICI therapy. Furthermore, our data suggests a potential benefit of combining ICI therapy with treatments targeting NK cells to improve immune responses.

## REFERENCES

1. Martinez-Jimenez F, Priestley P, Shale C, Baber J, Rozemuller E, Cuppen E. Genetic immune escape landscape in primary and metastatic cancer. *Nat Genet.* 2023;55(5):820-31.
2. Jenkins RW, Barbie DA, Flaherty KT. Mechanisms of resistance to immune checkpoint inhibitors. *Br J Cancer.* 2018;118(1):9-16.
3. de Vries NL, van de Haar J, Veninga V, Chalabi M, Ijsselsteijn ME, van der Ploeg M, et al. gammadelta T cells are effectors of immunotherapy in cancers with HLA class I defects. *Nature.* 2023;613(7945):743-50.
4. Hsu J, Hodgins JJ, Marathe M, Nicolai CJ, Bourgeois-Daigneault MC, Trevino TN, et al. Contribution of NK cells to immunotherapy mediated by PD-1/PD-L1 blockade. *J Clin Invest.* 2018;128(10):4654-68.
5. Karre K, Ljunggren HG, Piontek G, Kiessling R. Selective rejection of H-2-deficient lymphoma variants suggests alternative immune defence strategy. *Nature.* 1986;319(6055):675-8.
6. Ljunggren HG, Karre K. In search of the 'missing self': MHC molecules and NK cell recognition. *Immunol Today.* 1990;11(7):237-44.
7. Dubrot J, Du PP, Lane-Reticker SK, Kessler EA, Muscato AJ, Mehta A, et al. In vivo CRISPR screens reveal the landscape of immune evasion pathways across cancer. *Nat Immunol.* 2022;23(10):1495-506.
8. Grasso CS, Tsoi J, Onyshchenko M, Abril-Rodriguez G, Ross-Macdonald P, Wind-Rotolo M, et al. Conserved Interferon-gamma Signaling Drives Clinical Response to Immune Checkpoint Blockade Therapy in Melanoma. *Cancer Cell.* 2021;39(1):122.
9. Wang, R., J. J. Jaw, N. C. Stutzman, Z. Zou and P. D. Sun (2012). "Natural killer cell-produced IFN-gamma and TNF-alpha induce target cell cytolysis through up-regulation of ICAM-1." *J Leukoc Biol* 91(2): 299-309.
10. Watzl C. How to trigger a killer: modulation of natural killer cell reactivity on many levels. *Adv Immunol.* 2014;124:137-70.
11. Melaiu O, Lucarini V, Cifaldi L, Fruci D. Influence of the Tumor Microenvironment on NK Cell Function in Solid Tumors. *Front Immunol.* 2019;10:3038.
12. Nayyar G, Chu Y, Cairo MS. Overcoming Resistance to Natural Killer Cell Based Immunotherapies for Solid Tumors. *Front Oncol.* 2019;9:51.
13. Platonova S, Cherfils-Vicini J, Damotte D, Crozet L, Vieillard V, Validire P, et al. Profound coordinated alterations of intratumoral NK cell phenotype and function in lung carcinoma. *Cancer Res.* 2011;71(16):5412-22.
14. Hoogstad-van Evert, J. S., J. Cany, D. van den Brand, M. Oudenampsen, R. Brock, R. Torensma, R. L. Bekkers, J. H. Jansen, L. F. Massuger and H. Dolstra (2017). "Umbilical cord blood CD34(+) progenitor-derived NK cells efficiently kill ovarian cancer spheroids and intraperitoneal tumors in NOD/SCID/IL2Rg(null) mice." *Oncoimmunology* 6(8): e1320630.
15. de Jonge, P., P. M. M. van Hauten, L. D. Janssen, A. L. de Goede, M. M. Berrien-Elliott, J. M. R. van der Meer, C. M. Mousset, M. W. H. Roeven, M. Foster, N. Blijlevens, W. Hobo, T. A.

- Fehniger, J. H. Jansen, N. P. M. Schaap and H. Dolstra (2023). "Good manufacturing practice production of CD34(+) progenitor-derived NK cells for adoptive immunotherapy in acute myeloid leukemia." *Cancer Immunol Immunother* 72(10): 3323-3335.
16. van Hauten, P. M. M., L. Hooijmaijers, M. Vidal-Manrique, A. B. van der Waart, W. Hobo, J. Wu, N. M. A. Blijlevens, J. H. Jansen, B. Walcheck, N. P. M. Schaap, P. de Jonge and H. Dolstra (2023). "Engineering of CD34+ progenitor-derived natural killer cells with higher-affinity CD16a for enhanced antibody-dependent cellular cytotoxicity." *Cytotherapy*.
  17. Cattaneo CM, Dijkstra KK, Fanchi LF, Kelderman S, Kaing S, van Rooij N, et al. Tumor organoid-T-cell coculture systems. *Nat Protoc.* 2020;15(1):15-39.
  18. Dijkstra KK, Cattaneo CM, Weeber F, Chalabi M, van de Haar J, Fanchi LF, et al. Generation of Tumor-Reactive T Cells by Co-culture of Peripheral Blood Lymphocytes and Tumor Organoids. *Cell.* 2018;174(6):1586-98 e12.
  19. Jamieson, A. M., A. Diefenbach, C. W. McMahon, N. Xiong, J. R. Carlyle and D. H. Raulet (2002). "The role of the NKG2D immunoreceptor in immune cell activation and natural killing." *Immunity* 17(1): 19-29.
  20. Maas, R. J., J. S. Hoogstad-van Evert, J. M. Van der Meer, V. Mekers, S. Rezaeifard, A. J. Korman, P. K. de Jonge, J. Cary, R. Woestenenk, N. P. Schaap, L. F. Massuger, J. H. Jansen, W. Hobo and H. Dolstra (2020). "TIGIT blockade enhances functionality of peritoneal NK cells with altered expression of DNAM-1/TIGIT/CD96 checkpoint molecules in ovarian cancer." *Oncoimmunology* 9(1): 1843247.
  21. Dolstra H, Roeven MWH, Spanholtz J, Hangalapura BN, Tordoir M, Maas F, et al. Successful Transfer of Umbilical Cord Blood CD34(+) Hematopoietic Stem and Progenitor-derived NK Cells in Older Acute Myeloid Leukemia Patients. *Clin Cancer Res.* 2017;23(15):4107-18.
  22. Hosomi, S., Chen, Z., Baker, K., Chen, L., Huang, Y. H., Olszak, T., Zeissig, S., Wang, J. H., Mandelboim, O., Beauchemin, N., Lanier, L. L., & Blumberg, R. S. (2013). CEACAM1 on activated NK cells inhibits NKG2D-mediated cytolytic function and signaling. *Eur J Immunol*, 43(9), 2473-2483.
  23. Fantini, M., David, J. M., Annunziata, C. M., Morelli, M. P., Arlen, P. M., & Tsang, K. Y. (2020). The Monoclonal Antibody NEO-201 Enhances Natural Killer Cell Cytotoxicity Against Tumor Cells Through Blockade of the Inhibitory CEACAM5/CEACAM1 Immune Checkpoint Pathway. *Cancer Biother Radiopharm*, 35(3), 190-198.
  24. Chalabi M, Fanchi LF, Dijkstra KK, Van den Berg JG, Aalbers AG, Sikorska K, et al. Neoadjuvant immunotherapy leads to pathological responses in MMR-proficient and MMR-deficient early-stage colon cancers. *Nat Med.* 2020;26(4):566-76.
  25. Boudin L, de Nonneville A, Finetti P, Mescam L, Le Cesne A, Italiano A, et al. CSPG4 expression in soft tissue sarcomas is associated with poor prognosis and low cytotoxic immune response. *J Transl Med.* 2022;20(1):464.
  26. Viel, S., Marcais, A., Guimaraes, F. S., Loftus, R., Rabilloud, J., Grau, M., Degouve, S., Djebali, S., Sanlaville, A., Charrier, E., Bienvenu, J., Marie, J. C., Caux, C., Marvel, J., Town, L., Huntington, N. D., Bartholin, L., Finlay, D., Smyth, M. J., & Walzer, T. (2016). TGF-beta inhibits the activation and functions of NK cells by repressing the mTOR pathway. *Sci Signal*, 9(415), ra19.
  27. van Hall, T., Andre, P., Horowitz, A., Ruan, D. F., Borst, L., Zerbib, R., Narni-Mancinelli, E., van der Burg, S. H., & Vivier, E. (2019). Monalizumab: inhibiting the novel immune checkpoint NKG2A. *J Immunother Cancer*, 7(1), 263.
  28. Bexte, T., J. Alzubi, L. M. Reindl, P. Wendel, R. Schubert, E. Salzmann-Manrique, I. von Metzler, T. Cathomen and E. Ullrich (2022). "CRISPR-Cas9 based gene editing of the immune checkpoint NKG2A enhances NK cell mediated cytotoxicity against multiple myeloma." *Oncoimmunology* 11(1): 2081415.
  29. Dobin A, Davis CA, Schlesinger F, Drenkow J, Zaleski C, Jha S, et al. STAR: ultrafast universal RNA-seq aligner. *Bioinformatics.* 2013;29(1):15-21.

30. Robinson MD, McCarthy DJ, Smyth GK. edgeR: a Bioconductor package for differential expression analysis of digital gene expression data. *Bioinformatics*. 2010;26(1):139-40.
31. Ritchie ME, Phipson B, Wu D, Hu Y, Law CW, Shi W, et al. limma powers differential expression analyses for RNA-sequencing and microarray studies. *Nucleic Acids Res*. 2015;43(7):e47.
32. Ewels PA, Peltzer A, Fillinger S, Patel H, Alneberg J, Wilm A, et al. The nf-core framework for community-curated bioinformatics pipelines. *Nat Biotechnol*. 2020;38(3):276-8.
33. Love MI, Huber W, Anders S. Moderated estimation of fold change and dispersion for RNA-seq data with DESeq2. *Genome Biol*. 2014;15(12):550.
34. Zhu A, Ibrahim JG, Love MI. Heavy-tailed prior distributions for sequence count data: removing the noise and preserving large differences. *Bioinformatics*. 2019;35(12):2084-92.
35. Thorsson V, Gibbs DL, Brown SD, Wolf D, Bortone DS, Ou Yang TH, et al. The Immune Landscape of Cancer. *Immunity*. 2018;48(4):812-30 e14.

## METHODS

### Organoid models and culture

Tumor organoids were established from resection or biopsy material of NSCLC, MMR-d and MMR-p CRC tumors (Extended Data Table 1). Normal organoids were derived from healthy colon of lung tissue. Establishment of the organoids was performed as previously reported<sup>17,18,24</sup>. In short, tumor or normal tissue was dissociated mechanically and by digestion with 1.5 mg/mL of collagenase II (Sigma-Aldrich), 10 mg/mL of hyaluronidase type IV (Sigma-Aldrich) and 10 mM Y-27632 (Sigma-Aldrich). After dissociation, cells were embedded in Cultrex® RGF BME Type 2 (cat no. 3536-005-02, R&D systems) and incubated at 37° upside down for 20 min. In the first two weeks of organoid culture establishment 1x Primocin (Invivogen) was added to prevent microbial contamination. Depending on tissue origin organoids were cultured in presence of the respective medium. Human CRC organoid medium is composed of Ad-DF+++ (Advanced DMEM/F12 (GIBCO) supplemented with 2 mM Ultraglutamine I (Lonza), 10 mM HEPES (GIBCO), and 100/100 U/mL Penicillin/Streptomycin (GIBCO), 10% Noggin-conditioned medium, 20% R-spondin1-conditioned medium, 1x B27 supplement without vitamin A (GIBCO), 1.25 mM N-acetylcysteine (Sigma-Aldrich), 10 mM nicotinamide (Sigma-Aldrich), 50 ng/mL human recombinant EGF (Peprotech), 500 nM A83-01 (Tocris), 3 µM SB202190 (Cayman Chemicals) and 10 nM prostaglandin E2 (Cayman Chemicals). For normal colon organoids, the base medium composition was adjusted to 50% Wnt3A-

conditioned medium, 20% Ad-DF+++ , 10% Noggin-conditioned medium and 20% R-spondin1-conditioned medium. NSCLC and normal airway organoid medium is composed of Ad-DF+++ (Advanced DMEM/F12 (GIBCO) supplemented with 2 mM Ultraglutamine I (Lonza), 10 mM HEPES (GIBCO), and 100/100 U/mL Penicillin/Streptomycin (GIBCO), 10% Noggin-conditioned medium, 10% R-spondin1-conditioned medium, 1x B27 supplement with vitamin A (GIBCO), 1.25 mM N-acetylcysteine (Sigma-Aldrich), 10 mM nicotinamide (Sigma-Aldrich), 25 ng/mL human recombinant FGF-7 (Peprotech), 100 ng/mL human recombinant FGF-10 (Peprotech), 500 nM A83-01 (Tocris), 1  $\mu$ M SB202190 (Cayman Chemicals) and 5 mM Y-2763 (Sigma-Aldrich). Depending on the growth, organoids were passaged every 1-2 weeks by incubation with TrypLE Express (Gibco) for 5-15 min followed by embedding in BME, 20 min incubation at 37° and addition of the respective culturing medium. Medium was changed every 3-4 days. Organoids were authenticated by SNP array or STR profile and frequently tested for Mycoplasma using Mycoplasma PCR43 and the MycoAlert Mycoplasma Detection kit (cat no. LT07-318). Procedures performed with patient specimens were approved by the Medical Ethical Committee of the Netherlands Cancer Institute – Antoni van Leeuwenhoek hospital (study NL48824.031.14 and previously reported clinical trial NCT03026140<sup>2</sup>). Written informed consent was obtained from all patients.

#### Phenotyping of tumor organoids by flow cytometry

To analyze surface protein expression, tumor organoids were dissociated to single cells using pre-warmed TrypLE (Gibco). After sufficient dissociation cells were washed with cold PBS and filtered through a 40 mm filter (Corning). Cold FACS buffer (PBS (Gibco), 5 mM EDTA (Lonza), 1% bovine serum albumin (Sigma-Aldrich)) was used for a second washing step and as staining buffer. For NK cell ligand phenotyping cells were stained with ULBP1-AF647 (1:20,

170818, R&D Systems), ULBP3-PE (1:10, 166510, R&D Systems), ULBP2/5/6-BV421 (1:20, 165903, R&D Systems), CD112-AF488 (1:20, 610603, R&D Systems), PD-L1-APC (1:200, MIH1, Invitrogen), ULBP4-PE (1:10, 709116, R&D Systems), HLA-E-BV421 (1:20, 3D12, BD Biosciences), CD155-FITC (1:100, SKIL4, BioLegend), MICA/B-PECy7 (1:20, 6D4, BioLegend), HLA-C-PE (1:10, DT9, BD

Biosciences), Fas-BV421 (1:20, DX2, BioLegend), ICAM-FITC (1:80, HCD54, BioLegend), CD58-APC (1:20, TS2/9, BioLegend), HLA-A, B, C-PE (1:20, W6/32, BD Biosciences), HLA-DP-BV421 (1:40, B7/21, BD Biosciences), CD80-PECy7 (1:30, 2D10, BioLegend), TRAIL-R2-PE (1:20, DJR24, BioLegend), FasL-BV421 (1:20, NOK1, BioLegend), HLA-DP, DQ, DR-FITC (1:20, TU39, BD Biosciences), TRAIL-R1-APC (1:40, DJR1, BioLegend) and near-infrared viability dye (1:2000, Life Technologies Thermo Fisher). Cells were incubated for 30 min at 4°C in the dark and washed twice with cold FACS buffer before recording a Becton Dickinson Fortessa.

#### Reactivity assay autologous NK cells

PBMCs were isolated from peripheral blood using Ficoll-Paque and cryopreserved for later usage. For further analysis PBMCs were thawed one day prior to the experiment. Isolation of untouched NK cells from PBMCs was performed using a MicroBeads NK cell isolation kit (Miltenyi) according to manufacturer's protocol. To test NK cell reactivity, either PBMC's or isolated NK cells were co-cultured with tumor organoids similarly to a previous publication from our group (Extended Data Table 3)<sup>17,18</sup>. In brief, one day prior to the experiment PBMCs were thawed and resuspended at  $2 \times 10^6$  cells/mL in culture medium (RPMI (Gibco) supplemented with 10% human serum (Sigma-Aldrich), 1% Ultraglutamine I (Lonza), 1% Penicillin/Streptomycin (GIBCO)) and 150 U/mL IL-2 (Peprotech). 200 ng/mL IFN $\gamma$  (Peprotech) was added to tumor organoids 24h before reactivity assay. The next day, tumor organoids were dissociated to single cells using TrypLE Express (Gibco) and resuspended at  $5 \times 10^4$  cells/mL in culture medium. Then either PBMCs or NK cells, isolated from PBMCs using a microbeads untouched NK cell isolation kit (Miltenyi Biotec), were resuspended at  $1 \times 10^6$  cells/mL in culture medium before plating at a 1:1 ratio tumor organoids in a 96-well round bottom plate and 150 U/mL IL-2. Culture medium including IL-2 was refreshed after 2-3 days. Reactivity readout was performed after one week. Tumor organoids were again pre-stimulated with IFN $\gamma$  24h before readout, dissociated to single cells and resuspended at  $1 \times 10^6$  cells/mL in culture medium. PBMCs or NK cells were collected and resuspended at  $2 \times 10^6$  cells/mL in culture medium before 50ml were added to a 96-well round bottom plate. Depending on the

condition 50ml of tumor organoid suspension, culture medium alone or PMA (Sigma-Aldrich) / Ionomycin (Sigma-Aldrich) was added. CD107a-PE (1:50, H4A3, BD Biosciences) was added to all conditions before one hour incubation at 37°C and subsequent addition of 4x GolgiSTOP/PLUG (BD Biosciences). After 3.5 hours cells were washed with FACS buffer and stained for surface marker CD3-FITC (1:50, SK7, BD Biosciences), 1:40 CD16-AF700 (1:40, B73.1, BioLegend), CD56-BV605 (1:40, HCD56, BioLegend). Intracellular staining with IFN $\gamma$ -APC (1:40, B27, BD Biosciences) was performed after fixation/ permeabilization solution kit (BD Biosciences). After appropriate washing steps, cells were resuspended in FACS buffer and recoded at a Becton Dickinson Fortessa.

#### HSPC-NK cell establishment and phenotyping

HSPC-NK cells were derived from CD34+ progenitor cells isolated from UCB units. These units were either derived from the Radboudumc cord blood bank (banked after written informed consent) (donor 1) or collected at caesarean sections after written informed consent (approved by the Radboudumc Committee for Medical Research Ethics CMO 2014/226) (donor 2-4).

NK cells were cultured and phenotype was determined at the end of the 35-day culture process as previously described method<sup>15</sup>. Donor 1 was cultured and stained according to the GMP compliant method, while donor 2-4 were cultured and stained according to the pre-validation method. Briefly, isolated CD34+ cells were cultured in NK MACS medium (Miltenyi Biotec) with 10% Human serum (HS, Sanquin Bloodbank, Amsterdam, The Netherlands), that contained a specific mix of TPO (25 ng/ml, Immunotools, 500 U/ml, Miltenyi Biotec), FLT3L (25 ng/ml, Immunotools or 25 U/ml, Miltenyi Biotec), SCF (25 ng/ml, Immunotools or 25 U/ml, Miltenyi Biotec), IL7 (25 ng/ml, Immunotools or 2000 U/ml, Miltenyi Biotec), IL15 (50 ng/ml, Immunotools or 1000 U/ml, Miltenyi Biotec), IL12 (0.2 ng/ml, Immunotools or 0.25 U/ml, R&D systems) and/or SR1 (5  $\mu$ M, Ardena) as described. Donor 1 was cultured in VueLife 118 (day 1-7) and 750 AC (day 7-35) cell culture bags (Saint-Gobain) with cytokines in U/ml, while donor 2-4 were cultured in 6-well plates (Corning) with cytokines in ng/

ml. Every 3-4 days, cells were diluted to around 2 million/ml based on Trypan Blue cell counting by adding fresh culture medium in a 1:3, 1:4 or 1:5 ratio.

For phenotyping, cells were stained for CD56-BV510 (Biolegend, #318340), NKG2A-PE-Cy7 (Beckman Coulter, #B10246), DNAM-1-FITC (Biolegend, #337104), NKp46-PE (Biolegend, #311908) and NKG2D-APC (Biolegend, #320808) (donor 1) or CD56-PE-Cy7 (Biolegend, #318318), NKG2A-APC (Beckman Coulter, #A60797), DNAM-1-FITC (BD, #559788), NKp46-PE (Biolegend, #331908) and NKG2D-APC (Biolegend, #320808) (donor 2-4). Approximately 200,000 cells were stained in PBS/0.5% BSA at 4°C for 30 min. Cells were washed before staining and twice after staining. Cells were then resuspended in PBS/0.5% BSA containing 7-AAD (1:1000, Sigma, #A9400) (donor 1) or PBS/0.5% BSA containing Sytox Blue (1:5000, Invitrogen, #S34857) (donor 2-4). Cells were acquired using the Navios (donor 1) or Gallios (donor 2-4) flow cytometers and analyzed by Kaluza V2.1.3.

PD-1 expression was determined on 3 different HSPC-NK cell donors generated using the pre-validation method. Briefly, approximately 200,000 cells were stained for CD56-BV510 (Biolegend, #318340) and CD279-BV421 (BD, #562516) and eFluor 780 (Invitrogen, #2082592, 1:1000 diluted) in PBS/0.5% BSA at 4°C for 20 min. Cells were washed before staining and twice after staining. Cells were resuspended in PBS/0.5% BSA and acquired using the Gallios flow cytometer and analyzed by Kaluza.

#### Reactivity assay HSPC-NK cells

HSPC-NK cells were thawed one week prior to the reactivity assay and resuspended at  $1.5 \times 10^6$  cells/mL in NK MACS medium (Miltenyi Biotec) supplemented with 10% human serum, 1% Penicillin/Streptomycin, 50 ng/mL IL-15 (Peprotech) and 0.2 ng/mL IL-12 (Peprotech). HSPC-NK cells were plated in a 6-well plate at 3 mL/well and 1 / 1.5 mL of NK MACS medium including supplements was added at day 2 and 5 respectively. At the day of the reactivity assay HSPC-NK cells were resuspended at  $2 \times 10^6$  cells/mL in NK cell medium (IMDM (Gibco), 10% human serum, 1% Penicillin/Streptomycin). For comparison of the effect of IFN $\gamma$  tumor organoids were or were not pre-stimulated with 20 ng/mL IFN $\gamma$  24h prior to the readout. Then, tumor organoids



were dissociated to single cells and resuspended at  $1 \times 10^6$  cells/mL in NK cell medium. CD107a-FITC (1:50, H4A3, BioLegend) and PMA/Ionomycin control were prepared in NK cell medium. Depending on the desired condition, 50 mL of NK cell medium, for the alone control, tumor organoid suspension or PMA/Ionomycin were added to 50 mL of HSPC-NK cells and 50 mL CD107a staining solution in a 96-well round bottom plate. Cells were incubated for one hour at  $37^\circ\text{C}$  before adding GolgiSTOP/PLUG to a total volume of 200 mL/well. After 3.5h cells were first stained with CD56-BV605 (1:40, HCD56, BioLegend), followed by intracellular staining of Perforin-PE (1:50, DG9, BioLegend) and IFN $\gamma$ -APC (1:40, B27, BD Biosciences) after permeabilization and fixation. Finally, cells were resuspended in FACS buffer and recoded at a Becton Dickinson Fortessa.

#### Killing assay HSPC-NK cells

HSPC-NK cells were thawed and prepared as described above and resuspended at  $0.3 \times 10^6$  cells/mL in NK cell medium. Tumor organoids were collected and similarly to the previously described protocol<sup>14</sup> adjusted to a concentration of  $0.3 \times 10^6$  single cell equivalents/mL in NK cell medium with 10 mM Y-2763. 100 mL of HSPC-NK cells or NK cell medium, for the alone control, were then added to 100 mL of tumor organoid suspension in a 96-well flat bottom plate. Light microscopy pictures were taken using a Axio Vert.A1 (Zeiss) immediately after plating and after 48h.

#### NICHE study data

Raw RNA reads (FASTA files) of microsatellite instable cancers before and after dual immune checkpoint blockade (anti-PD-1 plus anti-CTLA-4) were obtained from the NICHE study<sup>24</sup> (ClinicalTrials.gov: [NCT03026140](https://clinicaltrials.gov/ct2/show/study/NCT03026140)) and aligned to the human reference genome (GRCh38) with STAR (v.2.7.7a)<sup>29</sup> using the default settings in two-pass mode. For gene expression quantification, we used the gencode.v35.annotation.gtf annotation file.

#### Differential gene expression analysis (NICHE)

Differential RNA expression of CSPG4 between microsatellite instable cancers in the NICHE trial before and after dual immune checkpoint blockade was tested using EdgeR<sup>30</sup> (v.3.28.1) and Limma/Voom<sup>31</sup> (v.3.42.2), following standard procedures: (i) filtering of low-expressed genes, (ii) normalization factors calculation using EdgeR, (iii) residual calculation using Voom, (iv) differential expression testing using Limma with empirical Bayes smoothing.

#### RNA sequencing tumor organoids

Cells were homogenized in the RLT buffer (79216, Qiagen) and total RNA was isolated using the RNeasy Mini Kit (74106, Qiagen) including an on-column DNase digestion (79254, Qiagen), according to the manufacturer's instructions. Quality and quantity of the total RNA was assessed on the 2100 Bioanalyzer instrument following manufacturer's instructions "Agilent RNA 6000 Nano" (G2938-90034, Agilent Technologies). Total RNA samples were subjected to TruSeq stranded mRNA library preparation, according to the manufacturer's instructions (Document # 1000000040498 v00, Illumina). The stranded mRNA libraries were analyzed on a 2100 Bioanalyzer instrument following the manufacturer's protocol "Agilent DNA 7500 kit" (G2938-90024, Agilent Technologies), diluted to 10nM and pooled equimolar into multiplex sequencing pools for paired end sequencing on the NovaSeq 6000 Illumina sequencing instrument. Paired-end sequencing was performed using 54 cycles for Read 1, 19 cycles for Read i7, 10 cycles for Read i5 and 54 cycles for Read 2, using the NovaSeq6000 Reagent Kit v1.5 (100 cycles) (20028401, 20028318, Illumina). On average 20 M paired reads per sample were generated. Reads were processed using the nf-core RNAseq analysis pipeline (v3.1.20)<sup>32</sup>. Briefly, raw reads were first filtered for low sequencing quality and read length using Trim Galore (v0.6.7). Next reads were then aligned to the GENCODE human reference genome (GRCh38, v35) using STAR (v2.7.9a)<sup>29</sup> with default settings in two-pass mode. Lastly, gene abundances were quantified from alignments using feature Counts (v2.0.1).

#### Differential gene expression analysis (PDTOs, TCGA)

Count normalization and differential gene expression analysis was performed using DESeq2 (v.1.38.3)<sup>33</sup> after pre-filtering genes with low expression (<10 counts across samples). The lfcShrink function with the apeglm (v.1.20.0)<sup>34</sup> package was used to shrink log<sub>2</sub> fold changes. Pre/post-ICB organoids were compared using a paired design (expression ~ patient + timepoint). In the tumor organoid panel, to identify genes for which expression was linearly associated with the level of HSPC-NK cell reactivity, a linear regression of log<sub>2</sub> gene expression on NK reactivity rank was performed (expression ~ NK\_reactivity\_rank). Genes were defined as significantly differentially expressed at a Benjamini-Hochberg/FDR adjusted P value <0.1, and for the pre/post-ICB organoid comparison, additionally an absolute (shrunk) fold change >1.5. Raw counts were vst-normalized for subsequent principal component analysis (PCA) and generation of heatmaps. Genes encoding for surface-expressed proteins were defined as those belonging to the gene ontology (GO) terms GO: 0009986 ('cell surface') and/or GO: 0009897 ('external side of plasma membrane').

#### TCGA data and abundance of activated NK cells

Public RNA gene expression data (raw counts) from The Cancer Genome Atlas (TCGA) colorectal adenocarcinoma (COADREAD) datasets were downloaded through the GDC data portal (<https://portal.gdc.cancer.gov>). Samples were matched to the COADREAD samples used in the extensive immunogenomic analysis published by Thorsson et al., which includes the data on the tissue fraction (abundance) of activated NK cells and immune gene expression signature scores used in this work<sup>35</sup>. This resulted in a total of 597 samples available for downstream analysis.

#### Acknowledgements

We would like to thank Martijn van Baalen, Frank van Diepen and Guido de Roo from the NKI-AVL Flow Cytometry Facility for flow cytometry support. We would like to thank Marja Nieuwland and the team from the NKI-AVL Genomics Core Facility for support with next generation sequencing of tumor organoids. We would like to acknowledge the Hartwig Medical Foundation for authentication of tumor organoids. We thank Iris Mimpen, Allard van Renterghem, Gabriele Picco, Matthew Coelho and

Mathew Garnett for scientific input and discussions. This work was supported by the NWO Gravitation program (NWO 2012-2022), and by an Open Targets grant for Identification of targets modulating lymphocyte-mediated tumour cell killing. (iFuncOnc) and Onco Institute (to E.E.V.) This work was supported by the Dutch Cancer Society KWF, grant numbers 10100 and 11564 (to H.D).

#### **Author contribution**

VV, PKJDJ, HD and EEV contributed to the experimental concepts and design. PKJDJ and HD generated HSPC-NK cell product. VV and DS performed, analyzed and interpreted experiments. SLCK analyzed data. YLV and MC provided Niche study data. VV and SLCK wrote the first draft of the manuscript. All authors reviewed the manuscript.

#### **Competing Interests**

E.E.V is non-executive board member of Clade Therapeutics, Sanofi and founder and strategic advisor of Mosaic Therapeutics. These positions did not provide a conflict of interest. Radboudumc is patent holder of the improved method for ex vivo expansion CD34<sup>+</sup> HSPCs into NK cells using an aryl hydrocarbon receptor antagonist (PCT/EP2016/071660). The authors have no other relevant financial or non-financial interests to disclose.

#### **Index of supplemental information**

**Extended Data Fig. 1:** Phenotyping of autologous and HSPC-NK cells and reactivity of autologous sub-populations by flow cytometry.

**Extended Data Fig. 2:** Extended analysis of HSPC-NK cell tumor organoids reactivity, including mutational profile of tumor organoid panel and MHC-I/II expression.

**Extended Data Fig. 3:** Extensive NK cell ligand surface expression phenotyping of tumor organoids.

**Extended Data Fig. 4:** RNA expression analysis of patient-derived tumor organoids.

**Extended Data Fig. 5:** Genes linearly associated with order of HSPC-NK cell reactivity.

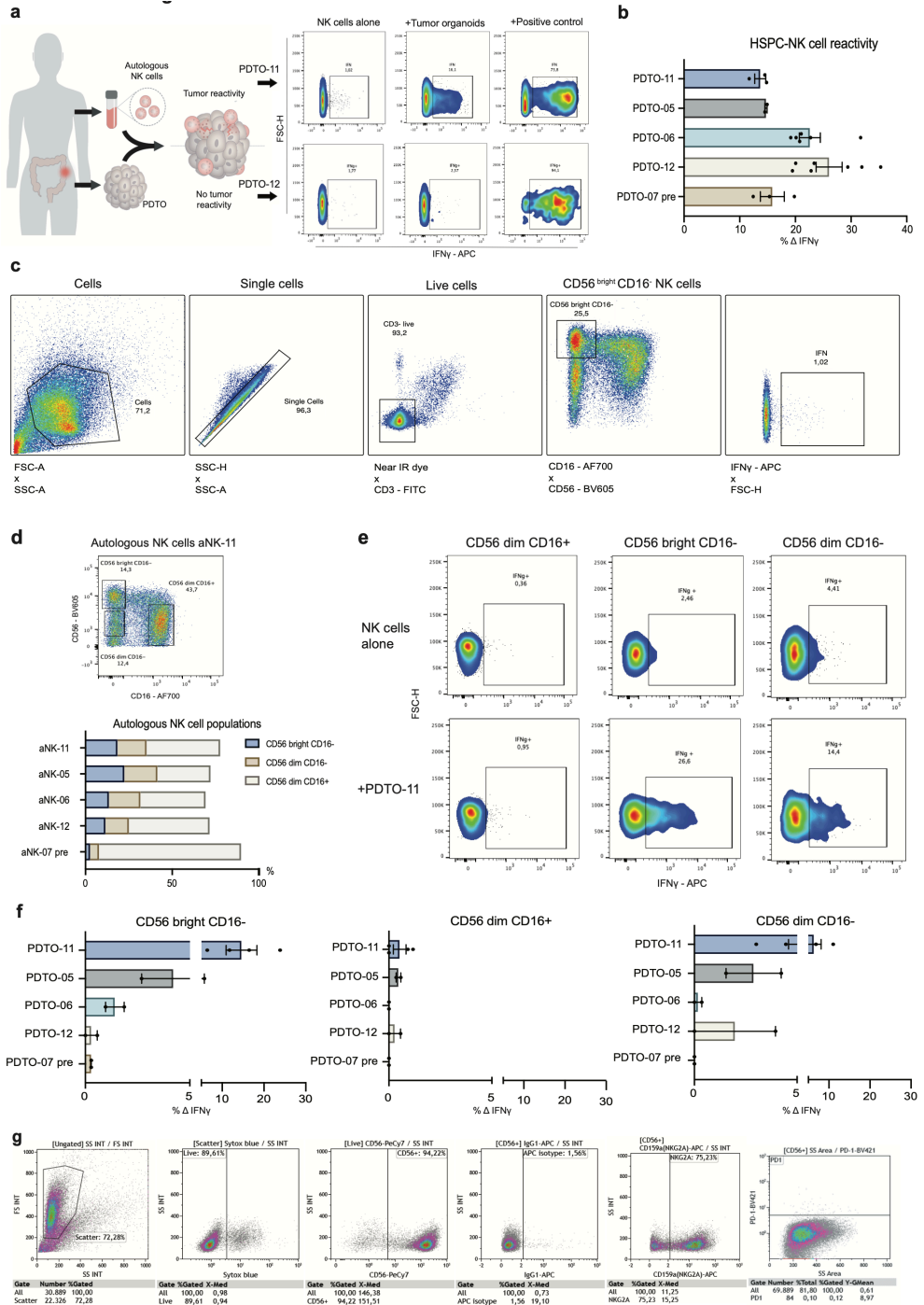
**Extended Data Table 1:** Patient derived (tumor) organoid information.

**Extended Data Table 2:** Information pre and on/post samples for PDTOs and patient treatment response.

**Extended Data Table 3:** Autologous NK cell reactivity by sub-populations.

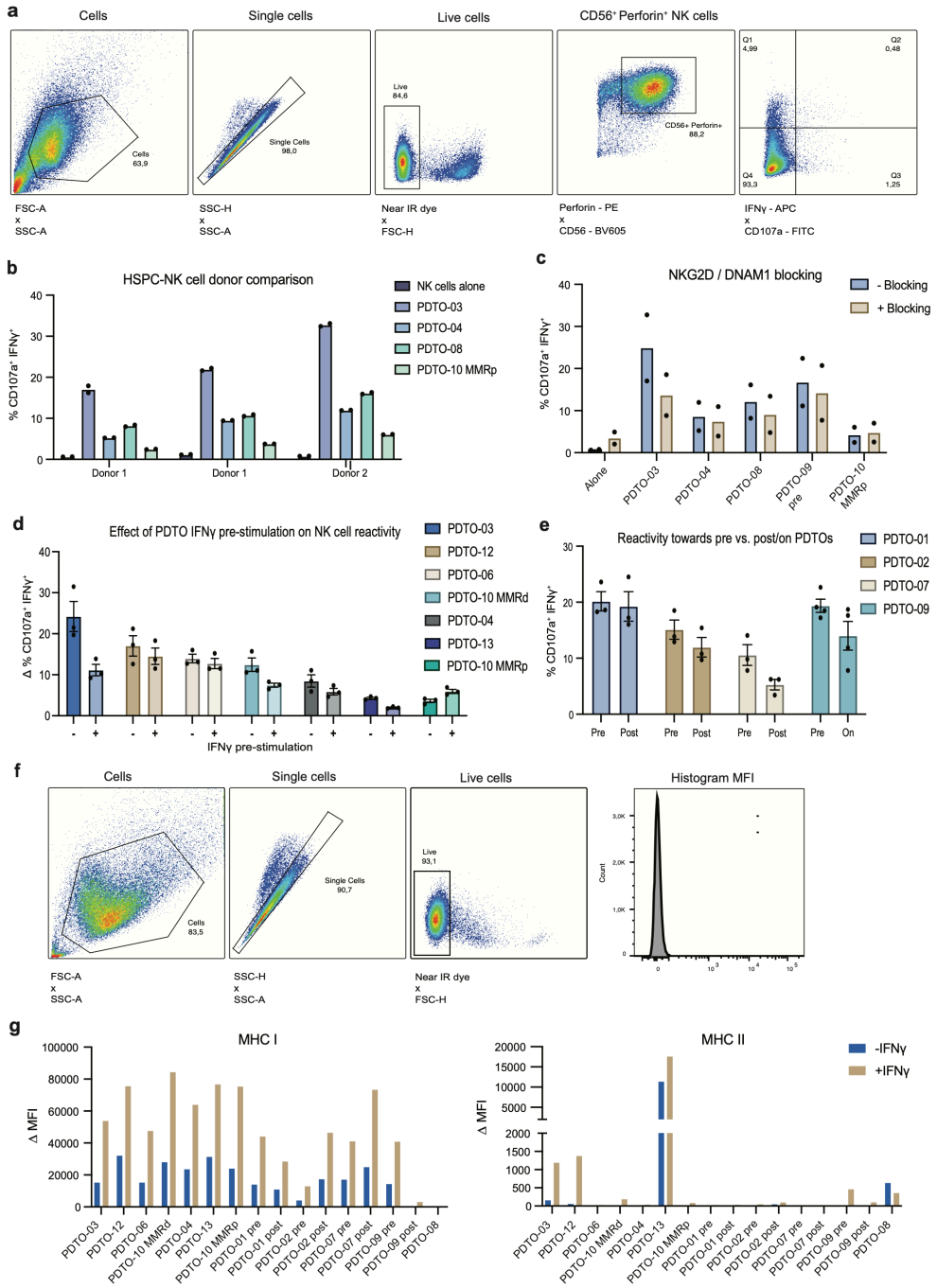
**Extended Data Table 4:** Antibodies used for phenotyping of PDTO's.

**Extended Data Table 5:** Phenotyping of HSPC-NK cells.



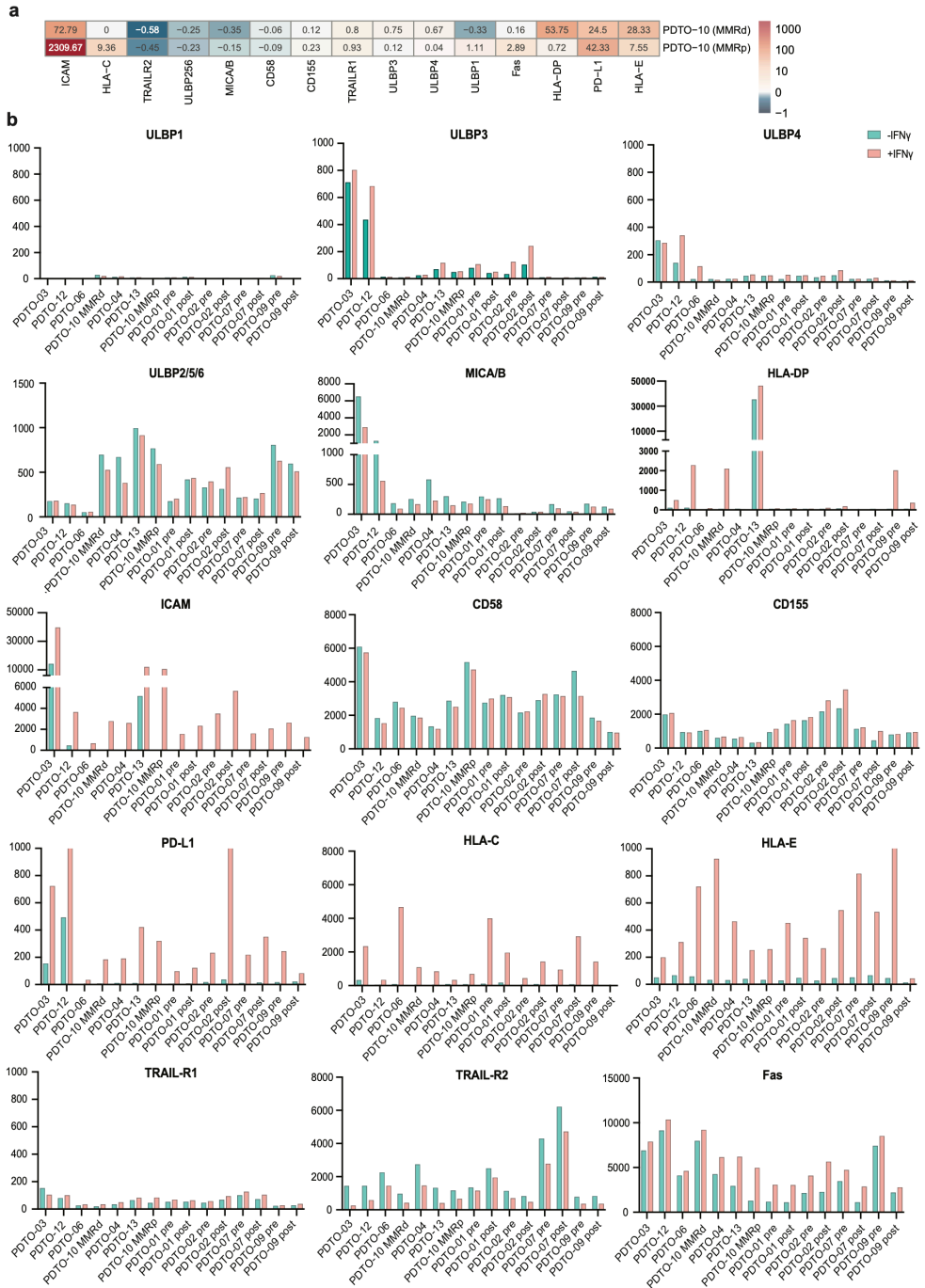
Extended Data Fig. 1: Phenotyping of autologous and HSPC-NK cells and reactivity of autologous sub-populations by flow cytometry. **a**. Schematic overview of the experimental setup and readout of the

autologous NK cell reactivity assays. NK cells derived from PBMCs were stimulated with tumor organoids, which were established from tumor material of the same patient as the collected PBMCs. Tumor reactivity of the autologous NK cells was assessed by IFN $\gamma$  expression. Representative flow cytometry plots showcase a tumor reactive, PDO-11, and non-reactive, PDO-12. **b.** Bar plots indicating mean background-subtracted IFN $\gamma$  expression of HSPC-NK cells after co-culture with PDOs. Data is shown for 3 or more biological replicates ( $n^3$ ). Whiskers indicate SEM. **c.** Flow cytometry gating strategy for single, live, CD56<sup>bright</sup> CD16<sup>-</sup> NK cells of a representative autologous NK cell sample showing sequential gating including percentages. Indicated gating strategy was used for all autologous NK cell reactivity assays to determine IFN $\gamma$  expression. **d.** Top: Representative flow cytometry plot of autologous NK cells (aNK-11) derived from patient PBMCs showing distribution of three sub-populations (CD56<sup>bright</sup> CD16<sup>-</sup>, CD56<sup>dim</sup> CD16<sup>-</sup> and CD56<sup>dim</sup> CD16<sup>+</sup>). Bottom: Bar plots presenting mean percentage of autologous NK cell sub-populations (CD56<sup>bright</sup> CD16<sup>-</sup>, CD56<sup>dim</sup> CD16<sup>-</sup> and CD56<sup>dim</sup> CD16<sup>+</sup>) after priming at the time of reactivity assay with respective tumor organoids. **e.** IFN $\gamma$  expression of unstimulated NK cells of each sub-population (top) and IFN $\gamma$  expression of NK cells stimulated with respective tumor organoids PDO-11 (bottom). **f.** Three bar plots of IFN $\gamma$  expression of autologous NK cell sub-populations (left to right: CD56<sup>bright</sup> CD16<sup>-</sup>, CD56<sup>dim</sup> CD16<sup>+</sup> and CD56<sup>dim</sup> CD16<sup>-</sup>) upon tumor organoid stimulation. Background signal of unstimulated NK cells has been subtracted from respective IFN $\gamma$  signal. Data is shown for at least 3 biological replicates ( $n^3$ ) except for PDO-12, -07 pre ( $n=2$ ). **g.** Flow cytometry gating strategy shows an example of the gating strategy used to determine markers expressed by the NK cells. First, a scatter gate is placed to gate out debris. Next, live cells are gated followed by gating on CD56<sup>+</sup>. Receptor expression is then determined by gating within the CD56<sup>+</sup> cells based on IgG isotype controls which were set between 1 and 2% as shown for NKG2A-APC. Right flow cytometry plot showing PD-1 expression.



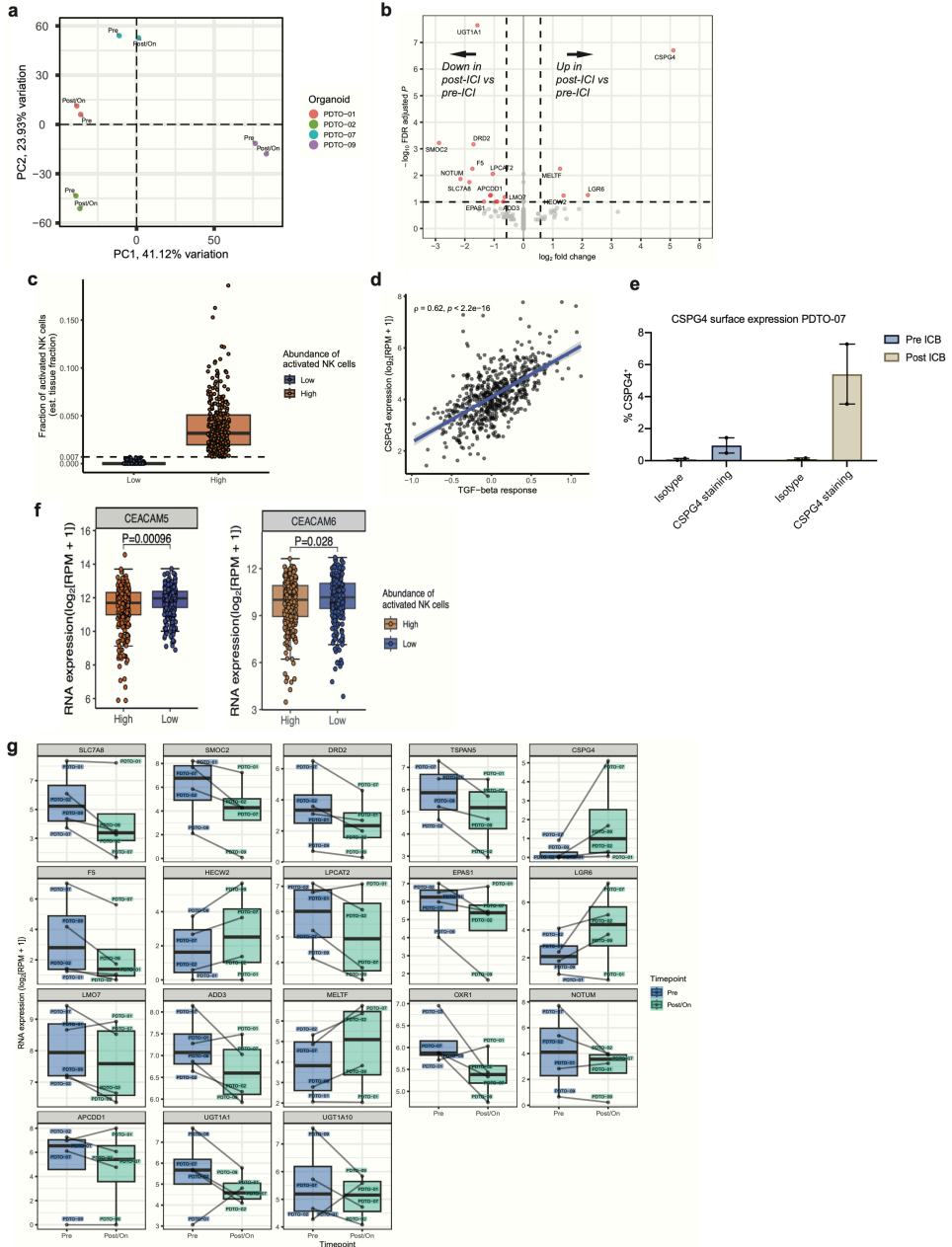
**Extended Data Fig. 2: Extended analysis of HSPC-NK cell tumor organoids reactivity, including mutational profile of tumor organoid panel and MHC-I/II expression.** **a.** Flow cytometry gating strategy for single, live, CD56<sup>+</sup> Perforin<sup>+</sup> NK cells of a representative HSPC-NK cell donor sample showing sequential gating including percentages. Indicated gating strategy was used for all HSPC-NK cell reactivity assays to determine IFN $\gamma$  and CD107a expression. **b.** Bar plots of IFN $\gamma$  and CD107a expression of two HSPC-NK cell donors (donor 1 and 2) and three independent experiments upon stimulation with PDTO-03, -04, -08, -10 MMRp or no tumor organoids stimulation (NK cells alone). Bars indicate mean of two technical replicates. **c.** Bar plots indicating IFN $\gamma$  and CD107a expression of unstimulated HSPC-NK cells (alone) or stimulated with tumor organoids (PDTO-03, -04, -08, -09 pre and -10 MMRp) in presence (sand color) or absence (blue color) of combined NKG2D and DNAM-1 ligand blocking (n=2). **d.** Bar plots indicate D IFN $\gamma$  and CD107a expression of HSPC-NK cells upon stimulation with tumor organoids (PDTO-03, -12, -06, -10 MMRd, -04, -13 and -10 MMRp) with (+) or without (-) IFN $\gamma$  pre-stimulation for 24h (n=3). Whiskers indicate SEM. **e.** Bar plots indicate D IFN $\gamma$  and CD107a expression of HSPC-NK cells upon stimulation with tumor organoids derived pre and on/post ICB treatment (n=3 except PDTO-09 with n=4). Whiskers indicate SEM. **f.** Flow cytometry gating strategy for single and live cells from a representative tumor organoids sample showing sequential gating including percentages. Indicated gating strategy was used for NK cell ligand and MHC surface expression analysis. **g.** Two bar plots indicating D MFI of MHC-I (left) and MHC-II (right) surface expression on tumor organoids. Surface expression analysis was performed on tumor organoids without IFN $\gamma$  (blue color) and with IFN $\gamma$  pre-stimulation (sand color).



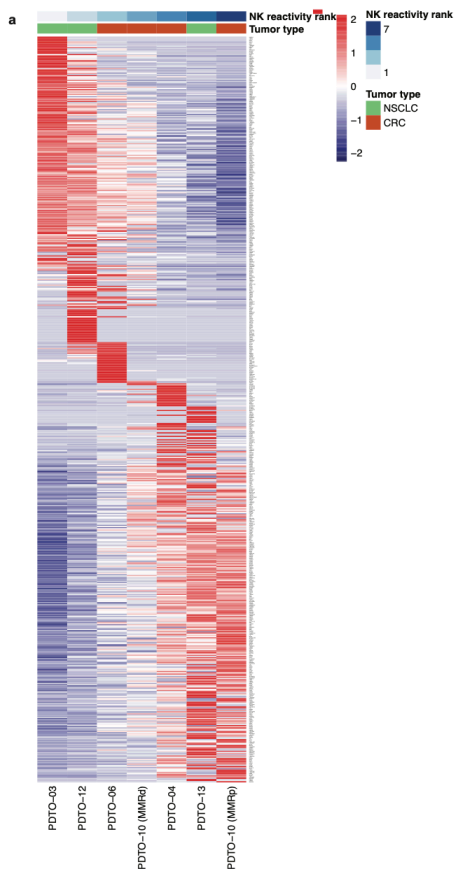


7

**Extended Data Fig. 3: Extensive NK cell ligand surface expression phenotyping of tumor organoids. a.** Heatmap presenting fold change of NK cell ligand surface expression of tumor organoid pair PDO-10 MMR-d and MMR-p stimulated with IFN $\gamma$  compared to no IFN $\gamma$  stimulation. Red color indicates increased DMFI upon IFN $\gamma$  stimulation (value > 0), whereas blue color indicates decreased DMFI upon IFN $\gamma$  stimulation (value < 0). Rows indicate tumor organoid samples and columns indicate NK cell ligands. **b.** Bar plots indicating D MFI of surface expression of whole NK cell ligand panel on tumor organoids included in HSPC-NK cell reactivity assays. Surface expression analysis was performed on tumor organoids without IFN $\gamma$  (mint color) and with IFN $\gamma$  pre-stimulation (coral color). Bars show mean of two biological replicates (n=2).



**Extended Data Fig. 4: RNA expression analysis of patient-derived tumor organoids.** **a.** PCA plot of the gene expression profiles of the four pre/post-ICI therapy PDO pairs. **b.** Volcano plot indicating differential gene expression between post-ICI and pre-ICI therapy PDOs of three pairs which elicited lower HSPC-NK cell reactivity by stimulation with post-ICI PDOs. Vertical and horizontal dotted lines indicate absolute 1.5-fold change differential expression threshold and 10% false discovery rate (FDR) threshold, respectively. **c.** Boxplot depicting the dichotomization of the abundance of activated NK cells in the TCGA-COADREAD dataset (n=597). The dotted line indicates the median, used to define low and high abundance of activated NK cells. **d.** Dot plot depicting the normalized expression of CSPG4 and the TGF-beta response signature score in the TCGA-COADREAD samples (n=597). A two-tailed Spearman correlation analysis was performed.  $\rho$  = Spearman correlation coefficient. **e.** Bar plots indicating surface expression of CSPG4 of PDO-07 pre vs. post ICI (n=2). Whiskers indicate SEM. **f.** CEACAM5 and CEACAM6 expression in TCGA-COADREAD samples with high or low abundance of activated NK cells (n=597). **g.** Paired boxplots depicting the normalized expression level of selected differentially expressed genes between pre-ICI and post-ICI therapy PDOs. Box plots indicate the median (line), interquartile range (box), minima and maxima (whiskers). Statistical significance was tested with a Wilcoxon signed-rank test.



**Extended Data Fig. 5: Genes linearly associated with order of HSPC-NK cell reactivity.** **a.** Heatmap of normalized RNA expression (column z-scores) of genes whose expression was linearly associated with the order of HSPC-NK cell reactivity in the tested PDOs (decreasing from left-to-right) per Fig. 2a.

Extended Data Table 1: Patient derived (tumor) organoid information

PD(T)O	Tumor type	MMR-d/-p status	Authenticated STR or SNP	Mycoplasma	Other
PDO-01	Normal colon	-	Yes	Negative	
PDTO-01 pre	CRC	MMR-p	Yes	Negative	
PDTO-01 post	CRC	MMR-p	Yes	Negative	
PDO-02	Normal colon	-	Yes	Negative	
PDTO-02 pre	CRC	MMR-p	Yes	Negative	
PDTO-02 post	CRC	MMR-p	Yes	Negative	
PDO-03	Normal lung	-	Yes	Negative	
PDTO-03	NSCLC	-	Yes	Negative	Luciferase transduced
PDTO-04	CRC	MMR-d	Yes	Negative	
PDTO-05	NSCLC	-	Yes	Negative	
PDTO-06	CRC	MMR-p	Yes	Negative	
PDTO-07 pre	CRC	MMR-p	Yes	Negative	
PDTO-07 post	CRC	MMR-p			
PDTO-08	CRC	MMR-d	Yes	Negative	B2M mutation
PDTO-09 pre	CRC	MMR-d	Yes	Negative	
PDTO-09 on	CRC	MMR-d			
PDTO-10 MMRd	CRC	MMR-d	Yes	Negative	
PDTO-10 MMRp	CRC	MMR-p	Yes	Negative	
PDTO-11	NSCLC	-	Yes	Negative	
PDTO-12	NSCLC	-	Yes	Negative	
PDTO-13	NSCLC	-	Yes	Negative	

Extended Data Table 2: Information pre and on/post samples for PDTOs and patient treatment response.

PDTO	Pre/ post treatment	Date biopsy for PDTOs	Treatment start / end	Treatment type	Response	Other treatment during time period
PDTO-01	Pre	08/05/2017	First: 08/05/2017	Nivolumab	PD	No other
PDTO-01	Post	13/06/2017	Last: 22/05/2017			
PDTO-02	Pre	20/03/2018	First: 23/03/2018	Nivolumab and Ipilimumab	PD	No other
PDTO-02	Post	20/04/2018	Last: 06/04/2018			
PDTO-07	Pre	06/10/2017	First: 10/10/2017	Pembrolizumab	PD	No other
PDTO-07	Post	29/01/2018	Last: 24/11/2017			
PDTO-09	Pre	23/01/2017	First: 27/10/2017	Nivolumab	SD	No other
PDTO-09	On	17/07/2018	Last: 25/09/2019			

Extended Data Table 3: Autologous NK cell reactivity by sub-populations.

Samples	PBMC / isolated NK cells	PDTO added in co- culture	% CD56 dim CD16 <sup>+</sup>	NK cells alone %IFN $\gamma$	+ PDTO %IFN $\gamma$	% CD56 high CD16 <sup>+</sup>	NK cells alone %IFN $\gamma$	+ PDTO %IFN $\gamma$	% CD56 dim CD16 <sup>+</sup>	NK cells alone %IFN $\gamma$	+ PDTO %IFN $\gamma$
<b>PDTO-12</b>	PBMCs	yes	49,20	0,42	0,38	15,60	2,47	3,04	5,70	3,60	2,17
	PBMCs	yes	43,80	4,76	5,33	7,50	7,82	7,15	21,40	1,88	5,83
<b>PDTO-06</b>	PBMCs	yes	26,10	6,37	4,92	16,10	6,34	7,31	18,90	5,27	4,09
	NK cells	no	49,00	9,14	8,24	11,00	5,69	7,55	17,50	7,34	7,70
<b>PDTO-11</b>	PBMCs	yes	33,80	2,87	2,15	19,90	5,44	11,85	20,30	3,51	6,52
	NK cells	yes	51,30	0,22	1,14	22,50	0,86	17,30	16,00	0,90	5,35
	NK cells	yes	43,40	0,91	0,39	13,90	2,84	26,70	12,60	4,26	15,30
<b>PDTO-05</b>	NK cells	yes	41,30	2,08	3,25	17,60	3,64	15,40	18,30	4,65	11,50
	PBMCs	yes	25,40	3,55	4,13	24,20	3,66	6,35	14,90	8,57	12,80
	NK cells	yes	35,90	0,10	0,45	20,70	0,58	6,31	23,20	0,69	2,23
<b>PDTO-07 pre</b>	NK cells	yes	82,10	8,15	4,58	2,59	3,09	3,37	5,11	0,21	0,21
	NK cells	no	81,70	5,69	1,93	2,84	1,59	1,88	5,20	0,13	0,10
<b>Average</b>			46,92			14,54			14,93		

Extended Data Table 4: Antibodies used for phenotyping of PB-NK cells and PDTO's.

Antibody	Fluoro- chrome	Clone	Supplier	Catalog number	Lot number	Dilution
ULBP1	AF647	170818	R&D Systems	FAB1380R	1628980	1:20
ULBP2/5/6	BV421	165903	BD Biosciences	748128	1112036	1:20
ULBP3	PE	166510	R&D Systems	FAB1517P	ABPX0720051	1:10
ULBP4	PE	709116	R&D Systems	FAB6285P	ADXP0520061	1:10
CD112	AF488	610603	R&D Systems	FAB2229 G	ACHM032102 1	1:20
PD-L1	APC	MIH1	invitrogen	17598342	2142932	1:200
HLA-E	BV421	3D12	BD Biosciences	567425	2098516	1:20
CD155	FITC	SKIL4	BioLegend	337627	B317987	1:100
MICA/B	PECy7	6D4	BioLegend	320918	B354808	1:20
HLA-C	PE	DT9	BD Biosciences	566372	1113595	1:10
Fas	BV421	DX2	BioLegend	305623	B333164	1:20
FasL	BV421	NOK1	BioLegend	306411	B312564	1:20
ICAM	FITC	HCD54	BioLegend	322720	B304243	1:80
CD58	APC	TS2/9	BioLegend	330917	B314901	1:20
HLA-A, B, C	PE	W6/32	BD Biosciences	567582		1:20
HLA-DP	BV421	B7/21	BD Biosciences	750875	1216456	1:40
CD80	PECy7	2D10	BioLegend	305218	B341123	1:30
TRAIL-R1	APC	DJR1	BioLegend	307207	B331654	1:40
TRAIL-R2	PE	DJR24	BioLegend	307405	B289920	1:20
HLA-DP, DQ, DR	FITC	TU39	BD Biosciences	550853	2059649	1:20
CD107a	PE	H4A3	BD Biosciences	555801	8130821	1:50
CD107a	FITC	H4A3	BioLegend	328606	B367980	1:50
CD3	FITC	SK7	BioLegend	344804	B322367	1:50
CD16	AF700	B73.1	BioLegend	360703	B317474	1:40
CD56	BV605	HCD56	BioLegend	318334	B324998	1:40
IFN $\gamma$	APC	B27	BD Biosciences	554702	1284406	1:40
Perforin	PE	DG9	BioLegend	308106	B317271	1:50
Live/Dead	Near-IR		Thermo Fisher	L34976	249465	1:2000

Extended Data Table 5: Phenotyping of HSPC-NK cells.

	CD56%	NKG2a%	NKG2d%	DNAM-1%	NKp46%
Donor 1	89	68	99	80	99
Donor 2	97	70	89	82	91
Donor 3	85	75	88	89	92
Donor 4	98	83	79	98	99
Donor 5	97	83	96	89	92

Each and every one of us has been born into a given historical reality, ruled by particular norms and values, and managed by a unique economic and political system. We take this reality for granted, thinking it is natural, inevitable and immutable. We forget that our world was created by an accidental chain of events, and that history shaped not only our technology, politics and society, but also our thoughts, fears and dreams. The cold hand of the past emerges from the grave of our ancestors, grips us by the neck and directs our gaze towards a single future. We have felt that grip from the moment we were born, so we assume that it is a natural and inescapable part of who we are. Therefore, we seldom try to shake ourselves free, and envision alternative futures.

Yuval Noah Harari

General Discussion and  
Summary







The success stories of cancer immunotherapy in the past decade have undoubtedly changed clinical treatment of cancer patients and allowed scientists to dream bigger. From trispecific NK cell engagers<sup>1</sup> over epigenetic engineering of chimeric antigen receptor (CAR) T cells<sup>2</sup> to in vivo gene immunotherapy using RNA interference (RNAi)<sup>3</sup>, the possibilities seem endless.

In this thesis we focused to a large extent on immune checkpoint inhibitor (ICI) treatment, which utilizes antibodies that block certain inhibiting signals to unleash anti-tumor immune responses. Even though it will be difficult to find any cancer immunotherapy publication that does not cite the impressive patient response rate to ICI treatment (rightfully so)<sup>4,5,6,7,8</sup>, the underlying principle is rather simple compared to the above-mentioned cancer immunotherapy strategies. So why is there no end in sight of research on ICI treatment? Why are we still in the dark when it comes to accurate treatment response prediction? I don't have the full answer, but I believe it is, at least to some extent, due to the fact that we try to decipher the interplay of two unique and vastly complex systems – the immune system and the tumor.

In order to capture such complexity and facilitate translation to clinical therapies, choosing the right model system is of high importance. Using patient-derived tumor organoids not only allowed us to capture characteristics of the original tumor<sup>9,10</sup> but also to use autologous immune cells to dissect personalized immune responses.

In this thesis, we present our initial findings of a whole genome CRISPR Cas9 screen in tumor organoids which identified a novel resistor gene to autologous CD8<sup>+</sup> T cell killing. Further, we explored the potential of combining tumor organoid and autologous co-cultures with chromatin accessibility analysis to better characterize T cell subsets and relevant regulatory elements for anti-tumor responses. By looking beyond T cells, we were able to explain how tumors invisible to CD8<sup>+</sup> T cells can respond to ICI treatment and how tumors may evade NK cell recognition. Although the research of this thesis covers only a tiny area of the field of cancer immunotherapy, it provides an idea of the complexity we embark on.

In **Chapter 2**, Emile Voest and I provide an extensive overview of the potential of patient-derived tumor organoids for precision medicine. Summarizing immense efforts in preclinical and fundamental research, we describe the opportunities that tumor

organoids offer for a better understanding of, for example, immunotherapies, genomic screens or proteomic focused approaches. Their versatility makes them accessible for numerous technologies and drug testing. However, we considered clinical implementation more challenging due to sometimes slow establishment rates, missing prospective studies and lack of a tumor microenvironment or vascular system. Since the review was published in mid 2021, genomic screens and CRISPR engineering of tumor organoids have gained further popularity<sup>11</sup>. Notable is the recent enthusiasm from the Pharma industry to invest in organoids for drug discovery and development, as done by Roche<sup>12</sup>. Although limitations of organoid cultures should not be neglected and a combination of different model systems, as well as integrated clinical data, is likely most beneficial for cancer research, tumor organoids are help us improve our understanding of personalized cancer biology.

Given those considerations and opportunities of tumor organoids, we embarked on a mission to perform a fully autologous whole genome CRISPR Cas9 knockout screen in patient-derived tumor organoids to identify mediators of T cell killing. This effort and its initial results are described in **Chapter 3**. Tumor reactive CD8<sup>+</sup> T cells were generated as previously described<sup>13,14</sup> and then co-cultured with library transduced tumor organoids. Using this screening effort in combination with an IFN $\gamma$  cytokine screen, showed that T cell killing was mainly mediated by IFN $\gamma$  and identified galactosyltransferases as potential modulators. The technical challenge of this endeavor was mainly the production of sufficient autologous tumor reactive T cells, since only a few pairs of tumor organoids and PBMCs elicit high T cell cytotoxicity and expansion potential can deviate. Using a minimal whole genome library improved the feasibility of using an autologous system but future screens may consider tissue specific or otherwise targeted screens to reduce complexity. Another obstacle, which needs to be addressed by future experiments, were missing hits in the antigen presenting machinery pathway. Likely as a result of T cell unrelated cell death due to a bystander effect or culture conditions, demonstrated challenges of this project and highlight the importance of validation experiments. Currently, additional screens of other pairs are being performed and analyzed as they should help to evaluate shared or patient model specific hits. Of special interest for future research is also to unveil

the role of proteoglycans, specifically galactosyltransferase B4GALT7, in respect to anti-tumor T cell responses.

While Chapter 3 looked at influences of T cell cytotoxicity on the tumor side, in **Chapter 4** we focused on the changes of T cells upon tumor organoid interaction. Here, we assessed the feasibility of scATAC sequencing of co-culture cell products, which comes with some challenges. Autologous PBMCs from cancer patients are a limited source. To ensure true representation of all T cell populations each condition should be established with a cell count that sufficiently represents the various T cell populations, hence the number of conditions needed to be carefully considered. Also, while taking into account that a certain loss of cells will occur during sample processing. Using a plate-based approach, which requires sorting of single cell nuclei, turned out to be not optimal for handling of small and perhaps fragile PBMCs. We speculated that a droplet-based approach, as offered by 10x Genomics, could improve our readout. Furthermore, our comparison to bulk ATAC taught us that this approach was technically more feasible but deconvolution of smaller immune subsets is dependent on available ATAC datasets, which are scarce compared to RNA sequencing data. An optimal setting for future experiments is likely to first select optimal conditions, including time points which represent T cell changes upon tumor organoid interaction and to lesser extent of culturing conditions, and then scaling up to a larger sample size. Such experiments could perhaps be based on RNA sequencing as deconvolution of sub-populations would be easier, a combination with bulk ATAC to reduce costs and then performing scATAC with an improved protocol as the final readout. A combination of scATAC with scRNA sequencing would be ideal but is costly. This approach could eventually facilitate the identification of T cell subsets and regulatory elements which are crucial for anti-tumor immune responses. Moreover, it would be interesting to test if such T cell subsets differ between ICI treatment responder or non-responder as it may have predictive value to treatment response. Overall, I believe that there is much more to learn from PBMCs, especially peripheral blood T cells, than we are currently grasping.

In **Chapter 5** we step away from conventional T cells and focus on  $\gamma\delta$  T cells, an immune cell type that bridges the adaptive and innate immunity. Starting with a riddle of how HLA class I deficient MMR-d CRC can respond to ICI treatment when CD8<sup>+</sup> T cells are excluded as effectors, we identified V $\delta$ 1 T cells as potential mediators of ICI response. We combined extensive phenotype analysis by scRNA sequencing of tumor infiltrating  $\gamma\delta$  T cells, data analysis on large patient's cohorts including ICI responder and non-responder, B2M wildtype and knockout isogenic tumor organoid models and imaging mass cytometry on patient tumor samples from the NICHE study pre and post ICI treatment, in an outstanding team effort. Our results expand our knowledge on cellular mechanisms that drive ICI response and suggest that  $\gamma\delta$  T cell therapies may overcome limitations of conventional T cells. However, the insights we gained led to even more questions. The full mechanism of tumor recognition by V $\delta$ 1 T cells remains unclear and identification of the respective TCR is under investigation. A possible immune cell-cell crosstalk with, for example, CD4<sup>+</sup> T cells is another avenue that may be pursued in the future. Moreover, it is yet to be determined if the presence of likely more active CD103<sup>+</sup> PD1<sup>+</sup>  $\gamma\delta$  T cells in MMR-d tumors<sup>15</sup> is a result of presence of other activated immune cells or if MMR/MSI status has a direct effect on  $\gamma\delta$  T cell.

This brings us to **Chapter 6** which follows up on this open question. Here, we present initial findings that indeed CRC cells with an MSI signature seem to elicit stronger V $\delta$ 1 T cell reactivity compared to CRC with an MSS signature. Using an isogenic HT29 cell line model system, established by the Bardelli group, we also showed that interference with B2M in MMR-p/MSS CRC cells increases V $\delta$ 1 T cell reactivity. To confirm the results and draw more conclusions we first need to expand our findings to a larger sample size of V $\delta$ 1 T cells and tumor models. However, these initial results will be interesting to follow up on as they suggest that a. in depth mechanistic characterization why and how MMR/MSI status influences V $\delta$ 1 T cell reactivity can open up opportunities to make MMR-p tumors more immunogenic and b. therapies targeting B2M or other components of the HLA class I could improve V $\delta$ 1 T cell responses in patients that are currently not responding to ICI treatment.

Lastly, in **Chapter 7** we fully transition to innate immunity and focus on NK cells, more specifically CD34<sup>+</sup> progenitor cell derived HSPC-NK cells. Compared to autologous NK cells, HSPC-NK cells offer the benefit of an unlimited off-the-shelf product which can be genetically engineered to improve its anti-tumor response. We, demonstrate the potential of combining patient-derived tumor organoids and HSPC-NK cells to discover relevant mediators of HSPC-NK cell reactivity. Following up on our findings and gaining mechanistic insights into a possible inhibiting role of CSPG4 on NK cells and its upregulation in post ICI treatment tumors, could provide rationale for genetic engineering of HSPC-NK cells to overcome an inhibitory effect. Moreover, our results emphasize the delicate balance of activating and inhibiting receptor ligand pairs that influence NK cell reactivity and make it challenging to identify and target the 'most relevant' ones. IFN $\gamma$  overall seemed to negatively influence HSPC-NK cell reactivity, which is in line with recent findings of an in vivo CRISPR screen on immune evasion mechanisms<sup>16</sup>. Chapter 3 touched upon the relevance of IFN $\gamma$  signaling for effective T cell responses which underlines the dual role of IFN $\gamma$  in the context of anti-tumor immunity. Demonstrating that a therapy with sole focus on one immune cell type might reduce the reactivity of another immune cell type. Although this is speculative, I could foresee that in some cases strategic targeting of different immune cell types yield improved anti-tumor responses.

### Final remarks

All chapters of this thesis focus on the attempt to increase our understanding of anti-tumor immune responses. We analyzed conventional T cells, with a focus on CD8<sup>+</sup> T cells,  $\gamma\delta$  T cells and HSPC-NK cells in respect to their interaction mostly with patient-derived tumor organoids. Our work generated a wealth of insights but even more questions and unknowns became apparent. This taught me how I am only grasping the complexity of anti-tumor immunity. Understanding the immune system and its fine-tuned balance and then leveraging the power of its network to eliminate cancer cells is something truly beautiful. That said, I cannot wait to find myself right in the middle of the exciting world of cancer immunotherapy research and its future innovations.

## REFERENCES

1. Gauthier, L., A. Morel, N. Anceriz, B. Rossi, A. Blanchard-Alvarez, G. Grondin, S. Trichard, C. Cesari, M. Sapet, F. Bosco, H. Rispaud-Blanc, F. Guillot, S. Cornen, A. Roussel, B. Amigues, G. Habib, F. Caraguel, S. Arrufat, R. Remark, F. Romagne, Y. Morel, E. Narni-Mancinelli and E. Vivier (2019). "Multifunctional Natural Killer Cell Engagers Targeting NKp46 Trigger Protective Tumor Immunity." *Cell* 177(7): 1701-1713 e1716.
2. Lynn, R. C., E. W. Weber, E. Sotillo, D. Gennert, P. Xu, Z. Good, H. Anbunathan, J. Lattin, R. Jones, V. Tieu, S. Nagaraja, J. Granja, C. F. A. de Bourcy, R. Majzner, A. T. Satpathy, S. R. Quake, M. Monje, H. Y. Chang and C. L. Mackall (2019). "c-Jun overexpression in CAR T cells induces exhaustion resistance." *Nature* 576(7786): 293-300.
3. Mai, D., C. H. June and N. C. Sheppard (2022). "In vivo gene immunotherapy for cancer." *Sci Transl Med* 14(670): eabo3603.
4. Hodi, F. S., S. J. O'Day, D. F. McDermott, R. W. Weber, J. A. Sosman, J. B. Haanen, R. Gonzalez, C. Robert, D. Schadendorf, J. C. Hassel, W. Akerley, A. J. van den Eertwegh, J. Lutzky, P. Lorigan, J. M. Vaubel, G. P. Linette, D. Hogg, C. H. Ottensmeier, C. Lebbe, C. Peschel, I. Quirt, J. I. Clark, J. D. Wolchok, J. S. Weber, J. Tian, M. J. Yellin, G. M. Nichol, A. Hoos and W. J. Urba (2010). "Improved survival with ipilimumab in patients with metastatic melanoma." *N Engl J Med* 363(8): 711-723.
5. Topalian, S. L., F. S. Hodi, J. R. Brahmer, S. N. Gettinger, D. C. Smith, D. F. McDermott, J. D. Powderly, R. D. Carvajal, J. A. Sosman, M. B. Atkins, P. D. Leming, D. R. Spigel, S. J. Antonia, L. Horn, C. G. Drake, D. M. Pardoll, L. Chen, W. H. Sharfman, R. A. Anders, J. M. Taube, T. L. McMiller, H. Xu, A. J. Korman, M. Jure-Kunkel, S. Agrawal, D. McDonald, G. D. Kollia, A. Gupta, J. M. Wigginton and M. Sznol (2012). "Safety, activity, and immune correlates of anti-PD-1 antibody in cancer." *N Engl J Med* 366(26): 2443-2454.
6. Ribas, A. and J. D. Wolchok (2018). "Cancer immunotherapy using checkpoint blockade." *Science* 359(6382): 1350-1355.
7. Larkin, J., V. Chiarion-Sileni, R. Gonzalez, J. J. Grob, P. Rutkowski, C. D. Lao, C. L. Cowey, D. Schadendorf, J. Wagstaff, R. Dummer, P. F. Ferrucci, M. Smylie, D. Hogg, A. Hill, I. Marquez-Rodas, J. Haanen, M. Guidoboni, M. Maio, P. Schöffski, M. S. Carlino, C. Lebbe, G. McArthur, P. A. Ascierto, G. A. Daniels, G. V. Long, L. Bastholt, J. I. Rizzo, A. Balogh, A. Moshyk, F. S. Hodi and J. D. Wolchok (2019). "Five-Year Survival with Combined Nivolumab and Ipilimumab in Advanced Melanoma." *N Engl J Med* 381(16): 1535-1546.
8. Chalabi, M., L. F. Fanchi, K. K. Dijkstra, J. G. Van den Berg, A. G. Aalbers, K. Sikorska, M. Lopez-Yurda, C. Grootsholten, G. L. Beets, P. Snaebjornsson, M. Maas, M. Mertz, V. Veninga, G. Bounova, A. Broeks, R. G. Beets-Tan, T. R. de Wijkerslooth, A. U. van Lent, H. A. Marsman, E. Nuijten, N. F. Kok, M. Kuiper, W. H. Verbeek, M. Kok, M. E. Van Leerdam, T. N. Schumacher, E. E. Voest and J. B. Haanen (2020). "Neoadjuvant immunotherapy leads to pathological responses in MMR-proficient and MMR-deficient early-stage colon cancers." *Nat Med* 26(4): 566-576.
9. Weeber, F., M. van de Wetering, M. Hoogstraat, K. K. Dijkstra, O. Krijgsman, T. Kuilman, C. G. Gadellaa-van Hooijdonk, D. L. van der Velden, D. S. Peeper, E. P. Cuppen, R. G. Vries, H. Clevers and E. E. Voest (2015). "Preserved genetic diversity in organoids cultured from biopsies of human colorectal cancer metastases." *Proc Natl Acad Sci U S A* 112(43): 13308-13311.
10. Sachs, N. and H. Clevers (2014). "Organoid cultures for the analysis of cancer phenotypes." *Curr Opin Genet Dev* 24: 68-73.
11. Geurts, M.H., Clevers, H. CRISPR engineering in organoids for gene repair and disease modelling. *Nat Rev Bioeng* 1, 32–45 (2023).
12. Clevers H. Mini-organs attract big pharma *Nature Reviews Drug Discovery* 22, 175-176 (2023)

13. Cattaneo, C. M., K. K. Dijkstra, L. F. Fanchi, S. Kelderman, S. Kaing, N. van Rooij, S. van den Brink, T. N. Schumacher and E. E. Voest (2020). "Tumor organoid-T-cell coculture systems." *Nat Protoc* 15(1): 15-39.
14. Dijkstra, K. K., C. M. Cattaneo, F. Weeber, M. Chalabi, J. van de Haar, L. F. Fanchi, M. Slagter, D. L. van der Velden, S. Kaing, S. Kelderman, N. van Rooij, M. E. van Leerdam, A. Depla, E. F. Smit, K. J. Hartemink, R. de Groot, M. C. Wolkers, N. Sachs, P. Snaebjornsson, K. Monkhorst, J. Haanen, H. Clevers, T. N. Schumacher and E. E. Voest (2018). "Generation of Tumor-Reactive T Cells by Co-culture of Peripheral Blood Lymphocytes and Tumor Organoids." *Cell* 174(6): 1586-1598 e1512.
15. de Vries, N. L., V. van Unen, M. E. Ijsselsteijn, T. Abdelaal, R. van der Breggen, A. Farina Sarasqueta, A. Mahfouz, K. Peeters, T. Holtt, B. P. F. Lelieveldt, F. Koning and N. de Miranda (2020). "High-dimensional cytometric analysis of colorectal cancer reveals novel mediators of antitumour immunity." *Gut* 69(4): 691-703.
16. Dubrot, J., P. P. Du, S. K. Lane-Reticker, E. A. Kessler, A. J. Muscato, A. Mehta, S. S. Freeman, P. M. Allen, K. E. Olander, K. M. Ockerman, C. H. Wolfe, F. Wiesmann, N. H. Knudsen, H. W. Tsao, A. Iracheta-Vellve, E. M. Schneider, A. N. Rivera-Rosario, I. C. Kohnle, H. W. Pope, A. Ayer, G. Mishra, M. D. Zimmer, S. Y. Kim, A. Mahapatra, H. Ebrahimi-Nik, D. T. Frederick, G. M. Boland, W. N. Haining, D. E. Root, J. G. Doench, N. Hacohen, K. B. Yates and R. T. Manguso (2022). "In vivo CRISPR screens reveal the landscape of immune evasion pathways across cancer." *Nat Immunol* 23(10): 1495-1506.



Who we are cannot be separated from where we're from

Malcolm Gladwell, *Outliers: The Story of Success*

## Addendum

Nederlandse samenvatting

Curriculum vitae

List of publications

Acknowledgments





## NEDERLANDSE SAMENVATTING

Dit proefschrift heeft als doel de anti-tumoractiviteit van verschillende type immuun cellen te begrijpen, waarbij de complexiteit van tumor-immuun cel interacties zorgvuldig wordt overwogen. Om anti-tumorimmunitet op een gepersonaliseerde manier te onderzoeken, wat kan bijdragen aan de vertaling naar de kliniek, is het kiezen van het juiste modelsysteem van groot belang. Van patiënt-afkomstige tumor organoïden (patient-derived tumor organoids; PDO) hebben dezelfde fenotypische en genetische kenmerken als de oorspronkelijke tumor en maken het onderzoeken van autologe immuunreacties mogelijk. Omdat PDO's van fundamenteel belang zijn voor het onderzoek van dit proefschrift, zal **Hoofdstuk 2** de kansen en uitdagingen belichten die verbonden zijn aan het modelsysteem met betrekking tot gepersonaliseerde geneeskunde. De review zal een uitgebreid overzicht bieden van de huidige staat van organoïden in het kankeronderzoek, waarbij hun voorspellende waarde voor kankerbehandelingen kritisch wordt geëvalueerd en de voortgang van de implementatie van dit modelsysteem in het veld van immuuntherapie wordt samengevat.

Na het beschrijven van de mogelijkheid om PDO's te gebruiken voor onderzoek naar genetische screens en immuuntherapie tegen kanker, rapporteert **Hoofdstuk 3** onze studie waarbij we een CRISPR Cas9 knock-out screen van het hele genoom uitvoeren op PDO's om modulators van tumorcel doding door autologe CD8+ T-cellen te identificeren. Op basis van twee onafhankelijke, volledig autologe screens van microsatelliet instabiele (MSI) colorectale kanker (CRC) PDO's met tumor-reactieve CD8+ T-cellen werden genen betrokken bij het stimuleren en remmen van het doden van tumorcellen door T-cellen geïdentificeerd en gevalideerd. Deze ambitieuze onderneming bracht talloze optimalisaties met zich mee, die in dit methode-gerichte hoofdstuk worden beschreven.

Overeenkomstig met het doel om het doden van tumorcellen door- en de reactiviteit van T-cellen beter te begrijpen, zal **Hoofdstuk 4** de dynamiek van T-cellen tijdens co-kweek met PDO's onderzoeken, echter uitgevoerd op kleinere



schaal. Hier probeerden we de verschillen in T-cel reactiviteit te begrijpen op basis van expressie- en chromatinetoegankelijkheidsprofielen. Daarnaast bespreken we recente ontwikkelingen bij het identificeren van relevante T-cel statussen voor tumorrespons en beschrijven we de mogelijkheden van ons modelsysteem om dit verder te onderzoeken.

In **hoofdstuk 5** presenteren we hoe tumoren, onzichtbaar voor CD8+ T-cellen, kunnen reageren op ICI-behandeling. Na een uitgebreide multi-omics-analyse van MMR-d CRC tumoren met genetische mutaties in B2M en klinische patiënten data, identificeerden we  $\gamma\delta$  T-cellen als effectoren van ICI-respons. Differentiële genexpressieanalyse van twee onafhankelijke patiënten cohorten behandeld met ICI, fenotypering van oppervlaktemarkers en single-cell RNA-analyse van tumorinfiltrerende  $\gamma\delta$  T-cellen, samen met in vitro experimenten gebruikmakend van CRC-cellijnen en isogene B2M-mutante/ knock-out PDTO's, bevestigde een cytotoxisch fenotype en verhoogde reactiviteit van V $\delta$ 1/3 T-cellen tegen MMR-d CRC-tumoren met genetische mutaties in B2M. Met deze veelbelovende bevindingen verschuift dit proefschrift de focus naar immuun cellen anders dan conventionele T-cellen.

Om de ontdekkingen uit Hoofdstuk 5 een stap verder te brengen, hebben we onderzocht of onze bevindingen van verhoogde  $\gamma\delta$  T-cel tumorreactiviteit in de context van MMR-d CRC toepasbaar zijn op MMR-p CRC. Deze tumoren reageren over het algemeen niet goed op ICI-behandeling<sup>12</sup>, en elke ontwikkeling in het initiëren van een betere immuunreactie zou een veelbelovende vooruitgang zijn.

**Hoofdstuk 6** beschrijft onze meest recente bevindingen over het introduceren van een B2M-mutatie in MMR-p CRC met als doel om de  $\gamma\delta$  T-celreactiviteit te verhogen.

Ten slotte beschrijft **Hoofdstuk 7** de reactiviteit van hematopoietische stam- en voorlopercel-afgeleide NK-cellen (HSPC-NK-cellen) op PDTO's om activerende en remmende liganden te karakteriseren, evenals het onderzoek naar de rol van IFN $\gamma$  bij tumorherkenning. Deze studie, gebruikmakend van paren CRC-PDTO's afgeleid vóór en na ICI-behandeling, bracht aan het licht dat HSPC-NK-cellen verminderde reactiviteit laten zien op PDTO's gegenereerd na ICI-behandeling.

Overeenkomstig met Hoofdstuk 4 zou dit kunnen wijzen op de betrokkenheid van immuun cellen anders dan conventionele T-cellen, bij de respons op immuuntherapie.

Samengevat presenteren de bovenstaande hoofdstukken een reis door de complexiteit van anti-tumorimmunitet, die we, zoals ik geloof, nog maar net beginnen te begrijpen. Te beginnen met de uitdaging om onze grenzen te verleggen van het begrijpen van T-celreacties naar meer onontdekte wegen, zoals de relevantie van  $\gamma\delta$  T-cellen in respons op ICI of regulatoren van HSPC-NK-cel reactiviteit.



## CURRICULUM VITAE

Vivien Veninga was born on 13th of May 1992 in Nienburg (Weser) Germany. After attending the Marion Dönhoff Gymnasium, where she obtained her Abitur in 2011 majoring in Chemistry, Physics and Mathematics, she first moved to Sydney, Australia, for one year and then to Southern Germany to pursue her academic career.

She obtained her Bachelor of Science in Biochemistry from the Eberhard Karls University in Tübingen in 2015. During her bachelor studies, she performed a research internship at the Max Planck Institute for Developmental Biology. Her bachelor thesis focused on modulators of matrix metalloproteinases and TGF- $\beta$  in glioblastoma. In 2015 she started her Master of Science in Biochemistry at the Ludwig Maximilian University (LMU) of Munich with molecular and cellular genetics, virology and human biology as electives. Next to her studies, she worked as a research assistant at the LMU Institute of Pathology under supervision of Dr. Steffen Ormanns focussing on pancreatic cancer. She graduated in 2018 after completing her master thesis on patient-derived tumor organoids and T cell co-cultures under supervision of Prof. Emile Voest at the Netherlands Cancer Institute in Amsterdam, the Netherlands.

Before returning to Prof. Emile Voest's lab she stayed in Prof. Johanna Olweus' lab in Oslo, Norway, at the Institute of Cancer Research. In the summer of 2019 she re-joined the Voest lab and started her PhD in the division of Molecular Oncology and Immunology at the Netherlands Cancer Institute. During her PhD, she was part of the NKI Entrepreneur Club. Her scientific efforts on better understanding the interplay of immune cells and tumors are described in this thesis.

In 2024 she will start her postdoc in Dr. Ansu Satpathy's lab at Stanford University, California, USA.



## LIST OF PUBLICATIONS

Gabriele Picco\*, **Vivien Veninga\***, Sara F. Viera, Sarah Consonni, Chiara M. Cattaneo, Alex Wattson, Samantha Walker, Emre Karakoc, Matthew A. Coelho, Thomas Battaglia, Leon Potgeter, Iris Mimpen, Allard W.J. van Renterghem, Krijn Dijkstra, Xuhui Ma, Shriram Bhosle, Mathew J. Garnett#, Emile E. Voest#  
Whole genome CRISPR screen of patient-derived tumor organoids to identify mediators of autologous CD8+ T cell killing. Manuscript in preparation.

**Vivien Veninga\***, Steven L.C. Ketelaars\*, Paul K.J.D. de Jonge#, Don Schilder#, Joris van de Haar, Yara L. Verschoor, Allard W.J. van Renterghem, Myriam Chalabi, Noel F.C.C. de Miranda, Harry Dolstra, Emile E. Voest (2024). Unveiling determinants driving CD34+ progenitor-derived NK cell reactivity against patient-derived tumor organoids. Submitted to *Cancer Immunology Research*.

Coelho, M. A., S. Cooper, M. E. Strauss, E. Karakoc, S. Bhosle, E. Goncalves, G. Picco, T. Burgold, C. M. Cattaneo, **V. Veninga**, S. Consonni, C. Dincer, S. F. Vieira, F. Gibson, S. Barthorpe, C. Hardy, J. Rein, M. Thomas, J. Marioni, E. E. Voest, A. Bassett and M. J. Garnett (2023). "Base editing screens map mutations affecting interferon-gamma signaling in cancer." *Cancer Cell* 41(2): 288-303 e286.

de Vries, N. L.\* , J. van de Haar\*, **V. Veninga\***, M. Chalabi\*, M. E. Ijsselsteijn, M. van der Ploeg, J. van den Bulk, D. Ruano, J. G. van den Berg, J. B. Haanen, L. J. Zeverijn, B. S. Geurts, G. F. de Wit, T. W. Battaglia, H. Gelderblom, H. M. W. Verheul, T. N. Schumacher, L. F. A. Wessels, F. Koning, N. de Miranda and E. E. Voest (2023). "gammadelta T cells are effectors of immunotherapy in cancers with HLA class I defects." *Nature* 613(7945): 743-750.

**Veninga, V.** and E. E. Voest (2021). "Tumor organoids: Opportunities and challenges to guide precision medicine." *Cancer Cell* 39(9): 1190-1201.





Chalabi, M., L. F. Fanchi, K. K. Dijkstra, J. G. Van den Berg, A. G. Aalbers, K. Sikorska, M. Lopez-Yurda, C. Grootsholten, G. L. Beets, P. Snaebjornsson, M. Maas, M. Mertz, **V. Veninga**, G. Bounova, A. Broeks, R. G. Beets-Tan, T. R. de Wijkerslooth, A. U. van Lent, H. A. Marsman, E. Nuijten, N. F. Kok, M. Kuiper, W. H. Verbeek, M. Kok, M. E. Van Leerdam, T. N. Schumacher, E. E. Voest and J. B. Haanen (2020). "Neoadjuvant immunotherapy leads to pathological responses in MMR-proficient and MMR-deficient early-stage colon cancers." Nat Med 26(4): 566-576.

Guenther, M., **V. Veninga**, J. Kumbrink, M. Haas, C. B. Westphalen, S. Kruger, V. Heinemann, T. Kirchner, S. Boeck, A. Jung and S. Ormanns (2018). "POLE gene hotspot mutations in advanced pancreatic cancer." J Cancer Res Clin Oncol 144(11): 2161-2166.

Schotterl, S., M. Hubner, A. Armento, **V. Veninga**, N. M. Wirsik, S. Bernatz, H. Lentzen, M. Mittelbronn and U. Naumann (2017). "Viscumins functionally modulate cell motility-associated gene expression." Int J Oncol 50(2): 684-696.

\*, # These authors contributed equally

## ACKNOWLEDGMENTS

Finally coming to the important part... It goes without saying that none of this would have been possible without each and everyone of you. The past years have shaped me tremendously, scientifically as well as personally. It is thanks to you that I have not once regretted coming back to the NKI and the Voesties. Given the fact that my opinion about Amsterdam has not changed, that is an immense compliment. I will forever be grateful for this experience and am happy to have met so many incredibly smart and fun people. Just to be clear, I would not say that I trust anyone of you with my experiments or would stop listening to music (just kidding... maybe) but I certainly want you to know that I value all the moments we shared along this journey.

**Emile**, it is difficult to find the right words. There are maybe a handful of people I have met throughout my life that guided, taught and challenged me the way you did. It is not a secret that you were one of the main reasons why I decided to come back to your lab. I was looking for a mentor who puts his heart into leading PhD students and pushes them to become better not just as a scientist but as a person. Looking back, I can say that you have exceeded my expectations in every single way and I am certain that without you I would not be where I am today. You were able to give me the feeling that you are always available no matter what, which is rare. You care deeply but simultaneously gave me the freedom to explore and mistakes. What was most special to me was the help you provided beyond scientific questions. I am beyond grateful for the directions you pointed me towards, doors you opened and the support you provided along the way. Even though my mind is pretty much made up all the time already, you got through and made me question myself. That can be challenging at times but was needed for me to grow. It was definitely a wild ride and I apologize for the difficult times. That said, I get why you jumped on a plane to Australia the moment I submitted my thesis but if you haven't had enough I hope to keep learning from you. Thank you!



**Noel**, I am very happy that I got to know you through our team effort on the  $\gamma\delta$  T cell manuscript. I knew you would be an absolute perfect fit as my co-promotor and am glad that you accepted! You complement Emile with your opinion, scientific expertise, which was so helpful for immunology related questions (I hope Emile doesn't read further than his own paragraph) and personality. Thank you for being providing me with valuable advice.

**Chiara**, my paranymp and friend who constantly sends me 20 voice messages in a row and, even though you live in Milan, I basically know what Dori and Betty had for breakfast and if Ale has a fever of 0.01 degree (sorry Ale). Who could have thought that this is what happens when you save Krijn's master student from a 'snowstorm' in the Netherlands and serve her the most delicious pasta? To be honest, I did not and it is crazy looking back. We have shared so, so many hilarious moments in the lab, very sad moments at Tiffany's, Friday evenings on your and Ale's couch (thanks again for adopting me), OCD baking sessions, 'fun' bike rides, one sided emotional cinema visits and since you are back in Italy, and even though I can't provide you with dishwasher tabs anymore, the list went on with insanely good food, beach day, getting to know your family and many many rants over the phone. I am so absolutely proud of our friendship and how much I can count on you, thank you for being there! I have zero doubt that the list of shared memories will go on and on but what I should definitely also mention is how much I value your scientific opinion and exceptional instinct. It is so easy to switch with you from very stupid, inappropriate jokes to strategically thinking about an experiment or concept. You can be so proud of yourself and it is my absolute joy to watch you succeed. You are a role model in your career as well as your personal life.

Of course, I cannot thank you/ Chiara without thanking you as well, **Ale**. Not only because you support her and let her grow to the person she is but also for the person you are and friend that you have become. Thank you!



**Steven**, my paranyphm and friend who I can always count on to tell me 'fuck that'. I am not sure if it is a good idea to combine the personality of the devil and of Satan, probably not, but well here we are. It was one of the smartest decisions our group has possibly ever made in adopting you as our plus one. I have 100% enjoyed all of our shared moments because your level of honesty, sarcasm, dark sense of humor and intellect is right up my alley. Not only do we think alike in many ways and at times suffered together, you are incredibly reliable and bring a high level of scientific knowledge and smart thinking to the table that has helped me over the past year. Thank you for being my sleep deprived zombie friend!

**Chelsea**, even though we had very little overlap in the Voest lab, I am so happy to have you as my friend (and neighbor and landlord). I am so thankful that we share a common love for good restaurants, good food in general, wine, cozy couch evenings, brunches, halloween and scary movies and the color turquoise. That aside, you have supported me throughout my PhD by bringing joy to this grayness in Amsterdam and always giving me the best possible advice I could think of. You are not only one hell of a scientist but also incredibly driven, smart and strategic in the way you solve problems and interact with people. You should be so proud of yourself and in fact, right now I have a bottle of champagne in my fridge to celebrate your latest promotion ;) Thank you and I'm looking forward to many more restaurant visits. In that sense, also thank you to you, **Marco**, for always delivering on exceptional cocktails and food - the essentials for finishing a PhD.

**Paulien**, Daniela made one very smart choice in hiring you and perhaps I should thank her for that as well. You have not one bad bone in you and became a truly good friend to me. I am so happy that our paths crossed because I can be me around you and same goes for you. The way you manoeuvre your PhD is absolutely laudable and it is impressive to see how you have grown in a very short amount of time. Many people can learn from you how it should look like to cheer on other peers. Thank you for our many walks and support you have given me!



**Iris**, my ride or die in the Voesties group. I believe, I have once said to Emile that you are one of the very few people that I completely trust in the lab. I stand by it. You are hard working, dedicated and get things done. But what's more important is that you are just so much fun to have around. I will absolutely miss your laughter (and very frequent sigh), your facial expression that makes it so easy for me to understand what you are thinking, which is most often not good, and our weekly updates and chats that required a closed door. I am happy to count you as one of my friends. Thank you for your support throughout and that I can rely on you.

**Tom**, although you did not plan on having an interview with our group, it was a hard yes from Chiara and me after talking to you. Since then we have spend (survived) around four years together, organized a lab retreat, agreed with Iris that none of us can handle crying, definitely shared one or two drinks and oh sooooo many gym sessions. I am impressed how you handled all the fame as the only bioinformatician in our lab and I can definitely learn from you how to remain calm in certain situations, like receiving out of the world annoyingly emails. I would say that you are always welcome to visit me in the States, if I get there, but unfortunately that would be a spot under the bridge.

And as your better half, **Elselien**, it was my absolute pleasure to get to know you as well and I will keep a second spot free for you under the bridge. You are always most welcome.

**Joris**, it was very early on that Emile opened my eyes and said 'that's why you clash with Joris, because you are similar in that way'. Although I don't want to push your ego too much, I think you are amazing and I have my full respect for how much you are currently juggling at the same time. Keep it up! Thank you for always finding time to help me and share your advice when needed - or also when not.



**Allard**, have to say based on your instagram I was a bit skeptical about how well we would get along. Turns out, I could not have been more wrong! You have just the best sense of humor and are incredibly smart (although I knew that part after your literature report \*the second draft). I have great memories about our time together with Iris and Emile in Cambridge. You are one of a kind and please don't hesitate to ask for help in case I need to give Emile hints to adjust his behavior again...

**Paula**, I could not have imagined a better successor for our little  $\gamma\delta$  T cell team. You are very talented and made it so easy for me to get you up to speed in the lab. Since you have already figured out how to deal with Joris, I have no doubt that you will do just amazing during you PhD. It was my pleasure sharing a project with you!

**Esmeé**, on that note, thank you very much for bringing Paula to B6 in the first place. We are lucky to have her and likely also due to your fantastic mentoring skills. It was always fun meeting you and thank you for your advice along the way.

**Myriam**, long gone are the days when you came to our office once per week and sat at the most annoying desk of all, the phone desk. I'm sure you miss it... During my PhD I watched you finish yours, establish your own group and gain international fame. You are someone I look up to and it was my pleasure sharing projects with you.

Speaking of, **Yara**, pretty sure you are happy to observe the Voesties craziness from a safe distance although it was fun to have you around at one of our lab retreats. I have good memories of our time in the lab when we tried (successfully) to process tumor samples. Good luck finishing up but I have no doubt that you will do just amazing! **Pedro**, I hope you enjoy your time in Myriam's group and are still excited about single cell analysis. I will definitely come back to you as I will be desperate very soon, thank you for offering to help.



**Alice and Marlies**, I have started my PhD with your help, Alice, and am finishing with the support of you, Marlies. Both of you have/ are doing a tremendous job in keeping our group up and running. We would all be lost without you. Thank you so much!

**Salo**, not sure when I saw you at more random times. While you were still a PhD student in our group, but no one was able to figure out your schedule (especially not your student), or after your graduation at occasional dinners with Chelsea. Either way, I had a blast every time and especially our 'team effort' at the EU TalentOn in Leiden was... memorable. It's always fun to have you around, which reminds me to start the process of scheduling another dinner with you and Chelsea. (Sending you a message right now).

**Shannon**, should I start in German or English? Ich bin SO froh, dass wir uns kennen gelernt haben. Du bist eine absolute power Frau und ich hab unsere brainstorm sessions sehr wertgeschätzt. Behalte die Energie die du hast und ich hoffe sehr, dass wir in Kontakt bleiben auch wenn ich nicht mehr in Amsterdam bin.

**Luuk**, I miss all of your one million crazy project ideas in our lab meetings so much! You were such a nice, fun and happy person to have around as a colleague. Very much enjoyed the (a bit) drunk night at the OOA retreat and then you smashing a coconut on my balcony. Good times :)

**Pim**, how much fun was it to meet with all of us complaining about our daily terrors while you found your way into to the free world? It was a pleasure to have you around for some time and I think you can be very happy about your decision.

**Connor**, ja schade, dass du nicht mehr da bist aber ich freue mich so sehr für dich! Es war mir eine Freude mit dir und Steven auf einer Wellenlänge zu sein.



Vielen Dank noch einmal für die wunderschönen Magneten und ich hoffe wir halte uns weiterhin auf dem Laufendem (vor allem was besondere committees etc. betrifft).

**Leon**, immer wenn ich an Connor denke muss ich auch an die seer unterhaltsame Situation in der Zellkulturen denken, als er dich nach deinen Vorfahren gefragt hat. Was soll man sagen, die Schweizer... Anyway, vielen Dank dass du mein Vertrauen in Master Studenten wieder hergestellt hattest! Du warst ein absoluter Bilderbuch Student und ich bin mir ganz sicher, dass du eine steile Karriere vor dir hast!

**Don**, it still amazes me how you managed to bring whole B6 together. It's a talent very few people have. The day at Volendam will never be forgotten. I'm very proud of you to dared to move to Leiden and happy to hear that you are enjoying yourself.

**Krijn**, after reflecting on my own role as a supervisor (mostly very impatient), of course I have to thank you for being a very good example of how to do it better. I'm still not sure how you managed to explain 5238791 times to me how to use the Fortessa, but at least I helped you with parafilm in return. Thank you for teaching me and making sure that I had a smooth start as a PhD student.

**Minhi**, I am truly sorry for the mess you had to deal with when you started. You have my full respect in how you dealt with it! I am very glad you decided to stay, not just because of your work ethics, but also for the fun person you are. **Xuhui**, I hope you enjoyed your time with us even though it must have been a bit of a cultural adjustment in the beginning. All of us were able to learn a lot from you and it is impressive how you managed your stay here! You should be proud. **Lindsay**, thank you for trying hard to make our office look nice, appreciate the effort but sorry for your plants, **Maartje, Bea, Agnes, Joyce, Kristine**, it was my pleasure to work with all of you and I think Emile can be proud to have/had such an amazing





team. Enjoy the Voesties spirit, it is a special one ;) **Miguel**, I was very quick to judge that we should definitely try to keep you in the lab and you are not disappointing! I have enjoyed having you around a lot. **Laurien**, you made it! Yay! Thanks for sharing kind words with me towards the end of our PhD and I hope you know that you really kept the DRUP team together, you can be proud. That said, **Birgit, Soemeya, Gijs, Floor** and of course **Judith** and **Jeanette**, our lab people can be happy to have a supporting team like you to answer all of our clinical questions. Thanks for your help!

**Ewald**, it is thanks to Chelsea that we have met and I am very happy about it. I like being challenged by your opinion and you are undoubtedly one of the smartest people around. Thanks also for always making sure there is wine or Amarula around.

**Mathew, Gabriele** and **Matt**, it was my absolute pleasure to work with you. You have been part of my PhD journey from the very beginning until the last minute and I was able to learn a lot from you. Our bi-weekly Friday afternoon meetings were probably more consistent than our own lab meetings and it will probably take a minute to not panic on Friday morning remembering that I need to prepare slides. I especially enjoyed our visits in Cambridge/ Amsterdam very much. Hope to stay in touch and I wish you ongoing success in your careers. Thank you!

The office next door, sorry that we should have kept our door closed more often to prevent you from the crazy Voest office talk. Although you must admit, it can be entertaining. **Jos, Mireille, Marius, Björn, Ziva, Mercedes** and **Floris**, you are one amazing team and so much fun to have around. I'm very sure that I will not meet similar colleagues wherever I go. Thank you for being around and for never being annoyed when I dropped by. Will miss you.

Same goes for **Wouter, Anne** and **Meike**, Thank you for always making time to help and share your advice, back in the days in B6 or even now. I appreciate it a lot!



**Gabriel**, I am sorry that you have to keep up with me sitting 24/7 at the kitchen table right now and that there is no way of not listening to me complaining about stupid writing. I would have never thought to talk about V $\delta$ 1 T cells while having dinner and I have to say that I really enjoy your input and kindness. The whole Peeper lab can be lucky to have you! Talking about, **Zowi**, **Sofia**, **Chun Pu**, **Sebastiaan**, **Su Min**, **Kelly**, **Susan** and **Johanna** (you guys expand to fast, sorry to whomever I forgot) B6 would not be the same without and I am happy you guys came to appreciate the struggle of organoids as well. **Tim**, it was my pleasure to teach you and I think your scientific dedication is absolutely admirable. **David**, the moment has come... I am finally not there anymore. I know this must be very special to you too. I wish you and **Julia** all the best for your family and your future. **Georgi**, I will not let you pick an airbnb again but I am happy we are alive! It was a fun trip and, **Alex**, I was very happy to meet someone else with that much food enthusiasm. Last but not least, **Nils**, I have no idea how you keep up with all of us but you are truly doing an exceptional job. Thank you and don't ever lose your excellent sense of humor!

**Brenda**, although not at B6 anymore, it was my pleasure to have met you especially because we share the Hannover experience.

**Ton**, **Daniel** and **Daniela**, I believe you would all agree if I say that B6 is a very unique place and although we are all fighting for space, at the end of the day it is amazing to have that many talented people around. Thank you for your excellent input, willingness to share your advice and keeping the scientific standard high!

**Leila**, I am extremely happy that Emile was spot on when he pointed me into your direction after I told him that I am looking for mentorship. He believed I would listen to you and, according to him, that is a rare occasion - I would probably have to agree. I appreciate your directness, honesty and sharpness. Next to excellent scientific advice, I look up to you for the way you manage your lab and navigate yourself in the academic world. You provided me with clarity when needed and I am grateful for the time and guidance you offered. Thank you!



**Karin**, it was my pleasure to have you in my PhD committee as you guided me with your expertise. **Jonas**, thank you for being so approachable and always happy to make time to share your advice. Either for Shannon and my Entrepreneur Club endeavors or my questions about starting your own lab and grants. Thank you! Talking about the Entrepreneur Club, **Henri** you were the one who made it possible and I am very thankful for your enthusiasm and help.

There would not exist one single chapter (okay besides the review), if it would not be for the amazing **Flow Cytometry team**. You guys rock! Your facility is outstanding and I don't know what to do without you. Good that I have some of your phone numbers, because rest assured I will make use of them when I'm stuck at the flow in my next lab. **Martijn, Frank, Guido, Anita** and **Saurabh**, thank you so, so much!

Another facility without whom our research would not be possible and we could all go home is the **Cryobank**. If you guys didn't know, your hilarious emails are famous among our group and I so much appreciate you for all your work and flexibility. Thank you **Minze, Erwin** and **Jufry**!

**Marja Nieuwland** and the team of the Genomics Facility, it should not be left unsaid how much I appreciate your dedication and help you have provided to design experiments and provide me with guidance. Thank you.

**Maarten**, I already miss our ritual in me bringing you a tiny piece of tumor and every other time sending you a disappointed email about how we did not receive any material. Thank you for your help and flexibility!

**Luca, Elzo** and **Moreno**, thank you for taking the time, keeping up with my ideas and providing me with your advice. You guys have delivered all the way and I was impressed how perfectly structure and forthcoming you helped me when it came down to putting all the data together. Luca, I wish you all the best for your own lab and hope to stay in touch. Good luck!



**Harry and Paul**, it was my pleasure to learn more about HSPC-NK cells and collaborate with you. It made me happy to see how enthusiastic you are about your research and thank you for your kind help.

... coming to the people who bring joy to my daily life and signed up for one hell of a ride. Thank you for keeping up with my insanity!

**Marieke**, ich bin davon überzeugt, dass wenn ich mich damals in der 9. Klasse nicht neben dich gesetzt hätte, die zweite Hälfte meines bisherigen Lebens um einiges grauer gewesen wäre. Du bist ein so unglaublich toller Mensch, den ich für so viele Aspekte endlos wertschätze. Danke, dass du da bist, ich mich auf dich verlassen kann und es jedes mal wieder einfach nur pure Freude und Spass ist wenn wir uns wiedersehen. Vor dir kann ich Schwäche zeigen und mich fallen lassen. Ohne eine Freundschaft wie unsere wären die letzten Jahre mal so schwer gewesen. Danke! ... ich hoffe der Wein steht kalt, weil wenn du das liest bin ich sehr wahrscheinlich bald zu Besuch.

**Sarah**, ich denke es ist fair zu sagen, dass weder deine noch meiner Mutter damals in der Krabbelgruppe ahnen konnten wie sich unsere Wege immer wieder kreuzen und nie auseinander gehen. Es ist absolut spannend zu sehen wie wir beide uns Entwickelt haben. Auf der einen Seite fühlt es sich wie gestern an, als wir beide noch in Steyerberg gewohnt haben, aus dem Kreml kamen und ich den nächsten morgen wieder mit Brötchen vor eurer Tür stand, aber sobald ich darüber nachdenke was wir alles erlebt haben?! Wir sind durch Höhen und Tiefen gegangen, gemeinsam oder jeweils am anderen Ende der Welt. Allein wie viele andere Leute jeweils in meinem oder deinem Leben in der Zwischenzeit gekommen und gegangen sind... wir waren da und ich freue mich auf Alles was noch kommt. Auch wenn die letzten Wochen mir nichts gezeigt haben was ich nicht sowieso schon von dir weiss, du hast wieder bewiesen wie sehr du mir den Rücken stärkst, für mich da bist und wie selbstlos du sein kannst wenn es um



andere geht. Danke! Ich freue mich so unglaublich sehr, dass sich unsere Wege wenigstens für ein paar Monate wieder kreuzen.

**Freddy**, wirklich 12 Jahre schon? Das interessante bei uns beiden ist, dass ich dir nicht sagen kann ob du oder ich mehr Durchhaltevermögen hast es so lange mit mir/ dir auszuhalten. Vielleicht war es deine anfängliche mütterliche Art als ich dir eine mehr als widerliche Alkoholpraline in die Hand spucken durfte, die mir mein generelles Misstrauen gegenüber Menschen genommen hat. Das wird definitiv mit reingespielt haben, aber vermutlich auch deine (sehr) direkte, ehrliche und vor allem loyale Art. Auf dich kann ich mich verlassen und das angenehme dabei ist, du kannst auch noch richtig gut denken und bringst mich zum lachen. Ich bin stolz auf dich, unsere Freundschaft und danke, dass du immer ein offenes Ohr hast.

**Isaac**, jetzt gerade glaube ich nicht daran, dass es jemals fertig wird. Aber falls du noch am Leben bist, wenn du das hier liest, kann ich wider erwartend bestätigen, dass es tatsächlich ein Ende gibt. Wir haben zusammen angefangen und obwohl wir beide es nicht lange an dem Ort ausgehalten, bin ich SO dankbar dich kennen gelernt zu haben. Ohne dich hätte mich entweder Ben Li Zang umgebracht, ich wär im Airbnb eingesperrt oder es gäbe meinen Fuss nicht mehr. Ich werde dir für immer für deine Hilfe und Fürsorge dankbar sein. Wobei noch viel mehr, für all den Wein (es war so viel Wein), die Dinner am Freitag die ab montags geplant wurden und für deinen ausnahmslos schwarzen und sehr unangemessene Humor. Danke! ... und jetzt, mehr Wein!

**Jule**, du kennst mich so lange wie meine Eltern mich kennen. In manchen Dingen könnten wir uns nicht unterschiedlicher sein und dann wieder rum sind es knapp 32 Jahre später, wir beide sitzen an unserer Doktorarbeit und ich hab deine Stimme im Kopf "Oh Vivien". Ich muss zugeben manchmal die Zeit zu vermissen als wir dachten ein Sandwich mir Zitrone und Salami ist das was eine Kochshow braucht. Du hast meine Kindheit geprägt wie niemand sonst und ich bin so froh,

dass wir uns nie ganz aus den Augen verloren haben. Ich hoffe du weisst, dass ich immer für dich da sein werde. Danke, dass es dich gibt.

**Wiebke**, paar Jahre später und paar Häuser vor Jule's... Die drei aus Hoppi's Klasse und es ist jedes Jahr wieder schön wenn wir alle beisammen sind.

**Cathi**, ich brauch dir nicht sagen wie es mir gerade geht...Ich bin sehr stolz auf dich wie du deinen Weg die letzten Jahre gegangen bist! Absolut Hut ab und ich wünsche dir ganz viel Erfolg für die nächsten Schritte in deiner Karriere. Am meisten freue ich mich auf den Moment wenn wir beide bei einem Glas Champagner sagen können, dass es sich gelohnt hat. Bis dahin, danke für dein offenes Ohr, egal wie banal die Probleme waren, deinen guten Geschmack in Wein und Essen und deine offene, ehrliche und unkomplizierte Art.

**Niggel**, na wie lang waren deine Acknowledgments? Freddy wollte erst gross prahlen, dass er der einzige Mann sei der es mit mir seit 12 Jahren aushält. Er musste es mit einem Zusatz korrigieren. Du hast mir vor allem in den letzten Jahren das gegeben was ich selber nicht so gut kann, Vertrauen in mich selbst. Immer wenn es schwer wird, bist du da und sagst mir, dass die Welt nicht gegen mich ist. Danke!

**Trieu**, war ich froh, dass du auch weiss magst und mich die Gästehandtücher nach meinem Belieben falten lassen hast. Das war eine schöne Anfangszeit hier in Amsterdam und genauso schön war es als wir während Corona festgestellt haben keine Hobbys zu haben. Du bist über die Jahre eine wirklich tolle Freundin geworden und kannst so stolz auf deinen spektakuläre Karriere sein. Alles mehr als verdient also erlaub dir stolz auf dich selbst zu sein.

**Alex**, you are just so much fun to have around and so absolutely caring for other people. It was very wise when you once said that I would go crazy living with you, you were right because I'm still not recovered after watching you color your nails,



but besides that I am very happy to have you as a friend. Thank you for all your supportive words.

**Max**, ja glaubt es einer? Da bin ich fertig. Es kann sicher nur an deinem Ansporn von day 1 an gelegen haben. Ich glaube ich hatte den Vertrag noch nicht einmal und du hast schon gefragt "bist jetzt endlich fertig?". Motivational skills 10/10. Danke!

**Linda**: Es ist so toll, dass wir uns kennen gelernt haben! Ich werde nicht in Details gehen und Floskeln aus unserer Stuttgardia Zeit erzählen... Ich finde es schön, dass wir uns nicht aus den Augen verloren haben und danke dir für deine stets fröhliche und sorgsame Art.

**Toni**: Ich freue mich so sehr wenn wir uns das nächste mal sehen und beide auf unseren Erfolg anstossen können! Toll, dass es dich gibt und es tat gut zu hören das wir gleichzeitig durch den thesis Schreibmarathon gegangen sind.

Frau **Dr. Tommek**, dank Ihnen habe ich die Schule gewechselt und konnte meiner Leidenschaft nachgehen - Chemie. Ich weiss nicht ob Ihnen bewusst ist wie bedeutsam das damals für mich war, aber ich hoffe diese Doktorarbeit zeigt zu einem gewissen Anteil wie gut Sie Ihren Job gemacht haben. Das gleiche gilt auch für Sie, **Herr Kohlstedde**, ich habe Ihre Buchvorschläge, insbesondere den Mortimer, damals verschlungen. Vielen Dank, dass Sie meine Interessen erkannt und gefördert haben. In Erinnerung auch an **Herrn Adolf**.

**Mike**, Bruderherz. Im Vergleich zu Opa, hatte ich nie Zweifel 'ob aus dir etwas wird'. Du kannst extrem stolz auf dich sein und darauf was du erreicht hast. Eins deiner Talente, was bei mir ab und an zu kurz kommt, ist es mit Leuten umzugehen. Dazu kommt dein Humor, den haben wir von Papa, und deine Arbeitsmoral, da macht Mama uns nichts vor. Ich hoffe dich nie zu Enttäuschen und das ist tatsächlich einer meiner Gedanken der mich anspricht mehr zu erreichen. Danke für dein Vertrauen in mich!

**Opa**, ich wünschte **Oma** hätte den Moment noch miterlebt. Ich bin stolz auf dich wie du seitdem das Leben meisterst, weiter machst und für uns alle da bist. Danke, dass du all deine Enkel so nimmst wie wir sind und mir das Gefühl gibst, dass ich auf dich zählen kann.

In Erinnerung an **Opa Holland**, auch wenn ich leider 1 Jahr zu lange gebraucht habe.

**Papa**: Das grösste Geschenk was du mir in meinem Leben gegeben hast, war dass ich mich, seitdem ich denken, von dir ernst genommen fühle. Danke! Auch wenn du mein Interesse an der Wissenschaft nicht nachempfinden kannst, verstehst du meinen Drang nach Freiheit, Unabhängigkeit und das Streben nach einem Leben was mich erfüllt. Danke für all die Lektionen die du mir mit auf den Weg gegeben hast!

**Mama**: Du hast alles richtig gemacht. Du hast mir ein Leben lang ein Gefühl von bedingungsloser Liebe vermittelt und ich bin mir sicher, dass ich es dir nicht immer leicht gemacht habe. Es gibt kaum eine Person, die so stark ist, so viel Energie hat (Mike und ich haben keine Ahnung wie du das machst) und so selbstlos ist wie du. Danke für deine Geduld, deine Hingabe und konstante Unterstützung. Ich hoffe du bist stolz auf dich.





EVERY SECOND COUNTS

The Bear  
Season 2, Episode 7

